Numerical modeling of thermal and geotechnical response of soils in Canadian no-permafrost regions to climate warming

By

Mohammed Yassir Marrah

A thesis submitted

under the supervision of Dr. Mamadou Fall

and

co-supervision of Dr. Husham Almansour

In partial fulfillment of the

requirements for the degree of

Master of Applied Science

in Geotechnical Engineering

Department of Civil Engineering

University of Ottawa

Ottawa, Canada

July, 2021

The M.A.Sc. in geotechnical Engineering is a joint program

with Carleton University administrated by

Ottawa-Carleton Institute for Civil Engineering

Abstract

In the present study, methodological approaches to assess the impact of climate change on the thermal and thermo-hydro-mechanical (THM) regimes of the ground in some selected Canadian no-permafrost areas (Ottawa, Sudbury, Toronto) is proposed. A modeling study to evaluate ground temperature variations due to global warming is conducted using TEMP/W software from Geoslope ltd. The effect of future climate change projections, up to 2100, on the ground freeze-thaw cycle frequencies, frost penetration depth, and frost duration is assessed in some selected sites located in the Canadian no-permafrost region. Moreover, three softwares (TEMP/W, SEEP/W and SIGMA/W from Geoslope Ltd) have been used to establish a numerical tool that enable to assess the effect of global warming on THM response of the grounds in the selected Canadian no-permafrost areas. TEMP/W and SEEP/W were coupled in a thermo-hydraulic analysis to assess the impact of global warming on the hydraulic regime of the ground. Afterwards, SEEP/W and SIGMA/W were coupled in a hydraulic-mechanical analysis to study the impact of climate change induced porewater pressures change on the mechanical regime of the ground in some no-permafrost regions. Simulation study to assess the effect ground temperature changes on key geotechnical properties of the soils in the selected sites is conducted by using the aforementioned numerical tool. The change of the porewater pressure changes and distributions in the soil induced by global warming is studied. The effect of climate change on the ground consolidation or settlement in the selected no-permafrost sites is also investigated. Finally, this study provides a simulation of a bridge pile foundation ground to detect the THM changes around the pile structure due to climate warming.

The results indicate that climate change will affect the thermal regime of the ground in the selected Canadian no permafrost areas. Ground temperature in the studied no-permafrost regions will likely increase by 2 to 4° C by 2100 due to global warming. Furthermore, the frost penetration depth will be significantly reduced in all study areas. It is also found that the frost duration will experience a gradual reduction with time up to 2100. In addition, the simulation results showed minimal influence of global warming on the porewater pressure distribution and magnitude in the studied grounds. Aligned to this, climate change did not seem to have a significant effect on the consolidation behavior or settlement of the ground in the studied no-permafrost areas. The simulation of the foundation ground confirms the results mentioned above, as temperature changes around the pile structure falls within the same range found in the thermal analysis. Porewater pressure distributions and ground settlement are not significantly affected along the pile perimeter. Overall, the design of pile foundation in the Canadian no-permafrost region will not be significantly affected by climate change up 2100. The tools developed and results obtained will be useful for the geotechnical design of climate-adaptive civil engineering or transportation structures in Canadian no permafrost areas.

To My Parents

Acknowledgement

First of all, I would like to thank my academic supervisor, Dr. Mamadou Fall, and co-supervisor, Dr. Husham Almansour, for taking me on as a graduate student. I would like to express my deepest gratitude to my supervisor and mentor, Dr. Mamadou Fall, for his constant guidance, encouragement, support, motivation and continuous help during the course of my Master's degree.

Special thanks to Dr. Husham Almansour for his continual help and constructive inputs along the process.

I would like to thank all my professors, in my undergraduate and graduate studies at the university of Ottawa, for providing a stimulating and fun environment in which to learn and grow.

Finally, I would like to take this opportunity to express my profound gratitude from the deepest part of my heart to my beloved parents, my dear sister, and my beloved wife. I cannot imagine my current position without their love and support. To them, I dedicate this thesis.

Table of Contents

Abstract ii
Acknowledgement iv
List of Figures viii
List of Tables xii

Chapter 1 – General Introduction 1
1.1 Problem statement 1
1.2 Objectives of the research 2
1.3 Research approaches and methods 2
1.4 Organization of the manuscript 3
1.5 References 5
Chapter 2 – Background and Literature review 6
2.1 Introduction 6
2.2 Geographical borders of the Canadian no-permafrost region 6
2.3 Seasonal ground freezing and thawing parameters of soils 7
2.3.1 Freezing and thawing indices 7
2.3.2 Frost penetration depth 10
2.4 Geotechnical design challenges in seasonally frozen no-permafrost soils 13
2.5 Background on numerical modeling tools and the softwares used 16
2.6 Background on the climate model and climate change scenarios used 18
2.7 Summary and conclusion 21
2.8 References 22
Chapter 3 - Technical paper I – Numerical simulation of ground thermal response in Canadian no-permafrost regions to climate warming 24
3.1 Introduction 25
3.2 The study area: 26
3.2.1 Geographical description of the study area: 26
3.2.2 Climate conditions of the study area 28
3.2.3 Climate change models in the study area in the next 100 years 28
3.2.4 Representative soil profiles of the study area 30
3.3 Methodology: 31

3.3.1 Approach: 31
3.4 Description and validation of the thermal model 32
3.4.1 General formulations 32
3.4.2 Validation of the thermal model/simulation tool 34
3.5 Climate data collection: 38
3.6 Geometry and material properties of the thermal models: 39
3.6.1 Geometry: 39
3.6.2 Material properties: 40
3.7 Modeling of the thermal responses of the selected sites to climate changes 42
3.7.1 Boundary conditions 42
3.8 Simulation results and discussion: 46
3.8.1 Temperature profiles: 46
3.8.2 Climate change scenario - Sensitivity analysis: 49
3.8.3 Ground temperature at different depths 55
3.8.4 Snow depth - Sensitivity analysis: 61
3.8.5 Discussion of results: 63
3.9 Summary and conclusions 66
3.10 References: 68
Chapter 4 - Numerical simulation of the ground thermo-hydro-mechanical response in Canadian no-permafrost regions to climate warming 70
4.1 Introduction 71
4.2 The study area 73
4.2.1 Geographical description of the study area 73
4.2.2 Representative soil profiles of the study area 74
4.3 Methodology 76
4.3.1 Approach 76
4.3.2 Governing equations, constitutive models, and coupling procedures. 77
4.3.3 TEMP/W 78
4.3.4 SEEP/W 79
4.3.5 SIGMA/W 80
4.4 Validation of the simulation approach / tool 81
4.4.1 Model geometry, material properties and boundary conditions: 81
4.4.2 Discussion of the validation results 87

4.5 Climate data collection 94
4.5.1 Geometry 96
4.5.2 Material properties 96
4.6 Modeling of the THM responses of the selected sites to climate changes 100
4.6.1 Boundary conditions 100
4.7 Simulation results 103
4.7.1 Coupled thermo-hydraulic simulation results. 104
4.7.2 Coupled hydro-mechanical simulation results 106
4.8 Discussion of results 111
4.9 Conclusion 114
4.10 References 115
Chapter 5 – Synthesis and discussions of results, and practical engineering application 118
5.1 Introduction 118
5.2 Synthesis and discussions of results 118
5.3 Application to bride pile foundation ground 120
5.3.1 Model geometry: 121
5.3.2 Boundary conditions: 121
5.3.3 Simulation results 122
5.4 Discussions of results and conclusions 132
Chapter 6 – Summary, conclusions and future research recommendations 135
6.1 Summary 135
6.2 Conclusions 136
6.3 Recommendations 137
Appendix A 140
Appendix B 146
Appendix C 152
Appendix D 162
Appendix E 171
Appendix F 177
Appendix G 195

List of Figures:

Figure 1.4.1: Thesis manuscript organization chart 4
Figure 2.2.1: The geographical limits of the Canadian no-permafrost region (Booshehrian et al., 2020) 6
Figure 2.2.2: Location of Ottawa, Toronto and Sudbury within Ontario (Cambrian International, 2021) ... 7
Figure 2.3.1: freezing-thawing time sequence (Orlando & Ladanyi, 2004) 8
Figure 2.3.2: the correction factor λ – graphical correlation (Orlando & Ladanyi, 2004) 12
Figure 2.5.1: The Burland triangle (Burland, 1987) 16
Figure 2.6.1: Historical and predicted Change in global average temperature 1900-2100 (Government of Canada, 2018) 20
Figure 3.2.1: The geographical limits of the Canadian no-permafrost region (Booshehrian et al., 2020).. 27
Figure 3.2.2: Location of Ottawa, Toronto and Sudbury within Ontario (Cambrian International, 2021) . 27
Figure 3.3.1: flow chart of the analysis 32
Figure 3.4.1: a) Cross Section of the validation model, b) Model surface boundary Layer, (c) Steady state boundary condition 36
Figure 3.4.2: Monthly ground temperature in clay soil at Ottawa from May 1954 to April 1955, a) measured data, b) modeling results. 37
Figure 3.5.1: Climate change interactive map (Government of Canada, 2019) 39
Figure 3.7.1: Simulation model Steady state boundary conditions a) Ottawa b) Toronto c) Sudbury 43
Figure 3.7.2: Analysis's sequence established and implemented in the modeling tool. 45
Figure 3.8.1: Ground temperature profiles at a) March 1st and b) December 31 st for 2020 – 2040 – 2060 – 2080 – 2100 – RCP8.5 46
Figure 3.8.2: Ground temperature profiles at a) March 1st and b) December 31 st for 2020 – 2040 – 2060 – 2080 – 2100 47
Figure 3.8.3: Ground temperature profiles at a) March 1st and b) December 31 st for 2020 – 2040 – 2060 – 2080 – 2100 – RCP 2.5 47
Figure 3.8.4: Ground temperature profiles at a) March 1st and b) December 31 st for 2020 – 2040 – 2060 – 2080 – 2100 – RCP8.5 48
Figure 3.8.5: Ground temperature profiles at a) March 1st and b) December 31 st for 2020 – 2040 – 2060 – 2080 – 2100 – RCP8.5 48
Figure 3.8.6: Temperature profiles at Mach 1st and December 1st in 2040, 2060, 2080 and 2100 for different RCPs- Ottawa 50

Figure 3.8.7: Temperature profiles at Mach 1st and December 1st in 2040, 2060, 2080 and 2100 for different 52
Figure 3.8.8: Temperature profiles at Mach 1st and December 1st in 2040, 2060, 2080 and 2100 for different RCPs - Sudbury 54
Figure 3.8.9: Temperature profile at different depths -2020 – Ottawa 55
Figure 3.8.10: Temperature profile at different depths - RCP 8.5 - at 2040, 2060, 2080, 2100 – Ottawa .. 56
Figure 3.8.11: Temperature profile at different depths - RCP 4.5 - at 2040, 2060, 2080, 2100 – Ottawa .. 57
Figure 3.8.12: Temperature profile at different depths - RCP 2.5 - at 2040, 2060, 2080, 2100 – Ottawa .. 58
Figure 3.8.13: Temperature profile at different depths - 2020 - Toronto 59
Figure 3.8.14: Temperature profile at different depths - RCP 8.5 at 2040, 2060, 2080, 2100 - Toronto ... 59
Figure 3.8.15: Temperature profile at different depths - 2020 – Sudbury 60
Figure 3.8.16: Temperature profile at different depths - RCP 8.5 at 2040, 2060, 2080, 2100 – Sudbury .. 60
Figure 3.8.17: ground temperature profile in Mach 1st 2100 a) Ottawa, b) Toronto c) Sudbury 62
Figure 4.2.1: The geographical limits of the Canadian no-permafrost region (Booshehrian et al., 2020) .. 73
Figure 4.2.2: Location of Ottawa, Toronto and Sudbury within Ontario (Cambrian International, 2021) 74
Figure 4.2.3: a) Ottawa simulation model geometry, b) Toronto simulation model geometry, (c) Sudbury simulation model geometry 76
Figure 4.3.1: Developed methodology for assessing the THM response of the soils in Canadian no permafrost areas to climate change (CCM: climate change model) 77
Figure 4.4.1: Cross Section of the validation model (Flynn, 2015) 82
Figure 4.4.2: Thermal boundary conditions – TEMP/W - validation model 85
Figure 4.4.3: Hydraulic boundary conditions – SEEP/W- validation model 86
Figure 4.4.4: Mechanical boundary conditions – SIGMA/W - validation model 87
Figure 4.4.5: Monthly ground temperature of the ground at a) January 2013, b) July 2013, c) February 2014 and d) July 2014 – TEMP/W 89
Figure 4.4.6: Simulated porewater pressures profiles at a) the toe and b) centerline of the embankment-SEEP/W 90
Figure 4.4.7: Field porewater measurements at the toe and the centerline of the embankment (Flynn, 2015) 91
Figure 4.4.8: Simulated vertical settlement of the embankment – SIGMA/W 92
Figure 4.4.9: Field vertical settlement of the embankment (Flynn, 2015) 92
Figure 4.5.1: Climate change interactive map (Government of Canada, 2019) 95

Figure 4.6.1: Simulation model steady state boundary conditions - Ottawa..... 101
Figure 4.6.2: Hydraulic boundary conditions – transient analysis – Ottawa 102
Figure 4.6.3: Mechanical boundary conditions – transient analysis – Ottawa..... 103
Figure 4.7.1: Porewater pressure distribution at a) December 31st and b) March 1st, 2020, 2040, 2060, 2080 and 2100 – RCP 8.5 104
Figure 4.7.2: Porewater pressure distribution at a) December 31st and b) March 1st, 2020, 2040, 2060, 2080 and 2100 – RCP 4.5 104
Figure 4.7.3: Porewater pressure distribution at a) December 31st and b) March 1st, 2020, 2040, 2060, 2080 and 2100 – RCP 8.5 105
Figure 4.7.4: Porewater pressure distribution at a) December 31st and b) March 1st, 2020, 2040, 2060, 2080 and 2100 – RCP 4.5 105
Figure 4.7.5: Porewater pressure distribution at a) December 31st and b) March 1st, 2020, 2040, 2060, 2080 and 2100 – RCP 8.5 106
Figure 4.7.6: Porewater pressure distribution at a) December 31st and b) March 1st, 2020, 2040, 2060, 2080 and 2100 – RCP 4.5 106
Figure 4.7.7: Average ground surface settlement at a) March 1st and b) December 31st 2020, 2040, 2060, 2080 and 2100 – RCP8.5 107
Figure 4.7.8: Average ground surface settlement at a) March 1st and b) December 31st 2020, 2040, 2060, 2080 and 2100 –RCP4.5 108
Figure 4.7.9: Average ground surface settlement at a) March 1st and b) December 31st 2020, 2040, 2060, 2080 and 2100 –RCP8.5 109
Figure 4.7.10: Average ground surface settlement at a) March 1st and b) December 31st 2020, 2040, 2060, 2080 and 2100 –RCP4.5 109
Figure 4.7.11: Average ground surface settlement at a) March 1st and b) December 31st 2020, 2040, 2060, 2080 and 2100 –RCP8.5 110
Figure 4.7.12: Average ground surface settlement at a) March 1st and b) December 31st 2020, 2040, 2060, 2080 and 2100 –RCP4.5 111
Figure 5.3.1: Geometry configuration of the pile structure 121
Figure 5.3.2: Groundwater table boundary conditions - SEEP/W. 122
Figure 5.3.3: Ground temperature distribution around the pile structure in December 31st, a) 2020, b) 2060 and c) 2100 for RCP 8.5 124
Figure 5.3.4: Porewater pressure distribution along the pile structure. The results were reported in December 31s,a) 2020, b) 2060 and c) 2100 for RCP 8.5. 125

Figure 5.3.5: Ground deformation structure in December 31s, a) 2020, b) 2060 and c) 2100 for RCP 8.5. 127
Figure 5.3.6: Ground temperature profiles at a) December 31 st and b) March 1st for 2020– 2060– 2100 – RCP8.5 128
Figure 5.3.7: Ground temperature profiles at a) December 31 st and b) March 1st for 2020– 2060– 2100 – RCP4.5 128
Figure 5.3.8: Porewater pressure distribution at a) December 31st and b) March 1st, 2020, 2040, 2060, 2080 and 2100 – RCP 4.5 129
Figure 5.3.9: Porewater pressure distribution at a) December 31st and b) March 1st, 2020, 2040, 2060, 2080 and 2100 – RCP 4.5 130
Figure 5.3.10: Vertical Displacement at a) December 31st and b) March 1st, 2020, 2040, 2060, 2080 and 2100 – RCP 4.5 131
Figure 5.3.11: Vertical Displacement at a) December 31st and b) March 1st, 2020, 2040, 2060, 2080 and 2100 – RCP 8.5 132

List of Tables

Table 2.3.1: Typical values of “n” factors for different type of surface - (Orlando & Ladanyi, 2004) 9
Table 2.4.1: Typical values of uplift forces - (Orlando & Ladanyi, 2004) 13
Table 2.6.1: Representative Concentration Pathways description (Charron, 2016) 20
Table 3.2.1: Climate change data – Ottawa- (Government of Canada, 2019) 29
Table 3.2.2: climate change data –Toronto- (Government of Canada, 2019) 29
Table 3.2.3: climate change data – Sudbury - (Government of Canada, 2019) 30
Table 3.4.1: Thermal properties of the validation model (Orlando & Ladanyi, 2004) 35
Table 3.5.1: Climate stations at Ottawa, Toronto and Sudbury (Government of Canada, 2019) 39
Table 3.6.1: Material thermal properties – Ottawa model - (Orlando & Ladanyi, 2004) 40
Table 3.6.2: Material thermal properties – Toronto model - (Orlando & Ladanyi, 2004) 41
Table 3.6.3: Material thermal properties – Sudbury model - (Orlando & Ladanyi, 2004) 41
Table 3.8.1: n-freezing and n-thawing factors used in the sensitivity analysis in the study areas (Smith & Riseborough, 2002) 61
Table 4.4.1: Thermal properties of the validation model (Orlando & Ladanyi, 2004) 83
Table 4.4.2: Hydraulic and mechanical properties of the validation model (Budhu, 2007) 84
Table 4.4.3: Surface Modifying Factors in TEMP/W 84
Table 4.5.1: Climate stations at Ottawa, Toronto and Sudbury (Government of Canada, 2019) 95
Table 4.5.2: Material hydraulic properties – Ottawa model - (Budhu, 2007) 96
Table 4.5.3: Material hydraulic properties – Toronto model - (Budhu, 2007) 97
Table 4.5.4: Material hydraulic properties – Sudbury model - (Budhu, 2007) 97
Table 4.5.5: Material physical and mechanical properties – Ottawa model - (Budhu, 2007) 97
Table 4.5.6: Material mechanical properties – Toronto model - (Budhu, 2007) 98
Table 4.5.7: Material mechanical properties – Sudbury model - (Budhu, 2007) 98
Table 4.5.8: Material thermal properties – Ottawa model - (Orlando & Ladanyi, 2004) 99
Table 4.5.9: Material thermal properties – Toronto model - (Orlando & Ladanyi, 2004) 99
Table 4.5.10: Material thermal properties – Sudbury model - (Orlando & Ladanyi, 2004) 99
Table 4.6.1: Geothermal heat flux (Grasby et al., 2009) 100
Table 4.6.2: Total head boundary conditions (Natural Resources Canada, 2010) 102

Chapter 1 – General Introduction

1.1 Problem statement

The geotechnical stability and the safety of the civil engineering structures and their foundations mainly rely on the strength, bearing capacity, and settlement of the soils beneath and/or adjacent to the foundation structures (Hoeg, 1991). Temperature changes induced soil freezing and thawing significantly affect the strength, bearing capacity and consolidation behavior of the soils beneath and/or adjacent foundation structures. However, extensive evidence exists of increase in soil freezing and thawing cycles in Canadian no-permafrost regions over the past decades because of the climatic change (Government of Canada, 2018). This climate induced change in freezing and thawing cycles has been negatively affecting the performance of many civil engineering structures (solar panel transmission towers, roads, railways, etc.) constructed in Canadian no-permafrost regions, increasing their maintenance costs, decreasing their useful life span, and jeopardizing the population safety and economic activities in those regions (Wieditz & Penney, 2006).

Indeed, these changing soils freezing and thawing frequencies, and the resulting thaw-settlement and strength or bearing capacity change of foundation soils promote differential settlement and instability of these foundation systems; in other words, they affect the safety of these engineering structures. Moreover, an increasing body of scientific works shows clear evidence that climate change will continue for many decades, and even centuries irrespective of the success of global initiatives to decrease greenhouse gas emissions thereby impacting foundation systems and abutments, and thus causing serious socio-economic consequences (Government of Canada, 2018). Therefore, on the basis of this global warming scenario, such changes in soil freeze-thaw cycles and their aforementioned consequences on foundations in Canadian no-permafrost regions are anticipated to intensify. Consequently, in order to ensure that the engineering structures can safely provide essential services and support economic activities in Canadian no-permafrost regions, the design of their foundation systems must be updated and/or adapted to the impacts of climate change. This objective can only be achieved, if the impact of climate induced change in freezing and thawing cycles on the thermal responses, porewater pressure and consolidation behavior/settlement of soils is well-known and can be predicted. However, no modeling studies have been conducted on the impact of climate change on the thermal behavior and geotechnical properties (porewater pressure, consolidation/settlement) of Canadian no permafrost soils.

1.2 Objectives of the research

The main objective of this study is to acquire knowledge and develop tools to assess the impact of global warming on the thermal behavior and key geotechnical properties/behavior of soils in Canadian no permafrost regions. The specific objectives of the research are described as follows;

- To acquire and review the engineering properties of the soils, the climate data, and the climate change projections in the selected Canadian no-permafrost sites.
- To develop a methodology and numerical tool to assess the impact of global warming on the thermal response of the ground in the selected Canadian no-permafrost areas.
- To simulate the effect of global warning on the thermal regimes of grounds in the Canadian permafrost region.
- To acquire knowledge and develop a methodology and numerical tool to assess the impact of the changing soil freezing/thawing cycles on the consolidation behavior and settlement of foundation soils in the selected sites.
- To simulate the effect of global warning on the thermo-hydro-mechanical response of grounds in the Canadian permafrost region.
- To understand and assess whether the thermal behavior and geotechnical response (porewater pressure, consolidation, etc.) of the ground around/adjacent to a bridge pile foundation in a Canadian no permafrost area can be affected by the global warming.

1.3 Research approaches and methods

In order to achieve the objectives of this thesis, three cities (Ottawa, Sudbury, Toronto) located in the Canadian no-permafrost region were selected as a study area. The selected sites represent the north, the center, and the south of the Ontario no-permafrost regions. Following, a comprehensive literature review was performed to determine the geometry and the geotechnical composition of the soil in the study areas. Moreover, the review included an examination of the historical climate data in the selected sites and a compilation of the climate change projections in the next 80 years up to 2100. Three climate change scenarios were considered is this study: RCP 8.5 (high global emission), RCP 4.5 (medium global emission) and RCP2.5 (low global emission) (Government of Canada, 2018).

Subsequently, a methodological approach and simulation tool to assess the impact of climate change on the thermal behavior of the soils in Canadian no permafrost areas was established. After the validation of the thermal simulation tool against field data, the impact of global warming on the ground thermal behavior in the study area was then examined using the simulation tool. Furthermore, a snow depth sensitivity analysis was conducted to assess the impact of the variation of the snow cover depth on the thermal regime of the soil in the study area for the three climate change scenarios.

Thereafter, the effect of climate change on the porewater pressure distribution and settlement behavior of the ground in the study area was simulated using a thermo-hydro-mechanical simulation tool. Three softwares were coupled to establish the simulation tool: TEMP/W, SEEP/W and SIGMA/W from Geoslope package (GEO-SLOPE International Ltd, 2014). The simulation tool was validated against field measurements before proceeding to the simulations.

Finally, a simulation of the response of a foundation ground for bridge pile in a Canadian no permafrost to global warming area was performed.

1.4 Organization of the manuscript

The thesis is organized in the form of technical papers and divided into five chapters. Figure 4.1.1 shows the organization of the thesis manuscript.

Chapter One contains the introduction, while **Chapter Two** provides the literature review. Eight sections are included in Chapter Two; Section One includes a general introduction to the chapter; Section Two introduces the geographical borders of the Canadian no-permafrost region; Section Three includes a comprehensive review of the engineering properties of Canadian no-permafrost soils; section Four provides an introduction to the seasonal ground freezing and thawing parameters of Canadian no-permafrost soils; Section Five discusses the thaw behavior of Canadian no-permafrost soils; Section Six provides an overview about the geotechnical design challenges in seasonally frozen no-permafrost soils.

Chapter Three is the first technical paper. In this paper, a numerical simulation study of ground thermal response in Canadian no-permafrost regions to climate warming is established.

Chapter Four is the second technical paper, which contains a numerical simulation of ground thermo-hydro-mechanical response in Canadian no-permafrost regions to climate warming.

Chapter Five contains a synthesis and discussion of results, and a practical engineering application.

It should be mentioned that because the main results of the thesis are presented as technical papers, some information will be repeated. This is because each paper is independently written (i.e. without taking into account the contents of the other papers or the rest of the document) and in accordance with the manuscript preparation requirements of the corresponding publication medium.

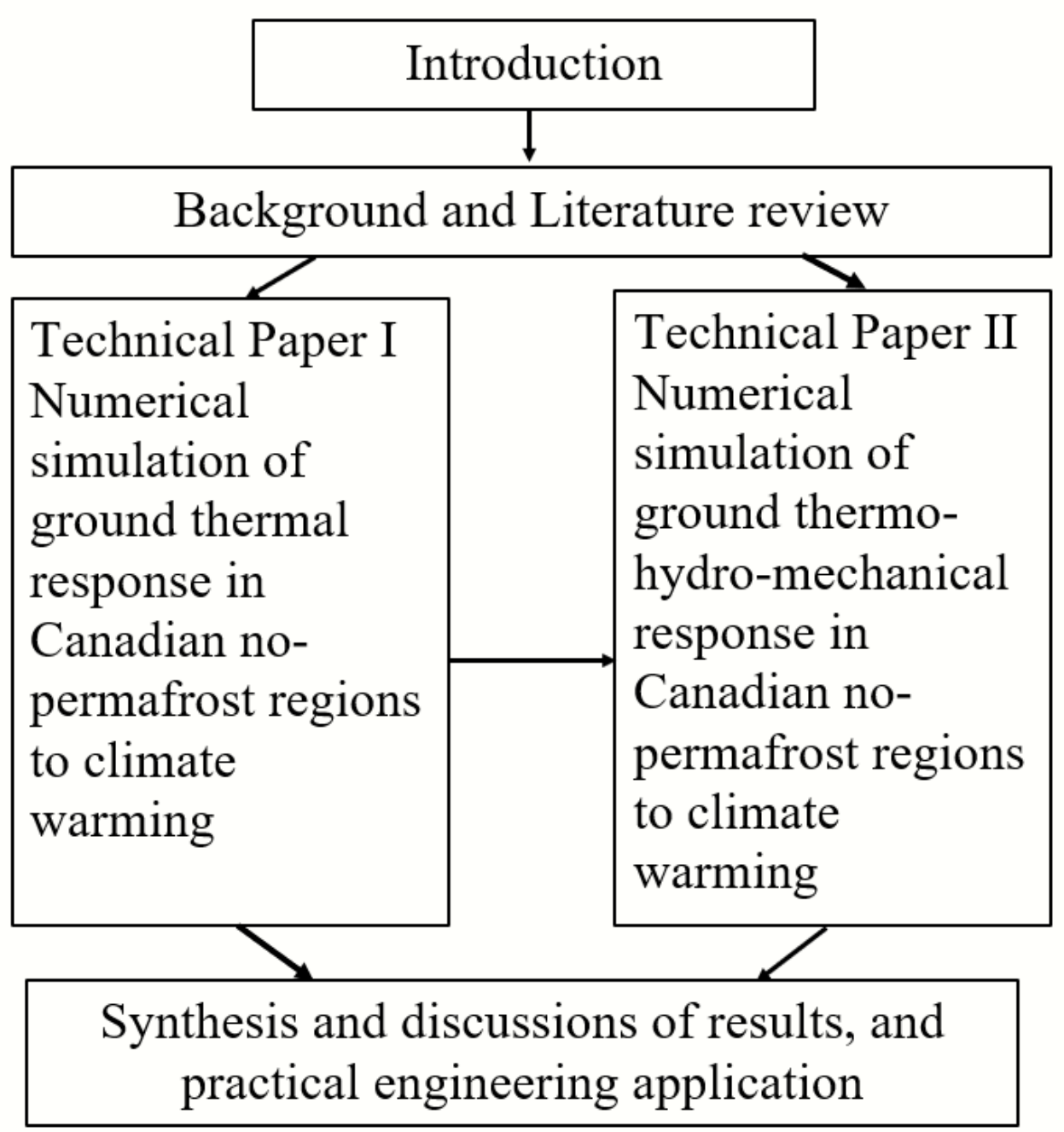

Figure 1.4.1: Thesis manuscript organization chart

1.5 References

GEO-SLOPE International Ltd. (2014). Thermal Modeling with TEMP / W. November.

Government of Canada. (2018). Senarios and climate models. https://www.canada.ca/en/environment-climate-change/services/climate-change/canadian-centre-climate-services/basics/scenario-models.html#toc2

Hoeg, K. (1991). Pile foundations. 2–3. https://doi.org/10.1201/9780429398452-8

Wieditz, I., & Penney, J. (2006). A scan of climate change impacts on toronto. Public Health Agency of Canada, 60.

Chapter 2 – Background and Literature review

2.1 Introduction

This chapter provides background information on the Canadian no-permafrost region, its distribution and location within the Canadian territory and a comprehensive review of the geotechnical, the physical and thermal properties of frozen soils. The chapter goes on to discuss the seasonal ground freezing and thawing parameters and the thaw behavior of the seasonally frozen ground before briefly reviewing the geotechnical design challenges in no-permafrost soils. Subsequently, background information on the climate change model and scenarios used in this thesis is provided.

2.2 Geographical borders of the Canadian no-permafrost region

The region of interest in this study is the no-permafrost region in Canada. This region extends from the Atlantic coast in the east to the pacific west coast running mainly through the whole south of Canada. This region comprises the major Canadian cities and hosts an important demographic distribution. It extends from the border with the United States in the south to the Hudson's Bay south shore in the north incorporating the whole New-Brunswick, Nova scotia, the southern part of Quebec, majority of Ontario, Manitoba, Saskatchewan, Alberta and British Columbia (Booshehrian et al., 2020). The geographical boundaries between zones of continuous permafrost, discontinuous permafrost, and no-permafrost regions are poorly defined but are approximately represented in (Figure 2.2.1).

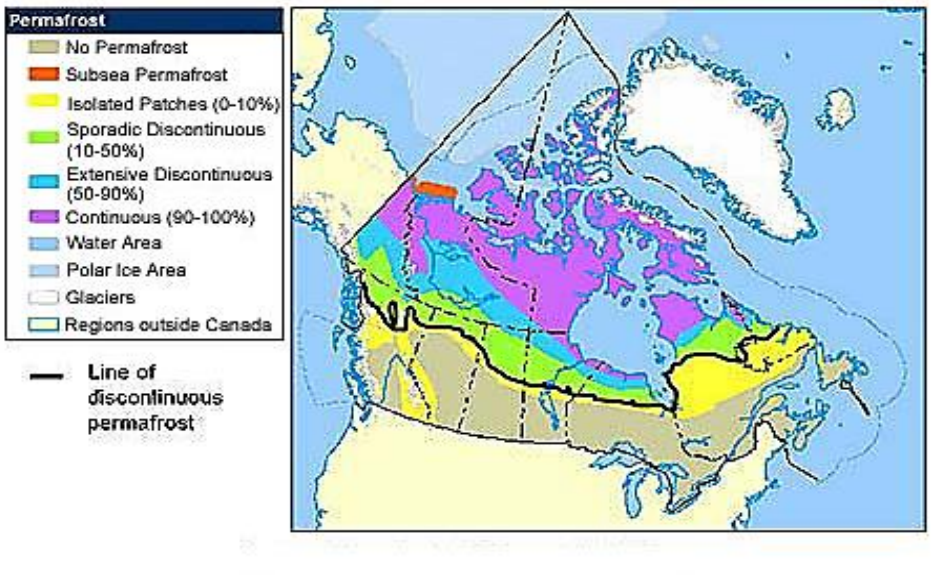

Figure 2.2.1: The geographical limits of the Canadian no-permafrost region (Booshehrian et al., 2020)

Figure 2.2.2: Location of Ottawa, Toronto and Sudbury within Ontario (Cambrian International, 2021)

2.3 Seasonal ground freezing and thawing parameters of soils

2.3.1 Freezing and thawing indices

In no-permafrost regions, ground surface temperature follows a seasonal classification including two main periods: the freezing and thawing seasons. To summarize the annual regime, each period is described using quantitative freezing (I_f) and thawing (I_t) indices (Orlando & Ladanyi, 2004).

Freezing period occurs in winter, staring from the autumn change over month (figure 2.3.1) and ends in the following spring in the spring change over month (figure 2.3.1). The thawing period begins at the spring change over month to the following autumn change over month (Orlando & Ladanyi, 2004).

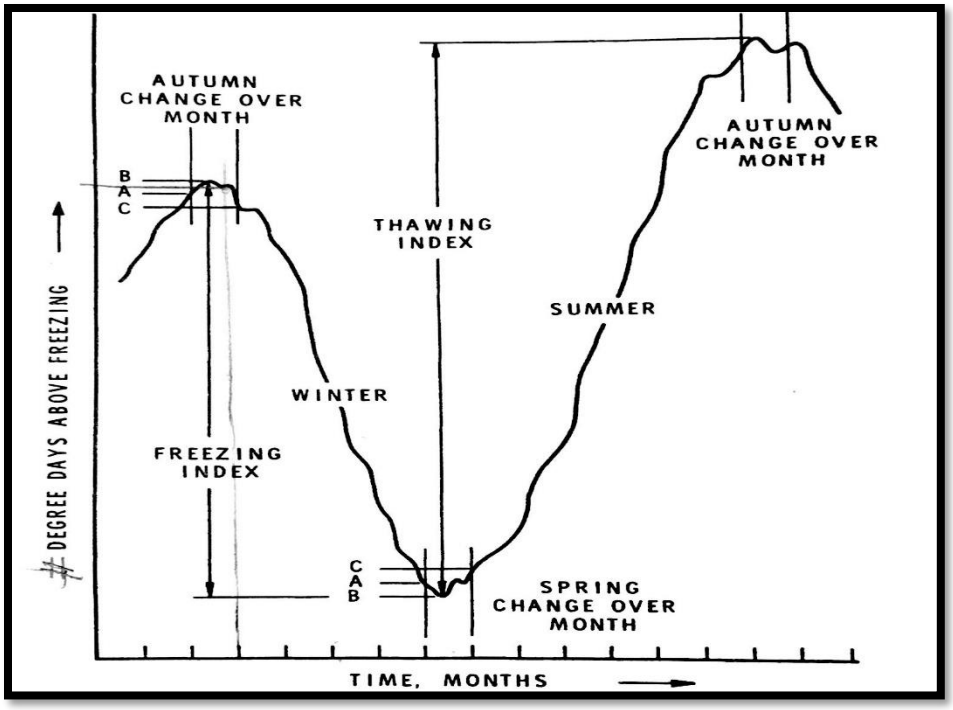

Figure 2.3.1: freezing-thawing time sequence (Orlando & Ladanyi, 2004)

Air freezing, and thawing indices are computed for air temperature in both seasons. They rely on the degree day concept, which describes the intensity of the air temperature variations daily. For example, a mean temperature of -4 ℃ for 3 days equals -12 ℃. days degree days (Orlando & Ladanyi, 2004).

Air freezing index could be computed as the sum of negative degree days in the freezing period. Similarly, the thawing index is calculated as the sum of the of positive degree days in the thawing period.

Klene et al. (2001) calculated the air thawing index using the following equation:

Equation 2.3.1: Air thawing index equation (Klene et al., 2001):

$$I_{at} = \int_0^{\theta_t} T_{at}\, dt \approx \sum_{k=0}^{\theta_t} (T_{at,avg} - T_{freezing,air})\ (\text{degree. days})$$

Where:

- I_{at}: Air thawing index,
- T_{at} : Air temperature > 0 ℃,
- $T_{freezing,air} = 0$ ℃
- θ_t : Duration of the thawing season,

- $T_{at,avg}$: Daily mean air temperature in the thawing period,

The freezing index I_{af} can be calculated using similar equation, with replacing the thawing parameters by the freezing period climate data where T_{af} is air temperature < 0 °C, θ_f : Duration of the freezing season and $T_{af,avg}$: Daily mean air temperature in the freezing period.

Ground surface indices are computed based on the air ones using an empirical factor "n_f" defined as the ratio of the ground surface freezing index I_{sf} to the air freezing index I_{af}. Similarly, the ground thawing index is found using thawing empirical factor "n_t" defined as the ratio of the ground surface thawing index I_{st} to the air thawing index I_{at} (Lunardini, 1978).

The conversion factors "n_f" and "n_t" depend on many factors including radiation, vegetation, snow cover, wind speed and ground thermal properties (Klene et al. 2001, Jorgenson and Kreig 1988, Taylor 1995, 2000). "n" factors for several surface types are presented in table 2.3.1.

Table 2.3.1: Typical values of "n" factors for different type of surface - (Orlando & Ladanyi, 2004)

Surface	**Freezing** n_f	**Thawing** n_t
Snow	1	----
Pavement free of snow and ice	0.9	----
Sand and gravel	0.9	2
Turf	0.5	1
Spruce trees, brush, moss over peat soil	0.29 (under snow)	0.37
Trees and brush cleared moss over peat soil	0.25 (under snow)	0.73
Vegetation and 6-cm soil stripped, mineral soil surface	0.33	1.22
Gravel	0.6-1.0	1.3-2
(Probable range, northern conditions)	(0.9-0.95)	
Asphalt pavement	0.29-1.0 or greater	1.4-2.3
(Probable range, northern conditions)	(0.9-0.95)	
Concrete pavement	0.25-0.95	1.3-2.1
(Probable range, northern conditions)	(0.7-0.9)	

2.3.2 Frost penetration depth

In no-permafrost regions, the top layer of the ground experiences a seasonal freezing during winter period. The depth to which ground freezes is called the frost penetration depth. It is governed by several factors including, the thermal properties of the soil, severity of winter, vegetation cover, ground water conditions and surface relief (Armstrong, 1963).

Frost penetration depth can be determined using empirical computation techniques and numerical modeling software. Hand calculations are used for simple applications, with simple geometry and well-defined boundary conditions. On the other hand, numerical methods may be used to model complex geometries, boundary conditions and time-dependent thermal properties (Orlando & Ladanyi, 2004).

Stefan equation and the modified Berggren equation are both used to estimate the frost penetration depth. Stefan (1889) equation assumes that in the freezing period, the latent heat of soil moisture is the only heat that is dissipated, neglecting the release of the thermal energy of the soil itself. Stefan emphasizes that the latent heat released by the ground moisture is the only heat loss responsible of soil freezing (Romanovsky and Osterkamp 1997). Therefore, the frost depth as per Stefan equation, is calculated as follows (Orlando & Ladanyi, 2004):

Equation 2.3.2: Frost depth - Stefan equation (Romanovsky and Osterkamp 1997):

$$X = \left(\frac{2k_f}{L}\int T_s \, dt\right)^{1/2}$$

Where:

- X (m) : frost depth penetration,
- L ($\frac{J}{m^3}$): Volumetric latent heat of the soil,
- k_f $\left(\frac{W}{°C* m}\right)$: frozen thermal conductivity of the soil,
- T_s (°C): The difference between the ground surface temperature and the freezing temperature of the soil moisture,

The freezing index I_{sf} (degree.days) is defined as follows:

Equation 2.3.3: Freezing index I_{sf} equation (Klene et al. 2001);

$$I_{sf}\,(°C.\text{days}) = \int T_s \, dt$$

Therefore, Stefan equation can be expressed as follows:

Equation 2.3.4: : Frost depth - Stefan equation (Orlando & Ladanyi, 2004):

$$X = \left(\frac{2k_f I_{sf}}{\rho * L}\right)^{1/2}$$

Aldrich and Paynter (1953) reported the Stephan equation in the imperial units as follows:

Equation 2.3.5: Frost depth - Stefan equation (Aldrich & Paynter, 1953):

$$X = \left(\frac{48kI_{sf}}{L}\right)^{1/2}$$

Where:

- X (ft) : frost depth penetration,
- L ($\frac{Btu}{ft^3}$): latent heat of the soil,
- k_f $\left(\frac{Btu}{hr*ft*°F}\right)$: frozen thermal conductivity of the soil,
- I_{sf} (°F. days): the difference between the ground surface temperature and the freezing temperature of the soil moisture,
- The "48" stands for $2 * (24\ h/day)$,

The modified Berggren equation for the frost penetration depth is expressed as follows:

Equation 2.3.6: Frost depth - Modified Berggren equation (Orlando & Ladanyi, 2004):

$$X = \lambda * \left(\frac{2 * k * T_s * \theta_f}{L}\right)^{\frac{1}{2}}$$

Where λ is a dimensionless correction factor, and all variables are as defined in the Stefan equation.

The modified Berggren equation relies on fundamental assumptions including that the soil is homogenous, at a steady state, with uniform thermal properties. It was also assumed that the surface temperature changes from its initial values T_o> freezing temperature (°C) to T_s < freezing temperature (°C) at the beginning of the freezing period, where $T_s = \frac{I_{sf}}{\theta_f}$ and θ_f is the duration of the freezing period (Orlando & Ladanyi, 2004).

The dimensionless correction factor λ is a function of the thermal ratio (α) and the fusion parameter (μ). Both parameters are computed as follow:

Equation 2.3.7 : Thermal ratio (α) equation (Orlando & Ladanyi, 2004):

$$\alpha = \frac{T_o}{T_s} = \frac{T_o \theta_f}{I_{sf}}$$

Equation 2.3.8: Fusion parameter (μ) equation (Orlando & Ladanyi, 2004):

$$\mu = \frac{c_v}{L} T_s = \frac{c_v I_{sf}}{L \theta_f}$$

Where:

- c_v : Volumetric heat capacity of the soil,
- I_{sf}: Soil freezing index,
- θ_f : Duration of the thawing season,
- The other terms are as defined above,

The correction coefficient factor λ is given as a function of α and μ in the figure below:

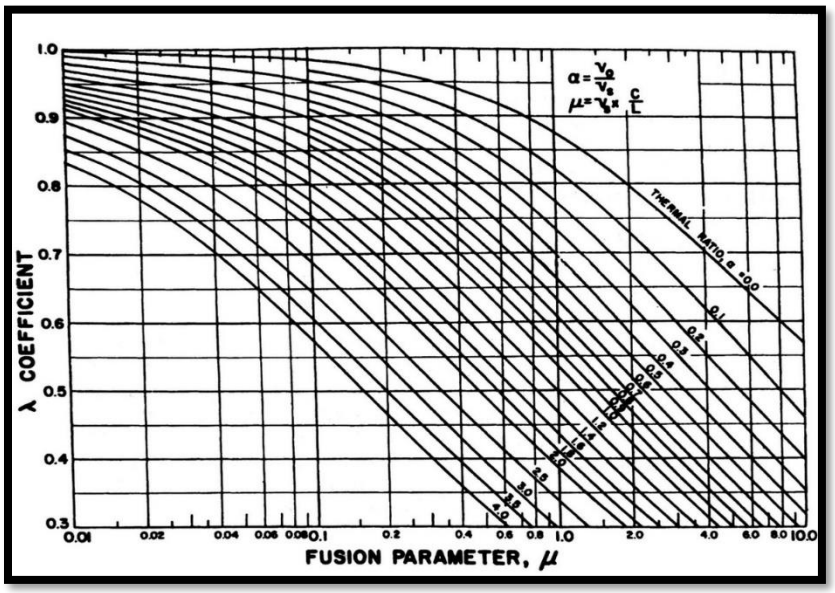

Figure 2.3.2: the correction factor λ – graphical correlation (Orlando & Ladanyi, 2004)

2.4 Geotechnical design challenges in seasonally frozen no-permafrost soils

The Ground in no-permafrost regions experiences a cyclic freezing-thawing process, which affects the structural properties of the ground and rises significant design challenges. Essentially, frost actions represent a significant matter in the design of pile foundations in the cold regions. Frost actions develop due to the formation of ice in the soil pores during the freezing period followed by thaw weakening in the thawing season (Orlando & Ladanyi, 2004). In the thawing season, the settling soil layers experience downward movement inducing down drag forces on the piles and developing negative skin friction. The negative skin friction applies additional loads on the pile and reduces the pile load capacity (Briaud & Tucker, 1997). Only 1mm of settlement is needed to cause the negative skin friction.

In the winter season, frost action induces tangential stresses along the pile length which pull out the pile out of the ground (Péwé & Paige, 1963). Typical lifting force (kN) values acting on piles made of different materials are listed in table 2.4.1:

Table 2.4.1: Typical values of uplift forces - (Orlando & Ladanyi, 2004)

Material	Lifting force with side grip (kN) for freezing index, F100 (h. °C)		
	10,000	30,000	50,000
Steel	50	100	140
Wood	30	50	60
Concrete	30	80	100
Concrete wall (per meter length)	25	40	50

The up-lifting forces acting on a pile can be estimated through field investigations; however, Vyalov and Porkhaev (1976) provided design values which could be used in the absence of field data. For soils having a temperature below -3 °C, uplift forces should be taken as 60 kPa; similarly, for soils having a temperature of -3 °C or higher, Vyalov and Porkhaev (1976) estimated an uplift force equal to 80 kPa (Vyalov and Porkhaev, 1976). These forces depend on many factors including the soil type, the pile surface material, soil water content and ground temperature (Péwé & Paige, 1963). In another investigation, Crory and Reed (1965) measured a maximum pile heave force of 250 kPa in frozen silty ground. They concluded that the maximum rate of heave occurs in the beginning of the winter at relatively shallow depths (1m) (Orlando & Ladanyi, 2004). Tong et al. (1988) proposed design values for the uplift forces based on field investigations and observations. They take into consideration soil type, water content, soil degree of saturation, and the distance above the water table to estimate the uplift stresses acting on the piles (Tong et al., 1988).

Ladanyi and Foriero (1995) proposed an analytical solution to compute the uplift forces acting on piles in

frozen ground. This method relies on fundamental assumptions inclining:

1- Sinusoidal seasonal temperature variation at the ground surface,
2- Frost penetration depth is computed using the modified Berggren equation,
3- Proportional relationship between surface heave and the thickness of the frozen soil,
4- Displacement and displacement rate of the heaving soil linearly decreases with depth,
5- Linear temperature variation along the pile in the frozen zone,

If these assumptions are met, the surface frost heave can be calculated based on the assumption 3 as follows:
Equation 2.4.1: Surface frost heave equation (Ladanyi & Foriero, 1995):

$$s_s = K\, x_o(t)$$

Where:

- K : coefficient of proportionality,
- $x_o(t)$: the frost penetration depth as computed by the modified Berggren equation in section 4.3.2,

The surface heave rate is then calculated by deriving the equation of the surface frost heave as follows:
Equation 2.4.2: Surface frost heave rate equation (Ladanyi & Foriero, 1995):

$$s'_s = K\, x_o^{\prime(t)}$$

The heave rate at any location along the pile is noted "s'_i" and can be computed based on the assumption 4 as follows:
Equation 2.4.3: Frost heave rate equation at any location along the pile (Ladanyi & Foriero, 1995):

$$s'_i = s'_s(t)\left(1 - \frac{x_i}{x_o(t)}\right)$$

Where:

- x_i: the depth at the specific location and all variables are as defined above.

The uplift stresses mobilized at the interface between the pile and the soil can be computed using Johnston and Ladanyi (1972):

Equation 2.4.4: Uplift stresses equation (Johnston & Ladanyi, 1972):

$$\tau_{a,i} = \tau_{c,\theta_i} \left[\frac{n-1}{\gamma_c}\right]^{\frac{1}{n}} \left[\frac{s_i'(t)}{a}\right]^{\frac{1}{n}}$$

Where:

- τ_{c,θ_i}: Temperature dependent shear creep modulus,
- $n \geq 1$: Experimental creep exponent,
- γ_c : Arbitrary reference shear strain,
- a : Pile radius,

The shear creep modulus can be calculated using the general creep modulus, σ_{co} and temperature as follow:

Equation 2.4.5: Shear creep modulus equation (Johnston & Ladanyi, 1972):

$$\tau_{c,\theta_i} = \sigma_{co} \left(1 + \frac{\theta_i}{\theta_o}\right)^w$$

Where:

- θ : the absolute value of the negative temperature of the soil at the specific location (depth),
- $\theta_o = 1\ C^o$
- w : experimental temperature exponent,

The general creep modulus σ_{co} as well as the experimental temperature exponent w can be both graphicly determined by conducting uniaxial tests on soil samples in different temperatures.

The temperature at any depth along the pile can be computed using the surface temperature T_s and based on assumption 5 as follows:

Equation 2.4.6: Temperature equation at any depth along the pile (Ladanyi & Foriero, 1995):

$$\theta_i = T_s \left(1 - \frac{x_i}{x_o(t)}\right)$$

Where all the variables are as defined above.

The uplift forces applied on the pile can be computed considering the radius of the pile “a” and the depth of the frozen layer of the pile "L_f" as follows:

Equation 2.4.7: Uplift forces equation (Ladanyi & Foriero, 1995):

$$F_{uplift} = 2\pi a * \tau_{a,i} * L_f$$

2.5 Background on numerical modeling tools and the softwares used

Burland (1987) summarized the numerical modeling in geotechnical engineering in three fundamental components: the ground profile, the soil behavior, and the modeling (Burland, 1987). He represented these components in the Burland triangle as illustrated in figure 2.5.1:

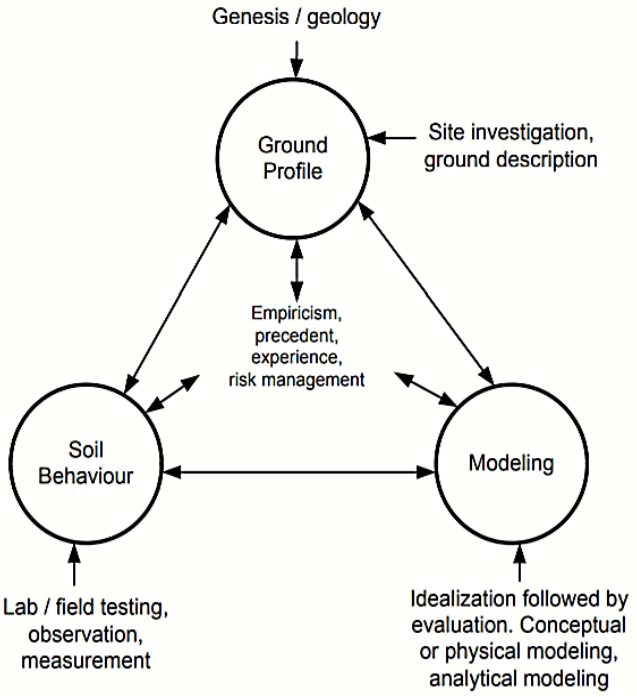

Figure 2.5.1: The Burland triangle (Burland, 1987)

Numerical modeling tools provide an extremely powerful calculator to do highly complex computations and simulate complex geometries and boundary conditions that are not otherwise humanly possible to model. Numerical tools rely on the ability of the user to deploy the appropriate geotechnical models, his understanding of soil mechanics constitutive models and his ability to interpret the results. Several types of numerical tools are used to solve geotechnical problems, this includes spreadsheet software programs, finite

element methods and programing-based tools. Finite element methods tools are widely used in the industry in the last two decades; this form of numerical modelling provides an efficient platform to understand the fundamental behavior of geomaterials and geostructures and simulate the real physical interactions and process occurring in the soil. There are various commercial FEM software tools used in the geotechnical industry including Abaqus, Palxis 2D/ 3D and Geostudio package. The latter comprises multiple programs simulating a variety of geotechnical applications. TEMP/W is the software used to simulate the thermal behavior of the ground in the present study. TEMP/W can model almost any geothermal problem, including the degradation of permafrost beneath civil structures and/or around a heated buried pipeline, freeze-thaw action beneath roadways and airport runways and many more complex geothermal problems. The first version of TEMP/W was initially released as part of geoslope package in 2007 and since then new versions of TEMP/W were released. The latest version of TEMP/W will be released in the 2021 version of geostudio. SEEP/W is another software from geostudio analyzing the groundwater seepage within the soil. SEEP/W is coupled with TEMP/W in the present analysis to establish the convective heat and water transfer in the ground. If used properly, SEEP/W can model almost any groundwater problem including the hydraulic response of a dam to water level fluctuations, water flow nets within soil dams and groundwater flow in freezing and thawing soils. Improvements of SEEP/W software are continuously released to empower its efficiency and capacity to model more complex seepage problems. The last software used in this study is SIGMA/W, the latter performs the stress and deformation analyses of the ground under external and/or soil self-weight loads. SIGMA/W comprises several constitutive deformation models including linear elastic, elastic-plastic, and highly sophisticated models such as hyperbolic and cam clay models. SIGMA/W is used in applications such as fully coupled consolidation analysis, and deformation beneath and around buried structures. The selection of the mechanical model depends on several factors including the material stiffness, tolerable displacement, and stability (GEO-SLOPE International Ltd, 2013). The employment of a realistic constitutive model is paramount to reproduce the important aspects of the soil stress-strain behavior under different loading conditions (Lade, 2005). The linear elastic uses the Hooke's law to model the behavior of the soil. It provides reasonable soil's representation for stress states not approaching failure. Therefore, all processes that occurs near and beyond failure including irreversibility of the strains, stress path dependency, volume changes due to shear stresses cannot be modelled by the elasticity theory (Lade, 2005). To overcome the shortcoming of the linear elastic theory, the hardening plasticity-based models were developed (Ti et al., 2009). Mohr-Coulomb model is a first order elastic-perfectly plastic model used to capture the soil behavior in general stress state conditions. The model's stress-strain relationship comprises a linear portion describing the elastic range followed by a perfectly plastic portion capturing the yield behavior and the irreversible change in volume due to shearing. Many research have shown by means of true triaxial tests that the stress state causing failure in real soil samples follow quite well the failure

criteria modeled by the Mohr-Coulomb model. Nevertheless, this model does not include strain hardening or softening effect of the soil (Ti et al., 2009). The Modified Cam Clay model (MCC) is an elastic plastic strain hardening model used to capture the irreversible straining and the residual strains that develop with the increase of the stress (Ti et al., 2009). The hardening theory of plasticity used to develop the MCC model provides accurate results in describing the behavior of normally consolidated or lightly over-consolidated clay. The modified Cam-Clay model is more appropriate to describe the deformation behavior than failure in applications including embankment or foundation involving normally consolidated clay soils (Ti et al., 2009).

2.6 Background on the climate model and climate change scenarios used

Climate is one of the main governing factors of ground behavior, the soil-climate complex interactions affect the geotechnical properties of the ground including its strength, texture, and compressibility. Other parameters such as soil structure, stability, topsoil water holding capacity, and soil erosion are also affected by climate patterns. Nevertheless, the actual climate conditions are significantly changing.

Global warming has caused a set of changes to the Earth's climate and ecosystems. It is induced by the release of greenhouse gases from humans' activities, such as industrial enterprises, transportation means, and cutting and burning forests. These greenhouse emissions capture the heat and sun light inside the earth air envelope but do not allow them to escape again. Therefore, the sun's heat stays in the Earth's atmosphere for a very long time and produce long terms impacts. Climate change is responsible not only for rising average air temperatures but also extreme weather events such as shifting wildlife populations and habitats, rising seas, and a range of other impacts (Nunez, 2019).

The government of Canada provides an estimation of future climate conditions using different emissions scenarios. These representative concentration pathways (RCPs) (climate scenarios) include consideration of future greenhouse gas emissions, deforestation, population growth and many other factors in estimating future climate changes (Government of Canada, 2018). RCPs were the basis of the latest, Fifth Assessment Report (AR5) published in 2013 by the IPCC and were developed in parallel with the development of climate models (Charron, 2014).

Climate models relay on complex software and numerical tools to represent the evolution of the climate in the future. These models are based on empirical equations derived from the physical, chemical, hydrological, cryogenic, lithographic, oceanographic and biological data collected through observations and experiments (Government of Canada, 2018).

Two main categories of models are regularly used: global climate models (GCMs) (called also "Earth System Models") which simulate climate change in the entire globe, and Regional Climate Models (RCMs)

covering only part of the globe. GCMs have a special resolution of the order of 200 to 300 km, while the RCMs have a resolution grid of 50 km or less (Charron, 2014).

GCMs include three sub-types; the first category comprises atmospheric general circulation models (AGCM). These schemes are developed first, to model only the physical interactions between climate system and the continental land surface. The second group of models, referred to as atmosphere-ocean general circulation models (AOGCM), combined the interactions between atmosphere and land with physical ocean models. The last category is Earth system models (ESM), which include the biogeochemical interactions and cycles, as well as changes in vegetation cover (Charron, 2014).

Indeed, each model type has its strengths and weaknesses, and can give different results. The combination of models gives reliable results. The difference in results is related to the type of the numerical scheme, the degree of simplification, application of boundary conditions (parameterization) and the degree of the spatial resolution.

In fact, the prediction of the climate change remains very challenging in the absence of precise estimation of how humans will behave in the future and how emissions of greenhouse gases will change. Therefore, Climate Canada, had established 3 different future climate scenarios (RCPs);

- **RCP8.5:** high global emission scenario. This scenario indicates global average warming levels of 3.2 to 5.4°C by 2090, with a mean temperature increase of 4.9 degree by 2100.
- **RCP4.5:** medium global emission scenario, includes measures to limit (mitigate) climate change. This scenario indicates global average warming levels of 1.7 to 3.2°C by 2090, with a mean temperature increase of 1.9 degree by 2100.
- **RCP2.6:** low emission global scenario, requires strong mitigation actions. This scenario indicates global average warming levels of 0.9 to 2.3°C by 2090, with a mean temperature increase of 4 degree by 2100 (Government of Canada, 2018).

The figure below represents the historical changes in the global average temperature between the year 1900 to 2005 and future projections for the period from 2006 to 2100 of the climate changes following the three proposed RCPs.

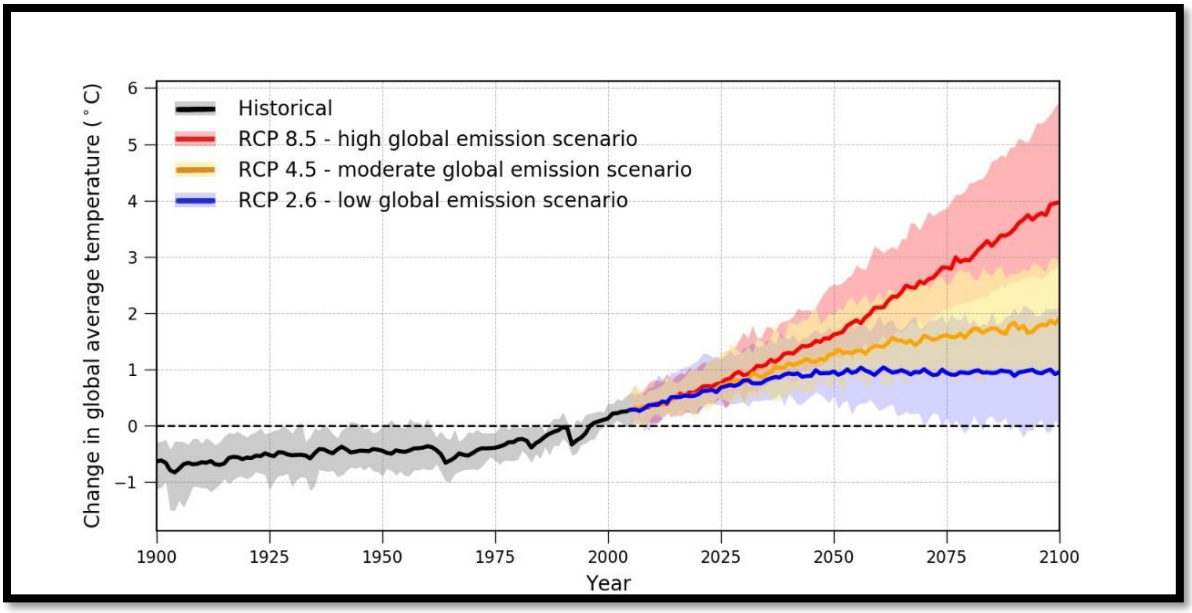

Figure 2.6.1: Historical and predicted Change in global average temperature 1900-2100 (Government of Canada, 2018)

RCPs are named based on the projection of the total radiative forcing (in W/m^2) around 2100. They also provide approximation of the concentration of CO_2 (ppm) in the atmosphere by 2100 and the increase in the average temperature.

The following table represents the different RCPs with an estimation of the radiative forcing, CO2 concentration, and the average temperature increase by 2100.

Table 2.6.1: Representative Concentration Pathways description (Charron, 2016)

Name	Radiative forcing	CO_2 equivalent (ppm)	Temp anomaly °C	Pathway
RCP8.5	8.5 W/m2 in 2100	>1370	4.9	Rising
RCP4.5	4.5 W/m2 post 2100	≈ 650	2.4	Stabilizing without overshoot
RCP2.6 (RCP3PD)	3W/m2 mid-century, decline to 2.6Wm2 by 2100	≈ 490	1.5	Peak and decline

2.7 Summary and conclusion

The Canadian no-permafrost region represents a major section of the Canadian territory. It includes a significant number of infrastructure and high importance civil engineering structures that have an important role in Canada's economy and industrial development. Contrary to the permafrost, the ground in the Canadian no-permafrost region is seasonally frozen during the winter season. Therefore, design matters associated with the impact of freeze-thaw cycles on the civil engineering infrastructure in this area are rising in a changing global climate.

All in all, this chapter has provided a general overview of the geographical borders of the Canadian no-permafrost region, a review of the engineering properties of the soils in this region and a discussion of the geotechnical, physical, and thermal properties of frozen soils. The chapter also covered the important parameters used in geotechnical applications in seasonally frozen ground. This includes the freezing and thawing indices, the frost penetration depth, and the thaw depth. Furthermore, a general overview of thaw settlement and thaw consolidation theories has been included in this chapter. Different estimation methods of the thaw settlement and thaw consolidation have been discussed. Additionally, the chapter covered the geotechnical design challenges of pile foundation systems in seasonally frozen soils related to freezing and thawing cycles. Many tools have been implemented to analyze the effect of the freeze thaw cycle on the geotechnical behavior of the ground; however, the advancement of numerical modeling methods made it possible to understand the complex thermo-hydro-mechanical of the soil subjected to freeze-thaw cycles. Accordingly, a comprehensive review of the history of numerical modeling in geotechnical engineering as well as the different types of numerical modeling methods used in the industry are being introduced. Moreover, a brief introduction to the main modeling software used in this present study has been included. Finally, background information on the climate model and climate change scenarios adopted in this study was provided.

2.8 References

Aldrich, H.P., and H.M. Paynter. (1953). Analytical Studies of Freezing and Thawing of Soils. Technical Report No. 42. U.S. Army Corps of Engineers, Arctic Construction and Frost Effects Laboratory, Boston, Mass.

Armstrong, M. D., & Csathy, T. I. (1963). Frost Design Practice in Canada. Ontario Department of Highways, 170–201. http://onlinepubs.trb.org/Onlinepubs/hrr/1963/33/33-008.pdf

Booshehrian, A., Wan, R., & Su, X. (2020). Hydraulic variations in permafrost due to open-pit mining and climate change: a case study in the Canadian Arctic. In Acta Geotechnica (Vol. 15, Issue 4). https://doi.org/10.1007/s11440-019-00786-x

Briaud, J. L., & Tucker, L. M. (1997). Design and construction guidelines for downdrag on uncoated and bitumen-coated piles. Nchrp, January 1996, 212. http://trid.trb.org/view.aspx?id=577429

Burland, J.B. (1987). Nash Lecture: The Teaching of Soil Mechanics – a Personal View. Proceedings, 9th ECSMFE, Dublin, Vol. 3, pp 1427-1447.Cambrian International. (2021). https://cambrianinternational.ca/

Charron, I. (2014). a Guidebook on Climate Scenarios : Using Climate Information to Guide Adaptation Research and Decisions. Ouranos.

Government of Canada. (2018). Senarios and climate models. https://www.canada.ca/en/environment-climate-change/services/climate-change/canadian-centre-climate-services/basics/scenario-models.html#toc2

Jorgenson, M.T. and Kreig, R.A. (1988). A model for mapping permafrost distribution based on landscape
component maps and climatic variables. Fifth International Conference on Permafrost, Trondheim, Norway: 176–182.

Klene A.E., Nelson, F.E., Shiklomanov, N.I., and Hinkel, K.M. (2001). The N-factor in natural landscapes: Variability of air and soil-surface temperatures, Kuraruk River Basin, Alaska, USA. Arctic, Antarctic and Alpine Research 33(2): 140–148.

Ladanyi, B., Foriero, A., Dallimore, S.R., Egginton, P.A., and Nixon, F.M. (1995). Modelling of deep seated creep in massive ice, Tuktoyaktuk Coastlands, N.W.T. Proceedings, 48th Canadian Geotechnical Conference, Vancouver, B.C., Vol. 2, pp. 1023–1030.

Lunardini, V.J. (1978). Theory of n-factors. Third Inter. Conf. on Permafrost, Edmonton, Canada: 40–46.

Nunez, C. (2019). Causes and effects of climate change. Crime, Violence, and Global Warming. https://www.nationalgeographic.com/environment/article/global-warming-overview

Orlando, B. A., & Ladanyi, B. (2004). Frozen Ground Engineering (4th ed.). John Wiley & sons.

Péwé, T. L., & Paige, R. A. (1963). Frost Heaving of Piles With an Example From Fair banks , Alaska. US Geological Survey Bulletin, 1111–1, 333–407.

Romanovsky, V.E. and Osterkamp, T.E. (1997). Thawing of the active layer on the coastal plain of th Alaskan Arctic. Permafrost and Periglacial Processes 8: 1–22

Taylor, A.E., (1995). Field measurements of n-factors for natural forest areas, Mackenzie Valley, Northwest Territories, Geological Survey of Canada Current Research. Geological Survey of Canada, 1995-B: 89–98.

Taylor, A.E., (2000). Relationship of ground temperatures to air temperatures in forests. The physical environment of the Mackenzie Valley, Northwest Territories: a base line for the assessment of environmental change; LD Dyke and CR Brooks eds. Geological Survey of Canada Bulletin 547: 111–117.

Vyalov, S.S., and Porkhaev, G.V. (1976). Handbook for the design of bases and foundations of buildings and other structures on permafrost. Translated by V. Poppe. National Research Council of Canada, Ottawa, Ont., Technical Translation No. 1865.

Ti, K. S., Huat, B. B., Noorzaei, S., Jaafar, S., & Sew, G. S. (2009). A review of Basic Soil Constitutive Models for Geotechnical Application. Electronic Journal of Geotechnical Engineering, 97(2), 375–391. http://www.academia.edu/download/40591375/A_Review_of_Basic_Soil_Constitutive_models

Tong, Ch., Yu, Ch. And Sun, W (1988). Investigation on tangential frost heaving forces, In Proceedings 5th International Permafrost conference, Trondheim, V.2, pp.1181-1185

Chapter 3 - Technical paper I – Numerical simulation of ground thermal response in Canadian no-permafrost regions to climate warming

Mohammed Yassir Marrah[a], Mamadou Fall[a], Husham Almansour[b]

a-Department of Civil Engineering, University of Ottawa, Ottawa, ON, Canada

b-National Research Council Canada, Ottawa, ON, Canada

Journal of Cold Regions Science and Technology (revised paper has been submitted)

Abstract:

Roads, railways, and other transportation infrastructure are of vital economic, social, and political importance in all Canadian regions, particularly in Canadian no-permafrost areas. The geotechnical design and stability of these structures and many other civil engineering structures require knowledge and understanding of the thermal regime/behavior (freezing/thawing cycles, frost depth, unfrozen states, frost heave) of the ground. The stability of the foundations of the structures mentioned above mainly relies on the strength, bearing capacity, heave and/or settlement of the soils beneath and/or adjacent to the foundation structures. Temperature change-induced soil freezing and thawing significantly affects the strength, heave, bearing capacity and settlement of soils. However, extensive evidence exists of the increase in soil freezing and thawing cycles in Canadian no-permafrost regions over the past decades because of the climatic warming. Furthermore, an increasing body of scientific works show clear evidence that climate change will continue for many decades, and even centuries, irrespective of the success of global initiatives to decrease greenhouse gas emissions. Consequently, in order to ensure that public infrastructure can safely provide essential services and support economic activities in no-permafrost regions, the design of their foundation systems must be updated and/or adapted to the impacts of climate change. This objective can only be achieved if the impact of global warming on the soil thermal behavior in Canadian no permafrost regions is well-known and can be predicted. In the present paper, the results of a modeling study to assess and predict the effect of global warming on the thermal regimes of grounds in Canadian no-permafrost regions are presented and discussed. The results show that future climate changes will significantly affect the soil thermal regimes in Canadian no-permafrost regions. The numerical tool developed, and results obtained will be useful for the geotechnical design of climate-adaptive transportation structures in Canadian no-permafrost areas.

3.1 Introduction

No-permafrost soils constitute a complex topic in frozen ground engineering. Unlike in the permafrost region, where soil remains frozen at a temperature below 0 °C continuously for more than two consecutive years, soils in the no-permafrost region are seasonally frozen only during the winter season (Orlando & Ladanyi, 2004). The complex thermo-mechanic behavior of no-permafrost grounds raises several issues related to the design of foundations and civil engineering facilities on these soils. The freezing-thawing cycle is a thermal sequence that affects the geotechnical properties and induces heave or settlement movements of the ground (Orlando & Ladanyi, 2004). Consequently, the impact of temperature on no-permafrost soils becomes significant. However, with a rapidly changing climate, the inadequacy of earlier no-permafrost ground theories and estimated seasonal frost depths has become evidently apparent.

The prediction of climate change remains very challenging in the absence of a precise estimation of how humans will behave in the future and how emissions of greenhouse gases will change (Charron, 2014). Many studies were conducted on this topic (Government of Canada, 2018), and all have raised serious warnings of a rapid global warming. Canada has not been immune from this fast climate warming, and, in fact, the most recent climate change report issued by the Government of Canada points out that Canada's climate is warming at twice the rate of the global average, with the highest level of warming happening in winter (Government of Canada, 2018; Bush and Lemmen, 2019). The annual average temperature in Canada raised by 1.7°C between 1948 and 2016 (Zhang et al. 2019), approximately twice the rise observed for the Earth as a whole (0.8°C for 1948–2016 according to Osborn and Jones, 2014). Moreover, country-wide annual average temperature projections for the late century (2081–2100) range from an increase of 1.8°C for a low emission scenario (RCP2.6; RCP = Representative Concentration Pathway) to 6.3°C for a high emission scenario (RCP8.5), compared to the reference period 1986–2005 (Government of Canada, 2018; Zhang et al. 2019; Panikom, 2020). These representative concentration pathways (RCPs) (climate scenarios) include consideration of future greenhouse gas emissions, deforestation, population growth and many other factors in estimating future climate changes (Government of Canada, 2018). RCP2.6 denotes a low emission pathway with a change in radiative forcing of approximately 2.6 W/m^2, whereas RCP8.5 represents a pathway with continuous growth in GHG emissions, leading to a radiative forcing of roughly 8.5 W/m^2 at the end of the century (Bush and Lemmen, 2019).

However, there is a paucity of technical information/data about the impact of climate change on the thermal behavior of seasonal frost soils. Previous studies were mainly conducted on permafrost soils. For example, Rasmussen et al. (2018) established a numerical model to understand the present and future permafrost thermal regimes in Northeast Greenland (Rasmussen et al., 2018). The study concluded that permafrost temperatures down to 18 m will likely increase by +1.5° to +3.5 °C due to global warming. Correspondingly, Zhou et al. (2009) provided a spatio-temporal simulation of permafrost geothermal

response to climate change scenarios in a building environment (Zhou et al., 2009). They concluded that around the middle of this century, the thickness of the active layer will likely increase at different rates underneath and around buildings, due to climate warming.

While no-permafrost soil spreads over a large portion of the Canadian territory (Slattery et al., 2011), the understanding of its complex thermal regime is still not addressed in the literature. Therefore, it is a relatively new topic that requires a serious focus, due to the significant amount of infrastructure and facilities existing on these soils. The change of the ground temperature and the freezing-thawing frequencies in the Canadian no-permafrost region, induce exhaustive differential settlement movements and bearing capacity variations of the soil (Orlando & Ladanyi, 2004). Therefore, many engineering structures, such as roads, bridges, transmission towers, solar panels, and houses built on no-permafrost soils will face serious serviceability and safety issues related to the impact of climate change. Consequently, these structures will require higher maintenance cost, while their useful life span will significantly decrease, thus, jeopardizing the population safety and economic activities in those regions. All in all, understanding the impact of climate change on the Canadian no-permafrost region will help geotechnical engineers optimize the design and develop safe and cost-effective alternatives to construct resilient foundation systems and infrastructure to meet the climate change requirements.

Due to the lack of research on this topic, this modeling study has been undertaken to understand and assess the effect of climate change on the temperature distribution and variation of grounds located in the Canadian no permafrost region. Thus, the main objectives of the present paper are: (i) to present the developed approach/tool for modeling and assessing the impact of climate change on the ground thermal regime; (ii) to present and discuss the main results of the simulation of the effect of climate warning on the thermal regime of grounds located in the Canadian no permafrost region. The no-permafrost areas selected in this study are in East-central Canada (Ontario, Canada).

3.2 The study area:

3.2.1 Geographical description of the study area:

The region of interest in this study is the no-permafrost area in Canada. This region extends from the Atlantic coast in the east to the pacific west coast running mainly through the whole south of Canada (Natural Resources Canada, 2010). Due to the large geographical extend, three sites located in the Ontario (east-central Canada) no-permafrost region were selected. These sites include Ottawa, Sudbury and Toronto

to represent the center, the north and the south of the Canadian no-permafrost region in Ontario, Canada.

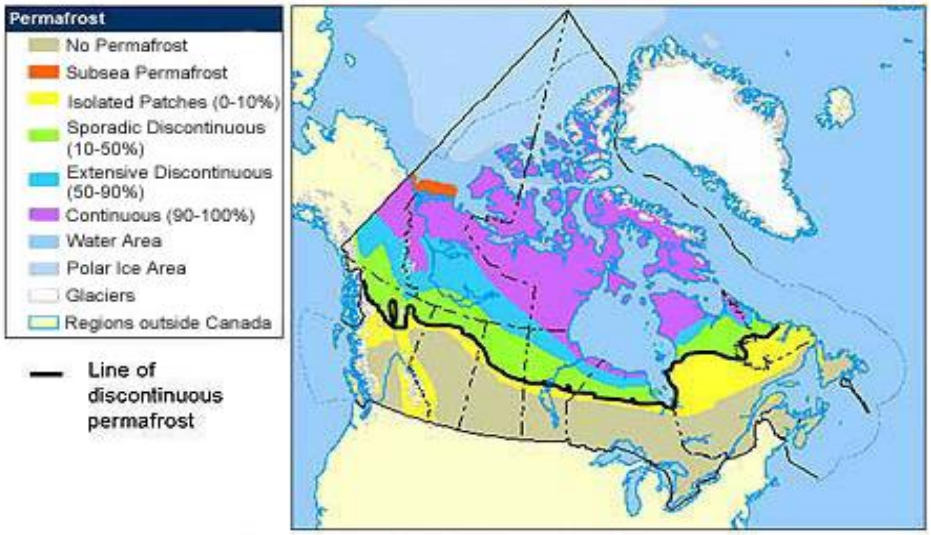

Figure 3.2.1: The geographical limits of the Canadian no-permafrost region (Booshehrian et al., 2020)

Figure 3.2.2: Location of Ottawa, Toronto and Sudbury within Ontario (Cambrian International, 2021)

3.2.2 Climate conditions of the study area

The climate of Ontario varies depending on the seasons and the locations (Government of Canada, 2011). For example, Ottawa has a humid continental climate with an average July maximum temperature of 26.6 °C and an average January minimum temperature of -14 °C (Meteoblue, 2019). Summers in Ottawa are warm and humid. Ottawa annual precipitation averages around 940 millimeters, snowfall occurs in early November and lasts for five months. Rainfall occurs mostly in summertime. The frost season in Ottawa region starts early November and lasts until early May (Meteoblue, 2019; Al-Umar et al. 2020).

Toronto lies farther south than Ottawa, resulting in significantly warmer winters. The winter in Toronto is cold and temperatures are usually below 0 ° (Meteoblue, 2018b). The average January maximum and minimum temperatures are -2 °C and –9 °C, respectively. The summer months are characterized by very warm temperatures with an average July maximum temperature of 27 °C. Toronto receives around 800 millimetres of precipitations per year, mostly in summertime. Precipitation is evenly distributed throughout the year, but summer is usually the wettest season. The frost season in the region of Toronto starts early December and lasts until mid-April (Meteoblue, 2018b).

Sudbury is located farther north at the edge of the Canadian no-permafrost region. Therefore, the winter season is long, snowy and very cold (Meteoblue, 2018a). Sudbury has a humid continental climate, with an average January minimum temperature of -18 °C. The snow cover is expected six months in the year. The duration of the frost period is approximately 180 days starting from early October to the end of April. The average yearly precipitation is about 540 mm in Sudbury (Meteoblue, 2018a).

3.2.3 Climate change models in the study area in the next 100 years

Temperature data gained by Climate Canada have indicated that annual and seasonal mean temperatures across Canada have increased, with the greatest warming occurring in winter. Between 1948 and 2016, the mean annual temperature increase is 1.7°C for Canada as a whole (Government of Canada, 2018; Bush and Lemmen, 2019). To project future temperature or climate changes across Canada, Climate Canada has adopted three different future climate scenarios (RCPs) (IPCC, 2015), RCP8.5 (high global emission scenario), RCP4.5 (medium global emission scenario) and RCP2.6 (low global emission scenario). Tables 1 to 3 show the projected average change in temperature and precipitations in Ottawa, Toronto and Sudbury and under three emissions scenarios (RCPs) for four future time periods: 2021-2040; 2041-2060; 2061-2080; 2081-2100 (Government of Canada, 2019).

Table 3.2.1: Climate change data – Ottawa- (Government of Canada, 2019)

Ottawa	RCPs	Annual Minimum Temperature Change	Annual Mean Temperature change	Annual Maximum Temperature change	Annual Precipitations change	Annual snow depth change	Annual surface wind velocity change
2021-2040	8.5	+1.6	+1.5	+1.5	+3.6%	-32.3%	-1.1%
	4.5	+1.2	+1.3	+1.6	+3.0%	-33.0%	-5.1%
	2.5	+1.2	+1.3	+1.4	+3.5%	-26.5%	-0.2%
2041-2060	8.5	+3.0	+2.9	+2.8	5.9%	-55.1	-1.7%
	4.5	+2.2	+2.3	+2.3	4.7%	-46.4%	-5.7%
	2.5	+1.7	+1.7	+1.8	+2.5%	-44.6%	0.2%
2061-2080	8.5	+4.6	+4.4	+4.3	+8.6%	-67.9%	-2.4%
	4.5	+2.9	+2.8	+2.7	+4.5%	-52.3%	-6%
	2.5	+1.7	+1.7	+1.7	+3.6%	-49.5%	0.5%
2081-2100	8.5	+6.1	+6.0	+5.7	+10.3%	-80.2%	-2.6%
	4.5	+3.2	+3.2	+3.1	+6.3%	-56.0%	-6.5%
	2.5	+1.6	+1.7	+1.8	+3.5%	-42.7%	+0.3%

Table 3.2.2: climate change data –Toronto- (Government of Canada, 2019)

Toronto	RCPs	Annual Minimum Temperature change	Annual Mean Temperature change	Annual Maximum Temperature change	Annual Precipitations change	Annual snow depth change	Annual surface wind velocity change
2021-2040	8.5	+1.5	+1.5	+1.5	+3.0%	-43.7%	-0.9%
	4.5	+1.4	+1.5	+1.5	+2.2%	-44.7%	-5.8%
	2.5	+1.3	+1.3	+1.3	+2.1%	-39.3%	-0.7%
2041-2060	8.5	+2.8	+2.9	+2.9	7.8%	-66.2%	-1.4%
	4.5	+2.2	+2.2	+2.4	+3.9%	-58.4%	-6.5%
	2.5	+1.8	+1.7	+1.8	+2.9%	-50.6%	-0.3%
2061-2080	8.5	+4.4	+4.3	+4.3	+8.0%	-78.9%	-1.8%
	4.5	+2.8	+2.7	+2.6	+5.8%	-66.2%	-7.7%

	2.5	+1.7	+1.8	+1.8	+4.0%	-59.2%	+0.0%
2081-2100	8.5	+5.6	+5.6	+5.5	+14.6%	-85.3%	-3.0%
	4.5	+3.1	+3.1	+3.0	+6.2%	-65.9%	-8.2%
	2.5	+1.8	+1.8	+1.8	3.30%	-54.60%	-0.20%

Table 3.2.3: climate change data – Sudbury - (Government of Canada, 2019)

Sudbury	**RCPs**	**Annual Minimum Temperature change**	**Annual Mean Temperature change**	**Annual Maximum Temperature change**	**Annual Precipitations change**	**Annual snow depth change**	**Annual surface wind velocity change**
2021-2040	8.5	+1.6	+1.5	+1.5	+3.9%	-36.7%	-0.7%
	4.5	+1.3	+1.4	+1.5	+2.9%	-34.4%	-6.0%
	2.5	+1.2	+1.3	+1.4	+2.4%	-31.6%	0.3%
2041-2060	8.5	+3	+2.9	+2.8	+8.9%	-57.7%	-1.6%
	4.5	+2.2	+2.2	+2.3	+5%	-49.2%	-6.8%
	2.5	+1.6	+1.7	+1.8	+4.5%	-47.5%	-0.1%
2061-2080	8.5	+4.6	+4.5	+4.4	+0.5%	-69.5%	-2.3%
	4.5	+2.9	+2.8	+2.7	+5.3%	-53.2%	-7.0%
	2.5	+1.7	+1.7	+1.8	+2.8%	-51.2%	+0.1%
2081-2100	8.5	+6.1	+6.0	+5.7	+9.6%	-80.1%	-2.9%
	4.5	+3.2	+3.2	+3.1	+7.4%	-58.0%	-7.7%
	2.5	+1.7	+1.7	+1.7	+3.4%	-45.6%	-0.1%

3.2.4 Representative soil profiles of the study area

The Canadian no-permafrost region embraces several geological patterns; therefore, soils have dissimilar geotechnical and physical properties within this region (Natural Resources Canada, 2010). The national geological survey of Canada provides borehole logs of several sites among the Canadian territory including Ottawa, Toronto and Sudbury. Accordingly, the geotechnical profiles of the three cities were developed based on the information included in the borehole logs of the national survey. Essentially, for the first 10 m into the ground, the soil composition comprises layers of clay, silt, sand and gravel. The bedrock layer was not detected in the representative boreholes (Natural Resources Canada, 2010). Beside the soil profile, the borehole logs include recordings of the relative density, temperature of the soil with depth and the velocity of the P waves in the sublayers of the soil stratum (Natural Resources Canada, 2010).

The geotechnical composition and geometry of the three selected sites for the thermal simulation are presented in the Section 3.7.

3.3 Methodology:

3.3.1 Approach:

Fig. 3.1.1 displays the developed approach or method for the assessment of the impact of future climate on the thermal regimes of grounds in the selected Canadian no-permafrost regions and the link between the different work stages of the studies performed. The method adopted comprises four main stages. The first stage (see Section 3.2) deals with the establishment of the simulation tool, which includes the determination of the suitable thermal model and its validation against field measurement data. The second stage (see Section 3.3) involves the acquisition of the actual climate conditions and the climate change predictions for the study area. The actual climate data was obtained from the Environment Canada, whereas climate change predictions were gained from the climate change interactive maps published on the Climate Change Canada website (Government of Canada, 2019). Three climate change scenarios, RCP 2.5, RCP 4.5 and RCP 8.5 were considered in the present study, as mentioned earlier. The third stage consists of (Section 3.4) of the acquisition of the required geotechnical, physical and thermal data of the grounds in the studied sites, which were used as input data in the modeling works to be conducted. In the fourth stage of this investigation (Section 3.5), numerical modeling and simulations of the effect of future climates on the thermal responses of the grounds in the studied sites were conducted. Subsequently, the simulation results were integrated and analyzed. The approach or method developed in this study can be also adopted or adapted to simulate the ground thermal regime under changing climate conditions in other no-permafrost regions in Canada or around the world. The aforementioned stages are described in detail below.

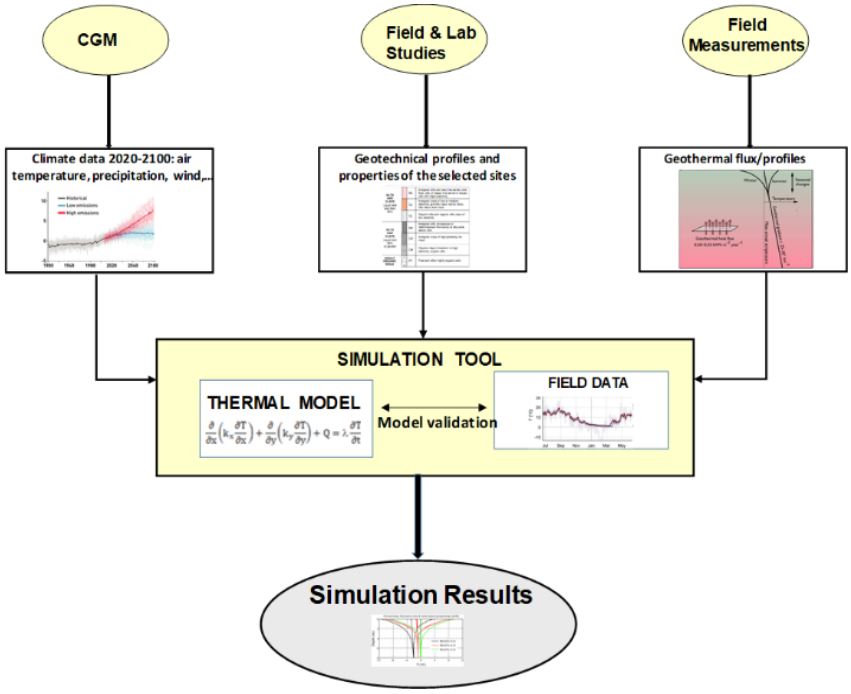

Figure 3.3.1: flow chart of the analysis

3.4 Description and validation of the thermal model

TEMP/W software package from Geo-Slope International Ltd. (GEO-SLOPE International Ltd, 2014) was used to develop a model of the ground thermal regime. TEMP/W provides a platform to simulate heat transfer through fully or partially saturated and fully or partially thawed material. The analysis of the thermal model requires three main elements; these elements are discretization, material properties, and boundary conditions. TEMP/W includes five thermal different material models: no-thermal, interface, coupled convective thermal, simplified, and full thermal model. The simplified thermal option was used in this study for all the simulations. This model is used for problems in which the latent heat of phase change is not considered in the freezing process and the phase change is assumed to occur at the phase change temperature instead of occurring over a range of temperatures (GEO-SLOPE International Ltd, 2014).

3.4.1 General formulations

Temperature changes in the soil are driven by four modes of heat transfer: radiation, conduction, convection, and phase changes. The radiative heat transfer is dominant at the soil–air interface where the soil receives direct solar shortwave radiation (Flynn, 2015). Nevertheless, the effect of radiations decreases with depth, therefore, radiative heat flow is often negligible in the formulation of heat transfer in the soil. Likewise, the convective heat transfer due to gas flow at the soil surface is neglected because the volumetric heat capacity of gas is three orders of magnitude smaller than the volumetric heat capacity of the solid or liquid (Orlando & Ladanyi, 2004). For the reasons described above, radiative, and convective heat transfers

were neglected in the present modeling study.

In most instances, conduction is the principal mode of energy transport in soils, although radiation and convection in very shallow layers also may transfer energy. Heat flow in soil can be considered analogous to heat flow in a solid to which Fourier's Law is applied:

Equation 3.4.1: Conduction equation:

$$q = -k * \left(\frac{dT}{dx}\right)$$

The heat flux, q (J/sec), directly depends on the thermal conductivity, k (J/(sec × m × °C)), and the change of temperature, T (°C), over a distance, x (m).

The differential equation that governs the formulation of 2D numerical solutions can be expressed as follows:

Equation 3.4.2 : General 2D heat flow formulation (Harlan & Nixon, 1978):

$$\frac{\partial}{\partial x}\left(k_x \frac{\partial T}{\partial x}\right) + \frac{\partial}{\partial y}\left(k_y \frac{\partial T}{\partial y}\right) + Q = l\frac{\partial T}{\partial t}$$

Where T = temperature, kx = thermal conductivity in the x-direction, ky = thermal conductivity in the y-direction, Q = applied boundary flux, l (J/(m^3 × °C) = capacity for heat storage, and t = time.

3.4.1.1 Steady state formulation

The difference between the heat flux entering and leaving an elemental volume of soil at a point in time is equal to the change in the stored heat energy. At steady state, the heat flux entering and leaving the system are equal, therefore, the equation for 2D heat flow becomes:

Equation 3.4.3: 2D heat flow formulation at steady state (GEO-SLOPE International Ltd, 2014):

$$\frac{\partial}{\partial x}\left(k_x \frac{\partial T}{\partial x}\right) + \frac{\partial}{\partial y}\left(k_y \frac{\partial T}{\partial y}\right) + Q = 0$$

3.4.1.2 Transient analysis formulation

In the transient analysis, the heat flux entering and leaving an elemental volume of soil at a point in time are not equal, therefore, heat energy is stored in the soil matrix. The amount of heat energy stored depends on the thermal properties of the soil. The capacity to store heat "l" is expressed as follows:

Equation 3.4.4: The capacity to store heat (Williams, 1964):

$$l = c + L\,\frac{\partial w_u}{\partial T}$$

Where c = volumetric heat capacity (material property), L (J/m^3) = latent heat of water, wu = total unfrozen volumetric water content and T = temperature,

Substituting for l in the main thermal equation leads to the complete 2D heat flow differential equation:

Equation 3.4.5: 2D heat flow formulation at transient analysis (GEO-SLOPE International Ltd, 2014):

$$\frac{\partial}{\partial x}\left(k_x \frac{\partial T}{\partial x}\right) + \frac{\partial}{\partial y}\left(k_y \frac{\partial T}{\partial y}\right) + Q = \lambda \frac{\partial T}{\partial t} = \left(c + L_w \theta \frac{\partial \theta_u}{\partial T}\right)\frac{\partial T}{\partial t}$$

where Q is the heat flux, kx and ky are the thermal conductivities in the x and y directions, λ the capacity for heat storage, t time. The capacity to store heat in the soil λ is composed of two parts: the volumetric heat capacity, c, that depends on whether the material is frozen or unfrozen, and L, the latent heat of fusion of the material. The latent heat calculation requires the volumetric water content, θ, the unfrozen volumetric water content, θu (m^3/m^3) and L_w the latent heat of water (GEO-SLOPE International Ltd, 2014).

3.4.2 Validation of the thermal model/simulation tool

The purpose of the validation model is to verify the accuracy of the selected thermal models from TEMP/W software to simulate the ground thermal regime. For this purpose, the validation model was built using field measurement data from previous geotechnical investigations conducted in the region of the national capital, Ottawa (Crawford & Legget, 2002).

3.4.2.1 Model geometry and material properties:

The geometry of the validation model is retrieved from a past geotechnical report of National Research Council Canada, which included temperature measurements of soil temperature from May 1954 to April 1955 under snow cleared surface (Crawford & Legget, 2002). The model geometry extended 15 m laterally from the centerline, and to a depth of 5 m below the natural ground surface. Different geometries that increased the lateral extent to 40 m were tested, however the isotherms (temperature contours) beyond 30 m were the same and did not affect the results. The temperature measurements provided in the geotechnical report were given to a depth of 5m, therefore, the depth of the model was selected as 5 m (Crawford & Legget, 2002). Mesh properties can be modified so that certain geometric objects can have a

finer mesh or a different pattern of mesh elements such as triangles or quadriparas (Flynn, 2015). A square mesh of 0.2 m diameter was selected. Finer dimensions were tested; however, the software was not able to establish the analysis due to storage limitations.

All materials were modelled using a simplified thermal model, which requires the volumetric heat capacities (cu and cf), thermal conductivities (ku and kf), the in-situ volumetric water content (VWC), and the unfrozen volumetric water content (GEO-SLOPE International Ltd, 2014). The Thermal properties used in the validation model were selected from previous studies on the Ottawa clay soil. The soil is assumed to be fully saturated. The soil properties are summarized in Table 3.4.1 (Orlando & Ladanyi, 2004)

Table 3.4.1: Thermal properties of the validation model (Orlando & Ladanyi, 2004)

Soil type	**Θ(m3/m3)**	**Unfrozen thermal conductivity (Kj/d/m.C)**	**Frozen thermal conductivity (Kj/d/m.C)**	**Unfrozen volumetric heat capacity (Kj/m3/C)**	**Frozen volumetric heat capacity (Kj/m3/C)**
Ottawa Clay	0.4	191	562	6556	4683

3.4.2.2 Boundary conditions

The validation model featured two analyses; a steady state and transient analysis. The purpose of the steady state analysis is to establish the thermal equilibrium in the soil during the first day of the transient analysis. At steady state, the top boundary condition is set to the average annual temperature at the year 1954. A constant unit heat flux representing the geothermal gradient was applied to the bottom extent of the model as shown in Figure 3.4.1. Geothermal gradients vary by location but generally range between 0.9 and 3.3°C per 100 m (Grasby et al., 2009). At the edges of the model, a zero-heat flux boundary condition was applied. A constant unit flux of 3.87 kJ/m2·day was used for Ottawa based on the Geothermal Map of Canada published in 2009 (Grasby et al., 2009).

The transient analysis comprises a whole year climate data. The climate data was obtained from the Environment Canada website. Climate data was downloaded for every day from the first day of May 1954 to the last day of April 1955 (Government of Canada, 2011).

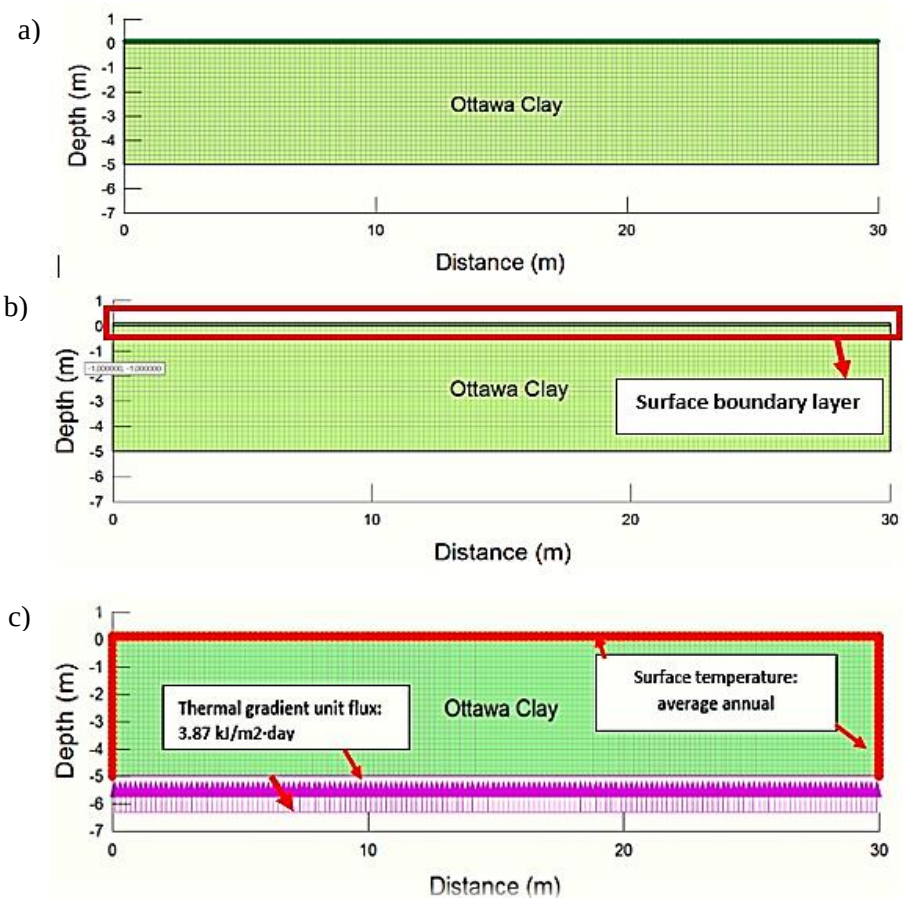

Figure 3.4.1: a) Cross Section of the validation model, b) Model surface boundary Layer, (c) Steady state boundary condition

3.4.2.3 Climate Boundary Condition -Validation model

The OTTAWA CDA weather monitoring station is a part of the cooperative climate network, and it is located at the Horizontal coordinates "Lat: 45.38, Long: -75.72". It provides a complete set of climate data for the region of the national capital (Government of Canada, 2011).

The climate boundary condition developed by TEMP/W required several input parameters which included: maximum and minimum daily temperatures, maximum and minimum daily relative humidity, daily average wind speed, and daily total precipitation. The latitude was set at 45.38° north to incorporate the effects of solar radiation(Government of Canada, 2011). A thin layer of finite elements called a surface layer was required at the top surface to apply the climate boundary condition in a TEMP/W model (GEO-SLOPE International Ltd, 2014).

To account for the fact that the air temperature at the surface differs from the ground temperature, even at shallow depths, "n" modifying factors were required. "n" factors are empirically based coefficients used to

estimate ground surface temperatures based on air temperatures. The n-factor is the ratio between thawing and freezing indices of the ground surface and the air (Orlando & Ladanyi, 2004). They vary depending on the geographic location and surface cover. Both the freezing and thawing n factors are required in the TEMP/W analysis.

Recommended n-factors were used based on values provided in TEMP/W manual. For a bare soil, the recommended thawing and freezing factors are respectively: $n_{th} = 1.4$ and $n_f = 0.7$ (GEO-SLOPE International Ltd, 2014).

3.4.2.4 Discussion of the validation results

The data provided in the National Research Canada report includes the monthly average temperature of an Ottawa clay soil between May 1954 and April 1955 (Crawford & Legget, 2002). The temperature graphs are represented in Figure 3.4.2 a. Ground temperature is provided for each month along the whole year. The validation model provides daily ground temperature measurement for an Ottawa clay ground. were processed to develop average monthly temperature graphs of the Ottawa clay ground similar to the graphs provided by the National Research Council Canada. The results of the validation simulation are presented in Figure 3.4.2b (Crawford & Legget, 2002).

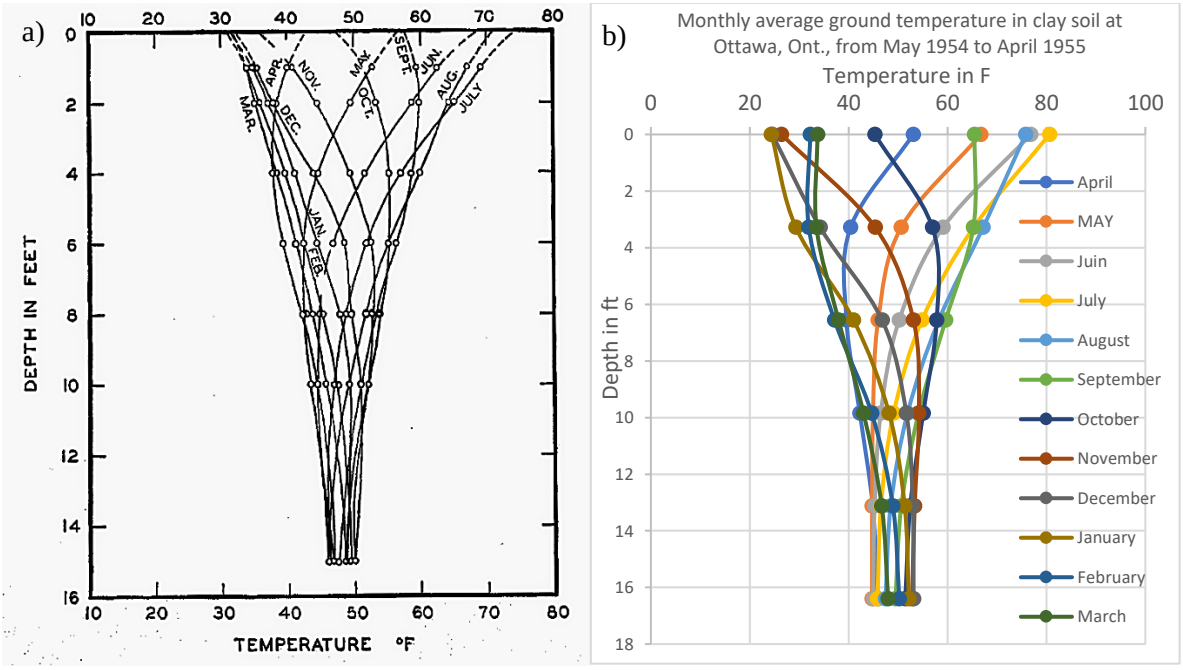

Figure 3.4.2: Monthly ground temperature in clay soil at Ottawa from May 1954 to April 1955, a) measured data, b) modeling results.

The simulation results obtained are approximately similar to the original (measured) ground temperature data. First, the validation model established similar thermal regimes in both the cold and the hot seasons. The graphs of the monthly average temperature in both seasons have approximately the same trend and shape as in the original report provided by the National Research Council Canada. At shallow depths (from 0 ft to 4 ft), some divergence was observed from the original temperature ground data. Nevertheless, at a depth of 6 ft, the thermal model succeeded to simulate to a large extent the original temperature data. For instance, at 6 ft, the temperature spectrum, ranges between 38 F to 58 F in the original and the simulation data. Likewise, the temperature spectrum at the bottom of the of the model ranges between 45 F to 52 F for the original ground temperature data, and between 43 F to 55 F for the simulation results. Thus, the divergence at the bottom of the model is very minor.

The divergence at shallow depths could be due to several reasons; first, the validation model used material properties retrieved from a different source for the Ottawa clay due to the absence of any information about the material properties in the original report. Second, TEMP/W 2012 considers the conduction as the main heat transfer mechanism even at shallow depths (GEO-SLOPE International Ltd, 2014); nevertheless, on the actual site, other processes affect the thermal regime of the ground including convection and radiation. Finally, climate data for the year 1954 – 1955 were retrieved from the Environment Canada website, separately from the original report. Therefore, the climate data used to build the model could be slightly different from the actual climate data used in the original report. All these factors might influence the validation model and might lead to the observed slight divergences. All in all, the adopted thermal model and the simulation tool provided a good understanding of thermal regime of the ground and could be used to simulate the impact of climate warming on the thermal regime of the ground.

3.5 Climate data collection:

It is commonly assumed that climate is relatively stable with no major climate changes within 20 years period (Government of Canada, 2019). Being said, for the aim of this study, climate conditions are defined in four-time segments of 20 years.

Climate data were collected from the Climate Canada website using projections map with temporal resolution available at a seasonal, and annual scale and spatial resolution approximately 10km (Government of Canada, 2019). The projection map provides information on the projected 20-year average changes in minimum, mean and maximum temperature. It also provides information on the average change in precipitations, snow depth and surface wind velocity.

These interactive maps simulate the climate change under the main three emission scenarios; RCP2.6, RCP4.5, RCP8.5 for Four-time frames starting from 2019 until 2100 (Government of Canada, 2018).

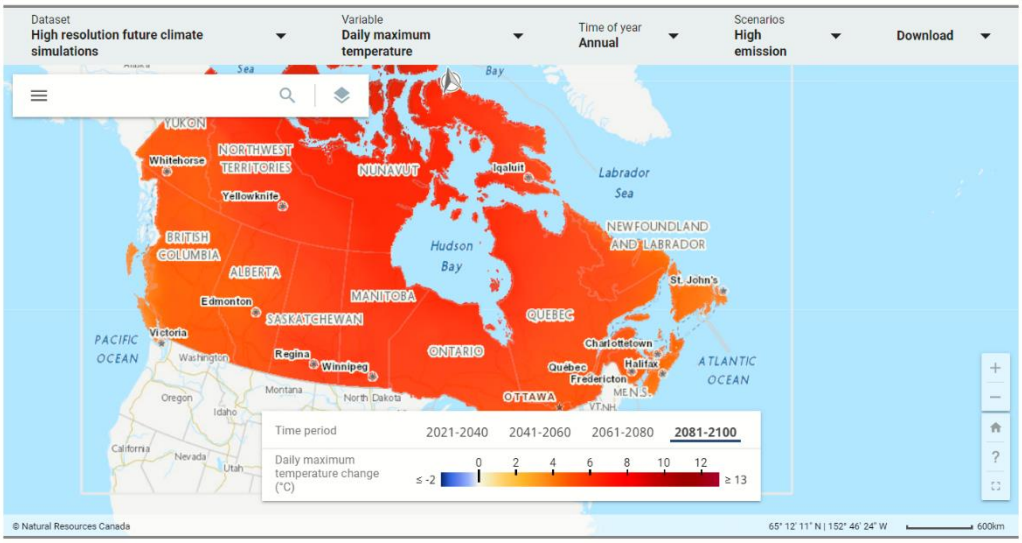

Figure 3.5.1: Climate change interactive map (Government of Canada, 2019)

Climate change is evaluated relatively to the reference period from 1900 to 2005. Climate conditions in 2019 are assumed to be similar to these of 2005 (within 20-year time period), therefore, climate change is assumed to occurs relatively to the climate condition in 2019.

The actual climate data were collected from the climate Canada official website. The selected climate monitoring stations are summarized in the Table 3.5.1 (Government of Canada, 2019).

Table 3.5.1: Climate stations at Ottawa, Toronto and Sudbury (Government of Canada, 2019)

City	Name	Latitude	Longitude
Ottawa	OTTAWA CDA	45.38	-75.72
Toronto	Toronto	43.67	-79.4
Sudbury	SUDBURY A	46.63	-80.8

3.6 Geometry and material properties of the thermal models:

3.6.1 Geometry:

The geometry of the simulation models was retrieved from Canada geological survey records for Ottawa, Toronto and Sudbury. Each model was developed based on two adjacent boreholes logs located at each city. All boreholes provide a continuous information on the sub-surface geotechnical profile to a depth of 20 m (Natural Resources Canada, 2010). The geometry of the three models extended 15 m laterally from the centerline, and to a depth of 20 m below the natural ground surface. A thin layer of finite elements

called a surface layer was required at the top surface to apply the climate boundary condition in a TEMP/W model (GEO-SLOPE International Ltd, 2014). The mesh properties are set to finite square of 0.2 m diameter for the three simulation models. The selected mesh dimensions provided accurate simulation results compared to a larger mesh. The software did not allow to use thinner mesh due to limited storage of the computer. Furthermore, thinner mesh, require a longer computation time (Flynn, 2015).

3.6.2 Material properties:

The thermal properties required to build the thermal model are the volumetric heat capacities (cu and cf), thermal conductivities (ku and kf), the in-situ volumetric water content (VWC), and the unfrozen volumetric water content. The material properties were retrieved from literature, for each material.
Table 3.6.1 to Table 3.6.3 summarize the thermal properties of simulation models for Ottawa, Toronto and Sudbury, respectively:

Table 3.6.1: Material thermal properties – Ottawa model - (Orlando & Ladanyi, 2004)

Soil type	**Θ(m3/m3)**	**Unfrozen thermal conductivity (Kj/d/m.C)**	**Frozen thermal conductivity (Kj/d/m.C)**	**Unfrozen volumetric heat capacity (Kj/m3/C)**	**Frozen volumetric heat capacity (Kj/m3/C)**
Brown silty clay	0.4	191.6	562.2	6556.3	4683.0
Grey soft silty clay	0.7	59.3	234.7	3488.7	2491.9
Grey firm silty clay	0.7	65.5	235.0	3567.0	2547.9

Table 3.6.2: Material thermal properties – Toronto model - (Orlando & Ladanyi, 2004)

Soil type	**Θ(m3/m3)**	**Unfrozen thermal conductivity (Kj/d/m.C)**	**Frozen thermal conductivity (Kj/d/m.C)**	**Unfrozen volumetric heat capacity (Kj/m3/C)**	**Frozen volumetric heat capacity (Kj/m3/C)**
Silty sand	0.52	84.9	83.1	1755.2	1253.7
Stiff grey silty clay	0.42	159.5	185.5	2519.8	1799.9
Dense silty clay	0.35	275.2	382.0	3438.3	2455.9

Table 3.6.3: Material thermal properties – Sudbury model - (Orlando & Ladanyi, 2004)

Soil type	**Θ(m3/m3)**	**Unfrozen thermal conductivity (Kj/d/m.C)**	**Frozen thermal conductivity (Kj/d/m.C)**	**Unfrozen volumetric heat capacity (Kj/m3/C)**	**Frozen volumetric heat capacity (Kj/m3/C)**
Clay	0.52	246.7	412.1	4261.2	3043.7
Silty clay	0.55	224.2	422.1	4635.1	3310.8
Clayey silt + trace of sand	0.52	171.1	240.7	3137.0	2240.7
Red clay	0.52	345.65	587.4	4771.7	3408.3
Sandy gravel	0.32	92	91.2	1831.0	1307.8

3.7 Modeling of the thermal responses of the selected sites to climate changes

3.7.1 Boundary conditions

3.7.1.1 Steady state boundary conditions:

At steady state, the boundary condition describes the initial thermal regime of the ground. A constant temperature was applied at the top boundary of the three models. It was assumed that at steady state, the ground surface temperature is equal to the average annual air temperature (GEO-SLOPE International Ltd, 2014). At the edges of the models, a zero-heat flux boundary condition was applied. At the bottom extent of each model, a constant heat flux was applied to take into consideration the impact of the geothermal gradient. The value of the heat flux depends on the location, but generally range between 0.9 and 3.3°C per 100 m (Grasby et al., 2009). The values of the thermal unit heat flux applied on the three models were retrieved from the thermal map of Canada.

Figure 3.7.1a), b) and c) represents the steady state boundary conditions for Ottawa, Toronto and Sudbury:

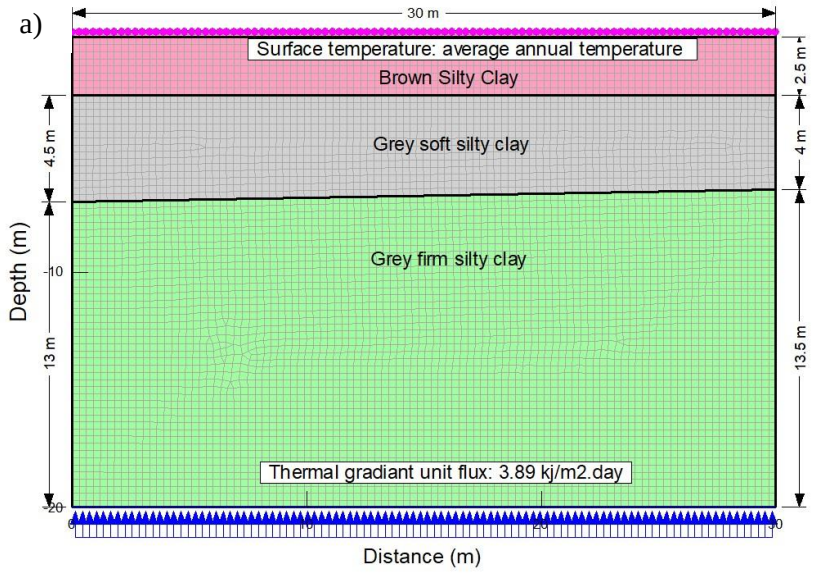

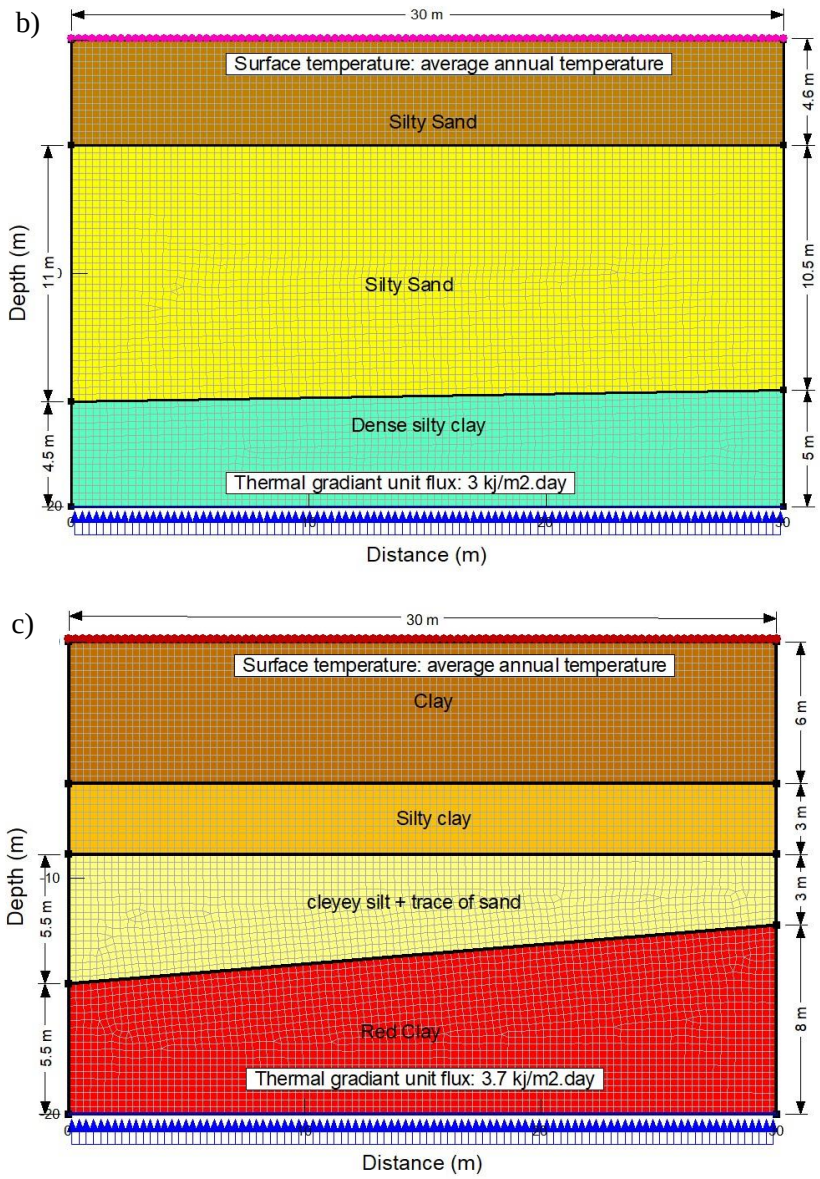

Figure 3.7.1: Simulation model Steady state boundary conditions a) Ottawa b) Toronto c) Sudbury

3.7.1.2 Transient analysis boundary conditions

The transient analysis comprises a whole year climate data. Climate data was downloaded for every day from the first day of January 2018 to the last day of December 2018. These data represent the actual climate data used to build the actual climate condition analysis. The transient simulation involves several steps; the first part of the analysis establishes the thermal regime of the ground for the actual climate conditions. For this purpose, five transient analyses were established using the actual climate data of 2018. The reason behind this, is to minimize the effect of the initial temperature through five cycles of the same actual climate conditions. After five transient simulations using the actual climate condition of 2018 the

simulation of climate change started. The simulations include four time periods; 2020-2040, 2041-2060, 2061-2080 and 2081-2100. The climate data used for each simulation are based on the actual climate data, including the climate change modifications listed in Table 3.2.1 through Table 3.2.3, to account for the impact of climate change. The climate values used in the simulations are modified for each time period, for example, following the RCP8.5, the daily maximum temperature of air will increase by 1.6 in Ottawa by 2040, given that the maximum temperature on March 1st was 4 °C in 2019, the maximum daily temperature in Ottawa on March 1st will be 5.6 °C by 2040 following the RCP 8.5. The same logic applies for the rest of the climate patterns used in the analyses (Government of Canada, 2018). For each city three models were built, each model simulates a climate change scenario; RCP 2.5, RCP 4.5 and RCP 8.5.

Below (Figure 3.7.2) a representation of the analyses sequence implemented in the modeling software for all the three thermal models.

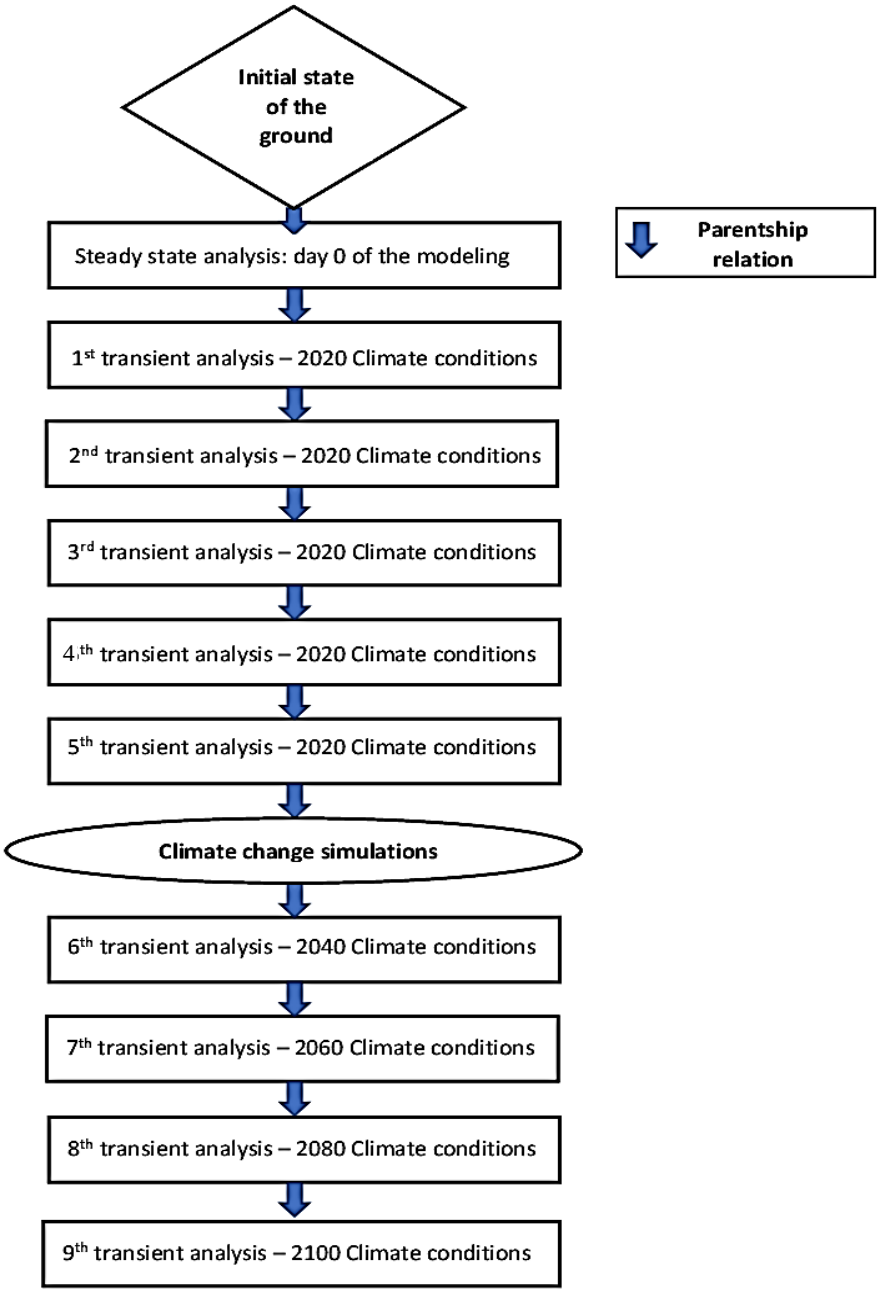

Figure 3.7.2: Analysis's sequence established and implemented in the modeling tool.

3.8 Simulation results and discussion:

A large amount of simulation results has been obtained. The results include ground temperature profiles and ground temperature at different depths along the sub-surface strata for December 31st and March 1st as well as the effect of the snow cover variation on the thermal regime of the studied grounds. These two days were selected to provide an understanding of the ground thermal regime at the beginning and the end of the winter season, respectively. For the sake of keeping the length of the manuscript and the number figures reasonable, only selected typical simulations results will be presented in this chapter. All simulation results obtained are available in the Appendix (A, B, C, D) of this thesis manuscript.

3.8.1 Temperature profiles:

Typical simulated ground temperature profiles for the three climate change scenarios, in Ottawa (Figure 3.8.1 to 3.8.3), Toronto (Figure 3.8.4 and Figure B-4 to Figure B-6) and Sudbury (Figure 3.8.5 and Figure B-7 to Figure B-9) at 2020, 2040, 2060, 2080 and 2100, are presented below as well as in the Appendix B.

3.8.1.1 Ottawa RCP 8.5:

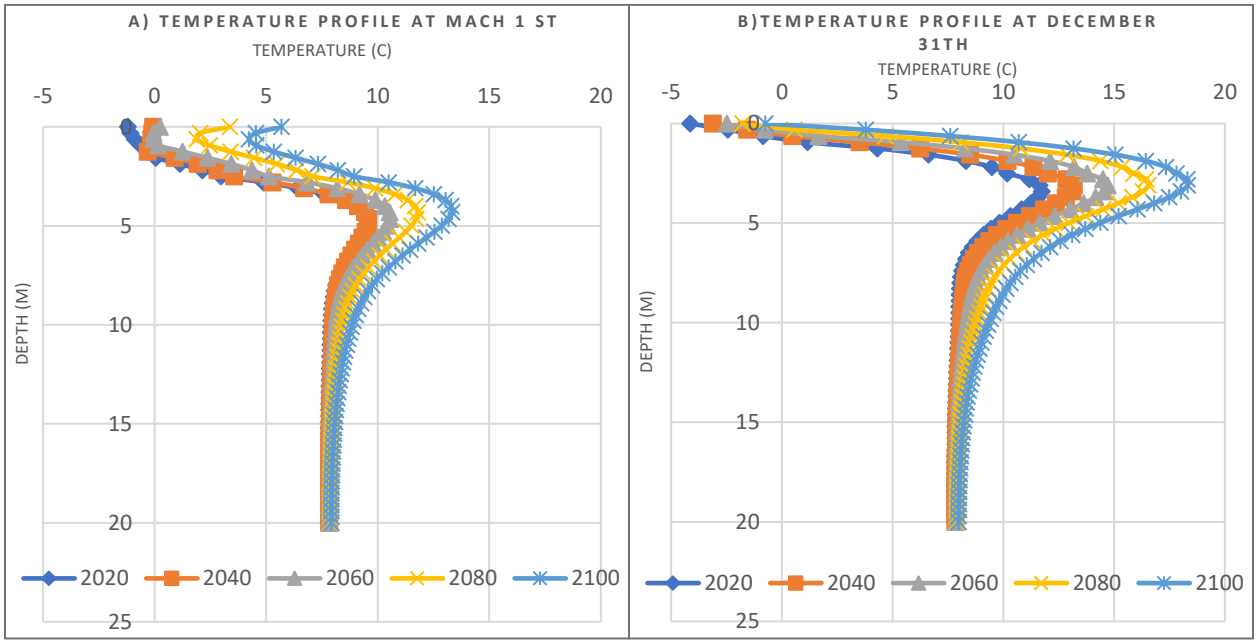

Figure 3.8.1: Ground temperature profiles at a) March 1st and b) December 31 st for 2020 – 2040 – 2060 – 2080 – 2100 – RCP8.5

3.8.1.2 Ottawa RCP 4.5:

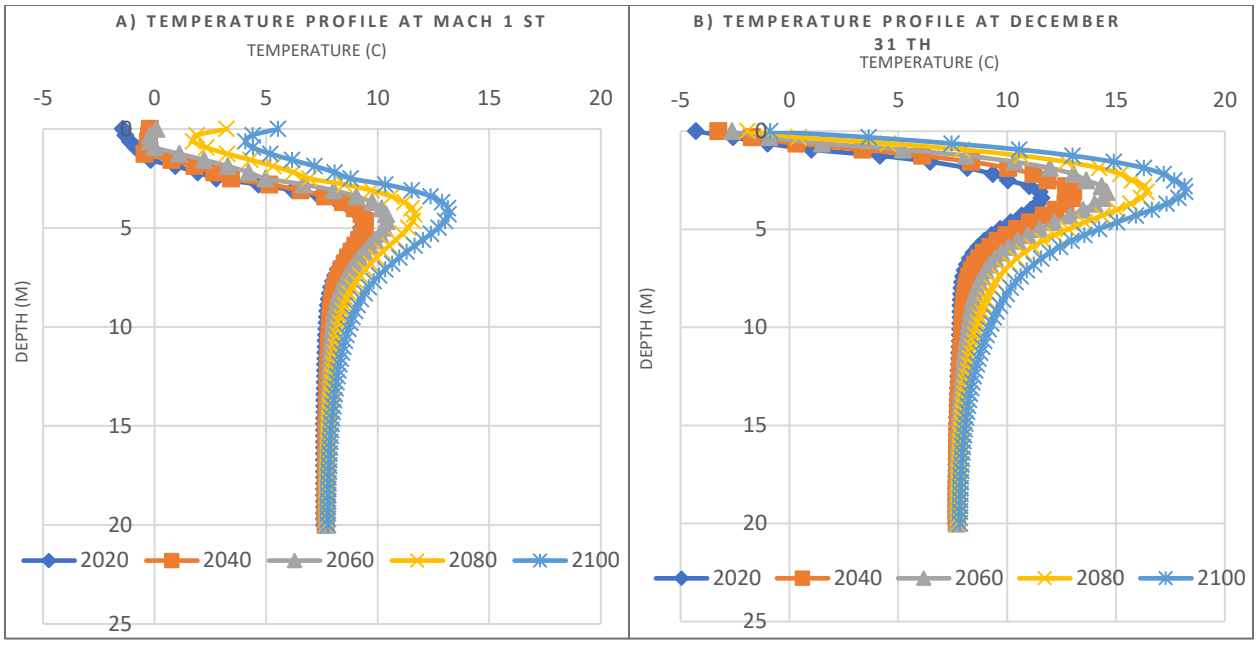

Figure 3.8.2: Ground temperature profiles at a) March 1st and b) December 31 st for 2020 – 2040 – 2060 – 2080 – 2100

3.8.1.3 Ottawa RCP 2.5:

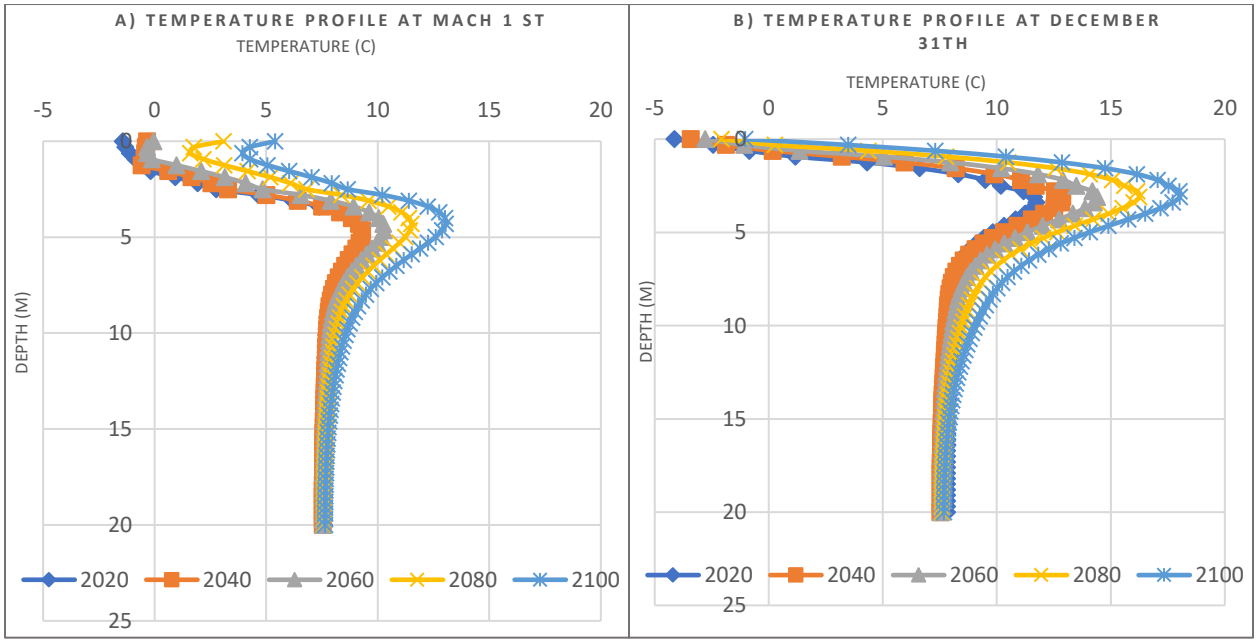

Figure 3.8.3: Ground temperature profiles at a) March 1st and b) December 31 st for 2020 – 2040 – 2060 – 2080 – 2100 – RCP 2.5

3.8.1.4 Toronto RCP 8.5:

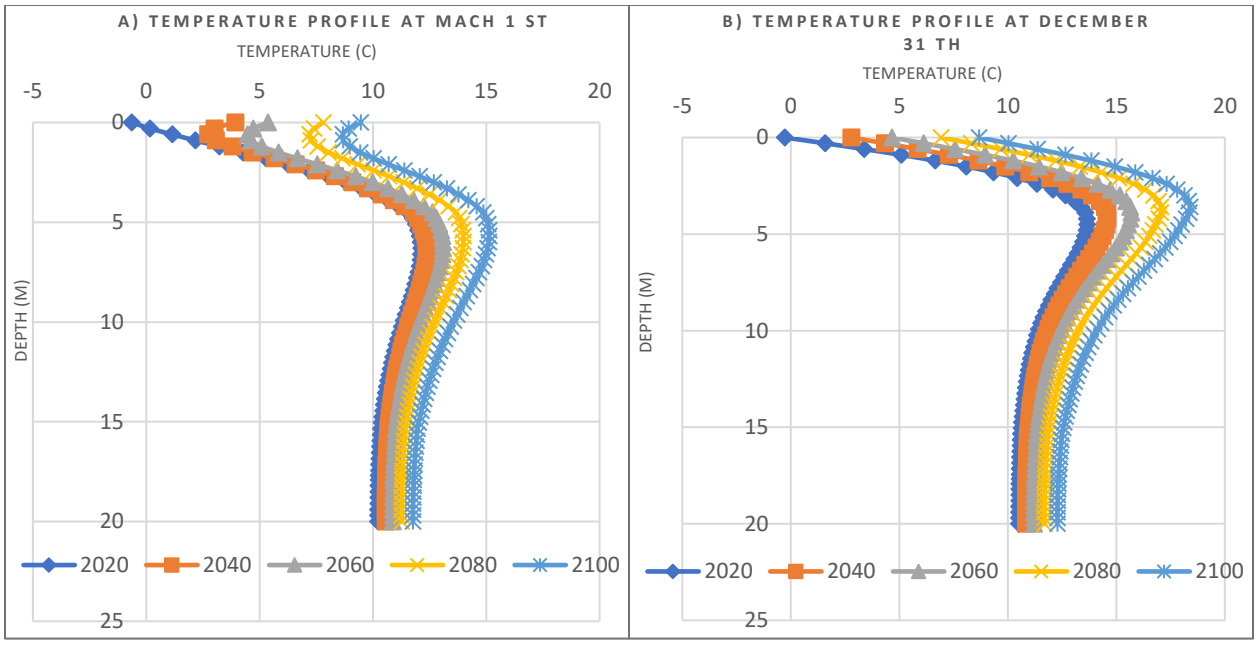

Figure 3.8.4: Ground temperature profiles at a) March 1st and b) December 31 st for 2020 – 2040 – 2060 – 2080 – 2100 – RCP8.5

3.8.1.5 Sudbury RCP 8.5:

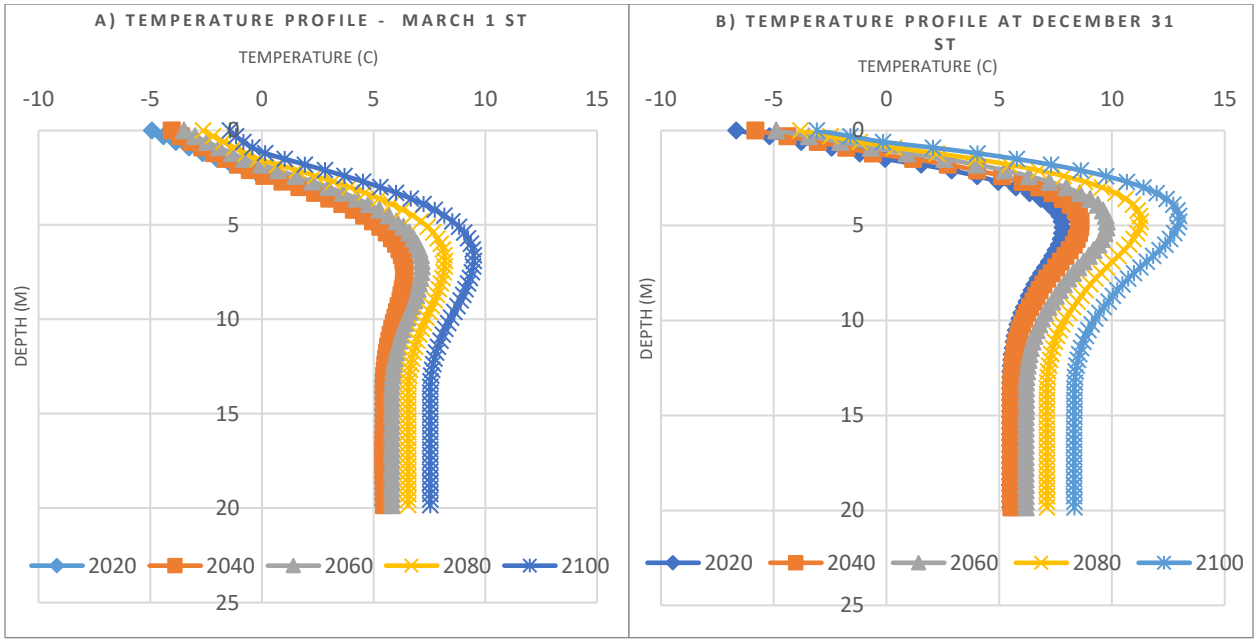

Figure 3.8.5: Ground temperature profiles at a) March 1st and b) December 31 st for 2020 – 2040 – 2060 – 2080 – 2100 – RCP8.5

3.8.2 Climate change scenario - Sensitivity analysis:

For comparison purposes the temperature profiles for March 1st and December 31st in 2040, 2060, 2080, 2100 for the three Climate change were combined in the same graph as illustrated in Figure 3.8.6 (Ottawa), Figure 3.8.7 (Toronto) and Figure 3.8.8 (Sudbury) below.

3.8.2.1 Ottawa:

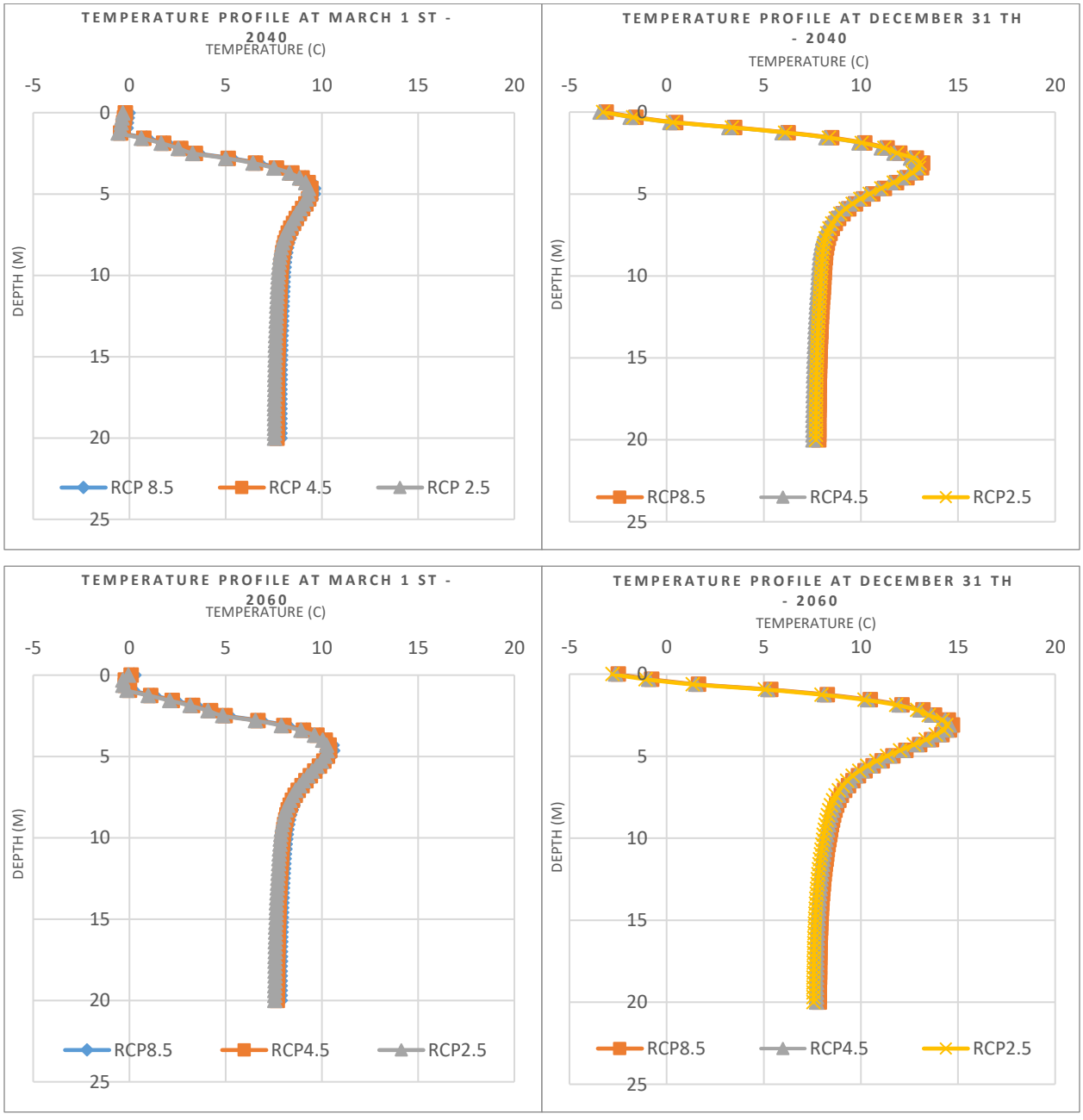

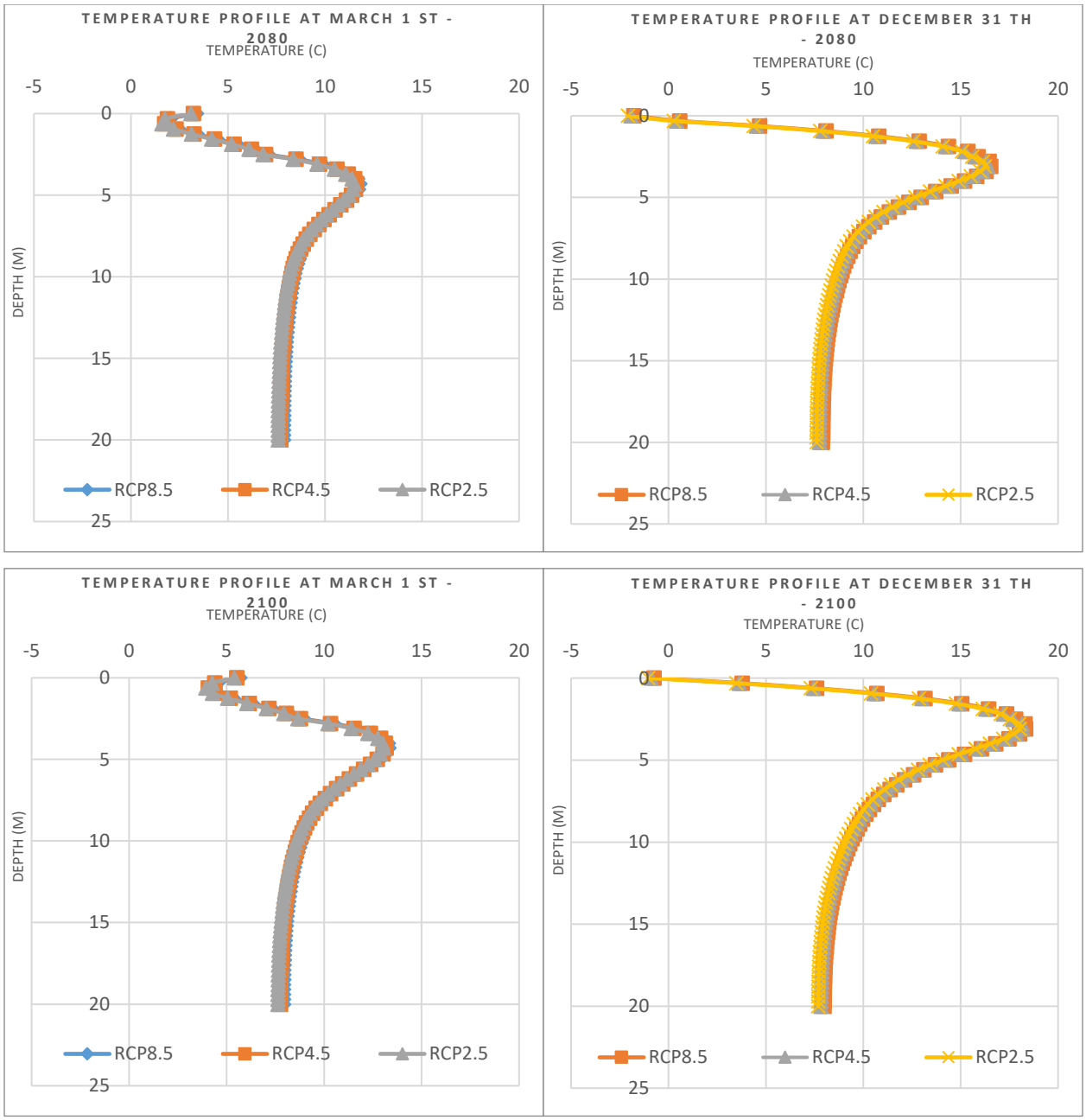

Figure 3.8.6: Temperature profiles at Mach 1st and December 1st in 2040, 2060, 2080 and 2100 for different RCPs- Ottawa

3.8.2.2 Toronto:

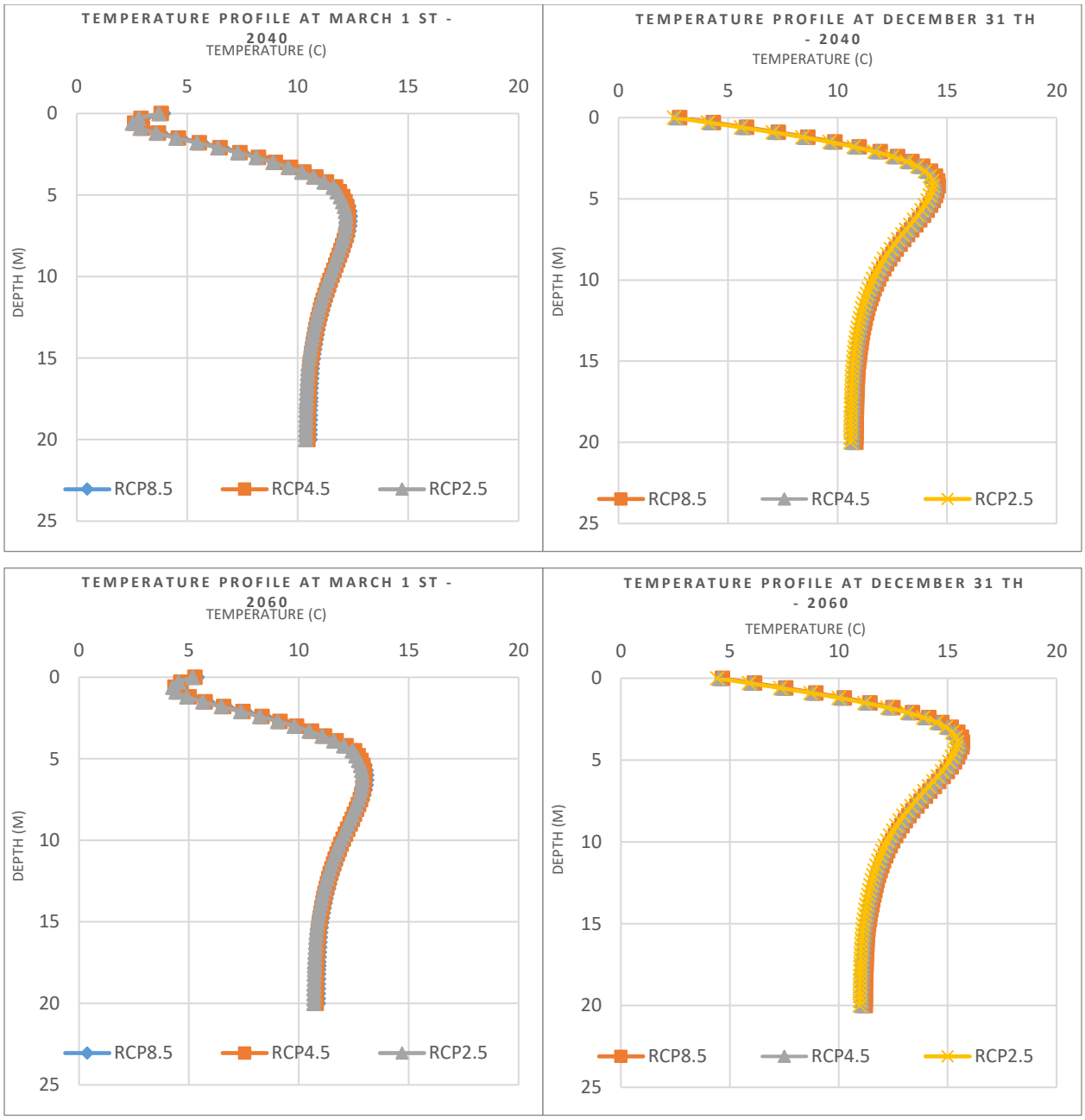

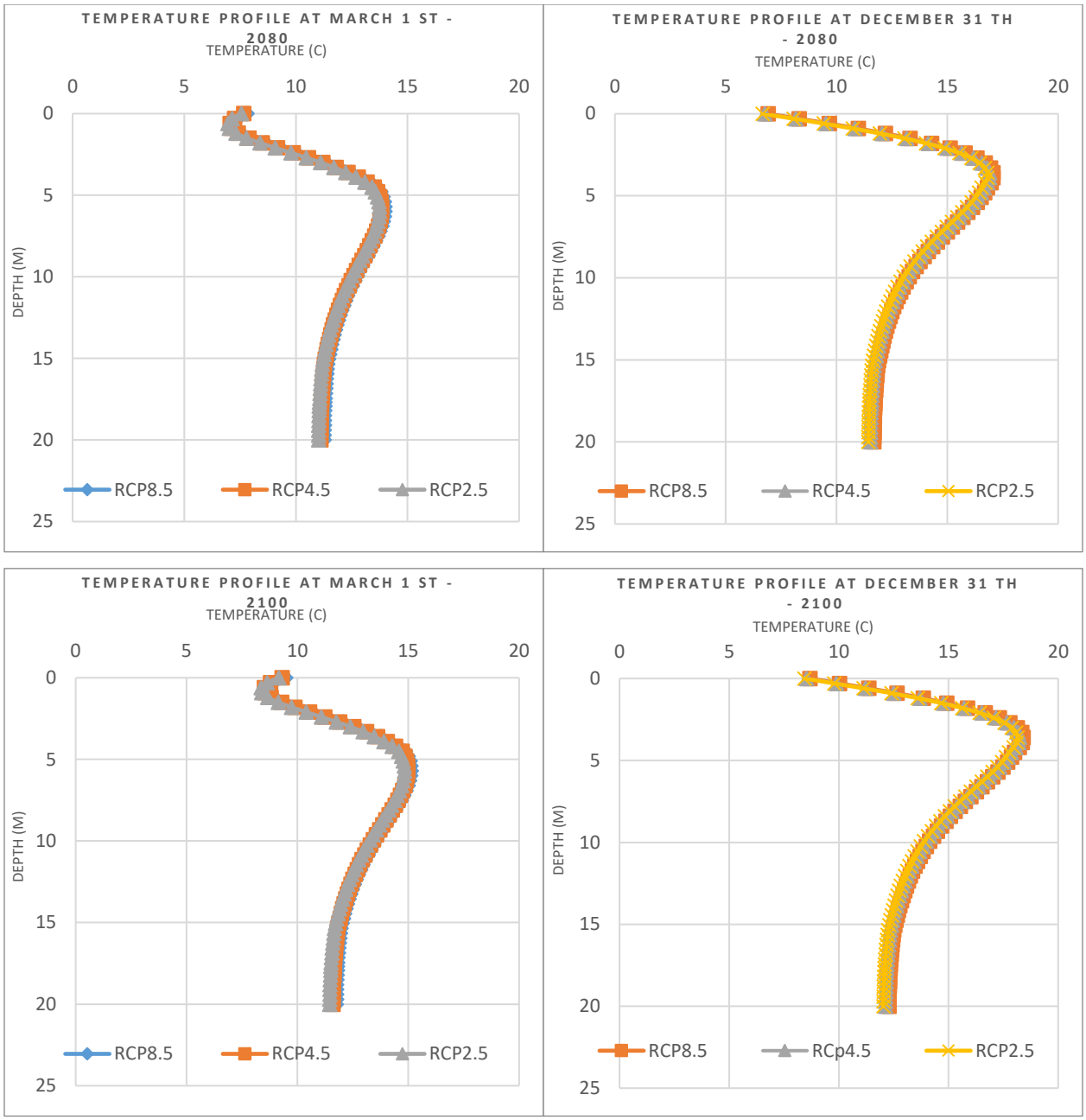

Figure 3.8.7: Temperature profiles at Mach 1st and December 1st in 2040, 2060, 2080 and 2100 for different

3.8.2.3 Sudbury:

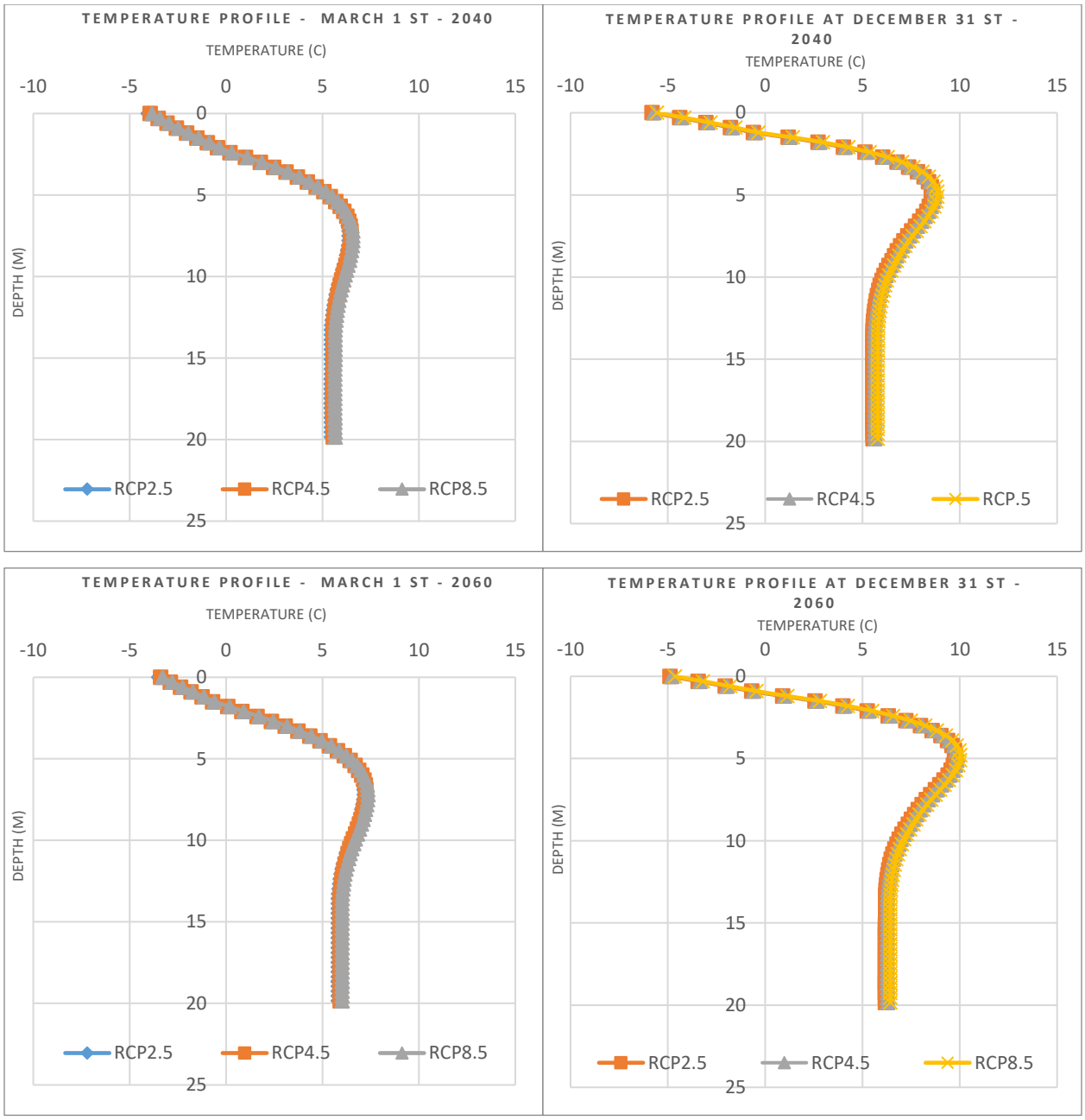

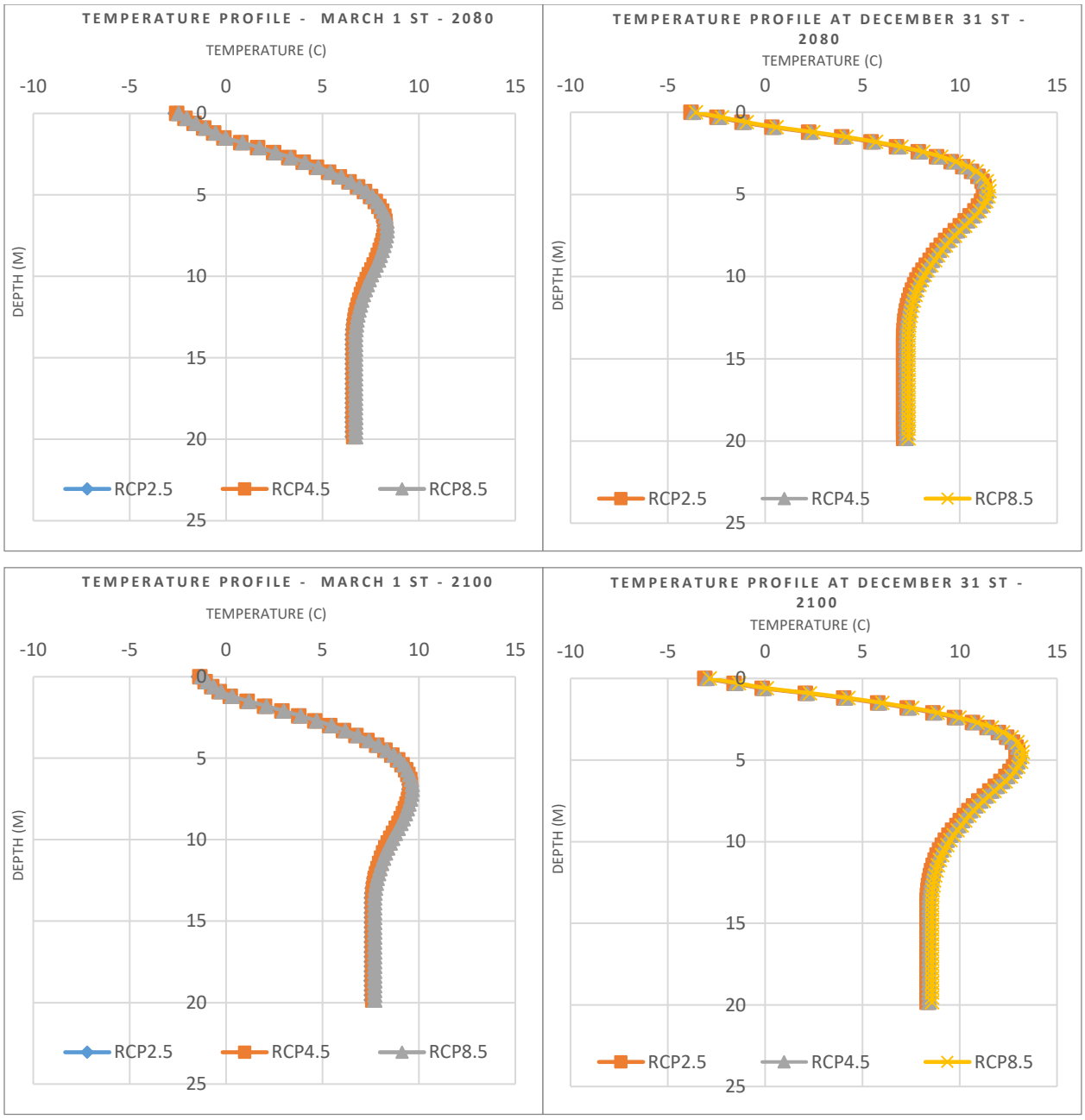

Figure 3.8.8: Temperature profiles at Mach 1st and December 1st in 2040, 2060, 2080 and 2100 for different RCPs - Sudbury

3.8.3 Ground temperature at different depths

Ground temperature at 1m, 2m, 3m, 4m, 15 m and 20m below the ground surface was reported along the full period of the analysis. These depths were selected to visualize the temperature variation and the impact of climate change at shallow and deep depths.

Since the climate conditions in 2020 represents the actual climate conditions, the ground temperature will not be affected by the climate change scenarios, thus, only one graph was reproduced to report the temperature at different depths of the sub-surface strata in the actual climate conditions.

Figures 3.8.9 to 3.8.12 summarize the ground temperature at 1m, 2m, 3m, 4m, 15 m and 20 m for Ottawa for the RCP8.5, RCP4.5 and RCP2.5, whereas Figures 3.8.13 to 3.8.16 present the temperature for Toronto and Sudbury for the RCP8.5 (all simulation results for RCP8.5, RCP4.5 and RCP2.5 are available in the Appendix C).

3.8.3.1 Ottawa:

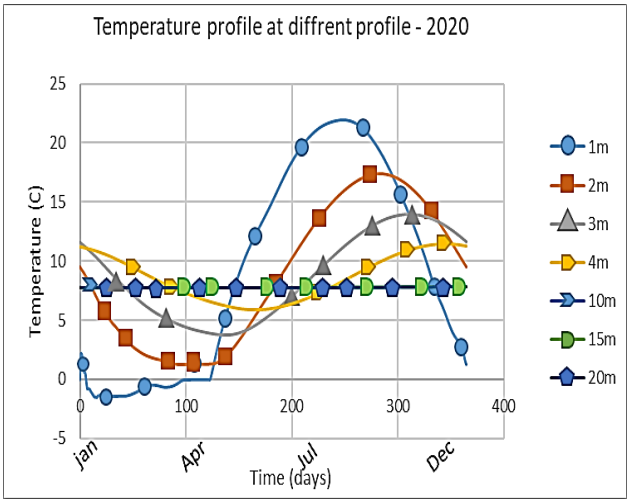

Figure 3.8.9: Temperature profile at different depths -2020 – Ottawa

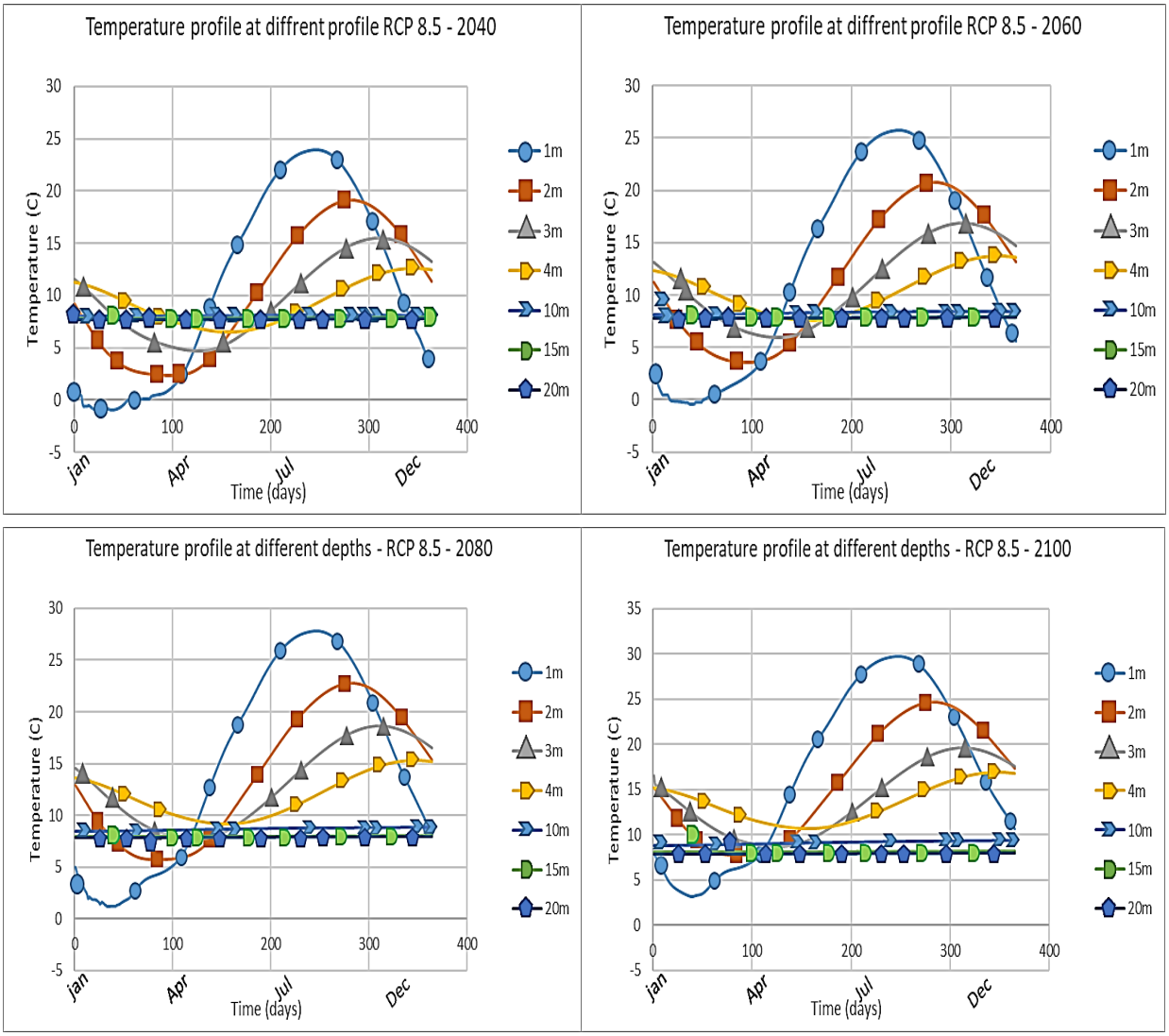

Figure 3.8.10: Temperature profile at different depths - RCP 8.5 - at 2040, 2060, 2080, 2100 – Ottawa

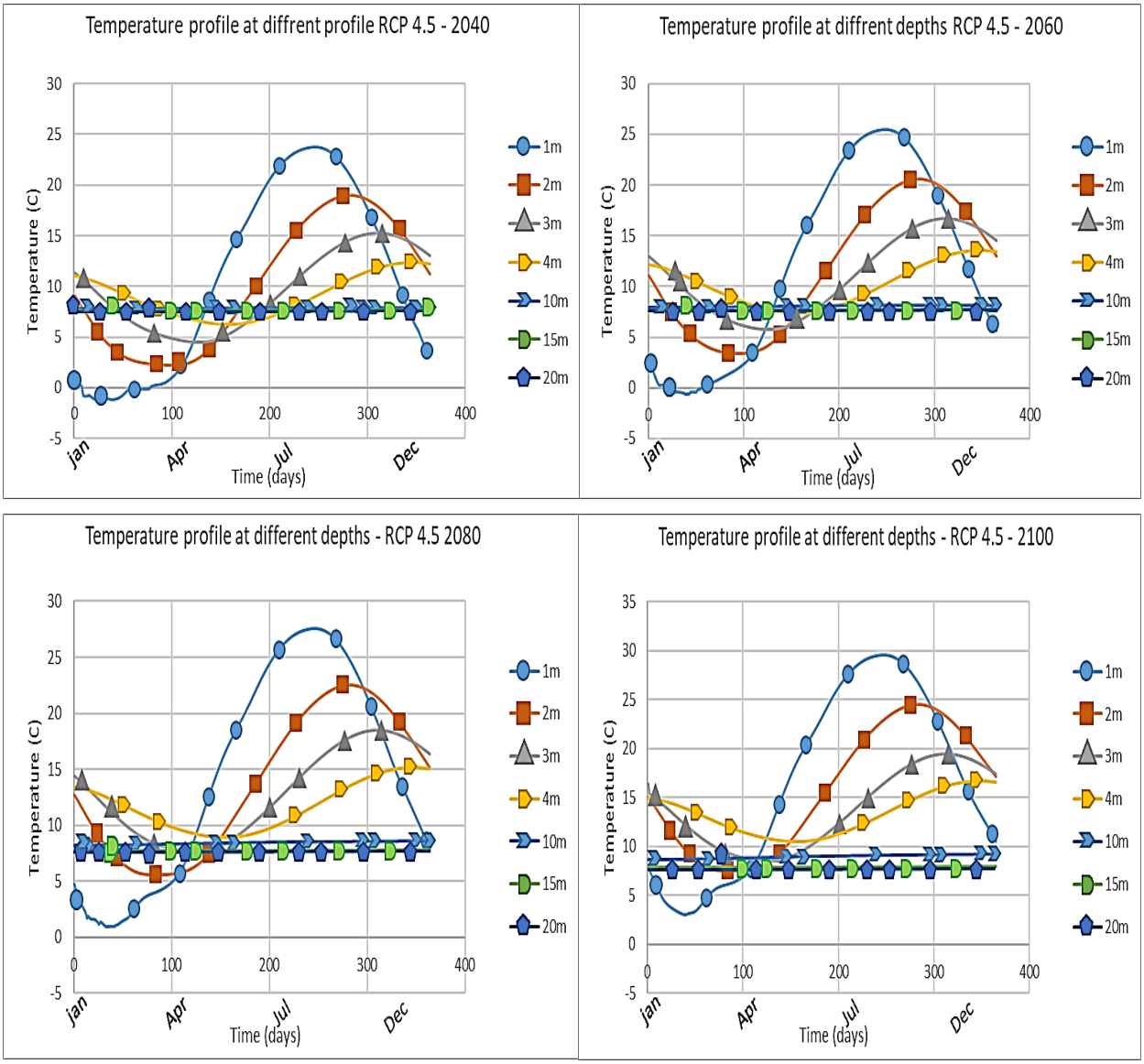

Figure 3.8.11: Temperature profile at different depths - RCP 4.5 - at 2040, 2060, 2080, 2100 – Ottawa

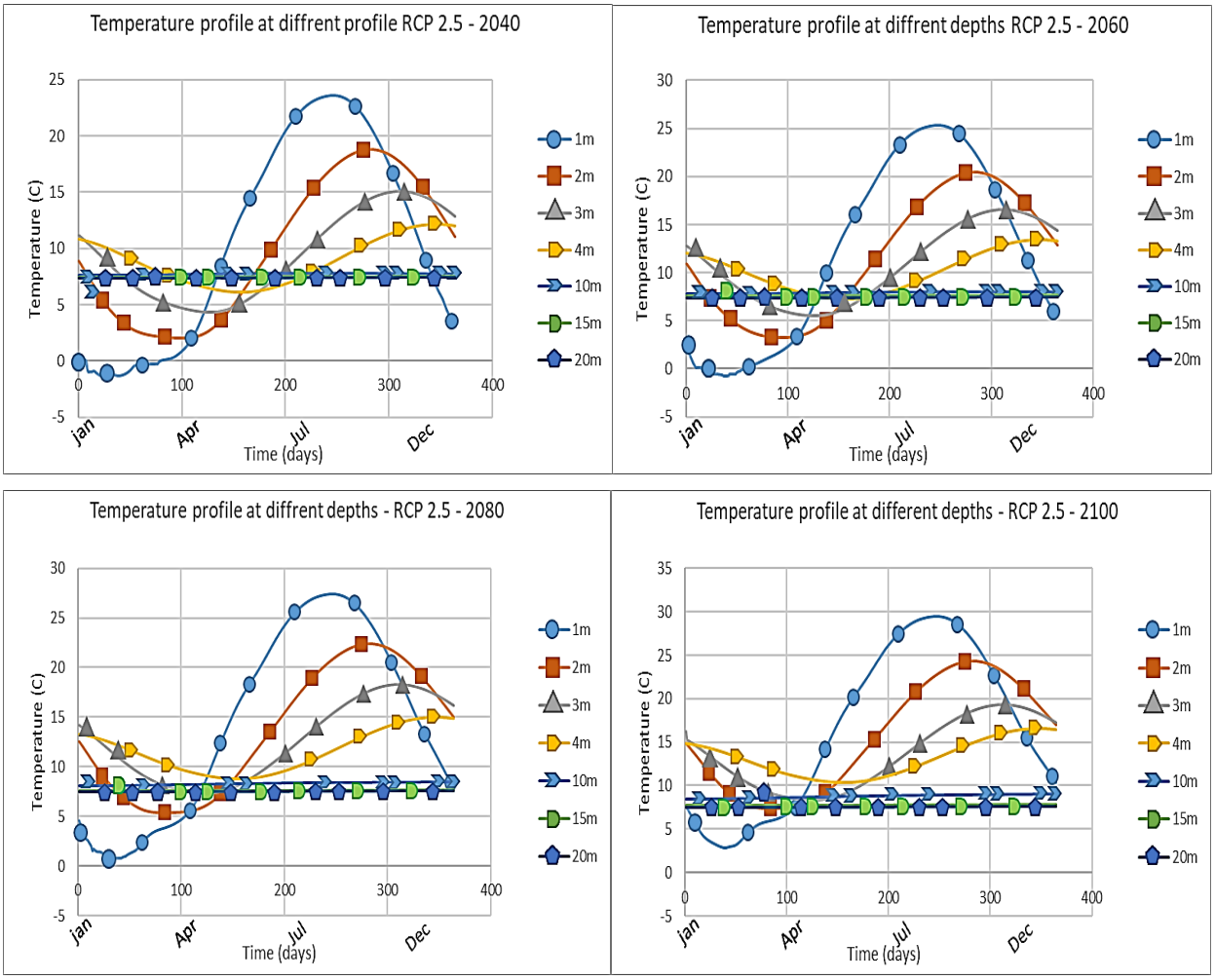

Figure 3.8.12: Temperature profile at different depths - RCP 2.5 - at 2040, 2060, 2080, 2100 – Ottawa

3.8.3.2 Toronto:

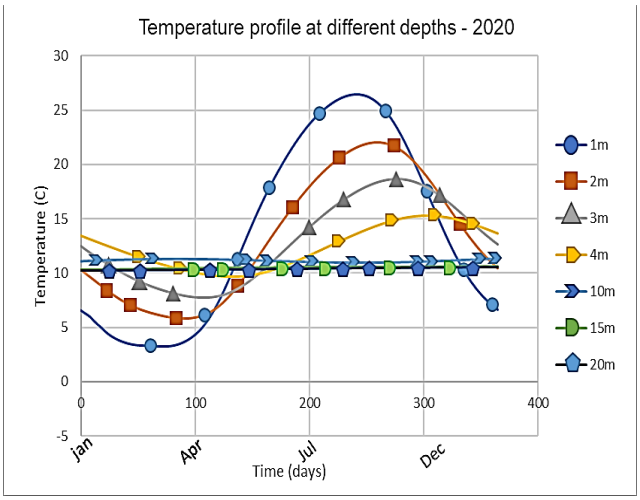

Figure 3.8.13: Temperature profile at different depths - 2020 - Toronto

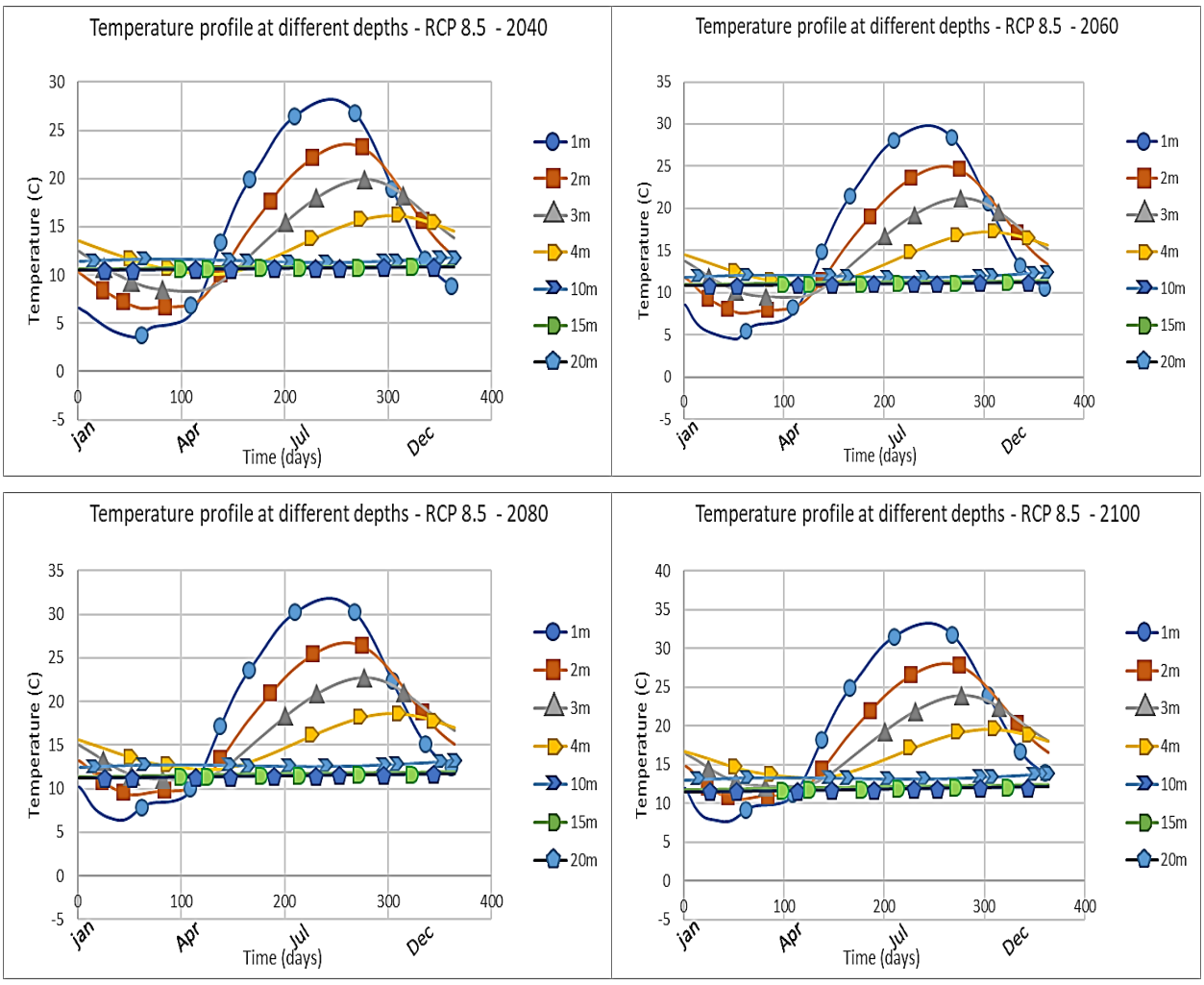

Figure 3.8.14: Temperature profile at different depths - RCP 8.5 at 2040, 2060, 2080, 2100 - Toronto

3.8.3.3 Sudbury:

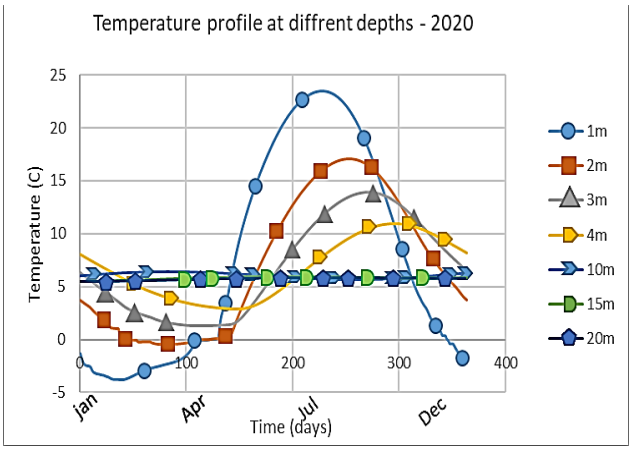

Figure 3.8.15: Temperature profile at different depths - 2020 – Sudbury

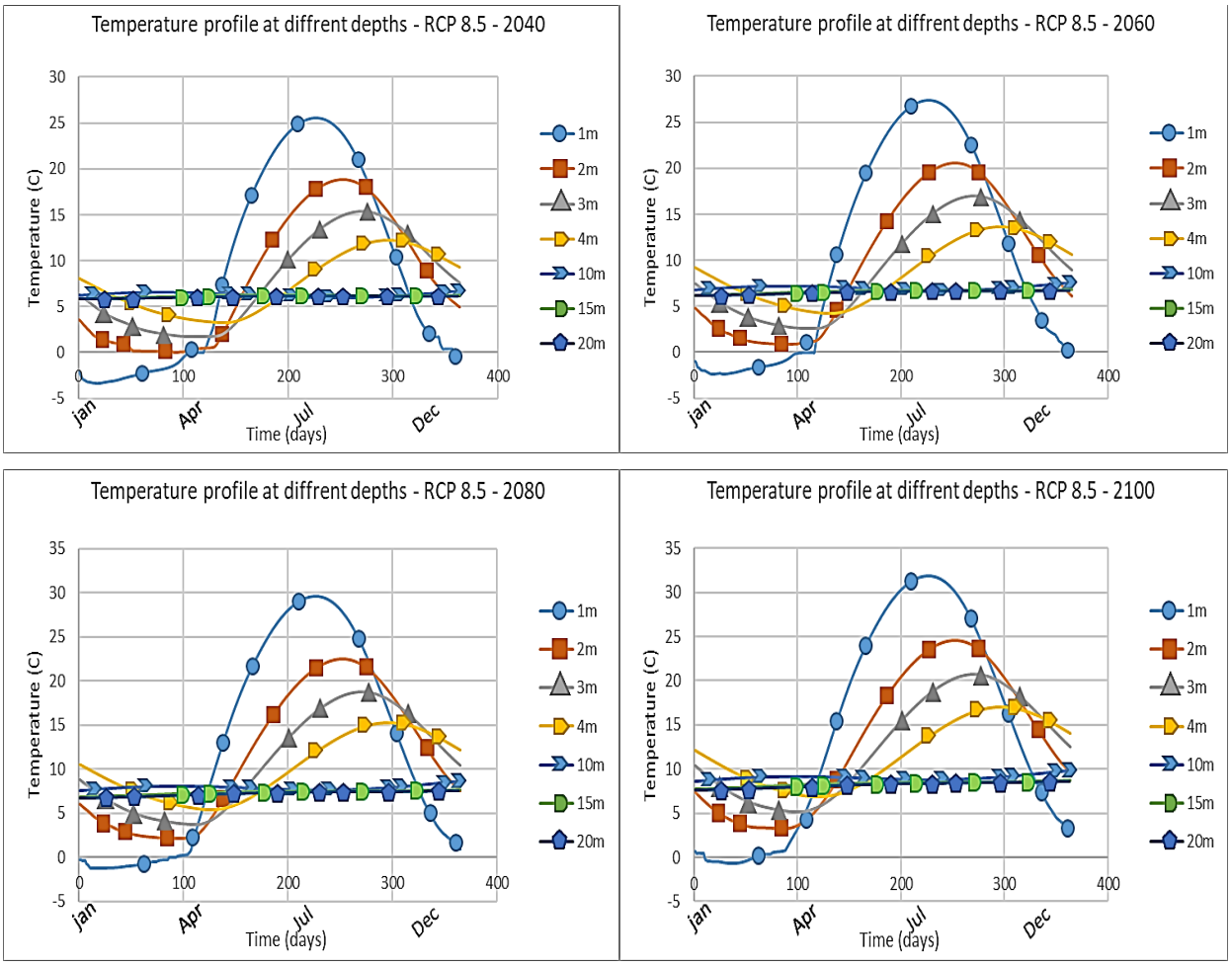

Figure 3.8.16: Temperature profile at different depths - RCP 8.5 at 2040, 2060, 2080, 2100 – Sudbury

3.8.4 Snow depth - Sensitivity analysis:

A sensitivity analyses was conducted to assess to the effect of the variation of snow cover in the study areas on the thermal regime of the ground. The variation of snow cover was modeled as a variation in the n_freezing factor in the cold season (Smith & Riseborough, 2002). In the summer season, the n_thawing factor varies with vegetation and surface cover (Klene et al. 2001), nevertheless, the variation of the summer cover conditions is not assessed. Therefore, the n_thawing factor remains constant in all the thermal simulations. Three additional case scenarios were considered in the sensitivity analysis; (i) a realistic higher n-factor that reflects a thinner snow depth, (ii) a realistic mean n-freezing factor reflecting a mean snow depth and (iii) a realistic lower n-factor that represents a thicker snow in the study areas (Smith & Riseborough, 2002). The sensitivity analysis was conducted only for the worst-case climate change scenario RCP8.5. Table 3.8.1 summarizes the values of the n-freezing and n-thawing factors used in the sensitivity analysis in the study areas.

Table 3.8.1: n-freezing and n-thawing factors used in the sensitivity analysis in the study areas (Smith & Riseborough, 2002)

Ottawa			
	Snow depth	n_thawing	n_freezing
Max Snow depth	47 cm	1.4	0.08
Min Snow depth	15 cm	1.4	0.35
Mean Snow depth	25 cm	1.4	0.15
Toronto			
	Snow depth	n_thawing	n_freezing
Max Snow depth	34 cm	1.4	0.05
Min Snow depth	6 cm	1.4	0.43
Mean Snow depth	15 cm	1.4	0.22
Sudbury			
	Snow depth	n_thawing	n_freezing
Max Snow depth	63 cm	1.4	0.11
Min Snow depth	20 cm	1.4	0.28
Mean Snow depth	35 cm	1.4	0.19

Figure 3.8.17 a, b, c represents the ground temperature profiles in March 1st, 2100 of Ottawa, Toronto and Sudbury for different snow cover conditions as follow:

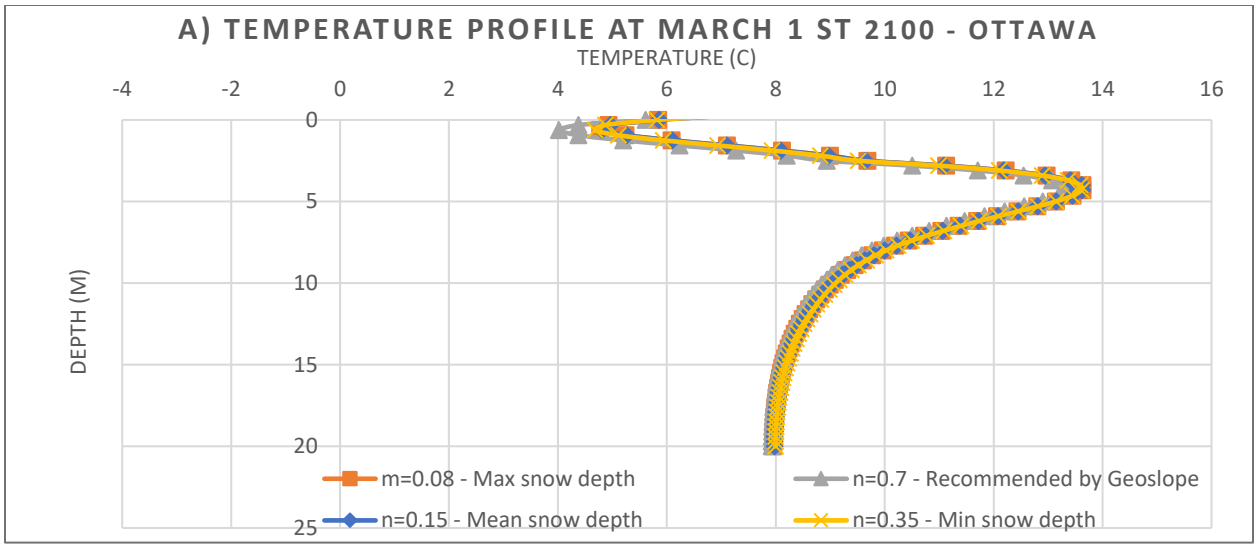

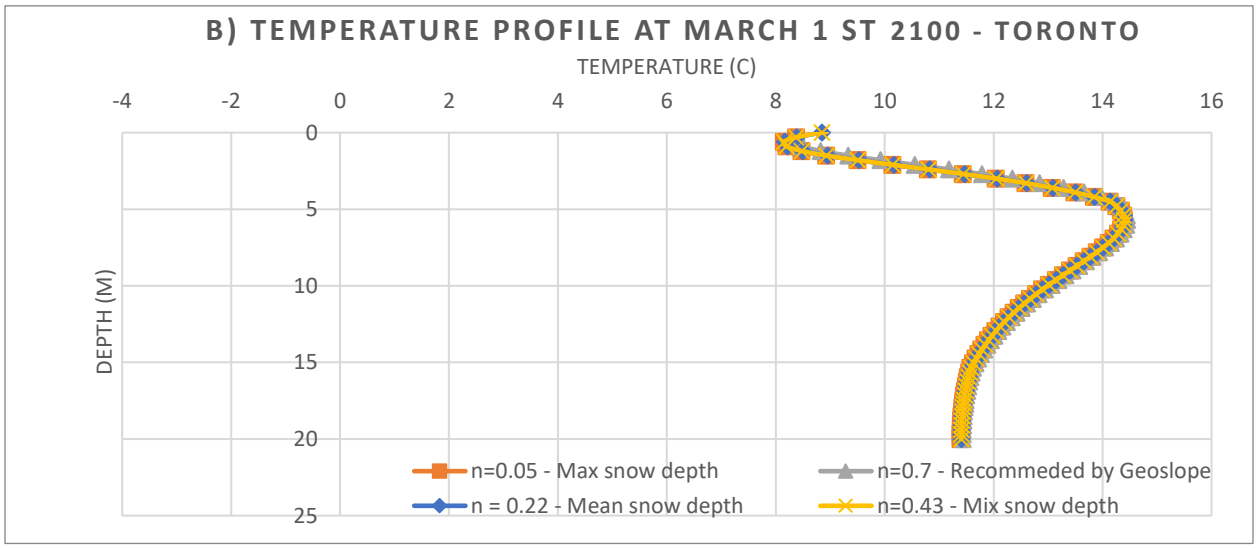

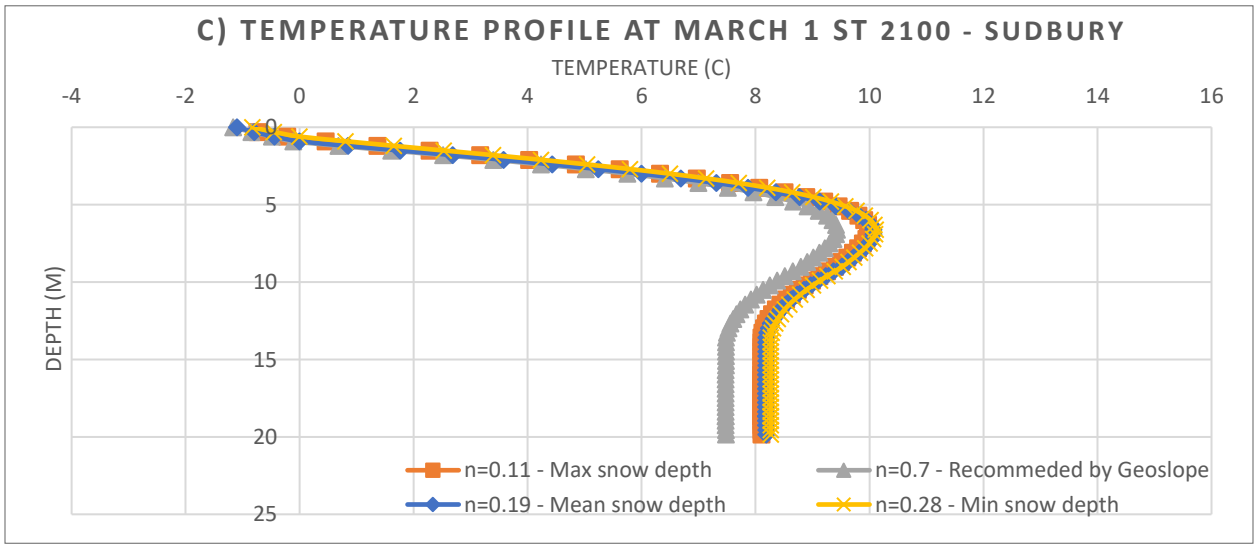

Figure 3.8.17: ground temperature profile in Mach 1st 2100 a) Ottawa, b) Toronto c) Sudbury

3.8.5 Discussion of results:

3.8.5.1 Impact of climate change on the ground temperature profiles in the study areas

Figure 3.8.1 through Figure 3.8.5 and Figures B-1 to B9 display the ground temperature profiles on March 1st and December 31st respectively in Ottawa, Toronto and Sudbury for the three climate change scenarios. The thermal regime in the beginning and the end of the winter season are similar in shape and profile with minor differences. It was observed that the general shape of the temperature profiles in the study areas show a nonlinear distribution of heat through the soil matrix. Temperature tends to become higher towards the bottom of all simulation models.

The temperature profile on December 31st reflects the expected behavior of the ground thermal regime within the three study areas during the winter season. Under the actual climate conditions, a frozen layer near the surface starts to form due to the impact of the cold air temperature in winter and continues to crawl down into the ground. On December 31st, 2020, the depth of the frozen layer is approximately 0.5 m in Ottawa, 0.1m in Toronto, and 0.9 m in Sudbury. The difference in the depth of the seasonally frozen layers in the study areas is mainly due to the climatic conditions. For instance, the higher frost depth is found in Sudbury where the climate is colder in winter. Accordingly, the lower frost depth is in Toronto where the climate is warmer is the winter season.

The temperature profile of March 1st represents the thermal behavior of the ground after 3 months of being exposed to the cold winter conditions. Although it is expected that ground temperature tends to become higher towards the bottom of the models, the results show an early warming stage of the frozen layer near the surface in Ottawa and Toronto. The development of the new thermal condition indicates that the freezing process had reached its maximum before March 1st. Accordingly, the thawing process starts to take effect within the seasonally frozen layer in Ottawa and Toronto. The maximum depths of the seasonally frozen layer observed in Ottawa and Toronto are approximately 1.3 m and 0.3m on March 1st, 2020, respectively. Due to the colder weather in Sudbury, the seasonally frozen layer is not yet affected by the early warming process on March 1st, 2020. Therefore, the ground surface temperature is colder than the layers underneath it. The maximum frost depth observed in Sudbury is 2.5 m on March 1st, 2020.

The ground temperature in the study areas undergoes a significant escalation from 2020 to 2100 for all the three Climate change scenarios. From 2020 to 2040, the ground temperature increases slightly due to the tiny increase in the air temperature. In fact, the effect of global warming will be clearly apparent by 2060 and will last for the whole duration of the simulation in the three study areas.

The thermal response of the ground varies according to the depth; it was noted that air temperature heavily influences the thermal regime of the first five meters of the sub-surface strata, but that effect gradually fades with depth. On the contrary, at deeper depths the ground thermal regime is controlled by the effect of the

geothermal gradient of the Earth.

The simulation results reveal a noticeable effect of climate change on the thermal regime of the top layers of the ground. From 2020 to 2100, the total increase in the temperature of the ground ranges between 1 °C at shallow depths to 4 °C at the depth of 5m in the three study areas. The ground surface and near surface layers temperatures experience a larger rise due to the direct interaction with the climate.

From a depth of 10 m to 20 m, the three sites showed a slightly different thermal behavior, in Ottawa, the ground temperature profiles at 2020, 2040, 2060, 2080, and 2100 overlap at the bottom of the model starting from a depth of 16 m. This behavior could be explained by the impact of the geo-thermal gradient on the model and the high thermal conductivity of the ground involved in the Ottawa model. In the presence of a ground with a high thermal conductivity, the impact of the geothermal gradient crawls up in the model leading to a constant ground temperature at greater depths (GEO-SLOPE International Ltd, 2014). However, in Toronto and Sudbury, there is no such convergence due to impact of climate change. The ground temperature will go on increasing with time even at greater depths. The ground thermal equilibrium is not observed at a depth of 20m in both study areas. In fact, the effect of the geothermal gradient will certainly be encountered at deeper level where ground temperature will become constant.

In the city of Ottawa, the frost depth is shifted up from 1.5m on March 1st, 2020 to 0 m on March 1st, 2100 for all the RCPs. Likewise, the frost depth completely disappears in Toronto on March 1st, 2100. The frost depth in Sudbury is shifted up from 2.5 m on March 1st, 2020 to 0.75 m in March 2100 for all the RCPs due to climate change.

A combined analysis was established to compare the results from the three-climate change scenarios. Figure 3.8.6 through figure 3.8.8 show the temperature profiles in 2040, 2060, 2080 and 2100 for Ottawa, Toronto and Sudbury for the three RCPs. The ground temperature slightly increases from RCP 2.5 to RCP4.5, and likewise, the temperature graphs slightly vary between RCP4.5 and RCP8.5. For instance, RCP8.5 provides the highest temperature values. The difference between the results provided by RCP 2.5 and 4.5 is in the order of a less than a half degree on March 1st and December 31st. Likewise, the difference between the RCP 4.5 and RCP8.5 does not exceed 0.2 degree Celsius in the three selected sites. All in all, the climate change scenarios do not seem to greatly affect the ground thermal response to global warming.

3.8.5.2 Effect of climate change on the ground profiles at specific depths

Figure 3.8.9 through figure 3.8.16 and Figures C-1 to C-12 display the ground temperature at depths of 1m, 2m, 3m, 4m, 10 m, 15m and 20 m for Ottawa, Toronto and Sudbury for the RCP 8.5, RCP4.5 and RCP 2.5. These depths were selected to provide an understanding of the thermal behavior at both shallow and deeper depths.

The temperature fluctuations of the ground are heavily impacted by the air temperature at shallow depths.

The ground thermal regime follows yearly periodic temperature cycles at 1m, 2m, 3m and 4m depth. The ground temperature fluctuates depending on the seasons creating a frost period where the ground freezes. The length of the frost period depends mainly on the climate conditions and the ground thermal properties. Therefore, it is different from a city to another. The longest frost period was observed in Sudbury, located in the north of the Canadian seasonal frost (no-permafrost) region and has the coldest climate in the winter between the three cities. The results showed that the frost period in Sudbury lasts for approximately 170 days under the actual climate conditions. Similarly, Ottawa experiences a frost period lasting for approximately 140 days. Toronto has the shortest frost period for approximately 120 days under the actual climate conditions.

Climate change had a significant impact on the length of the frost period in the three cities. It will gradually decrease from 2020 up to 2100. A loss of approximately 25% of the frost period was observed in the three cities by 2040. The frost period undergoes a continuous loss up to 2100 where it completely disappears in Ottawa and Toronto. In Sudbury the frost period becomes 65 days in the year. The three climate change scenarios showed approximately similar results.

3.8.5.3 Effect of snow cover on the thermal regime of the ground exposed to climate change

The effect of the snow cover on the thermal regime of the ground was assessed in a second sensitivity analysis in the three selected sites in the Canadian no-permafrost region. Figure 3.8.17 displays the soil temperature profiles on March 1st,2100 for different snow cover depths in Ottawa, Toronto and Sudbury.

Due to its low thermal conductivity, snow is as an excellent insulator between the atmosphere and the ground surface. The seasonal snow cover protects the ground from heat loss in winter resulting in higher ground temperatures (Goncharova et al., 2019). Essentially, the thicker the snow cover on the soil surface, the lesser is the heat loss from the ground to the atmosphere (Zhang, 2005).

The graphs reflect the expected thermal response of the ground to the variation of snow cover in all the study areas. However, results showed a minimal effect of the variation of the snow cover on the thermal regime of the ground in the three selected sites. The ground temperature difference is hardly noticeable between the realistic maximum, mean and minimum snow covers.

The value recommended by Geoslope for the n_freezing factors reflects an even thinner snow cover than the realistic minimum during the winter season in the three cities. Accordingly, it is interesting to note a slight drop in ground temperature in winter due to the minor insulation effect induced by the reduction of the snow cover in the three cities. In Sudbury, the excessive reduction of snow cover does not seem to influence the first 6m of the ground. However, a noticeable temperature drop, in the order of a degree Celsius, is observed starting from a depth of 6m and continues to the bottom of the model. As it is located

in the north of the Canadian no-permafrost region, Sudbury experiences the coldest winter weather of the three cities. Therefore, each winter, in the presence of a thick seasonal snow cover, the ground thermal equilibrium at greater depths is not affected by the cold air temperature, which helps the ground to maintain its temperature and prevents any heat loss at deeper levels. However, if the winter seasonal snow cover is thin, the insulation effect is reduced. This fact, affects the ground thermal equilibrium at greater depths, leading to an accumulated heat loss through the years. By 2100, The ground temperature at deeper depth will become colder in the presence of a thin snow cover than with a thicker one in Sudbury, which explains the temperature drop starting from a depth of 6m. In Ottawa and Toronto, the effect of the snow cover variation is not very apparent. The reduction of the snow cover appears not to have a significant effect on the ground thermal regime all along the depth of the models in both cities.

The net effect of snow cover on the thermal regime of the ground and its magnitude depend upon the timing and the severity of the climate condition in the winter season (Zhang, 2005). For example, in Sudbury, the climate is very severe in winter compared to Ottawa and Toronto (Meteoblue, 2018a); this helps the snow to accumulate and delays its melting process. Accordingly, the soil surface remains isolated from the atmosphere during the whole winter season without any interruption. On the other hand, in Ottawa and Toronto the climate is warmer during winter. On occasions, the air temperature on some winter days becomes higher than the freezing point, which induces a partial melting of the snow cover (Government of Canada, 2019). These air temperature fluctuations below and above the freezing point weakened the structure and the density of the snow cover leading to discontinuous snow covering. Due to all these reasons, the snow cover variation does not significantly influence the thermal regime in these two cities.

3.9 Summary and conclusions

This paper aims to study the impact of climate change on the thermal regimes of the ground in the Canadian seasonal frost region. The study was conducted for three cities (Ottawa, Sudbury and Toronto) located in different regions in the Canadian no permafrost area. The new research established future simulations of the ground thermal regime.

The first part of the research comprises the development and validation of an approach and simulation tool for the assessment of the impact of future climate on the thermal regimes of grounds in the study area. The second part of the research consists of assessing the impact of climate change on the thermal regimes of grounds in the study area by using the aforementioned simulation tool. Three climate change scenarios were considered in the study; RCP 2.5, RCP4.5 and RCP8.5. The RCP 8.5 represents the worst-case scenario in terms of climate change predictions. The RCP 2.5 is the optimistic climate change scenario. The study established the thermal regime of the ground in 2020, 2040, 2060, 2080 and 2100.

The study has come to the following conclusions:

1)- The developed numerical tool provided accurate results in simulating the ground thermal regime under different climate conditions. The validation model delivers good results in simulating the existing thermal conditions of the ground.

2)- The simulation results showed a gradual loss in the frost penetration depth due to the climate change, in the three representative sites. In Ottawa and Toronto, the seasonally frozen ground will disappear completely by 2100, in Sudbury, the frost penetration depth will become 0.75 m compared to 2.1 m in 2020.

3)-The frost period duration will be shorter due to climate change in the three selected sites and will totally vanish in Ottawa and Toronto. In Sudbury, the ground will likely remain frozen for only 80 days in 2100 compared to 180 days in 2020.

4)- The mean average ground temperature and the thickness of the seasonally frozen soil would have significant changes due to climate warming for the study period of 2020-2100. The mean average ground temperature would be much higher, and the frost penetration depth would be significantly reduced.

5)- The impact of climate change, would not appear clearly in the first 40 years “up to 2060”. The mean average ground temperature and the frost penetration depth would both slightly decrease in the first 40 years period followed by a significant decrease in the subsequent 40 years period in the three selected cities. This nonlinear effect implies that substantial changes could follow in a short timeframe and climate change will need at least 40 years to mobilize a significant change in the ground's thermal behaviour.

6)- The response of the ground to the impact of climate change varies with the geotechnical composition of the ground and the climate conditions. Overall, in the center and south of the study area, the changes are more significant than the north of the study area.

7)- Climate change scenarios would affect much the ground's thermal behavior, RCP2.5 and RCP4.5 would produce a similar impact, but slightly less severe than that RCP 8.5 could produce.

3.10 References:

Al-Umar, M., Fall, M., Daneshfar, B. (2020). GIS-based modeling of snowmelt-induced landslide susceptibility of sensitive marine clays. Geoenvironmental Disasters 7 (1), 1-18.

Booshehrian, A., Wan, R., & Su, X. (2020). Hydraulic variations in permafrost due to open-pit mining and climate change: a case study in the Canadian Arctic. In Acta Geotechnica (Vol. 15, Issue 4). https://doi.org/10.1007/s11440-019-00786-x

Bush, E., & Lemmen, D. . (2019). Rapport sur le climat changeant du Canada. https://www.rncan.gc.ca/sites/www.nrcan.gc.ca/files/energy/Climate-change/pdf/RCCC_FULLREPORT-FR-FINAL.pdf

Cambrian International. (2021). https://cambrianinternational.ca/

Charron, I. (2014). a Guidebook on Climate Scenarios : Using Climate Information to Guide Adaptation Research and Decisions. Ouranos.

Crawford, C. B., & Legget, R. F. (2002). NRC Publications Archive Archives des publications du CNRC Cool under fire.

Flynn, D. J. (2015). Field and Numerical Studies of an Instrumented Highway Embankment in Degrading Permafrost By.

GEO-SLOPE International Ltd. (2014). Thermal Modeling with TEMP / W. November.

Government of Canada. (2011). Historical Climate Record (Issue mm). https://climate.weather.gc.ca/

Government of Canada. (2018). Senarios and climate models. https://www.canada.ca/en/environment-climate-change/services/climate-change/canadian-centre-climate-services/basics/scenario-models.html#toc2

Government of Canada. (2019). Climate data viewer. https://climate-viewer.canada.ca/climate-maps.html#/?t=annual&v=tmax&d=dcs&r=rcp85&cp=-75.67013409675477,45.4091958833889&z=8&ts=2

Grasby, S. E., Majorowicz, J., & Ko, M. (2009). Geothermal maps of Canada. Geological Survey of Canada Open File 6167, 35.

Harlan, R.L., and Nixon, J.F. (1978). Ground thermal regime. Chapter 3 in Geotechnical Engineering for Cold Regions, ed. O.B. Andersland and D.M. Anderson. New York: McGraw-Hill, pp. 103-163.

Klene A.E., Nelson, F.E., Shiklomanov, N.I., and Hinkel, K.M. (2001). The N-factor in natural landscapes: Variability of air and soil-surface temperatures, Kuraruk River Basin, Alaska, USA. Arctic, Antarctic and Alpine Research 33(2): 140–148.

Meteoblue. (2018a). Weather Sudbury. https://www.meteoblue.com/en/weather/week/sudbury_united-kingdom_2636564

Meteoblue. (2018b). Weather Toronto.

https://www.meteoblue.com/en/weather/week/toronto_canada_6167865

Meteoblue. (2019). Weather Ottawa. https://www.meteoblue.com/en/weather/week/ottawa_canada_6094817

Natural Resources Canada. (2010). Geological Survey of Canada.

Orlando, B. A., & Ladanyi, B. (2004). Frozen Ground Engineering (4th ed.). John Wiley & sons.

Panikom, N. (2020). Climate change impact on rainfall-induced landslides in ottawa. University of Ottawa.

Rasmussen, L. H., Zhang, W., Hollesen, J., Cable, S., Christiansen, H. H., Jansson, P. E., & Elberling, B. (2018). Modelling present and future permafrost thermal regimes in Northeast Greenland. Cold Regions Science and Technology, 146 (April 2017), 199–213. https://doi.org/10.1016/j.coldregions.2017.10.011

Slattery, S. R., Andriashek, A. A., Jean, L. D., Stewart, G., Moktan, S. A., & Lemay T.G., H. (2011). Bedrock Topography and Sediment Thickness Mapping in the Edmonton–Calgary Corridor, Central Alberta: An Overview of Protocols and Methodologies. Energy Resource Conservation Board.

Smith, M. W., & Riseborough, D. W. (2002). Climate and the limits of permafrost: A zonal analysis. Permafrost and Periglacial Processes, 13(1), 1–15. https://doi.org/10.1002/ppp.410

Williams, P.J., (1964). Unfrozen Water Content of Frozen Soils and Moisture Suction. Geotehnique., vol. 14, pp. 133-142.

Zhang, T. (2005). Influence of the seasonal snow cover on the ground thermal Regime: an overview. In Simulation (Issue December). https://doi.org/10.1029/2004RG000157.1.Introduction

Zhou, F., Zhang, A., Li, R., & Hoeve, E. (2009). Spatio-temporal simulation of permafrost ge

othermal response to climate change scenarios in a building environment. Cold Regions Science and Technology, 56(2–3), 141–151. https://doi.org/10.1016/j.coldregions.2008.12.004

Chapter 4 - Numerical simulation of the ground thermo-hydro-mechanical response in Canadian no-permafrost regions to climate warming

Mohammed Yassir Marrah[a], Mamadou Fall[a], Husham Almansour[b]

a-Department of Civil Engineering, University of Ottawa, Ottawa, ON, Canada

b-National Research Council Canada, Ottawa, ON, Canada

Abstract:

Climate change, as noticed over the past decades, will inevitably changes in the thermo-hydro-mechanical behavior of Canadian no-permafrost soils. The thermal response of these soils to climate warming was assessed in a previous study, in which a significant increase in the ground temperature has been observed in different sites along the no-permafrost region in Canada. However, no study has been to examine the potential impact of climate warming on the hydro-mechanical response of these soils. Clear evidence confirm that climate change will continue for many decades and even centuries, irrespective of the success of global initiatives to decrease greenhouse gas emissions. Therefore, the understanding of the effect of climate warming on the thermo-hydro-mechanical behavior of the ground is of vital importance in designing resilient civil engineering structures that will meet the climate change requirements and support economic activities in all Canadian regions, particularly in Canadian no-permafrost areas. Within this framework, this paper presents the methodology and the results of modeling the thermo-hydro-mechanical response of grounds in three different sites located in the Canadian no-permafrost region to climate warming. The results show that future climate changes will affect the soil's hydro-mechanical regimes in Canadian no-permafrost regions. However, this effect is limited to the upper part of the ground. The numerical tool developed, and the results obtained will be useful for the geotechnical design of climate-adaptive transportation structures in Canadian no-permafrost areas.

4.1 Introduction

Temperature remains an important factor controlling both the hydraulic and the mechanical regimes of the ground. Particularly, in no-permafrost soils, the seasonal variation of ground temperature affects the equilibrium and motion of soil bodies creating a complex thermo-hydro-mechanical regime (Orlando & Ladanyi, 2004). The need for the analysis of the behavior of seasonally frozen soils arises often as a result of spectacular accidents, such as excessive settlements and failures of foundations. The freezing-thawing cycle changes the mechanical properties of soil through changing its structure and stiffness. It affects most geotechnical properties of the ground and induces upward movement of the soil body referred to as heave actions in winter and downward settlement action in the thawing season (Orlando & Ladanyi, 2004).

Frost actions require a supply of water and decrease in temperature to induce the freezing of water in the ground (Orlando & Ladanyi, 2004). In the cold season, the in-situ ground water freezes, forming ice layers within the soil body. When ice forms underground, it expands causing an upward or outward movement of the ground surface (National Snow and Ice data center, 2020).

Several factors influence the amount and distribution of ice in frozen ground. This includes for instance, composition and thermal properties of the soil and moisture and structural changes histories. The volumetric expansion (strain) during the freezing period is a function of the soil porosity (n) and the soil initial volume. Commonly, the formation of ice induces a volumetric strain estimated as 0.09 n (Orlando & Ladanyi, 2004). On the contrary, during the thawing season, the rise in temperature induces the melting of frozen water and causes structural change in the soil skeleton. The dissipation of water implies a change in the void ratio (e); therefore, the soil under the existing overburden and the applied (if any) pressures must adapt itself to the new equilibrium void ratio (Orlando & Ladanyi, 2004).

Thaw settlement represents a significant matter in the design of buildings, foundations, embankments, buried pipelines and road and highways in cold regions. It raises several design challenges including a significant loss of soil shear strength and excessive settlement, which may affect the serviceability of all structures mentioned above and could induce their entire failure (Zhang, 2005). The thawing process is defined as the movement of the surface thermal boundary condition (Ts> 0° C) through the frozen soil to a given depth. Two factors are responsible for soil thawing settlement: ice phase change (ice to water) and the dissipation of excess water out of the soil. Thaw settlement is more significant in fine-grained soils where slow freezing permits important ice segregation (Orlando & Ladanyi, 2004). Ice segregation induces local soil consolidation leading to more water in the thawing period.

The first thaw-consolidation tests were performed by Tsytovich approximately 70 years ago. Tsytovich conducted thaw consolidation tests using a simple oedometer and measured settlement in rapid thawing

soils under different loading conditions (Lesage, 2008). Tsytovich's experiments concluded that the compressible behaviour of the soil skeleton could be modeled using the Terzaghi consolidation theory. Morgenstern and Nixon (1971) used Tsytovich's results to establish the thaw consolidation theory and describe the mechanical, thermal and hydrological processes that occur in soils in the thawing season (Lesage, 2008).

Harlan (1973), Guymon and Luthin (1974), Taylor and Luthin (1978), and Jame and Norum (1980) have all contributed to establishing the first fundamental governing equations of the coupled thermo-hydro-mechanical process in soils. Numerical methods were provided to solve these governing partial differential equations; however, due to the lack of computational tools, the use of these solutions was very limited. As finite element methods developed, the THM modeling was widely used in both research and practice (Zhang, 2014).

The numerical modeling of the coupled thermo-hydro-mechanical interaction in no-permafrost soils using finite element method was established to a very limited extent in previous studies. THM models, however, were mainly established to simulate the THM mechanism in rocks. Veinović et al. (2020) developed a thermo-hydro-mechanical model using TEMP/W, SEEP/W and SIGMA/W software from geoslope package to detect the effect of the Spent Nuclear Fuel waste on the repository in crystalline rocks in the Krško nuclear power plant. The results of the THM model confirmed that the crystalline rocks are suitable to host the spent nuclear waste resulting from the Krško nuclear power plant (Veinović et al., 2020). The application of FEM to assess the coupled thermo-hydro-mechanical of the soils is used to a limited extent in literature. Studies focused mainly on the development of the constitutive models of the coupled THM analysis. Cui et al. (2000) established a thermomechanical model for saturated clays. The study proposes a modified Cam clay constitutive model to capture the coupling and hardening phenomena related to the combined effects of stress and temperature (Cui et al., 2000). In another study, an alternative coupled thermo-hydro-mechanical finite element formulation for fully saturated soils is established by Potts et al (2018). The research provides a bespoke finite element code to simulate the coupled THM processes in fully saturated soils. The proposed formulation was implemented in the Imperial College Finite Element Program (ICFEP) and validated against a triaxial undrained heating test reported by Abuel-Naga et al. The new THM formulation succeeded to simulate the thermally induced excess pore water under a constant applied load in fully saturated clay samples to a large extent (W. Cui et al., 2018).

The application of FEM to simulate the coupled thermo-hydro-mechanical of the ground in practical engineering problem remains very limited. Particularly, in no-permafrost or seasonal frost soils, no case study was found to simulate the complex THM interactions occurring in the soil in the freezing and thawing seasons, nor the impact of climate change on the THM regime of no-permafrost soils. Therefore, due to the lack of research on this topic, this modeling study has been undertaken with the aim to understand and

assess the effect of climate change on the thermal, hydraulic, and mechanical regime of grounds located in the Canadian no-permafrost region. The no-permafrost areas selected in this study are in East-central Canada (Ontario, Canada).

4.2 The study area

4.2.1 Geographical description of the study area

The region of interest in this study is the no-permafrost area in Canada. This region extends from the Atlantic coast in the east to the pacific west coast running mainly through the whole south of Canada (Natural Resources Canada, 2010). Due to the large geographical extend, three sites located in the Ontario (east-central Canada) no-permafrost region were selected. These sites include Sudbury and Toronto to represent the center, the north and the south of the Canadian no-permafrost region in Ontario, Canada.

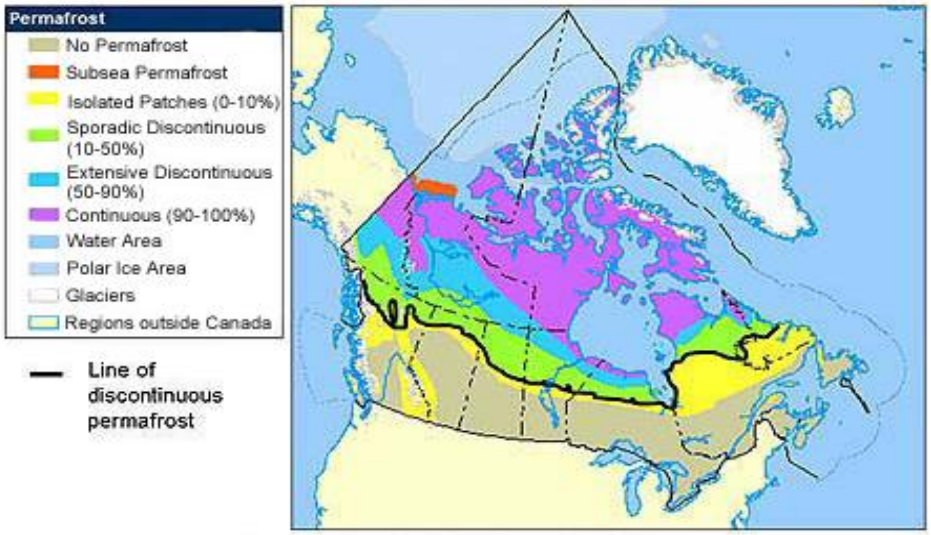

Figure 4.2.1: The geographical limits of the Canadian no-permafrost region (Booshehrian et al., 2020)

Figure 4.2.2: Location of Ottawa, Toronto and Sudbury within Ontario (Cambrian International, 2021)

4.2.2 Representative soil profiles of the study area

The Canadian no-permafrost region embraces several geological patterns; therefore, soils have dissimilar geotechnical and physical properties within this region (Natural Resources Canada, 2010). The national geological survey of Canada provides borehole logs of several sites among the Canadian territory including Ottawa, Toronto and Sudbury. Accordingly, the geotechnical profiles of the three cities were developed based on the information included in the borehole logs of the national survey. Essentially, for the first 20 m into the ground, the soil composition comprises layers of clay, silt, sand and gravel. The bedrock layer was not detected in the representative boreholes (Natural Resources Canada, 2010). Beside the soil profile, the borehole logs include recordings of the relative density, temperature of the soil with depth and the velocity of the P waves in the sublayers of the soil stratum (Natural Resources Canada, 2010). Figure 4.2.3 a, b and c represents the geotechnical composition and the geometry of the three selected sites for the THM simulation.

a)

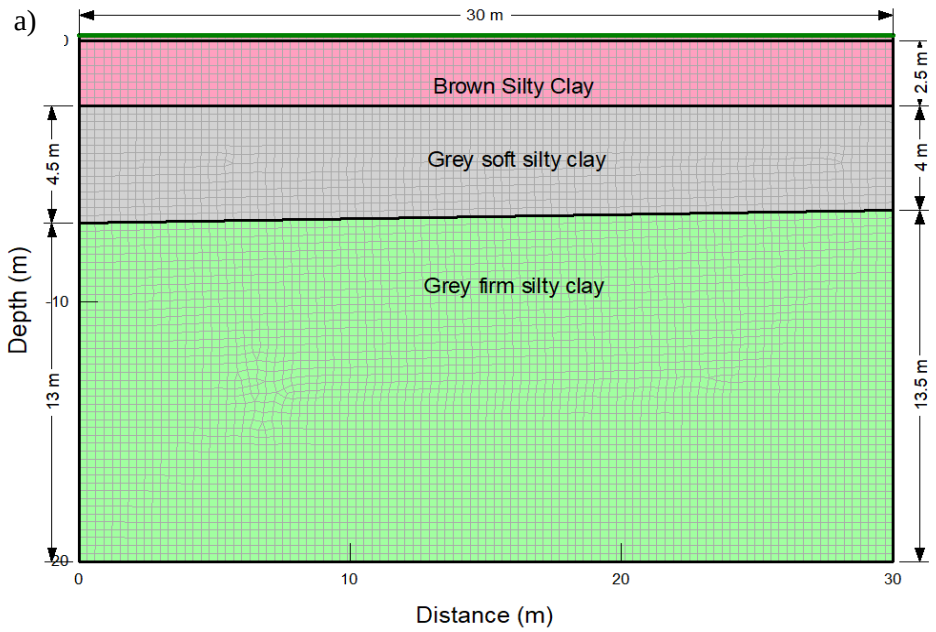
30 m
Brown Silty Clay
Grey soft silty clay
Grey firm silty clay
2.5 m
4 m
13.5 m
4.5 m
13 m
Depth (m)
0
10
20
30
Distance (m)

b)

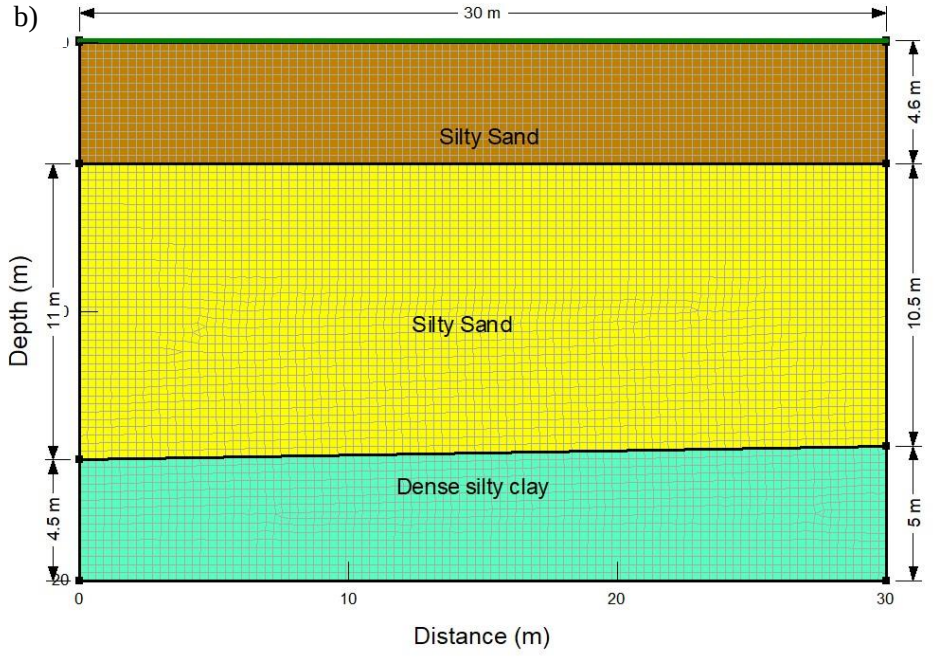
30 m
Silty Sand
Silty Sand
Dense silty clay
4.6 m
10.5 m
5 m
11 m
4.5 m
Depth (m)
0
10
20
30
Distance (m)

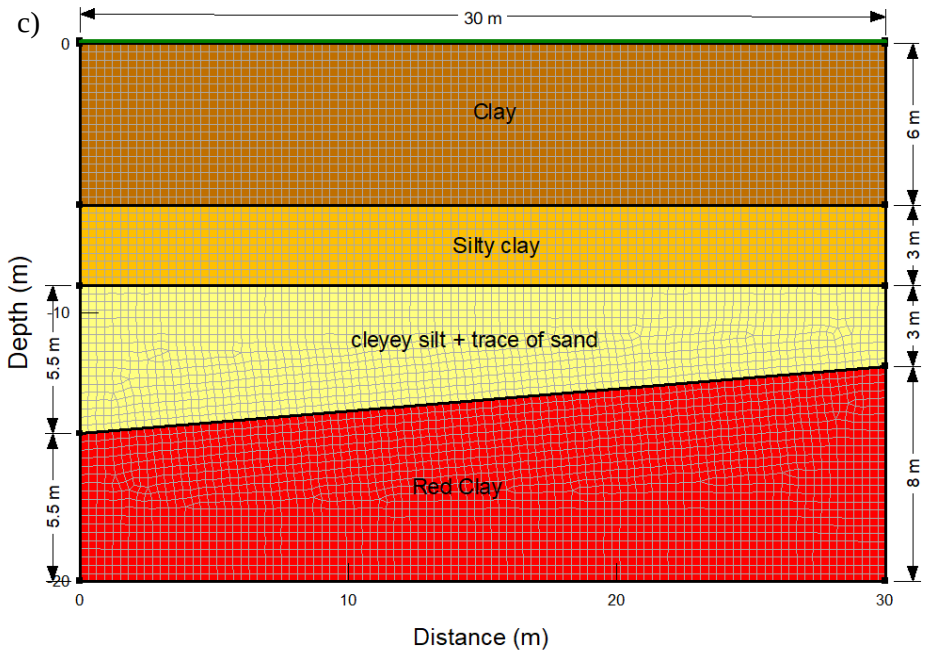

Figure 4.2.3: a) Ottawa simulation model geometry, b) Toronto simulation model geometry, (c) Sudbury simulation model geometry

4.3 Methodology

4.3.1 Approach

Figure 4.3.1 displays the developed approach or method for the assessment of the impact of future climate on the thermo-hydro-mechanical regimes of the grounds in the selected Canadian no-permafrost regions and the relationship between the different work stages of the studies performed. The first stage of the analysis deals with the establishment of the simulation tools used to build a coupled thermo-hydro-mechanical model. The development of numerical models and simulations were carried out with coupling three main softwares from GeoStudio package. The selected softwares are TEMP/W, SEEP/W and SIGMA/W. The second stage deals with the validation of the coupled softwares or simulation tool against field data. The third stage comprises the acquisition of the climate data and the climate change predictions for the study area to establish the thermal models in TEMP/W software (Government of Canada, 2019). For sensitivity analysis purposes, two climate change scenarios, namely RCP4.5 (medium global emission scenario) and RCP8.5 5 (high global emission scenario) were considered in the present study. The fourth stage entails the acquisition of the required thermal, hydraulic and mechanical properties of the grounds in the studied sites, in addition to the in-situ site conditions including the thermal, hydraulic and mechanical boundary conditions, which were used as input data in the thermo-hydro-mechanical models. In the fifth stage of this investigation, numerical modeling, and simulations of the effect of future climates on the

thermo-hydro-mechanical responses of the grounds in the studied sites were conducted. Subsequently, the simulation results were integrated and analyzed. The proposed approach or method developed in this paper can be also adopted or adapted to simulate the ground thermo-hydro-mechanical regime under changing climate conditions in other no-permafrost regions in Canada or around the world. The aforementioned stages are described in detail below.

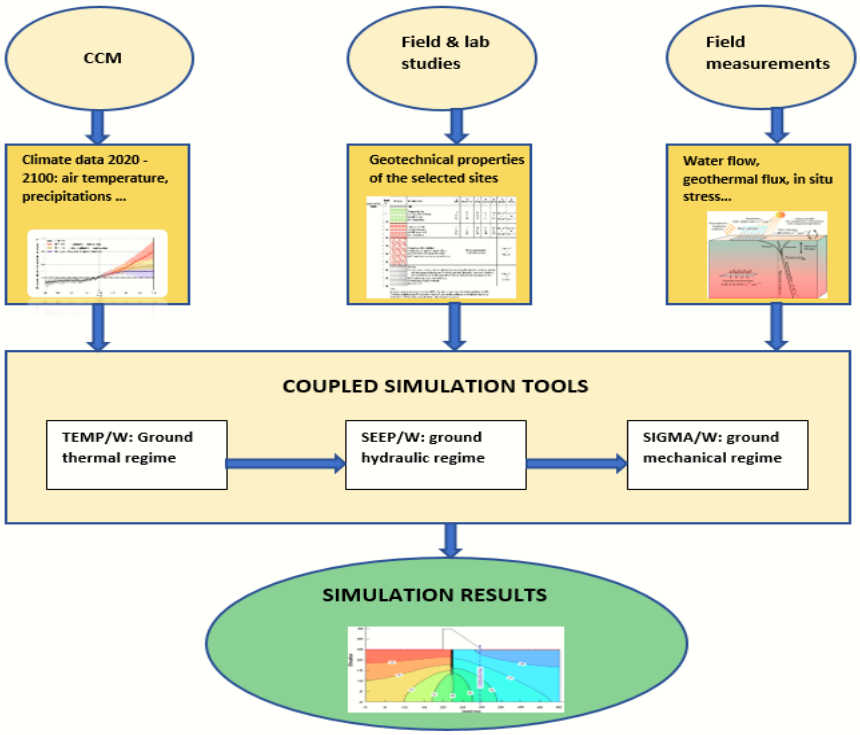

Figure 4.3.1: Developed methodology for assessing the THM response of the soils in Canadian no permafrost areas to climate change (CCM: climate change model)

4.3.2 Governing equations, constitutive models, and coupling procedures.

In the present study, Geostudio package was selected to proceed with the thermo-hydro-mechanical simulations. This software is a finite element package that comprises several modelling programs including, SEEP/W to model the groundwater flow in saturated and non-saturated conditions in porous materials (GEO-SLOPE International Ltd, 2012), SIGMA/W for stress and deformation analysis of soil and structural materials (GEO-SLOPE International Ltd, 2013) and TEMP/W for modeling heat transfer and phase changes through fully or partially saturated and fully or partially thawed material (Veinović et al., 2020). To establish the coupled thermo-hydro-mechanical analysis in this paper, TEMP/W, SEEP/W and SIGMA/W were coupled. The process of coupling these three programs is possible through a simulation sequence described below.

4.3.3 TEMP/W

TEMP/W governing equation describes the conduction as the main mechanism of the heat transfer in the soil (Harlan & Nixon, 1978). Therefore, the heat flow in soil can be considered analogous to heat flow in a solid to which Fourier's Law is applied:

Equation 4.3.1: Conduction equation:

$$q = -k * \left(\frac{dT}{dx}\right)$$

The heat flux, q (J/sec), directly depends on the thermal conductivity, k (J/(sec × m × °C)), and the change of temperature, T (°C), over a distance, x (m).

The differential equation that governs the formulation of 2D numerical solutions in TEMP/W can be expressed as follows:

Equation 4.3.2: General 2D heat flow formulation (Harlan & Nixon, 1978):

$$\frac{\partial}{\partial x}\left(k_x \frac{\partial T}{\partial x}\right) + \frac{\partial}{\partial y}\left(k_y \frac{\partial T}{\partial y}\right) + Q = \lambda \frac{\partial T}{\partial t}$$

Where T = temperature, kx = thermal conductivity in the x-direction, ky = thermal conductivity in the y-direction, Q = applied boundary flux, (J/ (m^3 × °C) = capacity for heat storage, and t = time.

The amount of heat energy stored depends on the thermal properties of the soil therefore the capacity to store heat "λ" is expressed as follows (GEO-SLOPE International Ltd, 2014):

Equation 4.3.3: The capacity to store heat (Williams, 1964):

$$\lambda = c + L \frac{\partial w_u}{\partial T}$$

Where c = volumetric heat capacity (material property), L (J/m3) = latent heat of water, wu = total unfrozen volumetric water content and T = temperature,

Substituting for λ in the main thermal equation leads to the complete 2D heat flow differential equation:

Equation 4.3.4: 2D heat flow formulation at transient analysis (GEO-SLOPE International Ltd, 2014):

$$\frac{\partial}{\partial x}\left(k_x \frac{\partial T}{\partial x}\right) + \frac{\partial}{\partial y}\left(k_y \frac{\partial T}{\partial y}\right) + Q = \lambda \frac{\partial T}{\partial t} = \left(c + L_w \theta \frac{\partial \theta_u}{\partial T}\right)\frac{\partial T}{\partial t}$$

where Q is the heat flux, kx and ky are the thermal conductivities in the x and y directions, λ the capacity for heat storage, t time. The capacity to store heat in the soil λ is composed of two parts: the volumetric heat capacity, c, that depends on whether the material is frozen or unfrozen, and L, the latent heat of fusion of the material. The latent heat calculation requires the volumetric water content, θ, the unfrozen volumetric water content, θu and L_w the latent heat of water.

In the coupled heat and water transfer analysis, both the thermal and hydraulic simulations are run simultaneously in order to take into account the convective heat transfer that occurs due to flowing water and examine the effect of temperature change on the water flow in the soil. Once coupled with SEEP/W, the TEMP/W governing equation of the heat transfer is modified to:

Equation 4.3.5: General 2D coupled water and heat flow formulation (Harlan, 1973 and Flerchinger & Saxton, 1989):

$$\left(\rho_s c_{ps} + L_w \theta_w \frac{\partial \theta_u}{\partial T}\right)\frac{\partial T}{\partial t} = \frac{\partial}{\partial y}\left(k_y \frac{\partial T}{\partial y}\right) + \rho_w c_{pw} \frac{\partial (q_w T)}{\partial y} + Q$$

Where $\rho_s c_{ps}$ is volumetric heat capacity of soil, $\frac{\partial \theta_u}{\partial T}$ the slope of the unfrozen water content function and q_w the specific discharge (Darcy velocity) of water.

4.3.4 SEEP/W

SEEP/W is formulated only for flow through both saturated and unsaturated soil that follows Darcy's law (GEO-SLOPE International Ltd, 2014). The general formulation of Darcy's law is as follows:

Equation 4.3.6: Darcy's law equation:

$$q = k * i$$

where: q = the specific discharge (m/sec), k (m/sec) = the hydraulic conductivity and i= the gradient of total hydraulic head.

The differential equation that governs the formulation of 2D numerical solutions in SEEP/W can be expressed as follows:

Equation 4.3.7: General 2D water flow formulation (Richards, 1931 and Childs & Collins-George, 1950):

$$\frac{\partial}{\partial x}\left(k_x \frac{\partial H}{\partial x}\right) + \frac{\partial}{\partial y}\left(k_y \frac{\partial H}{\partial y}\right) + Q = \frac{\partial \theta}{\partial t}$$

Where H = the total head (m), kx = hydraulic conductivity in the x-direction (m/sec), ky = hydraulic conductivity in the y-direction (m/sec), Q (m^3 /sec) = applied boundary flux, θ ($m^{3/}$ m^3) = the volumetric water content, and t = time.

SEEP/W is formulated for conditions of constant total stress; that is, there is no loading or unloading of the soil mass and assumes that the pore-air pressure remains constant at atmospheric pressure during transient processes (GEO-SLOPE International Ltd, 2012). Therefore, the change in volumetric water content can be related to a change in porewater pressure by the following equation:

Equation 4.3.8: porewater variation equation (GEO-SLOPE International Ltd, 2012):

$$\partial\theta = m_w \gamma_w \, \partial H$$

Where: m_w (m^3/KN) = the slope of the storage curve and γ_w (KN/ m^3) = the unit weight of water.

Therefore, the governing differential equation used in SEEP/W finite element formulation becomes:

Equation 4.3.9: General 2D water transfer formulation (GEO-SLOPE International Ltd, 2012):

$$\frac{\partial}{\partial x}\left(k_x \frac{\partial H}{\partial x}\right) + \frac{\partial}{\partial y}\left(k_y \frac{\partial H}{\partial y}\right) + Q = m_w \gamma_w \frac{\partial H}{\partial t}$$

4.3.5 SIGMA/W

The displacements are formulated based on incremental analysis in SIGMA/W (GEO-SLOPE International Ltd, 2013). For each time step, an incremental displacement is calculated based on the incremental load and cumulatively added to the displacement from the previous time step. SIGMA/W can only calculate the end conditions of a stress-strain problem if the in-situ conditions were defined prior to loading. The governing equation of SIGMA/W for two-dimensional plane strain analysis is as follow (Bathe, 1982, Smith and Griffiths, 1988, Segerlind, 1984 and Zienkiewicz and Taylor, 1989):

Equation 4.3.10: governing equation of SIGMA/W for two-dimensional plane strain analysis (GEO-SLOPE International Ltd, 2013):

$$t\int_a [B]^T[C][B]dA\{a\} = bt\int_l \langle N\rangle^T dA + pt\int_l \langle N\rangle^T dL$$

Where: t = constant unit element thickness, A = area along the boundary of an element, [B] = strain-displacement matrix, [C] = constitutive matrix, {a} = column vector of nodal increments x- and y-displacements, b = unit body force intensity, <N> = row vector of interpolating functions, p = incremental surface pressure and L = length along the boundary of an element.

Modeling in SIGMA/W requires information about the in-situ stress loading and the porewater condition; therefore, SEEP/W can be coupled with SIGMA/W to describe the in-situ hydraulic conditions required to run the mechanical simulation. Nevertheless, at the time of this study, GeoStudio cannot simulate thaw consolidation. Being said, a fully coupled thermo-hydro-mechanical analysis using SIGMA/W, TEMP/W and SEEP/W is not possible using the GeoStudio package. As an alternative, a coupled heat and water transfer analysis is to be established first, to investigate how thawing conditions affect water flow. Subsequently, a coupled water and stress analysis should be conducted to examine coupled consolidation. SIGMA/W includes three main different constitutive models for effective analysis with porewater pressure change: Linear elastic, Elastic-plastic (Mohr-Coulomb or Tresca) and soft Clay - Modified Cam-clay (Critical State). Moreover, SIGMA/W allows a fourth option to create a user add-in constitutive model that best describes the stress-strain behavior of the user's model.

4.4 Validation of the simulation approach / tool

4.4.1 Model geometry, material properties and boundary conditions:

4.4.1.1 Geometry:

The validation model was built using field measurement data from previous geotechnical investigations that focused on a section of highway embankment on Provincial Road (PR) 391 located 18 km north of Thompson, Manitoba (Flynn, 2015). The geometry of the validation model (Figure 4.4.1) is retrieved from a past master's thesis manuscript by Flynn (2015). This manuscript includes temperature, porewater pressures and vertical displacement field measurements of soil temperature from September 25th , 2012 to September 25th , 2014 (Flynn, 2015). The model geometry represents a half embanquement with a bare soil extention. It extends 40 m laterally from the centreline, and to a depth of 18 m below the natural ground surface. The model depth extends to the bedrock at a depth of 18 m and since the thermistor strings were installed to bedrock. The model used a finite element mesh size of 0.2 m by 0.2m. Finer dimensions were tested; however, the software was not able to establish the analysis due to storage limitations. The geometry of the validation model is represented in Figure 4.4.1.

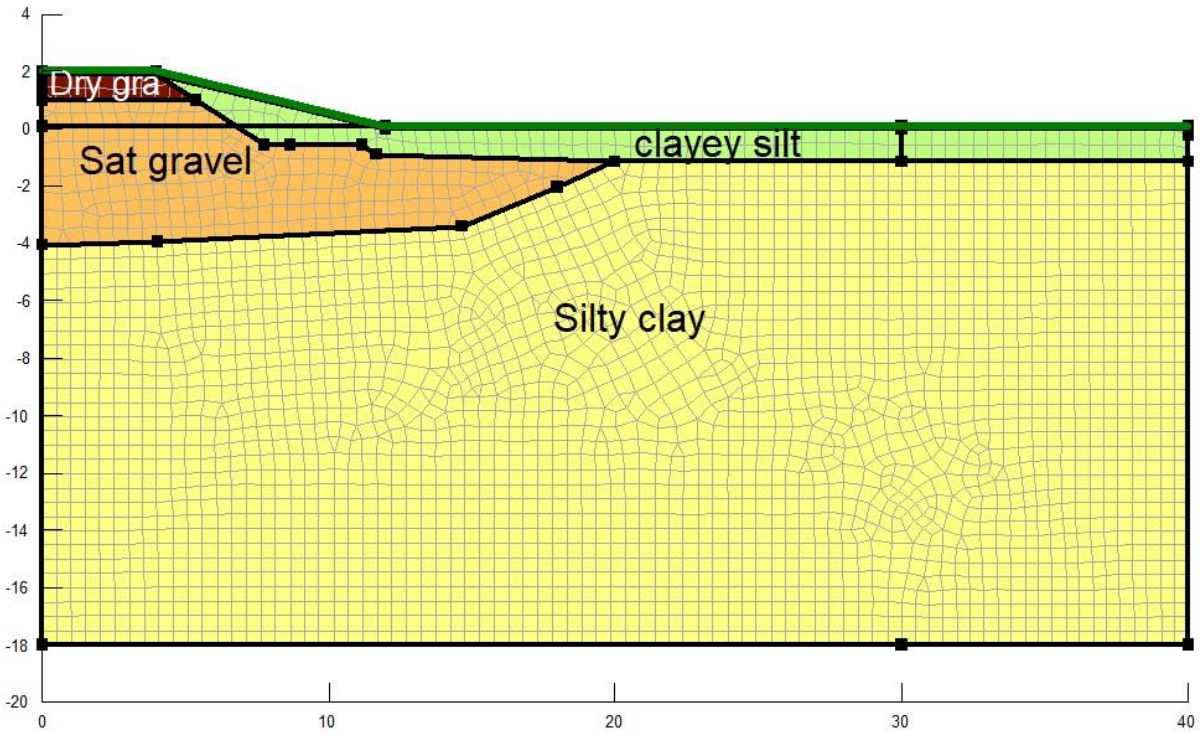

Figure 4.4.1: Cross Section of the validation model (Flynn, 2015)

4.4.1.2 Material properties

In a coupled analysis, the geotechnical proporties of the soil vary with temperature, therefore, in the thermal simulation, all materials were modelled using a full thermal model, which requires intrinsic properties in frozen and unfrozen states, including the volumetric heat capacities (cu and cf), thermal conductivities (ku and kf), the in-situ volumetric water content (VWC), and the unfrozen volumetric water content (GEO-SLOPE International Ltd, 2014). The Thermal properties used in the validation model were retrieved from the original manuscript (Flynn, 2015). The soil is assumed to be fully saturated. The soil properties are summarized in Table 4.4.1.

Table 4.4.1: Thermal properties of the validation model (Orlando & Ladanyi, 2004)

Soil type	Unfrozen volumetric heat capacity (Kj/m3/C)	frozen volumetric heat capacity (Kj/m3/C)	Unfrozen thermal conductivity (Kj/d/m.C)	Frozen thermal conductivity (Kj/d/m.C)	Θ(m3/m3)
Silty Clay	2760	1960	107	161	0.41
Clayey Silt w/ Organics	2850	2050	123	209	0.41
Gravel Sat.	2505	1958	233	328	0.28
Gravel Dry	1591	1472	130	86	0.06

In the coupled heat and water analysis, the soil was assumed completely saturated except the dry gravel layer and the clayey silt layer, therefore, a saturated material model was applied for all the soil layers beneath the dry gravel. An unsaturated /saturated material model was used for the dry gravel and clayey silt layers. In addition, the selection of the material model in the load deformation analysis represented an important stage in the modeling process. In general, the use of simpler constitutive models like linear elastic where stress is directly proportional to strain is recommended before progressing to more complex models such as Modified Cam Clay to account for critical state soil behavior. For this particular problem, the in-situ loading conditions did not give rise to the critical state and were not approaching the failure. The only load applied to the domain is a 100 kPa. Therefore, a linear elastic model with porewater pressure change was used for the soil layers in the validation model. The load was only applied to the road surface to account for the traffic loading.

The hydraulic and the mechanical properties of the soil layers were retrieved from the literature (Budhu, 2007). The hydraulic and mechanical properties used in the SEEP/W and SIGMA/W are summarized in Table 4.4.2.

Table 4.4.2: Hydraulic and mechanical properties of the validation model (Budhu, 2007)

Soil type	Unit Weight [kN/m3]	E [MPa]	Saturated hydraulic conductivity (m/day)
Silty Clay	15	3	$1\,x10^{-5}$
Clayey Silt w/ Organics	15	3	$8\,x10^{-4}$
Gravel Sat.	15	15	$3\,x10^{-2}$
Gravel Dry	19	200	$3\,x10^{-2}$

4.4.1.3 Boundary conditions

The validation model featured three analyses: a thermal analysis, seepage analysis and a volume change analysis. In the first analysis, the soil thermal equilibrium at the first day of the simulation was established using a spatial function. Thermistor string data placed on site were used to establish the thermal regime of the ground at steady state. The transient thermal analysis covers 2 full years. The climate data was obtained from the Environment Canada website. Climate data was downloaded for every day from September 25th 2012 to September 25th 2014 (Government of Canada, 2011).

"n" modifying factors were used in the thermal analysis to account for the fact that the air temperature at the surface differs from the ground temperature, even at shallow depths. "n" factors estimate ground surface temperatures based on air temperatures (Orlando & Ladanyi, 2004). Both the freezing and thawing n factors are required in the TEMP/W analysis. Recommended n-factors were used based on values provided in TEMP/W manual. The model surface was divided into three parts including the road surface, the mid slope and toe, therefore, n-freezing and thawing factors were selected for each segment separately. The values of the n freezing, and thawing factors are represented in Table 4.4.3.

Table 4.4.3: Surface Modifying Factors in TEMP/W

Material	Thawing nt	Freezing nf
Road Surface	0.3	0.3
Mid Slope	0.1	0.6
Toe	0.01	0.7

A constant unit heat flux representing the geothermal gradient was applied to the bottom extent of the model as shown in Figure 4.4.2. Geothermal gradients vary by location but generally range between 0.9 and 3.3°C per 100 m (Grasby et al., 2009). The thermal boundary conditions are represented in Figure 4.4.2,

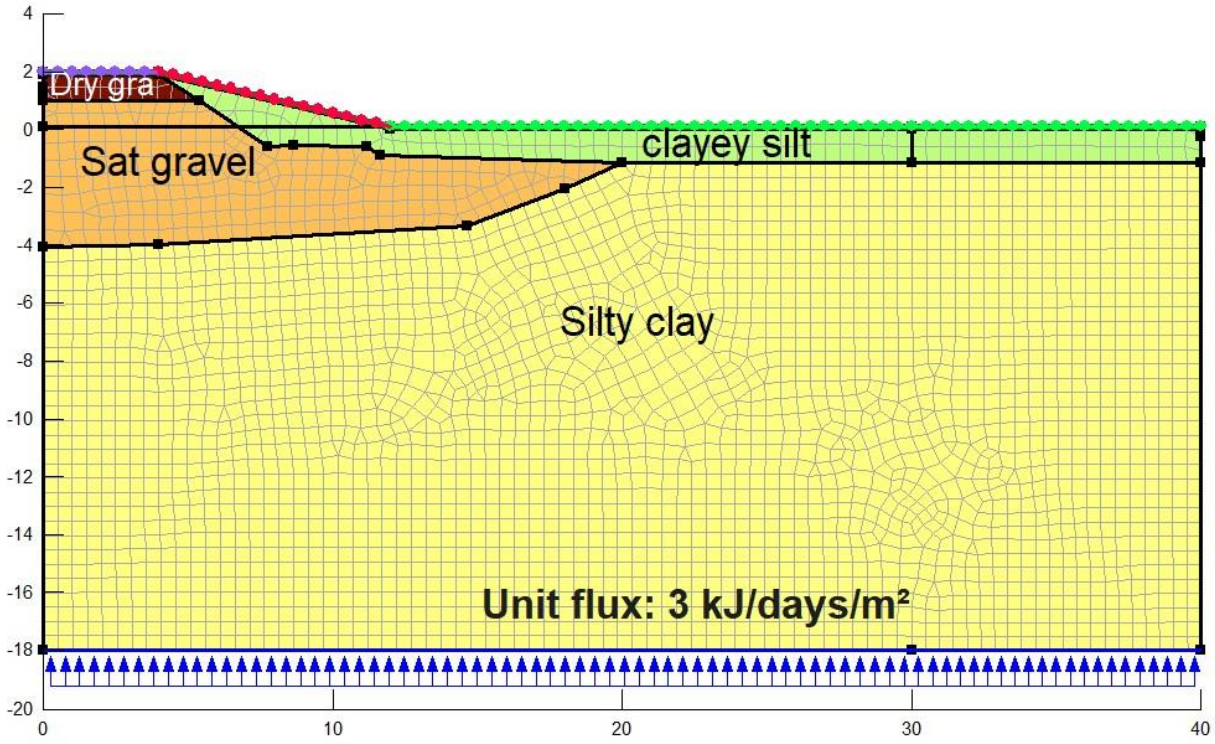

Figure 4.4.2: Thermal boundary conditions – TEMP/W - validation model

In the SEEP/W analysis, a total head boundary conditions were applied at the right and left extents of the model, the values of the total heads were recovered from the site measurement. Average values were used in the SEEP/W analysis. A total head of 1.2 m was applied to left side of the model when a total head of -0.2 m was applied to the right extent of the model. The initial head and porewater pressures were computed from the initial water table. The location of the water table was established from site investigations. The seepage boundary conditions are represented in Figure 4.4.3,

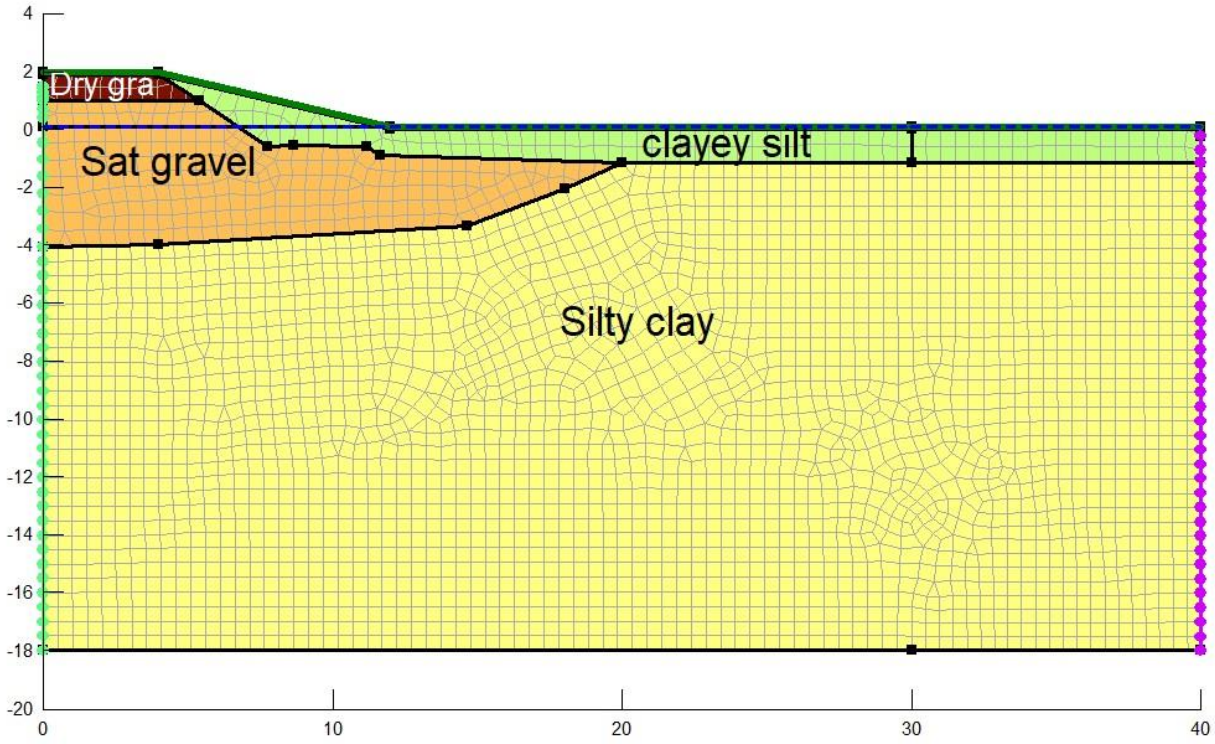

Figure 4.4.3: Hydraulic boundary conditions – SEEP/W- validation model

In the deformation model, the in-situ porewater pressure was imported from the convective heat transfer analysis for each day of the analysis. A potential seepage face was applied to the ground surface and both sides of the model to allow the dissipation of the excess water resulting from the consolidation of the soil. The stress-strain boundary conditions include a Fixed X/Y boundary along the bottom boundary at a depth of 18m. The Fixed X/Y boundary condition does not allow any movement laterally or vertically and was appropriate for the depth of bedrock. A Fixed X boundary condition was applied at all stages of the model to the left and right extents of the model assuming that movement at these locations could only happen in the vertical direction (Flynn, 2015). A cyclic spline data point function was used to represent the traffic load on the embankment. A load of 100 kPa, representing the average traffic loading, was selected after some sensitivity analysis with different loads to represent the cyclic traffic loading on the embankment. The mechanical boundary conditions are represented in Figure 4.4.4

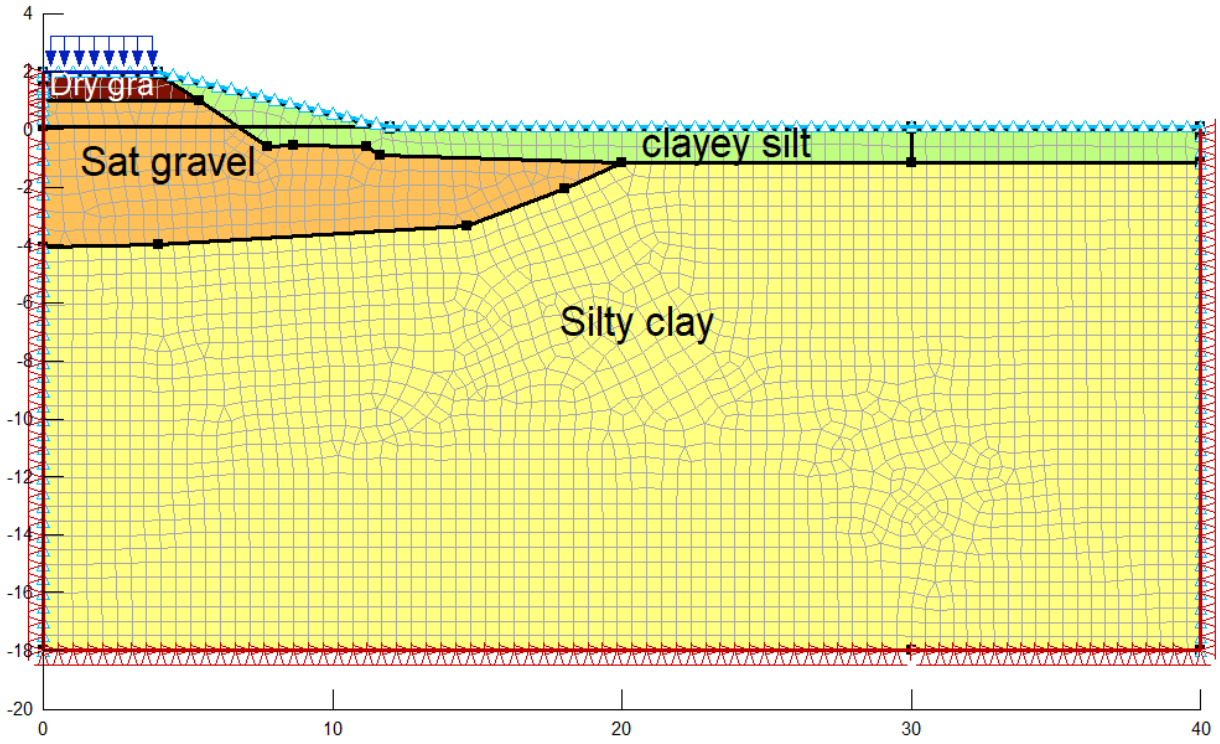

Figure 4.4.4: Mechanical boundary conditions – SIGMA/W - validation model

4.4.2 Discussion of the validation results

The simulation results were compared to site measurements included in the thesis manuscript (Flynn 2015) in order to validate the simulation tools. The site data included the monthly average ground temperature for different months as represented in Figure 4.4.5 (a,b,c,d). Accordingly, the thermal simulation provides daily ground temperature for each day of the analysis. For comparison purposes, the simulation results were processed and plotted on the same graphs with the site data for comparison purposes. The results of the thermal validation are presented in Figure 4.4.5b.

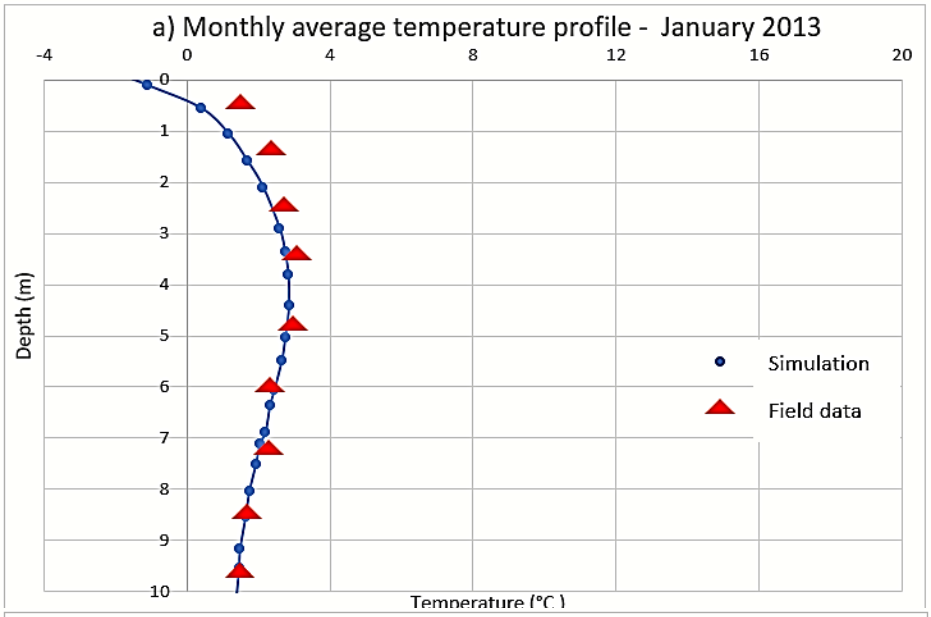
a) Monthly average temperature profile - January 2013
-4
0
4
8
12
16
20
0
1
2
3
4
5
6
7
8
9
10
Depth (m)
Simulation
Field data
Temperature (°C)

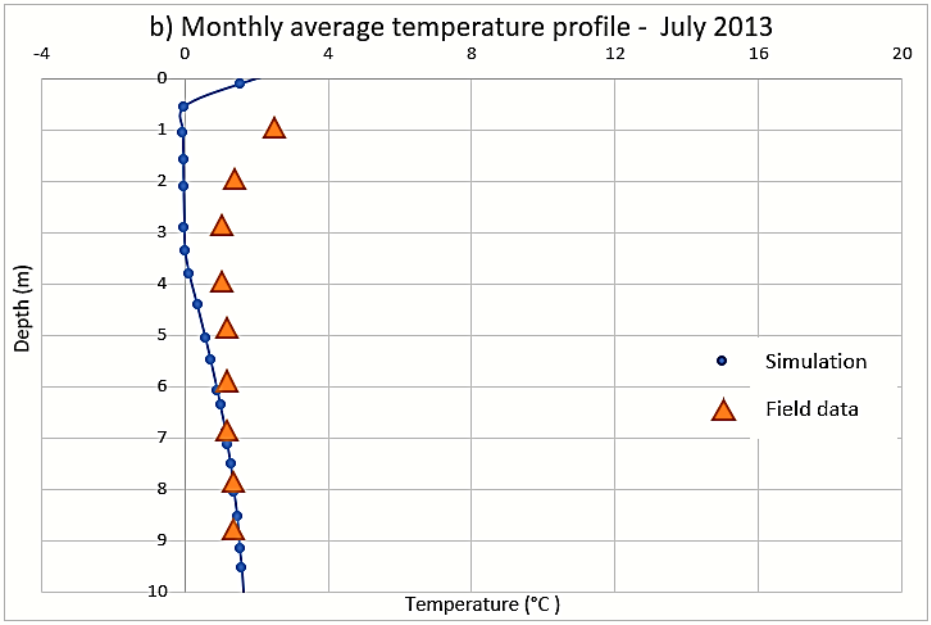
b) Monthly average temperature profile - July 2013
-4
0
4
8
12
16
20
0
1
2
3
4
5
6
7
8
9
10
Depth (m)
Simulation
Field data
Temperature (°C)

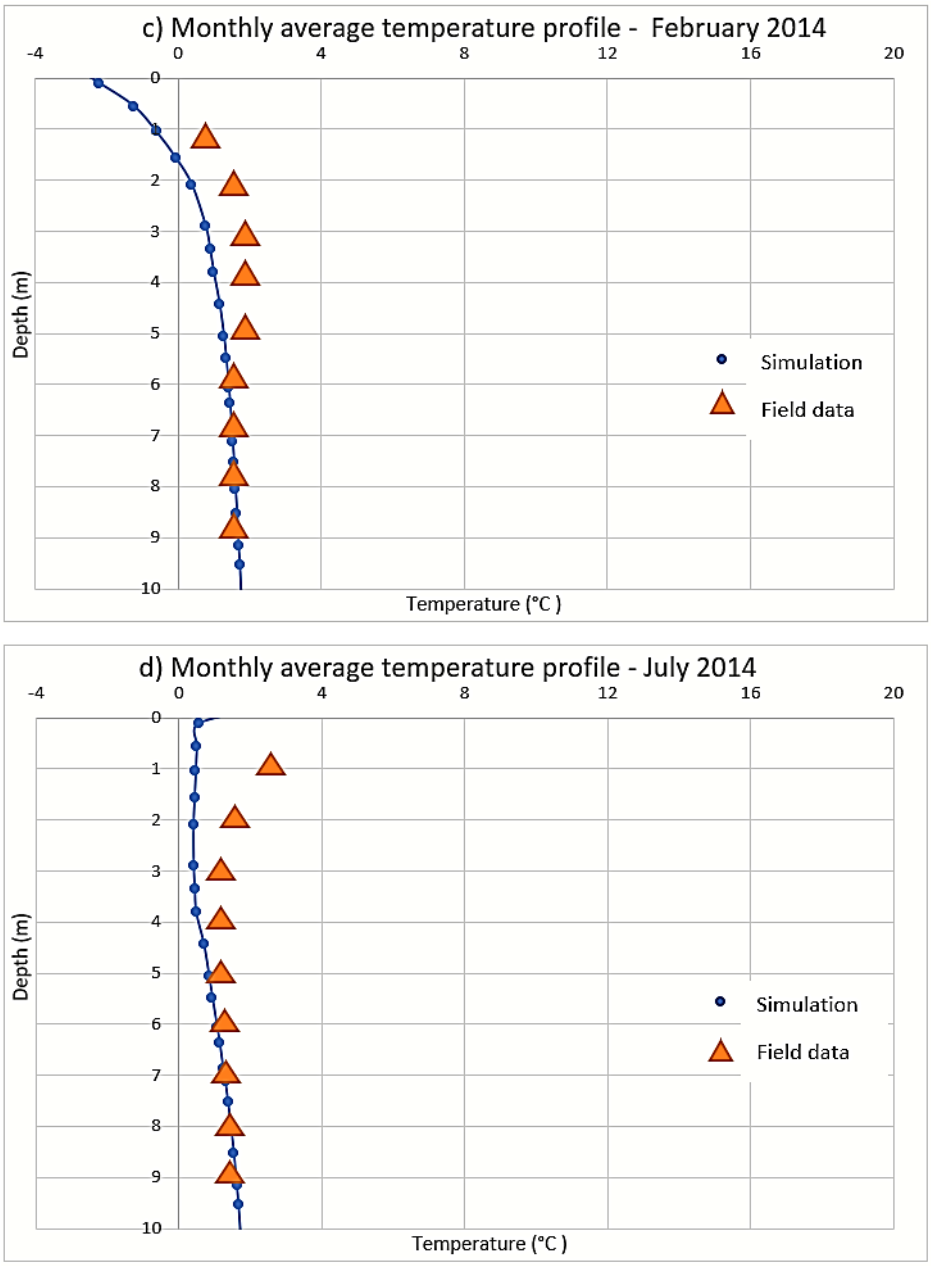

Figure 4.4.5: Monthly ground temperature of the ground at a) January 2013, b) July 2013, c) February 2014 and d) July 2014 – TEMP/W

The results of the convective heat transfer analysis were plotted for two different locations: the centerline and the toe of the embankment. Values of the porewater pressures were established for the two locations in the numerical simulation. In addition, site measurements included data of porewater pressures along the centerline and the toe of the embankment. The simulated porewater pressure distributions are represented in Figure 4.4.6 and b. The original field porewater measurement data are represented in Figure 4.4.7.

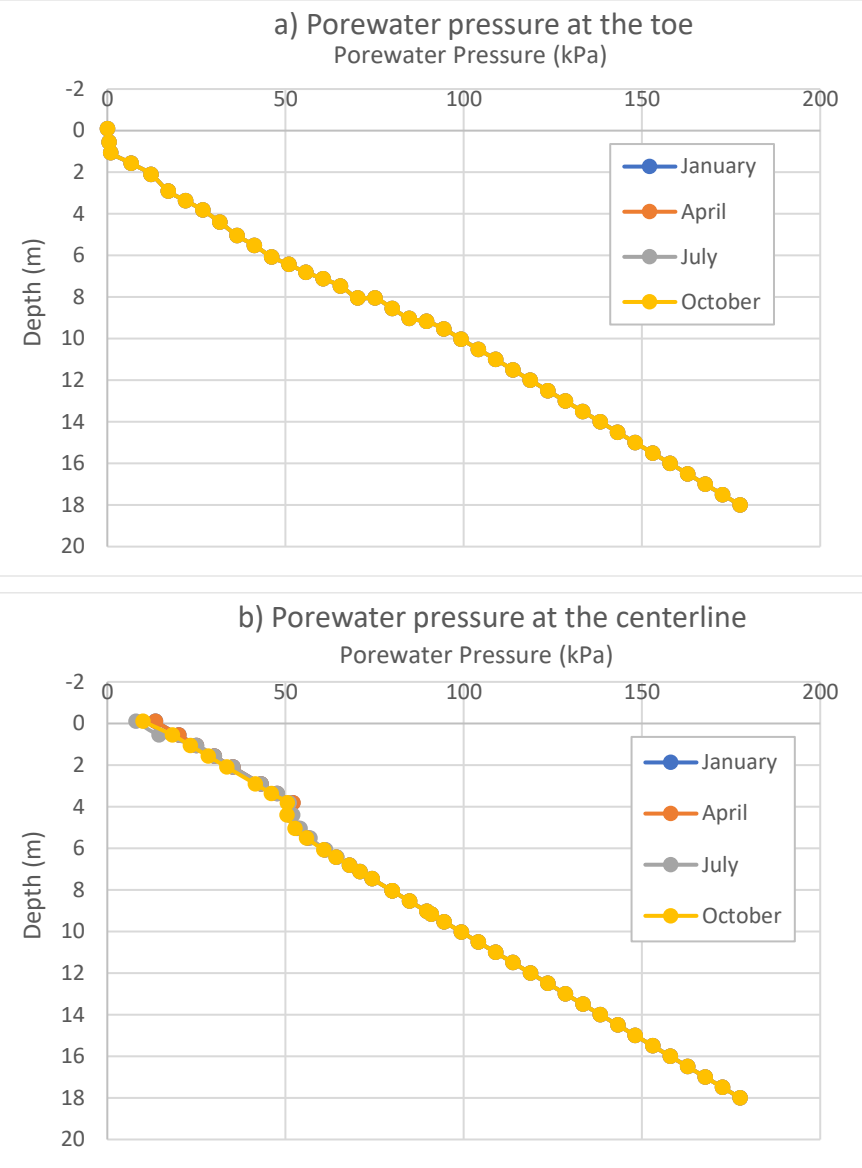

Figure 4.4.6: Simulated porewater pressures profiles at a) the toe and b) centerline of the embankment-SEEP/W

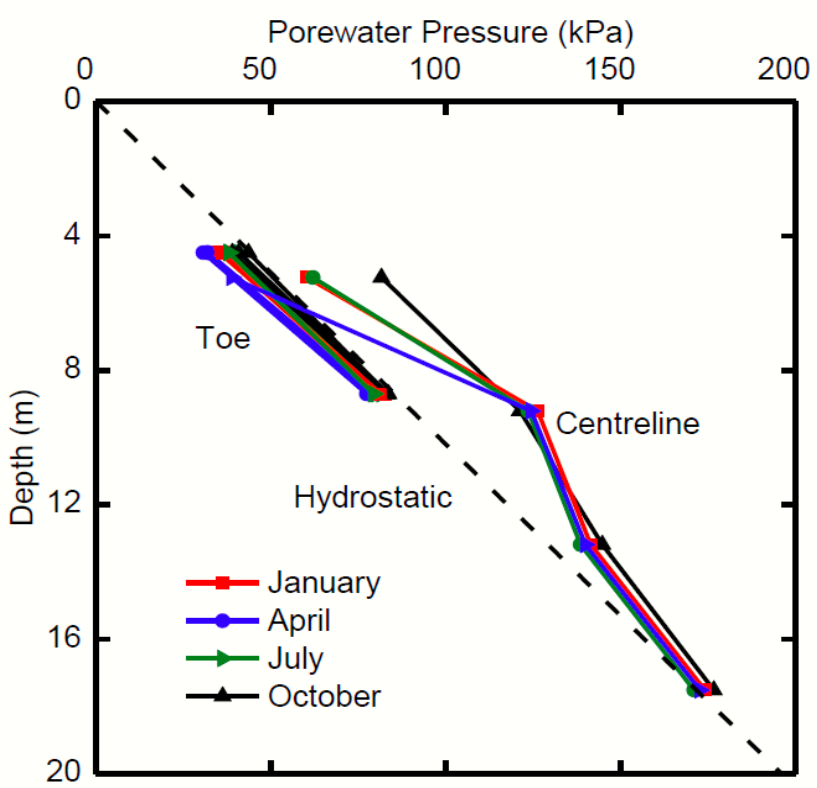

Figure 4.4.7: Field porewater measurements at the toe and the centerline of the embankment (Flynn, 2015)

The manuscript by Flynn (2015) included site measurement of the vertical displacement of the embankment at different days from September 2012 to October 2014. Similar graphs were plotted using the results from the coupled hydro-mechanical analysis established in the validation model. The simulation results are represented in Figure 4.4.8. In addition, the measured vertical displacements are included in Figure 4.4.9.

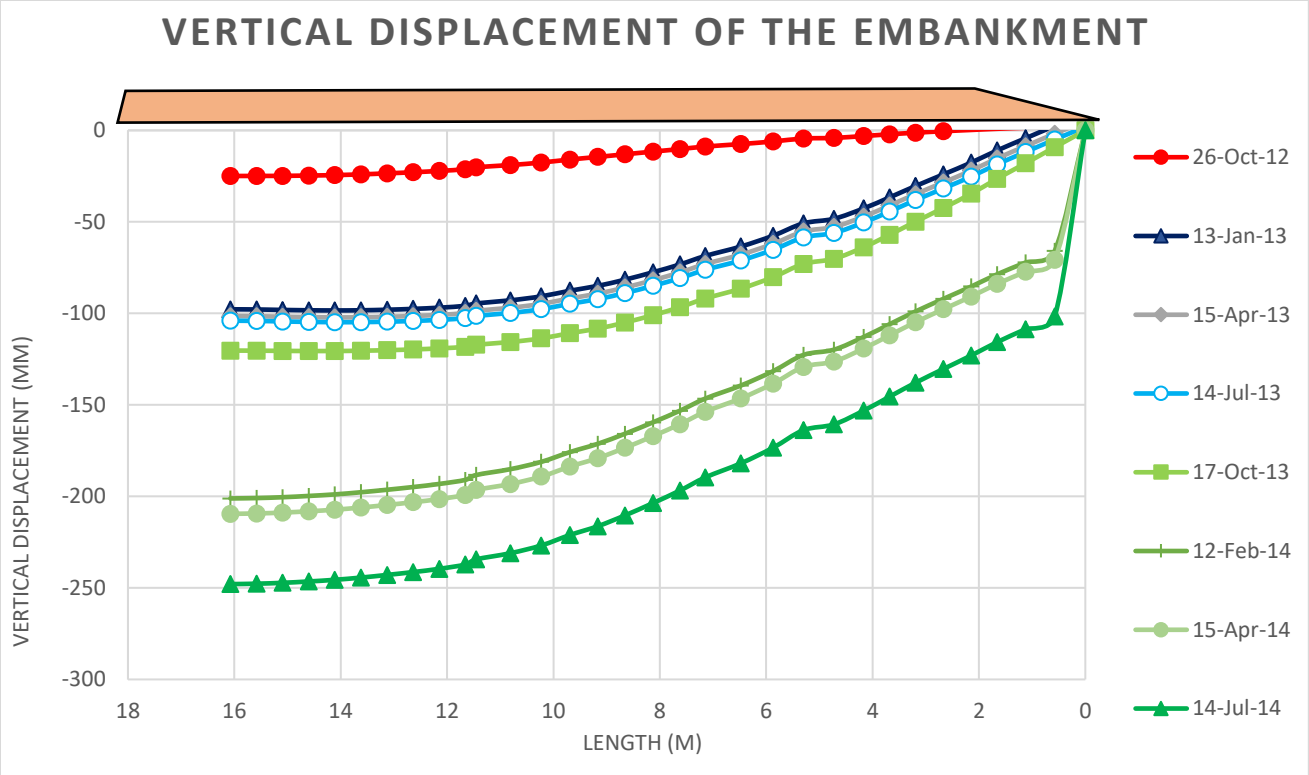

Figure 4.4.8: Simulated vertical settlement of the embankment – SIGMA/W

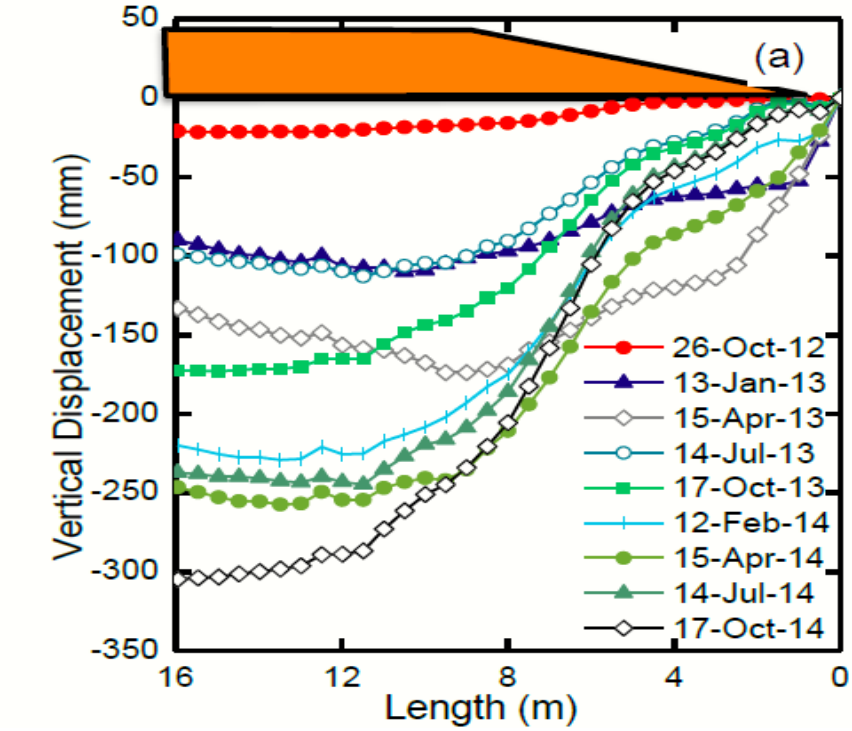

Figure 4.4.9: Field vertical settlement of the embankment (Flynn, 2015)

In the three stages of the analysis, the simulation results, approximate the general shape of the site measurements, for instance, the simulated ground temperatures are close to the field thermistor measurements. Therefore, the thermal simulation captures the thermal behaviour of the ground with a good precision in both the winter and the summer seasons. A small divergence from the original temperature data was noted in the simulation results. This divergence could be due to several factors. First, the thermal properties of the ground were not determined in the original studies (Flynn, 2005), no lab experiments were conducted on soil samples to determine the thermal properties of the soil layers. Therefore, due to the absence of any information about the material properties in the original studies, the validation model used material properties retrieved from a different literature source. Second, the value of the thermal gradient was not investigated for this specific site, therefore, the model used an estimated value from the literature for the region of Thompson airport area. Finally, the climate data between September 2012 to September 2014 were retrieved from the Environment Canada website, separately from the original studies. Therefore, the climate data used to build the model could be slightly different from the actual climate data used in the original report and could lead to the observed divergence.

In the coupled heat and water transfer analysis, the simulation results approximate the shape and the general trend of the hydraulic regime in the site. The original field studies (Flynn, 2005) provided site measurement of the porewater pressures at the centerline and the toe of the embankment, therefore, the simulation results were reported for the same locations. At the centerline, the simulated porewater pressures showed an increase of the porewater pressure due to the convective heat transfer at a depth of 4m similar to that represented by the site data. The field data showed a similar increase at a depth of 4m under the embankment. Nevertheless, the porewater pressure increase in the numerical simulation is slightly smaller than the site measurement. At the toe, the distribution of the porewater pressures fits perfectly the site measurements. The change of the porewater pressures due to the convective heat transfer is not significant at the toe of the embankment in the simulation results and the site measurements. The amount of the porewater increase represented in the simulation results is somewhat small compared to site measurements, nevertheless, site measurements included only four reading points, the graph represented in the original graph was developed based on numerical correlation between the four data points, therefore, the values of the porewater pressures along the centerline were not all measured in site. The difference between the simulation results and field data could be due to several factors. First of all, the flow of water at the site is not well understood (Flynn, 2015). The model used an average value for the total head at both sides of the model. Nevertheless, the total heads change with depth and do not follow a typical trend. Second, the values of the hydraulic conductivities of the soil layers were not measured in the lab for this specific location, therefore, standard values of hydraulic conductivities were retrieved from the literature to complete the model. Modification of the hydraulic properties of the soil layers can also impact the soil hydraulic behavior

in the model. Lastly, site investigations did not cover some processes such as infiltration and evaporation, their amounts were not discussed in the original studies, therefore, they were not considered in the numerical model. All these factors contributed in the observed difference between the results of the simulation and the site data.

The coupled hydro-mechanical model simulated the cumulative vertical settlement of the soil under specific loading condition. The cumulative vertical displacement of the embankment continuously increases over the entire simulation period, likewise, site measurements, showed a steadily increase of vertical settlement of the soil. The graphical representation of cumulative displacement of the embankment was reported for different days along the simulation period in the original study (Flynn, 2005). Similar graphs were established using the results of the load-deformation. The results of the coupled hydro-mechanical model agree with the site data in the general trend and shape. A maximum deformation of 250 mm was observed just beyond the centerline by July 2014 in both the site data and the numerical results. Nevertheless, minor dissimilarities were noted between the simulated and site data. The difference between the simulation results and the site measurement could be due to several factors. The displacement measurements were recorded using a ShapeAccelArrays (SAA) placed horizontally between the toe and the centerline. The anchored end of the SAA was modified twice to ensure it was fixed in position. Therefore, the modification of the anchored end of the SAA could induce a discrepancy in the deformation readings. Moreover, the embankment is maintained and re-graded every year. Though, the model was unable to consider the displacements with the amount of fill applied to the road as exact records of gravel application at this location were not kept (Flynn, 2015). Finally, the mechanical soil properties of the soil layers were not determined in the laboratory, therefore, the model used standard values retrieved from the literature to complete the simulation. All these factors could lead the observed minor divergence between the site data and the simulation results.

All in all, the adopted thermo-hydro-mechanical approach and the simulation tools provide a good understanding of the coupled thermal, hydraulic and mechanical regime of the ground and could be used to simulate the coupled impact of climate warming on the thermo-hydro-mechanical regime of the ground.

4.5 Climate data collection

The climate change simulations were developed based on the assumption that the climate is relatively stable with no major climate variances within 20 years period (Government of Canada, 2019). Therefore, the acquisition of climate data, included four-time segments of 20 years each. The climate change simulations cover the period from 2020 to 2100. Climate data for the next 80 years were available on the Climate Canada website. The website represent the climate change predictions using projections map with temporal resolution available at a seasonal, and annual scale and spatial resolution approximately

10km (Government of Canada, 2019). The climatic predictions include information on the projected 20-year average changes in minimum, mean and maximum temperature. It also provides information on the average change in precipitations, snow depth and surface wind velocity.

These interactive maps simulate the climate change under the main three emission scenarios; RCP2.6 (low global emission scenario), RCP4.5 (medium global emission scenario), RCP8.5 (high global emission scenario) for Four-time frames starting from 2019 until 2100 (Government of Canada, 2018).

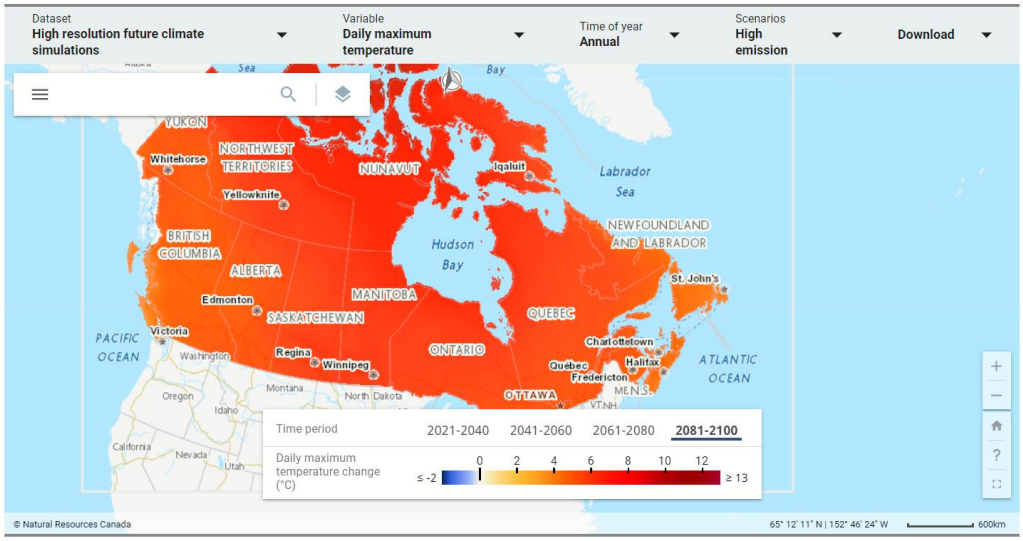

Figure 4.5.1: Climate change interactive map (Government of Canada, 2019)

For the aim of this study, three weather monitoring stations were selected. The selected climate monitoring stations are summarized in the Table 4.5.1 (Government of Canada, 2019).

Table 4.5.1: Climate stations at Ottawa, Toronto and Sudbury (Government of Canada, 2019)

City	Name	Latitude	Longitude
Ottawa	OTTAWA CDA	45.38	-75.72
Toronto	Toronto	43.67	-79.4
Sudbury	SUDBURY A	46.63	-80.8

4.5.1 Geometry

The Canadian geological survey includes a set of borehole logs in different cities of Canada including Ottawa, Toronto and Sudbury. Consequently, the geometry of the simulation models was developed based on two adjacent boreholes logs located at each city. All boreholes provide a continuous information on the soil beneath the surface to a depth of 20 m (Natural Resources Canada, 2010). The geometry of the three models extended 15 m laterally from the centerline, and to a depth of 20 m below the natural ground surface. For the aim of the numerical simulation, a thin layer of finite elements called a surface layer was added the top surface to apply the different boundary conditions in the three simulation tools (GEO-SLOPE International Ltd, 2014). The mesh properties are set to finite square of 0.2 m diameter for the three simulation models. The selected mesh dimensions provided accurate simulation results compared to a larger mesh. SEEP/W, SIGMA/W and TEMP/W software did not allow to use thinner mesh due to limited storage of the computer. Furthermore, thinner mesh, require a longer computation time (Flynn, 2015).

4.5.2 Material properties

4.5.2.1 Hydraulic properties:

The soil was assumed to be fully saturated in the simulation models, therefore, a saturated material model was used for all the soil layers in the numerical simulations. The hydraulic properties required to build the coupled convective heat transfer simulation are the hydraulic conductivities at saturation and the volumetric water content of the soil. The material properties were retrieved from literature, for each material (Budhu, 2007).

Tables 4.5.2 to 4.5.4 summarize the thermal properties of the simulation models for Ottawa, Toronto and Sudbury, respectively.

Table 4.5.2: Material hydraulic properties – Ottawa model - (Budhu, 2007)

Soil type	**Θ(m3/m3)**	**Hydraulic conductivity (m/day)**
Brown silty clay	0.4	$5x10^{-6}$
Grey soft silty clay	0.7	10^{-5}
Grey Firm silty clay	0.7	$5x10^{-7}$

Table 4.5.3: Material hydraulic properties – Toronto model - (Budhu, 2007)

Soil type	**Θ(m3/m3)**	**Hydraulic conductivity (m/day)**
silty Sand	0.5	$5x10^{-1}$
Stiff grey silty clay	0.4	10^{-5}
Dense silty clay	0.3	$5x10^{-4}$

Table 4.5.4: Material hydraulic properties – Sudbury model - (Budhu, 2007)

Soil type	**Θ(m3/m3)**	**Hydraulic conductivity (m/day)**
Clay	0.5	$8.6x10^{-8}$
Silty clay	0.5	$1x10^{-7}$
Clayey silt + trace of sand	0.5	$1x10^{-4}$
Red clay	0.5	$1x10^{-8}$

4.5.2.2 Mechanical properties:

The coupled hydro-mechanical simulations used linear elastic models with effective parameters for all materials. The linear elastic model was selected considering the low mechanical loading condition. The mechanical properties were retrieved from the literature for all the soil layers in the three cities.

Table 4.5.5: Material physical and mechanical properties – Ottawa model - (Budhu, 2007)

Soil type	**Unit Weight [kN/m3]**	**E [MPa]**
Brown silty clay	**15**	**20**
Grey soft silty clay	**15**	**3**
Grey Firm silty clay	**15**	**50**

Table 4.5.6: Material mechanical properties – Toronto model - (Budhu, 2007)

Soil type	**Unit Weight [kN/m3]**	**E [MPa]**
silty Sand	**17**	**10**
Stiff grey silty clay	**15**	**50**
Dense silty clay	**15**	**30**

Table 4.5.7: Material mechanical properties – Sudbury model - (Budhu, 2007)

Soil type	**Unit Weight [kN/m3]**	**E [MPa]**
Clay	15	15
Silty clay	15	10
Clayey silt + trace of sand	17	50
Red clay	15	25

4.5.2.3 Thermal properties:

The thermal properties required to build the thermal model are the (unfrozen, frozen) volumetric heat capacities (cu and cf), (unfrozen, frozen) thermal conductivities (ku and kf), the in-situ volumetric water content (Ɵ), and the unfrozen volumetric water content. The material properties were retrieved from literature, for each material (Orlando & Ladanyi, 2004).

Tables 4.5.8 to 4.5.10 summarize the thermal properties of simulation models for Ottawa, Toronto and Sudbury, respectively:

Table 4.5.8: Material thermal properties – Ottawa model - (Orlando & Ladanyi, 2004)

Soil type	Θ(m3/m3)	Unfrozen thermal conductivity (Kj/d/m.C)	Frozen thermal conductivity (Kj/d/m.C)	Unfrozen volumetric water content (Kj/m3/C)	Frozen volumetric heat capacity (Kj/m3/C)
Brown silty clay	0.4	191.6	562.2	6556.3	4683.0
Grey soft silty clay	0.7	59.3	234.7	3488.7	2491.9
Grey firm silty clay	0.7	65.5	235.0	3567.0	2547.9

Table 4.5.9: Material thermal properties – Toronto model - (Orlando & Ladanyi, 2004)

Soil type	Θ(m3/m3)	Unfrozen thermal conductivity (Kj/d/m.C)	Frozen thermal conductivity (Kj/d/m.C)	Unfrozen volumetric heat capacity (Kj/m3/C)	Frozen volumetric heat capacity (Kj/m3/C)
Silty sand	0.5	83.1	84.9	1755.2	1253.7
Stiff grey silty clay	0.4	159.5	185.5	2519.8	1799.9
Dense silty clay	0.3	275.2	382.0	3438.3	2455.9

Table 4.5.10: Material thermal properties – Sudbury model - (Orlando & Ladanyi, 2004)

Soil type	Θ(m3/m3)	Unfrozen thermal conductivity (Kj/d/m.C)	Frozen thermal conductivity (Kj/d/m.C)	Unfrozen volumetric water content (Kj/m3/C)	Frozen volumetric heat capacity (Kj/m3/C)
Clay	0.5	246.7	412.1	4261.2	3043.7
Silty clay	0.5	224.2	422.1	4635.1	3310.8
Clayey silt + trace of sand	0.5	171.1	240.7	3137.0	2240.7
Red clay	0.5	345.65	587.4	4771.7	3408.3

4.6 Modeling of the THM responses of the selected sites to climate changes

4.6.1 Boundary conditions

4.6.1.1 Steady state boundary conditions:

The simulation models required a thermal steady state analysis to establish the initial ground temperature at the first day of the analysis. A constant temperature was applied at the top boundary of the three simulation models. The ground surface temperature was assumed to be equal to the average annual air temperature at steady state (GEO-SLOPE International Ltd, 2014). At the edges of the models, a zero-heat flux boundary condition was applied. The bottom boundary conditions were represented by a constant heat flux. The thermal heat flux represents the impact of the geothermal gradient. The value of the heat flux depends on the location, but generally range between 0.9 and 3.3°C per 100 m (Grasby et al., 2009). The values of the thermal unit heat flux applied on the three models were retrieved from the thermal map of Canada. Table 4.6.1 summurizes the values of the geothermal heat flux used for Ottawa, Toronto and Sudbury.

Table 4.6.1: Geothermal heat flux (Grasby et al., 2009)

City	**Geothermal unit flux kj/m2.day**
Ottawa	3.9
Toronto	3.0
Sudbury	3.7

Figure 4.6.1 represents the thermal steady state boundary conditions for Ottawa, similar representation was used for Toronto and Sudbury.

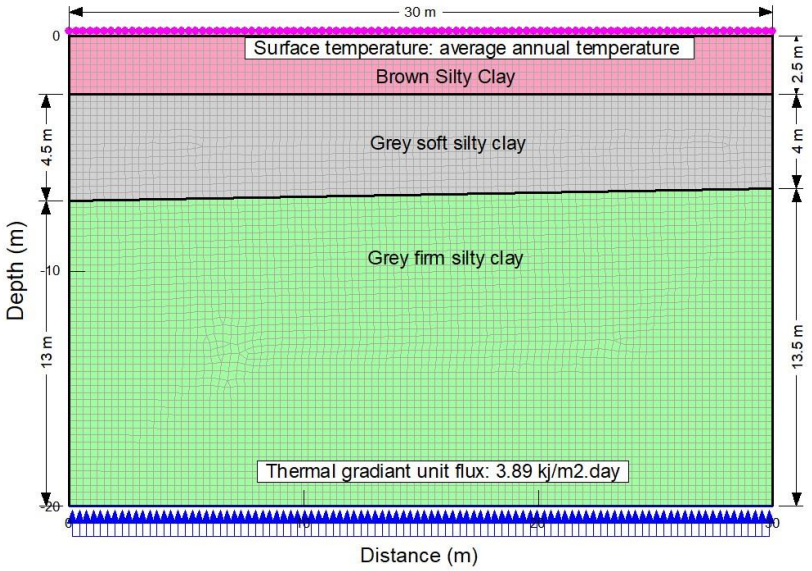

Figure 4.6.1: Simulation model steady state boundary conditions - Ottawa

4.6.1.2 Transient analysis boundary conditions

The transient analysis comprises two main stages: the coupled convective hydro-thermal simulations and the coupled hydro-mechanical simulations. In the first stage, the convective heat transfer analysis considers the convective heat transfer that occurs due to flowing water within the soil matrix to establish the distribution of the temperature and the porewater pressures in the soil. Therefore, both thermal and hydraulic boundary conditions were required. In TEMP/W, the model uses the climate data of a full year. The thermal analysis featured nine transient analyses. The first five transient analyses use the climate data from the first day of January 2018 to the last day of December 2018 to calibrate the steady state temperature of the ground. It was assumed that the climate data of the year 2018 are similar to 2020 to start the numerical simulations. After the thermal stabilization, the simulation of climate changes up to the year 2100 started. The simulation of global warming featured four transient analyses. Each analysis simulates the average change of air temperature within a 20 years' time period. Therefore, the thermal model includes four-time periods; 2020-2040, 2041-2060, 2061-2080 and 2081-2100. The climate values used in the simulations are modified for each time period, for example, following the RCP8.5, the daily maximum temperature of air will increase by 1.6 in Ottawa by 2040, given that the maximum temperature on March 1st was 4 °C in 2019, the maximum daily temperature in Ottawa on March 1st will be 5.6 °C by 2040 following the RCP 8.5. The same logic applies for the rest of the climate patterns used in the analyses (Government of Canada, 2018). Correspondingly, each thermal simulation was coupled with a hydraulic analysis using SEEP/W. An initial water table was used to establish the steady state distribution of the porewater pressures in the ground in the three cities. Afterward, total head boundary conditions were used

at both edges of the models to simulate the transient convective heat and water flow within the soil matrix. The values of the total heads were retrieved from the literature to represent the differential head in the three sites (Natural Resources Canada, 2010). Given the geometry of the model, the total differential head remains minor. Table 4.6.2 presents a summary of the total heads used to build the simulation models of the three cities.

Table 4.6.2: Total head boundary conditions (Natural Resources Canada, 2010)

City	Total head at left edge (m)	Total head at right edge (m)
Ottawa	-0.1 m	-0.6 m
Toronto	-0.2 m	-0.5 m
Sudbury	-0.1 m	-0.5 m

Figure 4.6.2 represents the graphical representation of the hydraulic boundary conditions in SEEP/W software, similar representation was used for Toronto and Sudbury.

Figure 4.6.2: Hydraulic boundary conditions – transient analysis – Ottawa

In the coupled hydro-mechanical simulations, SIGMA/W uses the porewater pressures calculated by SEEP/W for each transient to establish the settlement behavior of the soil. The boundary conditions used in SIGMA/W replicate loading conditions in the real world to represent the hydraulic and stress-strain conditions of the soil. A Fixed X/Y boundary condition was applied to the bottom boundary at a depth in all transient analyses in the three simulation models. A Fixed X/Y boundary condition allows no movement

laterally or vertically and was appropriate for the depth of bedrock (Flynn, 2015). Furthermore, a fixed X boundary condition was applied to the left and right extents of the models assuming that movement at these locations could only happen in the vertical direction (Flynn, 2015). To allow the dissipation of the excess porewater pressure due to the consolidation, a seepage face boundary condition was applied to the surface and the edges of each model. Figure 4.6.3 represents the boundary conditions used in the coupled hydro-mechanical simulation in Ottawa, similar representation was used for Toronto and Sudbury.

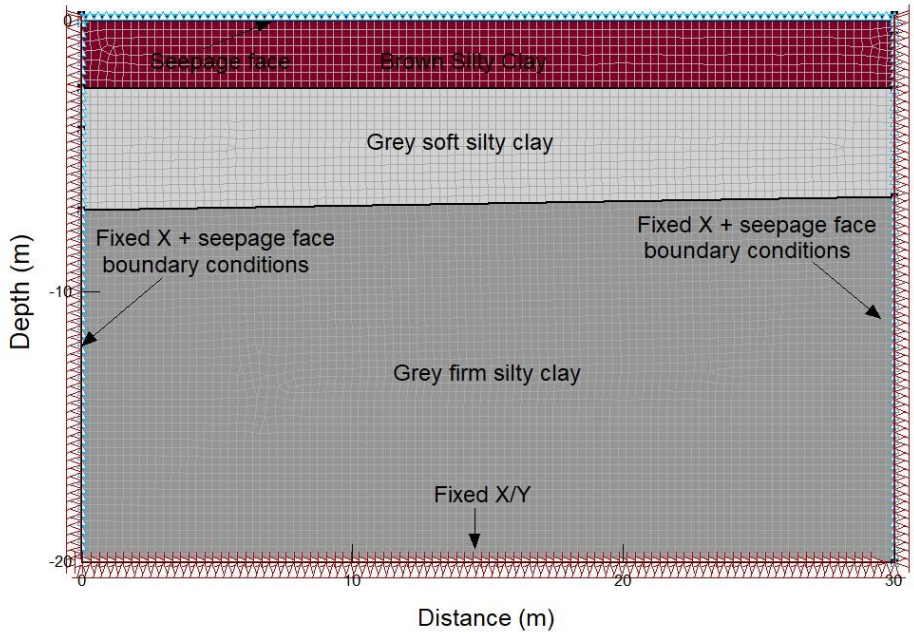

Figure 4.6.3: Mechanical boundary conditions – transient analysis – Ottawa

4.7 Simulation results

The results of the thermal simulation in the three selected sites are presented and discussed to a large extent in the paper entitled "Numerical simulation of ground thermal response in Canadian no-permafrost regions to climate warming" by Marrah et al., 2021 as well as in Chapter 3. For the sake of brevity, the thermal simulation results will not be detailed in this paper. The thermal simulation results showed a gradual increase of ground temperature from 2020 to 2100 in the three studied sites. The average temperature increase varies in the three selected cities. Nevertheless, the total increase in the temperature of the ground ranges between 1 °C at shallow depths to 4 °C at the depth of 5m in the three study areas. At greater depth, the ground temperature slightly changes due to the impact of the geothermal heat flux.

4.7.1 Coupled thermo-hydraulic simulation results.

The results of coupled thermo-hydraulic simulation include the distribution of the porewater pressures in the soil along the sub-surface strata for December 31st and March 1st. The selected days provide an understanding of thermally induced porewater pressure change at the beginning and the end of the winter season, respectively. The results display the impact of climate change on the porewater pressure distribution in the soil. The porewater pressure distribution is plotted for December 31st and March 1st for RCP8.5 and RCP4.5 in Ottawa (Figures 4.7.1 to 4.7.2), Toronto (Figures 4.7.3 to 4.7.4) and Sudbury (Figures 4.7.5 to 4.7.6).

4.7.1.1 Ottawa:

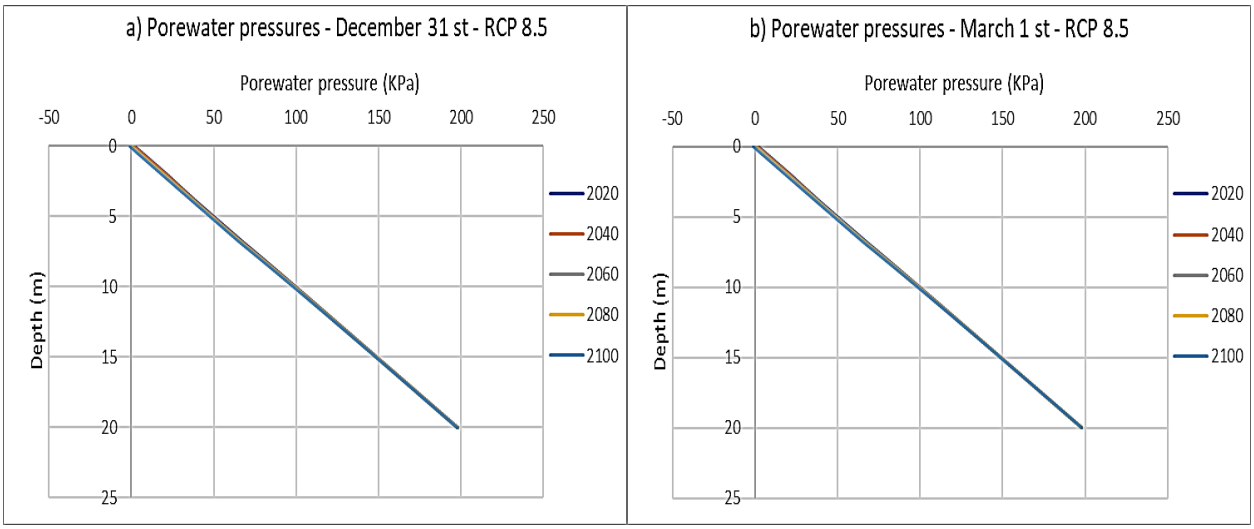

Figure 4.7.1: Porewater pressure distribution at a) December 31st and b) March 1st, 2020, 2040, 2060, 2080 and 2100 – RCP 8.5

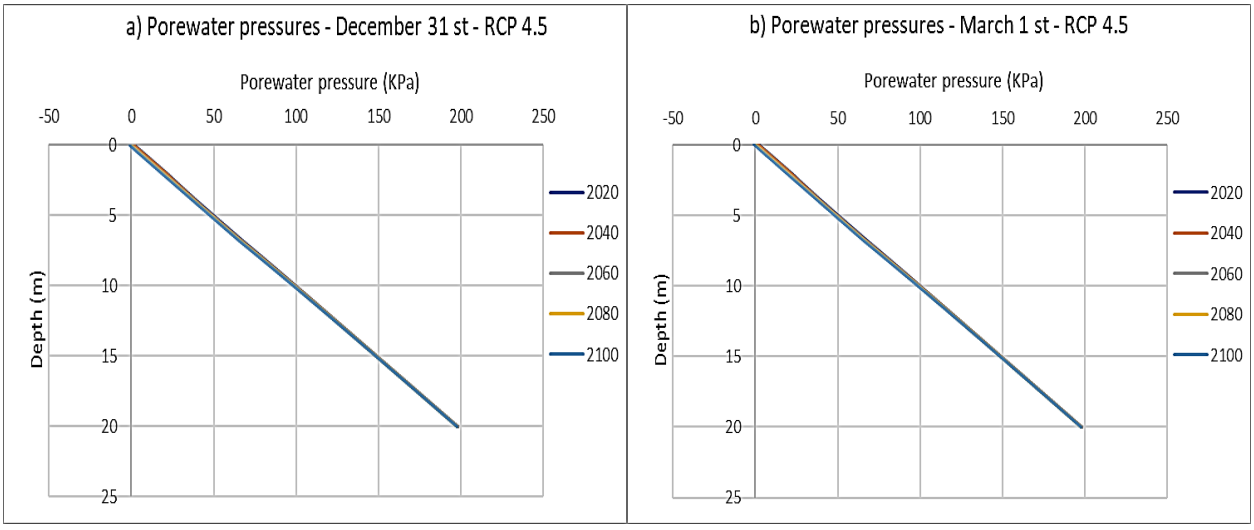

Figure 4.7.2: Porewater pressure distribution at a) December 31st and b) March 1st, 2020, 2040, 2060, 2080 and 2100 – RCP 4.5

4.7.1.2 Toronto:

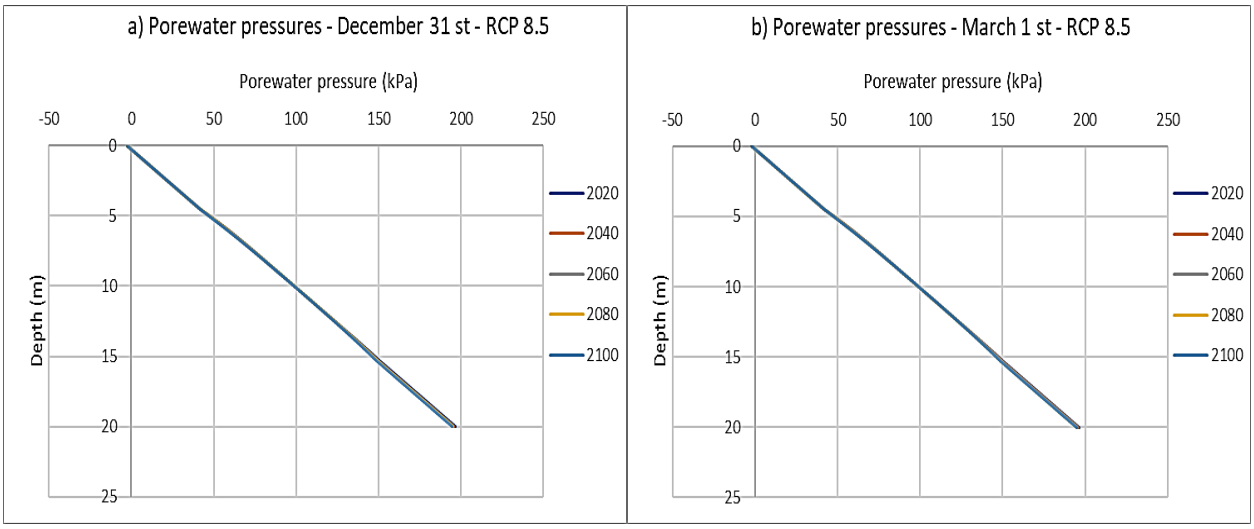

Figure 4.7.3: Porewater pressure distribution at a) December 31st and b) March 1st, 2020, 2040, 2060, 2080 and 2100 – RCP 8.5

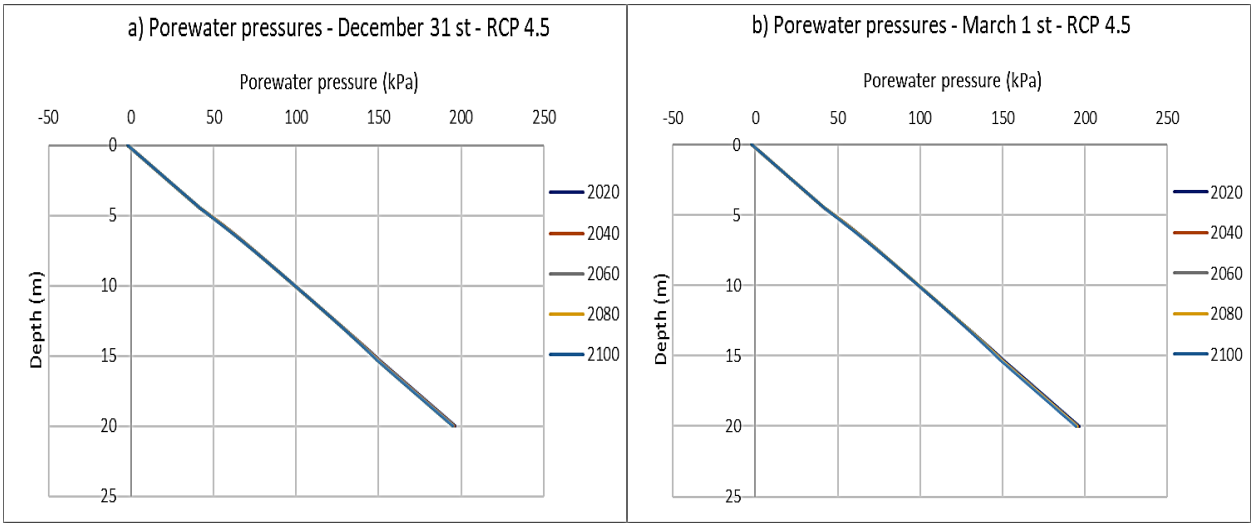

Figure 4.7.4: Porewater pressure distribution at a) December 31st and b) March 1st, 2020, 2040, 2060, 2080 and 2100 – RCP 4.5

4.7.1.3 Sudbury:

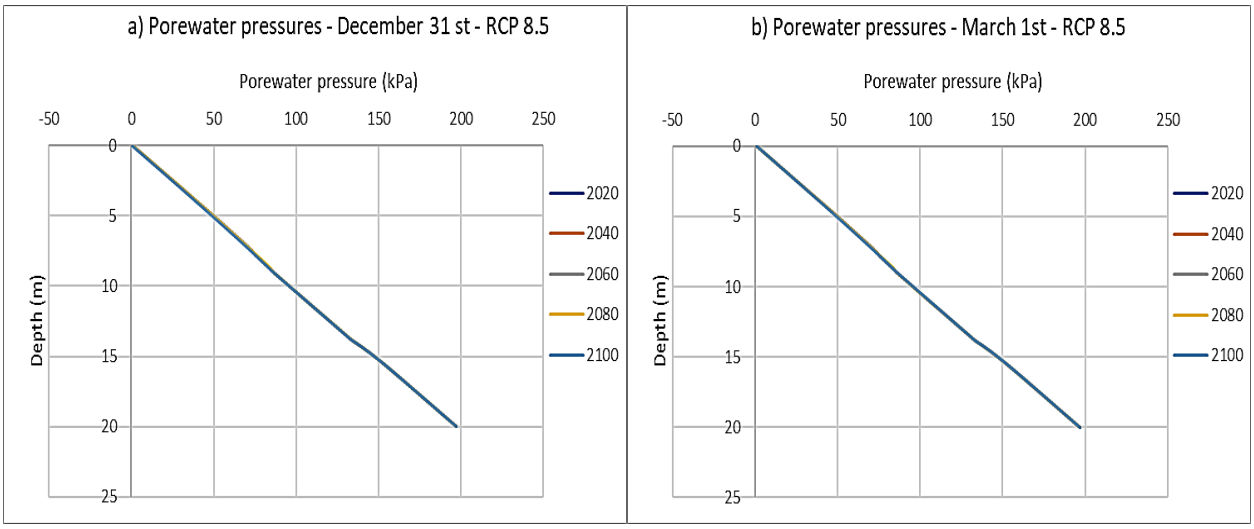

Figure 4.7.5: Porewater pressure distribution at a) December 31st and b) March 1st, 2020, 2040, 2060, 2080 and 2100 – RCP 8.5

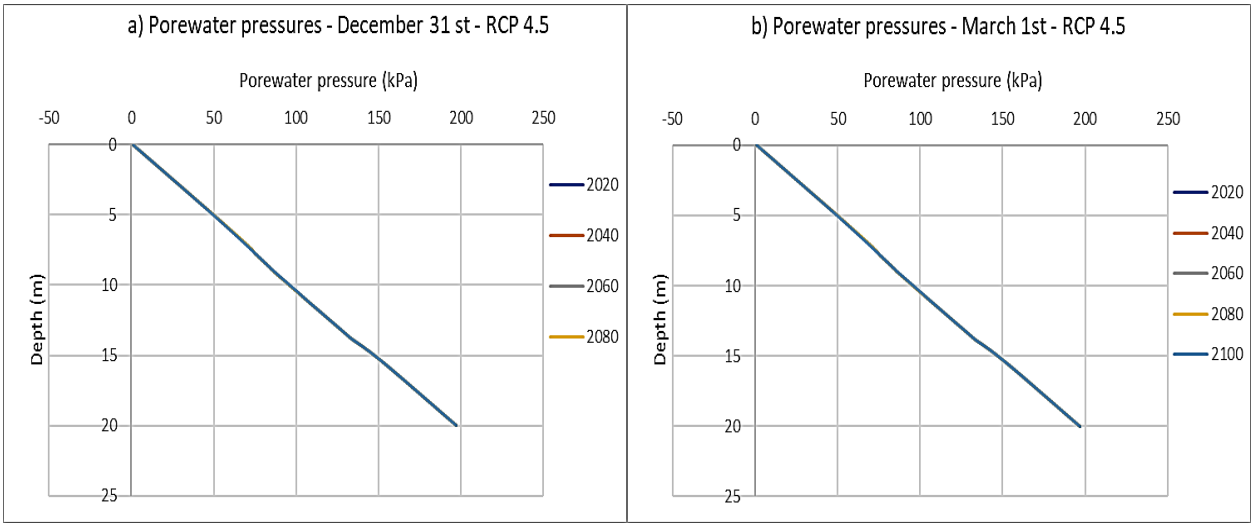

Figure 4.7.6: Porewater pressure distribution at a) December 31st and b) March 1st, 2020, 2040, 2060, 2080 and 2100 – RCP 4.5

4.7.2 Coupled hydro-mechanical simulation results

The distributions of the porewater pressure from the thermo-hydraulic analysis were integrated into a coupled hydro-mechanical model to study the settlement and the heave behavior of the ground in the three selected sited in response to climate change. The results were reported for December 31st and March 1st to detect the settlement at the end of the fall season and the frost heave at the peak of the winter season. The simulation tool provides a graphical representation of the vertical movement of the ground at each day of

the analysis for both RCPs.

The simulated settlement of the ground surface in Ottawa, Toronto and Sudbury at 2020, 2040, 2060, 2080 and 2100, for RCP 4.5 and RCP 8.5 are presented below. The results were reported on December 31st and March 1st of each year.

Figures 4.7.7 to 4.7.12 display the average ground surface settlement at 2020, 2040, 2060, 2080 and 2100 for RCP 8.5 and RCP 4.5 to visualize the impact of the global warming on the deformation behavior of the ground in Ottawa, Toronto and Sudbury.

4.7.2.1 Ottawa:

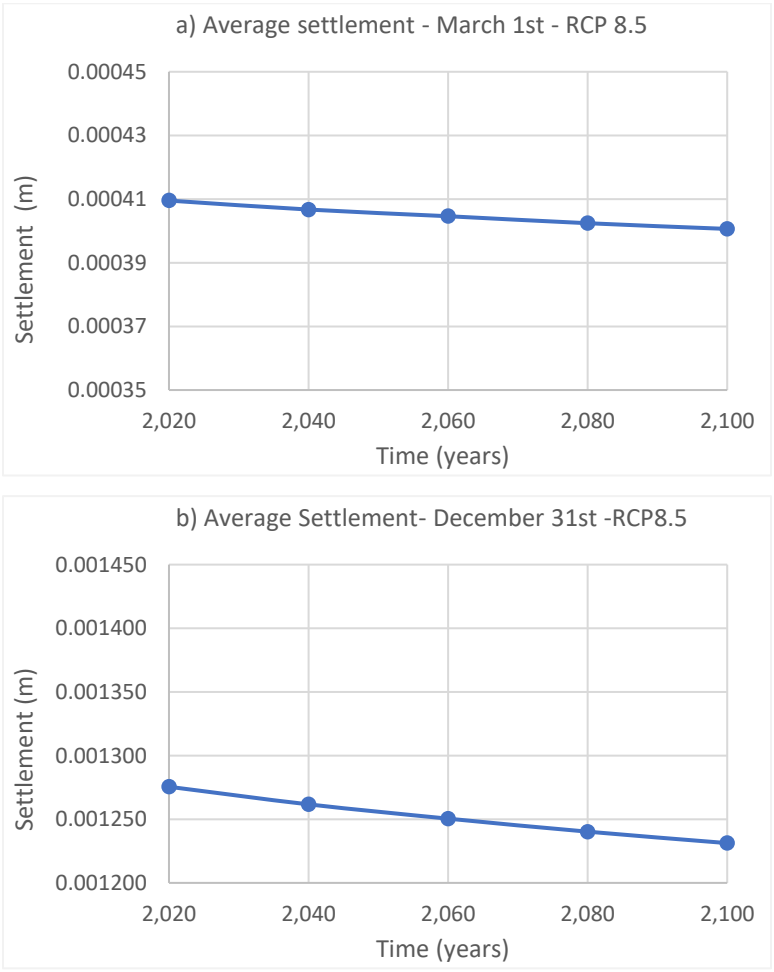

Figure 4.7.7: Average ground surface settlement at a) March 1st and b) December 31st 2020, 2040, 2060, 2080 and 2100 – RCP8.5

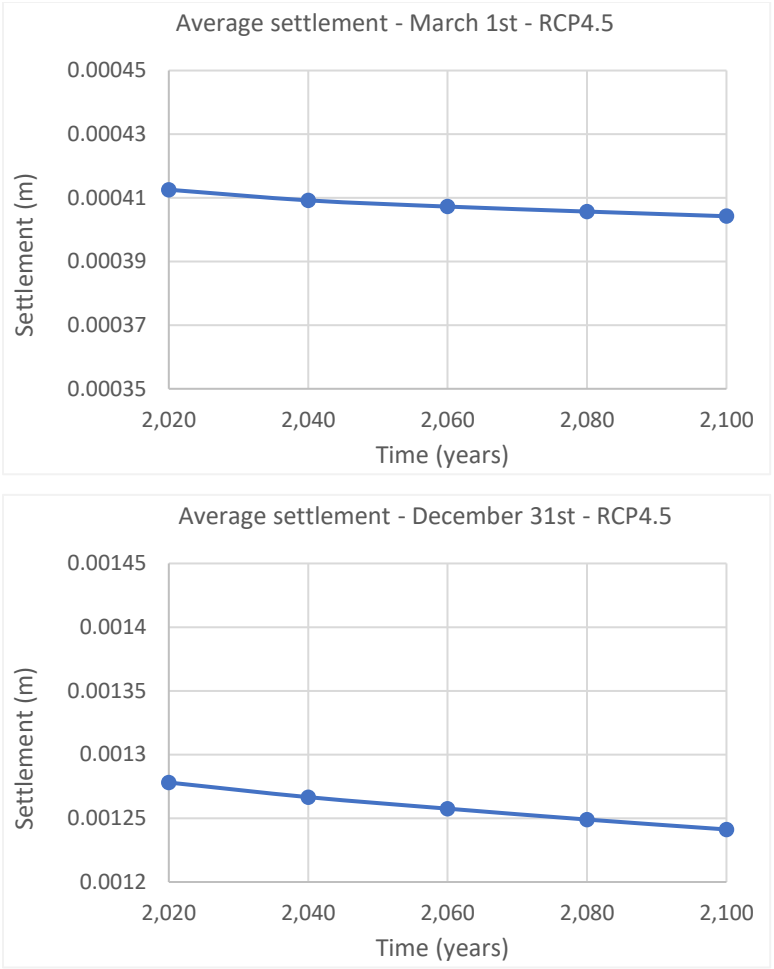

Figure 4.7.8: Average ground surface settlement at a) March 1st and b) December 31st 2020, 2040, 2060, 2080 and 2100 –RCP4.5

4.7.2.2 Toronto:

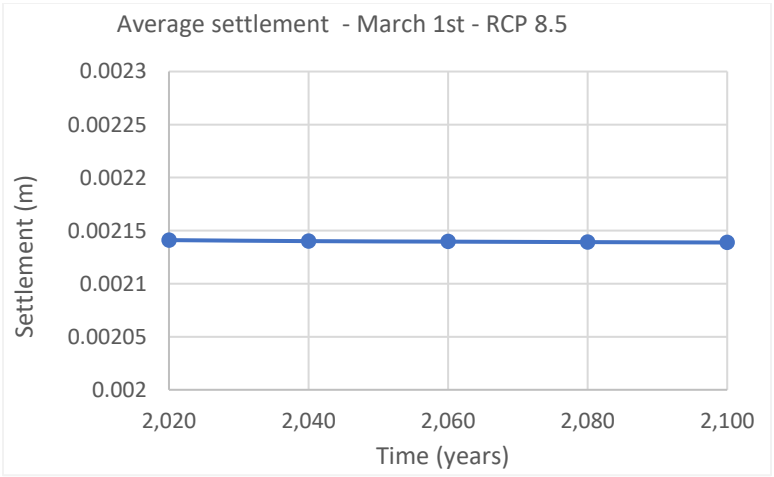

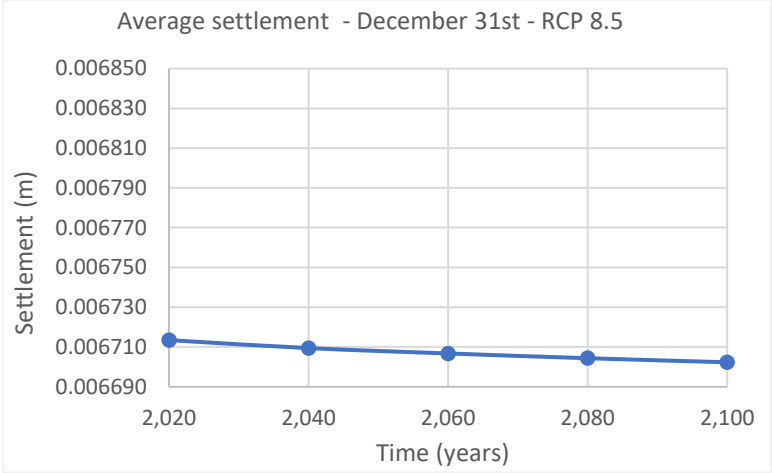

Figure 4.7.9: Average ground surface settlement at a) March 1st and b) December 31st 2020, 2040, 2060, 2080 and 2100 –RCP8.5

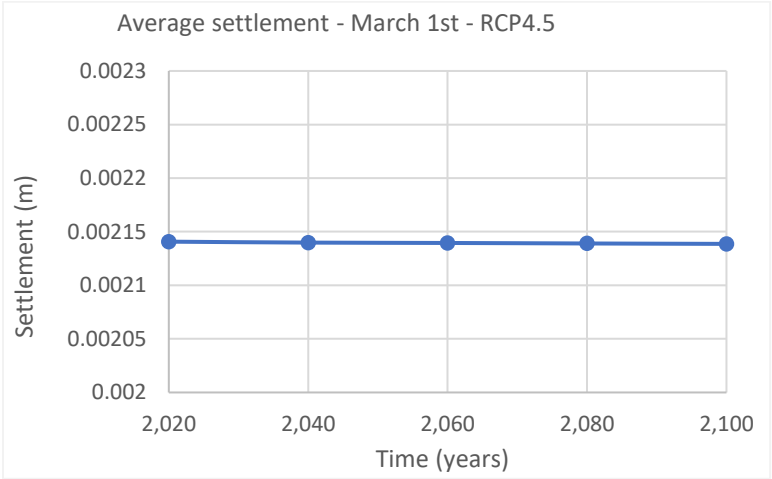

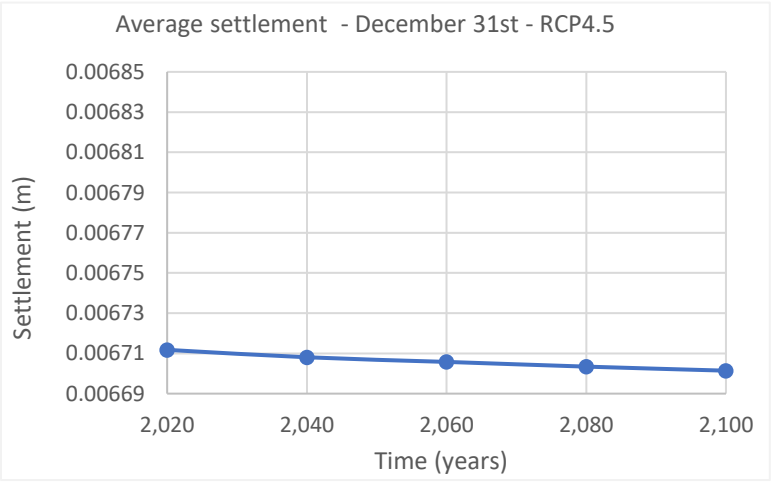

Figure 4.7.10: Average ground surface settlement at a) March 1st and b) December 31st 2020, 2040, 2060, 2080 and 2100 –RCP4.5

4.7.2.3 Sudbury:

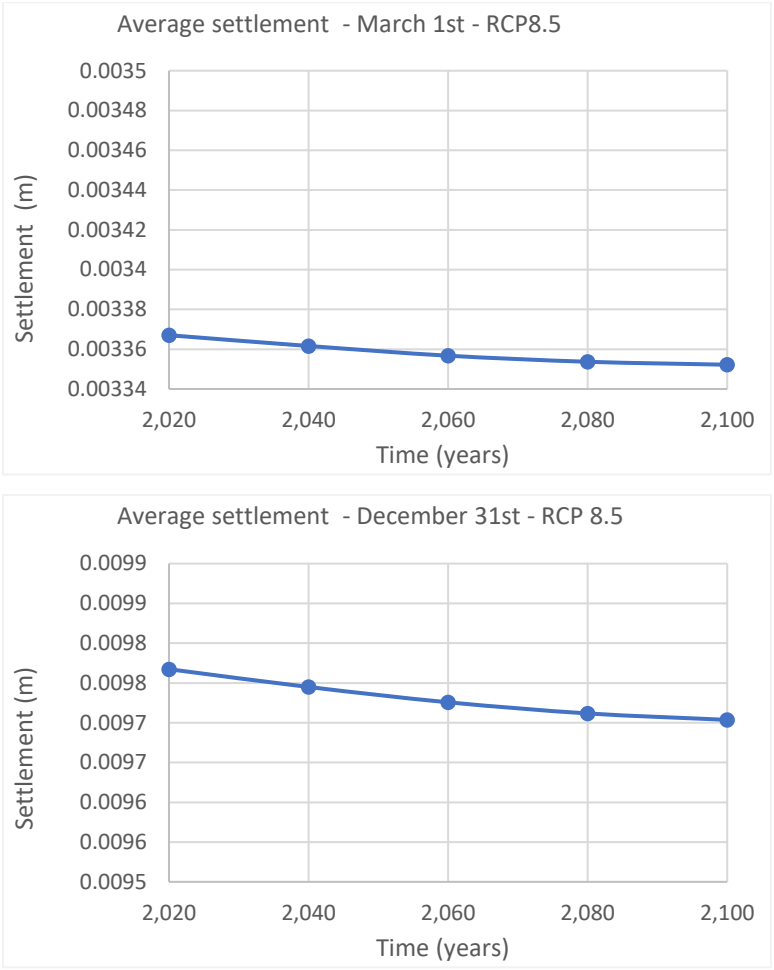

Figure 4.7.11: Average ground surface settlement at a) March 1st and b) December 31st 2020, 2040, 2060, 2080 and 2100 –RCP8.5

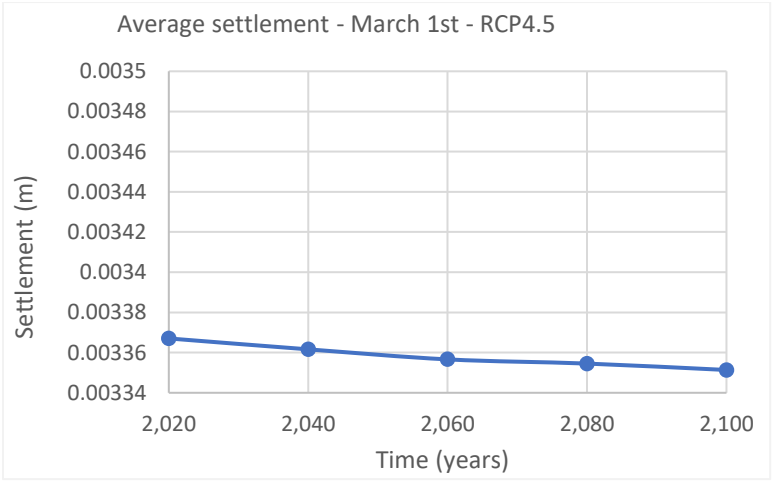

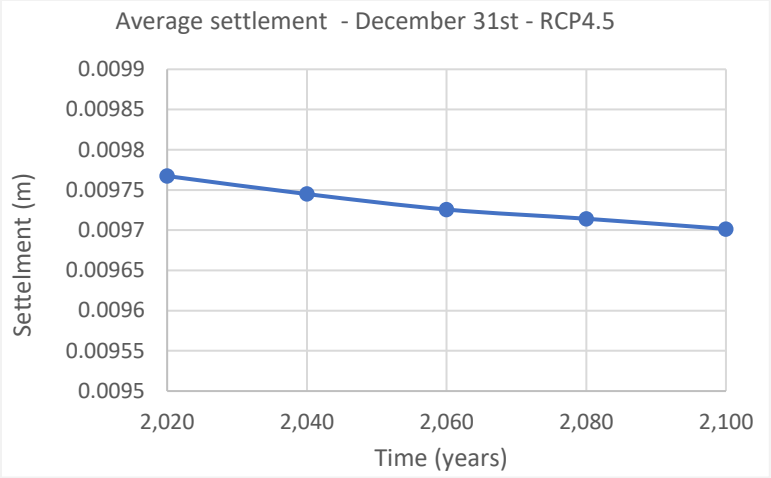

Figure 4.7.12: Average ground surface settlement at a) March 1st and b) December 31st 2020, 2040, 2060, 2080 and 2100 –RCP4.5

4.8 Discussion of results

The thermal component of the analysis showed an increase of the ground temperature from 2020 to 2100 in all the three cities for both climate change scenarios. The ground temperature rises gradually due to global warming. The ground temperature increase ranges between 4 °C at shallow depth (up to 5m) and 1°C at the bottom of the three models by 2100. Hence the thermal regime of the ground is impacted by climate warming. The impact of ground temperature rise on the hydraulic regime, specifically, the porewater pressure distribution in the soil matrix is assessed in a coupled thermo-hydraulic analysis. The change in the porewater pressure due to global warming was assessed to detect the impact of climate change on the hydraulic regime of no-permafrost soils. The porewater pressure profile was established at 2020, 2040, 2060, 2080 and 2100 for the same hydraulic boundary conditions. The hydraulic boundary conditions were kept intact over time to minimize the number of variants controlling the hydraulic regime of the ground. Therefore, the change in the porewater pressures will be mainly related to the impact of climate change on the water migration within the soil matrix.

Figures 4.7.1 to Figure 4.7.6 display the variation of the distribution of the porewater pressure in the soil in Ottawa, Toronto and Sudbury. The porewater pressure distribution is found to be linear along the depth of the soil model in the three cities for both climate change scenarios. The linear distribution was expected since the soils are fully saturated. Results showed a minimal drop of the porewater pressures with time in the three studied sites for both RCPs. The porewater distribution profile at 2020 has the steepest slope among the years. The slope of the distribution profile becomes mild with time inducing a reduction in the porewater pressures. The amount of reduction differs from city to another, nevertheless, it remains very small. A drop of 2 kPa was observed by 2100 in Ottawa at shallow depth (up to 3m) but then the porewater

profiles overlap again up to the bottom of the model. In Toronto, the same behavior was observed, however, the drop was not significant, a small shift was displayed in the porewater pressure graphs for both March 1st and December 31st. Lastly, in Sudbury, the change in the stress state is hardly noticeable. A very finite drop of the porewater pressure was observed throughout the study period. Overall, the temperature -induced alteration in stress history of the studied non-permafrost soils is not significant, therefore, the impact of global warming on the hydraulic regime on the three studied sites is not significant. The observed behavior could be due to several factors. First of all, the variation of the excess pore pressure is strongly dependent on the temperature. Studies have shown that porewater pressure decreases as ground temperature increases (Cuisinier et al., 2017). This behavior could be directly related to the decrease in the water viscosity as the temperature increases, which facilitates expulsion of the water (Cuisinier et al., 2017). Nevertheless, in the present study, the temperature rise due to global warming in the three studied sites varies between 1° C and 4° C. Therefore, it will have a little effect on the water flow within the soil body explaining the insignificant drop of porewater pressures observed in the simulation results. Furthermore, infiltration, evaporation and transpiration processes were not modelled in the coupled heat and water transfer analysis due to the absence of information on their amounts in the selected sites. Water in the ground may turn to vapor and evaporate and may leave the ground through plant transpiration, which will further induce change in the porewater pressure distribution. Finally, in the coupled heat and water transfer analysis the ground suction is estimated based on temperature and used to determine frozen ground hydraulic conductivity. Nevertheless, the hydraulic conductivities are not directly coupled with the thermal equation. Therefore, all potential impacts of temperature are not fully captured in the coupled heat and water transfer analysis. Second, SEEP/W does not take into consideration the cryogenic suction which can draw water towards the freezing front where it can accumulate and cause frost heave. Therefore, the seepage analysis in freezing ground can be very complicated, especially in the direct vicinity of the phase change region (GEO-SLOPE International Ltd, 2012).

The computed stress states in the coupled heat and water transfer analyses were integrated into the mechanical models to study the change in the settlement behavior of the ground due to global warming. At this moment in time, thermo-mechanical coupling with TEMP/W and SIGMA/W is not possible using Geslope package. Thereby, the porewater pressure changes computed in SEEP/W were used in SIGMA/W to do a volume change analysis, however, the thermal regime of the ground will not affect much the mechanical response. The computed ground settlement represents only the consolidation settlement due to the dissipation of previously established porewater pressures. Though thaw settlement due to water phase change and thaw consolidation could not be modeled at this moment in time using geoslope package. For the purpose of this study, the mechanical models do not include any external applied load, consequently, the resulting settlement is only due to the overburden soil self-weight.

Figure 4.7.7 to Figure 4.7.12 display the ground surface settlement at 2020, 2040, 2060, 2080 and 2100 in Ottawa, Toronto and Sudbury. The ground settlement was reported at March 1st and December 31st. For sensitivity analysis purposes, results were reported for both climate change scenarios; RCP4.5 and RCP8.5. The volume change analysis solved in SIGMA/W showed a parabolic settlement profile in the three studied cities where the maximum ground surface settlement was located at both edges of the model's surface. The smallest settlement values are detected at the centerline of the models. Moreover, a very small change in the settlement behavior of the ground was observed in the three studied sites with time. In Ottawa, the ground surface settlement is very small. A maximum settlement of 0.65 mm was observed in Ottawa at March 31st, 2020. A tiny shift up was noticed at the same day in 2100. Similarly, a maximum ground surface settlement of 2 mm was found at December 31st, 2020. At 2100, the maximum ground settlement drops to 1.8 mm in December 31st. Therefore, the settlement behavior variation is not very significant. In Toronto, the parabolic settlement behavior is displayed, however, the variation of the ground settlement with time is not captured. A maximum ground settlement of 2.6 mm was noted at March 1st, 2020. The settlement curves at 2020, 2040, 2060, 2080 and 2100 overlap at both days of the analysis. Therefore, approximately the same maximum settlement value was found at March 1st, 2100. Similarly, a maximum settlement of 7.6 mm was reported at December 31st. Finally, in Sudbury, the maximum ground settlement at March 1st, 2020 is 3.75 mm. at March 1st, 2100 the ground settlement slightly decreases, and the maximum settlement becomes 3.6 mm. Furthermore, the ground settlement at December 31st decreases from 10.4 mm in 2020 to 10.3 mm in 2100. Likewise, the variation of ground settlement is very small and in the range of 0.1 mm. Overall, the climate change scenarios do not seem to affect much the settlement behavior of the ground in the three cities. The difference between the simulation results of both RCP is in the range of 0.01 mm which remains insignificant. The variation of the average ground surface settlement was plotted to display the general trend of ground settlement change with time in the three studied sites. The results show a decreasing trend from 2020 up to 2100. This trend was present in the three cities and for both selected climate change scenarios.

The ground settlement simulated in SIGMA/W represents the settlement due to the dissipation of excess porewater pressure previously computed in SEEP/W. Since the variation of the porewater pressure was found to very small, the settlement variation due to temperature change is not very significant. Furthermore, the volume change analysis conducted in this study, do not allow the addition of an external applied load to the model.

At this time, SIGMA/W cannot simulate frost heave action, thaw consolidation or settlement due to temperature or phase change. Geoslope ltd are currently working hard to improve SIGMA/W and will be introducing a totally updated version for the next release. Though thaw consolidation will not be part of this initial release, it is something they plan to release in a future version of GeoStudio.

4.9 Conclusion

The following conclusions are made based on the research conducted:

1- The simulations of the future climate changes confirmed an increase of ground temperature in the three selected no-permafrost sites. The temperature of the ground will continuously increase in the Canadian no-permafrost region from 2020 up to 2100 and the rise will range between 1°C to 4° C at 2100 in the three selected sites. Additionally, climate change scenarios did not affect the simulation results as the ground temperature profiles of both RCPs provided approximately similar data.

2- The coupled convective heat and water simulations showed a very small reduction of the porewater pressures in the three studied locations, due to the increase of ground temperature. In fact, the future climate changes will not significantly affect the magnitude and distribution of porewater pressure in the soils in Canadian no-permafrost regions by 2100. Again, climate change scenarios did not significantly affect the results of the coupled thermo-hydraulic simulations. Both RCPs provided similar porewater pressure distributions.

3- The coupled hydro-mechanical analysis established using SEEP/W and SIGMA/W showed that the future climate changes will not significantly affect the settlement of the soils in Canadian no-permafrost regions. The simulation results displayed a decreasing trend from 2020 up to 2100 due to the temperature induced reduction of porewater pressures in the three no-permafrost sites. Nevertheless, the amount of settlement change dur to future climate changes is not significant, in Canadian no-permafrost region.

4- At the time being, a fully coupled THM simulation is not possible using Geoslope package, the company is working on a new version of Geoslpe package that will be released in 2021, however, the fully coupled THM will not be part of this version. It is a concept that will be developed in future releases.

4.10 References

Bathe, K-J., (1982). Finite Element Procedures in Engineering Analysis. Prentice-Hall.

Booshehrian, A., Wan, R., & Su, X. (2020). Hydraulic variations in permafrost due to open-pit mining and climate change: a case study in the Canadian Arctic. In Acta Geotechnica (Vol. 15, Issue 4). https://doi.org/10.1007/s11440-019-00786-x

Budhu, M (2007). Soil Mechanics and Foundations (2nd Ed.). Hoboken, United States: John Wiley & Sons.

Cambrian International. (2021). https://cambrianinternational.ca/

Childs, E.C., and Collis-George, N., (1950). The Permeability of Porous Materials. Proceedings of the Royal Society, pp. 392-405.

Cui, W., Potts, D. M., Zdravković, L., Gawecka, K. A., & Taborda, D. M. G. (2018). An alternative coupled thermo-hydro-mechanical finite element formulation for fully saturated soils. Computers and Geotechnics, 94, 22–30. https://doi.org/10.1016/j.compgeo.2017.08.011

Cui, Y. J., Sultan, N., & Delage, P. (2000). A thermomechanical model for saturated clays. Canadian Geotechnical Journal, 37(3), 607–620. https://doi.org/10.1139/t99-111

Cuisinier, O., Jarad, N., & Masrouri, F. (2017). Effect of temperature and strain rate on the consolidation behaviour of compacted clayey soils. European Journal of Environmental and Civil Engineering. https://www-tandfonline-com.proxy.bib.uottawa.ca/doi/full/10.1080/19648189.2017.1311806

Emerson, D. G. (1994). A heat and water transfer model for seasonally frozen soils with application to a precipitation-runoff model. US Geological Survey Water-Supply Paper, 2389. https://doi.org/10.3133/wsp2389

Flerchinger, G.N. and K.E. Saxton. (1989). Simultaneous heat and water model of a freezing snow-residuesoil system I. Theory and development. Trans. of ASAE, 32(2), 565-571.

Flynn, D. J. (2015). Field and Numerical Studies of an Instrumented Highway Embankment in Degrading Permafrost By.

GEO-SLOPE International Ltd. (2012). Seepage Modeling with SEEP / W. Geostudio Helpfile, July, 199. http://www.geo-slope.com

GEO-SLOPE International Ltd. (2013). Stress-Deformation Modeling with SIGMA/W. July, 223. http://downloads.geo-slope.com/geostudioresources/books/8/15/sigma modeling.pdf

GEO-SLOPE International Ltd. (2014). Thermal Modeling with TEMP / W. November.

Government of Canada. (2011). Historical Climate Record (Issue mm). https://climate.weather.gc.ca/

Government of Canada. (2018). Senarios and climate models. https://www.canada.ca/en/environment-climate-change/services/climate-change/canadian-centre-climate-services/basics/scenario-models.html#toc2

Government of Canada. (2019). Climate data viewer. https://climate-viewer.canada.ca/climate-maps.html#/?t=annual&v=tmax&d=dcs&r=rcp85&cp=-75.67013409675477,45.4091958833889&z=8&ts=2

Grasby, S. E., Majorowicz, J., & Ko, M. (2009). Geothermal maps of Canada. Geological Survey of Canada Open File 6167, 35.

Guymon, G. L., and J. N. Luthin. (1974). "A coupled heat and moisture transport model for arctic soils." Water Resour. Res., 10(5), 995-1001.

Harlan, R.L., (1973). Analysis of Coupled Heat-Fluid Transport in Partially Frozen Soil. Water Resource Res., vol. 9, pp. 1314 - 1323.

Harlan, R.L., and Nixon, J.F. (1978). Ground thermal regime. Chapter 3 in Geotechnical Engineering for Cold Regions, ed. O.B. Andersland and D.M. Anderson. New York: McGraw-Hill, pp. 103-163

Jame, Y. W. and Norum, D. I. (1980). "Heat and mass transfer in a freezing unsaturated porous medium." Water Resources Research, 16(4), 811-819.

Lesage, K. (2008). Experimental studies of thaw consolidation of fine grained frozen soils from the Mackenzie Valley.

National Snow and Ice data center. (2020). Frost actions. https://nsidc.org/cryosphere/glossary/term/frost-action

Natural Resources Canada. (2010). Geological Survey of Canada.

Orlando, B. A., & Ladanyi, B. (2004). Frozen Ground Engineering (4th ed.). John Wiley & sons.

Richards, L.A. (1931). Capillary conduction of liquids through porous mediums. Phys. J. Gen. Appl. Phys., 1, 318–333

Segerlind, L.J., (1984). Applied Finite Element Analysis, 2nd Ed. John Wiley and Sons, Inc

Smith, I.M. and Griffiths, D.V., (1988). Programming the Finite Element Method, 2nd Ed. John Wiley and

Sons, Inc.

Taylor, G. S. and Luthin, J. N. (1978). "A model for coupled heat and moisture transfer during soil freezing." Can. Geotech. J., 15, 548-555.

Veinović, Ž., Uroić, G., Domitrović, D., & Kegel, L. (2020). Thermo-hydro-mechanical effects on host rock for a generic spent nuclear fuel repository. Rudarsko Geolosko Naftni Zbornik, 35(1), 65–80. https://doi.org/10.17794/rgn.2020.1.6

Zhang, T. (2005). Influence of the seasonal snow cover on the ground thermal regime: an overview. In Simulation (Issue December). https://doi.org/10.1029/2004RG000157.1.INTRODUCTION

Zhang, Y. (2014). Thermal-Hydro-Mechanical Model for Freezing and Thawing of Soils. 201. https://deepblue.lib.umich.edu/bitstream/handle/2027.42/108828/zhyao_1.pdf?sequence=1%0Ahttps

://deepblue.lib.umich.edu/handle/2027.42/108828

Zienkiewicz, O.C. and Taylor, R.L., (1989). The Finite Element Method, 4th Ed., Vol. 1. McGraw-Hill.

Chapter 5 – Synthesis and discussions of results, and practical engineering application

5.1 Introduction

The impact of global warming on the thermal and thermo-hydro-mechanical behavior of the soils in selected Canadian no permafrost areas is studied in this thesis. The acquired results provide a clear understanding of the ground temperature changes due to global warming, the change in the porewater distribution in the soil and the resulting consolidation/settlement. The results obtained are synthesized and discussed in this chapter. Moreover, a practical geotechnical application of the simulation tools developed in this thesis and results obtained is established. This application focuses on understanding and simulating the thermal and geotechnical response of the soil around a bridge pile foundation in the Canadian no permafrost region to climate change. The simulation results enable to determine whether the geotechnical stability and design of pile foundations for the current and future transportation bridges in Canadian no permafrost regions may be affected by global warming.

5.2 Synthesis and discussions of results

The thermal simulations established in the first part of the present study displayed an important increase of the ground temperature in the three studied sites. All in all, the ground thermal regime of the Canadian no-permafrost will be affected by global warming. The rise of the ground temperature will impact the length of the frost period and the frost penetration depth in this area of the Canadian territory. A significant reduction of the annual frost period was noted in the three studied cities. In fact, the seasonally frozen ground layer will completely disappear in the center and the south of the Canadian no-permafrost region on March 1st by 2100. In the north of this region, the thickness of the seasonally frozen ground layer is reduced significantly, results confirmed that the frost penetration depth in Sudbury is reduced from 2.1 m on March 1st 2020 to 0.75 m in March 1st 2100 due to climate change. In addition to the above stated findings, the impact of climate change on the soil behaviour is found to be limited to the top layers of the soil. The thermal behavior of the first 5m into the ground follows a cyclic thermal sequence depending on the seasons. At shallow depths, the ground temperature varies greatly under the effect of changing air temperature between the seasons. The ground temperature difference between the winter season and the summer season varies between 20 °C at a depth of 1 m to 10 °C at a depth of 4 m. The effect of the climate on the soil fades with depth, results confirmed that the ground temperature remains constant starting at a depth of 10 m under the impact of the geothermal gradient. Consequently, the ground thermal regime at deep levels will not be affected by future climate changes. In addition, the assessment of the effect of the snow cover depth on the thermal regime of the ground revealed an unseizable change of the ground thermal

behaviour under different snow cover depths. Therefore, the snow cover depth does not represent a governing factor of the response of no-permafrost soils to future climate change in Canada. The results acquired in the present thermal analysis provide an understanding of the thermal regime of the ground in the Canadian no-permafrost region for the next 80 years. The methodology of the future thermal simulations could be used/ duplicated to assess the impact of future climate changes on other soil's geotechnical composition and geometries in the Canadian no-permafrost region.

The changes in the thermal regime of the ground will induce changes in the stress state of the soil and accordingly change in the settlement behaviour of the ground. Chapter 4 established the coupled thermo-hydro-mechanical analysis to simulate the effect of rising ground temperature on the in-situ porewater pressure regime and the consolidation/settlement behaviour of soils during the study time period. The results of the thermo-hydraulic simulation displayed a minimal effect of future climate changes on the hydraulic equilibrium of the soil with time. The ground temperature escalation due to global warming will not engender a noticeable change in the distribution and the magnitude of the in-situ porewater pressures in the ground in all Canadian no-permafrost regions by 2100. A small drop, in the first 4m of the ground, was displayed in the porewater pressures profiles in the three study areas. Nevertheless, the amount of reduction is less than 2 kPa in 2100. Consequently, the magnitude and the distribution of the effective stress in the ground will not be affected by future climate change.

The second stage of the THM analysis includes a coupled hydro-mechanical simulation to assess the impact of future climate changes on the settlement/ consolidation of the soil in the Canadian no-permafrost area. The resulting in-situ porewater pressures, computed in the coupled heat and water transfer analysis, were incorporated in the mechanical model to compute the soil settlement/consolidation. The simulation results displayed an unsignificant drop, in the order of 0.1 mm of the ground settlement due to global warming. This behaviour was observed in the three selected study areas. The strain and strength behaviour of soil is a function of the effective stress, in fact, the soil's in-situ effective stress controls the soil's motion and displacement, consequently, because of the minimal change of the in-situ effective stress due to global warming noticed in the thermo-hydraulic simulations, the ground settlement in Canadian no-permafrost region is not significantly affected by future climate changes.

The climate change scenarios; RCP2.5, RCP4.5 and RCP8.5 provide different projections of the air temperature future changes due to global warming. Indeed, RCP 8.5 provide the highest air temperature change by 2100 followed by RCP4.5 and then RCP2.5. Therefore, the simulated ground temperature using RCP8.5 projections is the highest among the three climate change scenario simulations. Nevertheless, in the present study, the soil's THM behaviour does not seem to be sensitive to climate change scenarios. The difference between the ground temperature profiles of the three RCPs is not very significant in the three-study area. Accordingly, the porewater pressure distribution and magnitude is not found to be sensitive to

climate change scenarios. Both RCPs, namely RCP4.5 and RCP8.5, considered in the thermo-hydraulic simulations provided almost similar results. this trend was observed in the three selected no-permafrost areas. As a result of the minimal effect of climate change scenarios on the distribution of the porewater pressures and the in-situ effective stresses, the settlement/ consolidation behaviour of the ground is not affected by future climate change scenarios.

5.3 Application to bride pile foundation ground

Roads, railways, and other transportation infrastructure are of vital economic, social, and political importance in all Canadian regions. Bridges play a critical role in the Canadian transportation infrastructure and network. Resilient and secure bridge infrastructure is vital for population safety and economic prosperity. Bridge structures are commonly supported by pile foundation systems. The geotechnical stability or safety of the bridge substructures and foundation mainly rely on the strength, bearing capacity, and settlement (consolidation behaviour) of the soils beneath and/or adjacent to the pile foundation structures. Climate warming induced changes in soil thermal behavior could alter the geotechnical response/behaviour (e.g., porewater pressure, consolidation, settlement, shear strength) of the soil around the bridge pile foundation), cause negative skin friction and impact the uplift force applied on a bridge pile in Canadian no permafrost areas. These changes may impact the geotechnical stability of the transportation bridge pile foundation, affect the safety of the bridges and/or result in increasing their maintenance costs and decreasing their useful life span. So, to address the aforementioned issues, numerical simulations of the impact of global warming on the thermal and THM response of the ground around a bridge pile in a Canadian no permafrost area are carried out by using the developed approach/tools. The thermal and THM changes of the soil around and beneath a 15 m long pile foundation of 1 m diameter are assessed. A coupled thermo-hydraulic simulation is first established to assess ground temperature and porewater pressure changes around the pile structure due to global warming. Afterwards, a coupled hydro-mechanical simulation was conducted to determine the settlement behavior around the shaft of the pile structure. Both climate change scenarios; RCP 8.5 and RCP4.5 are considered in this modeling case study. The simulation models use the geometry, climate conditions and future climate projections of the city of Ottawa. The main results of the modeling analysis are reported and discussed below. Additionally, the modeling process of the bridge pile foundation is described. Finally, the summary and the main conclusions of the analysis are conveyed. It should be underlined that simulating the response of pile groups and whole bridge structure is out of the scope of this master thesis.

5.3.1 Model geometry:

A simulation of a single pile foundation is established using the proposed approach in Chapter 4. This simulation aims to assess the temperature, porewater pressure and settlement variations around the perimeter of the pile structure. A steel pile of 1m diameter and a length of 15 m was modeled using the geotechnical profile of the City of Ottawa. The steel pile was assumed to have of modulus of elasticity of 200 GPa, a Poisson ratio of 0.3 and a unit weight of 75.8 kN/m^3. The pile structure is modeled using a linear elastic constitutive model in SIGMA/W.

Figure 5.3.1 represents the geometry configuration of the pile structure.

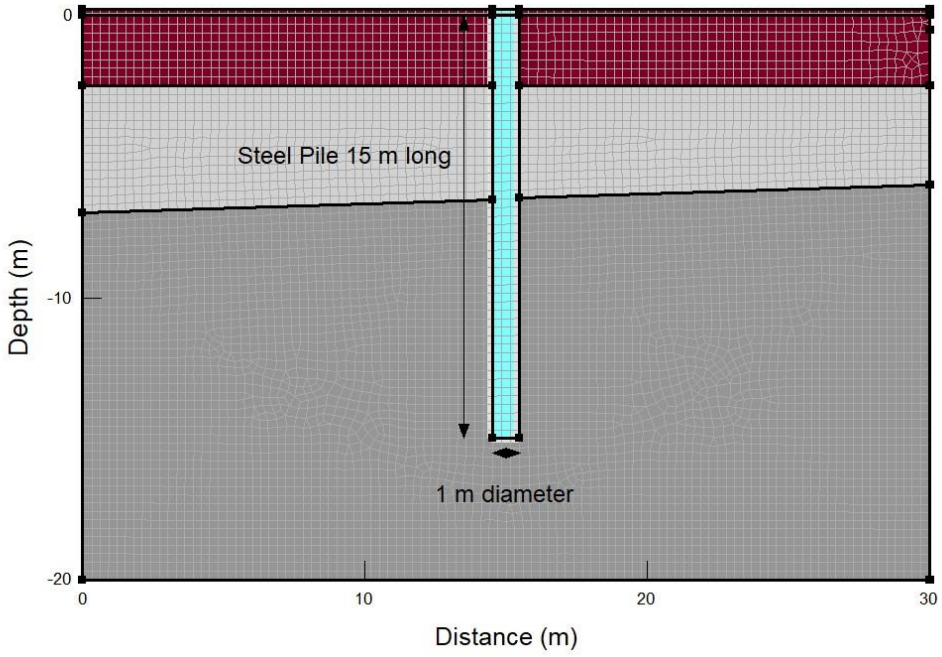

Figure 5.3.1: Geometry configuration of the pile structure

5.3.2 Boundary conditions:

The thermal and mechanical boundary conditions remain the same as in section 4.6.1. Nevertheless, a small change to the SEEP/W analysis was made. The groundwater table was shifted to the toe and around the edges of the pile foundation. The total heads at the edges of the models remained the same as in section 4.6.1. Figure 5.3.2 represents the groundwater table change in SEEP/W. The deformation model simulates the settlement of the soil around the pile foundation, therefore, there is no deformation of the pile foundation. The soil body is free to move laterally along the shaft of the pile, however, a fixed X boundary condition was applied along the shaft of the pile to restrain the horizontal movement of the pile and the soil body in order to force the no-deformation behaviour of the pile foundation.

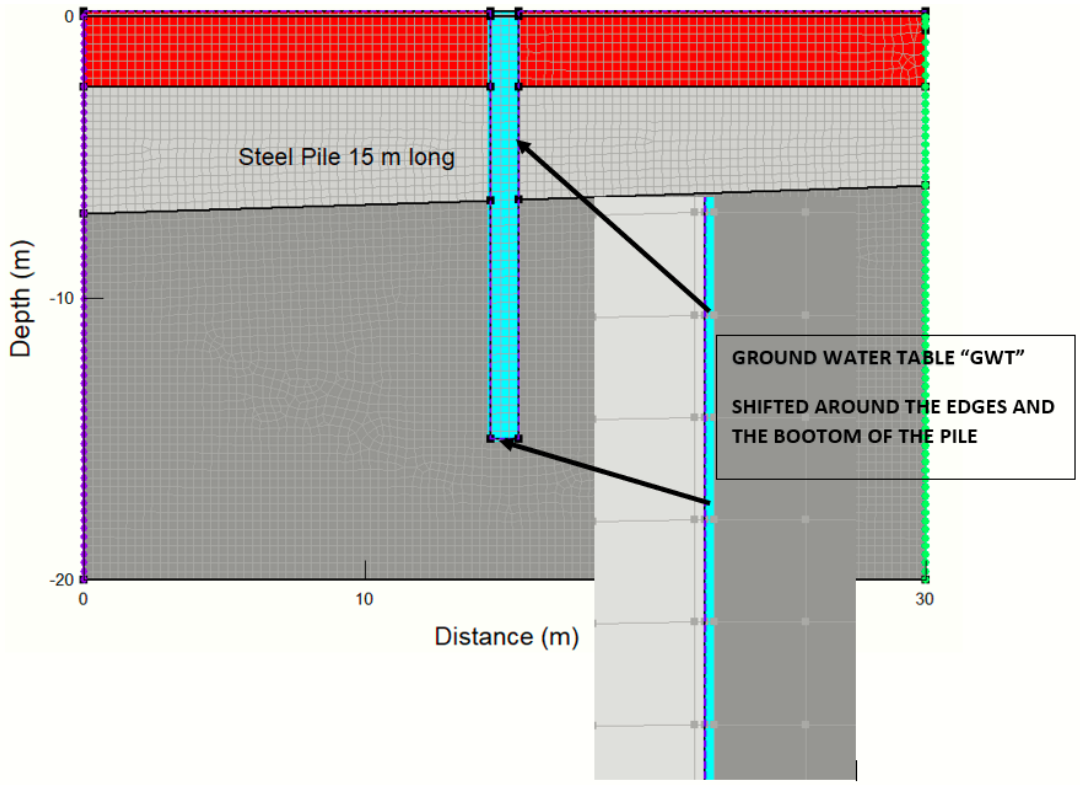

Figure 5.3.2: Groundwater table boundary conditions - SEEP/W.

5.3.3 Simulation results

The simulation results include temperature profiles around the perimeter of the pile structure, porewater distribution along the pile perimeter and the vertical displacement of the ground of the soil adjacent of the pile foundation. Results are reported on March 1st and December 31st of different years of the analysis to assess the impact of climate change of the THM behaviour of the foundations soil.

Figure 5.3.3 a, b, c represents the ground temperature distribution around the pile structure on December 31st, 2020, 2060 and 2100 for RCP 8.5.

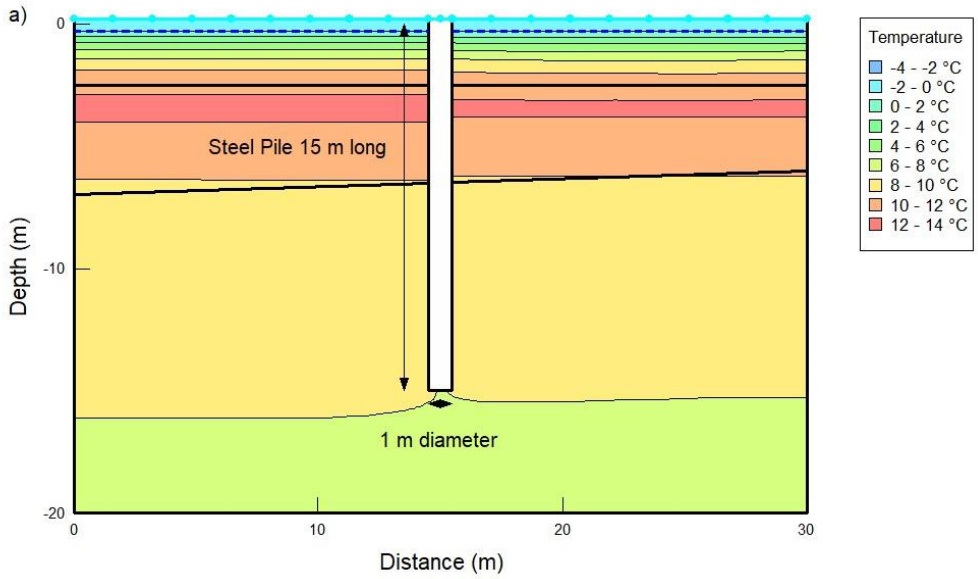
a)
Steel Pile 15 m long
1 m diameter
Depth (m)
Distance (m)
Temperature
-4 - -2 °C
-2 - 0 °C
0 - 2 °C
2 - 4 °C
4 - 6 °C
6 - 8 °C
8 - 10 °C
10 - 12 °C
12 - 14 °C

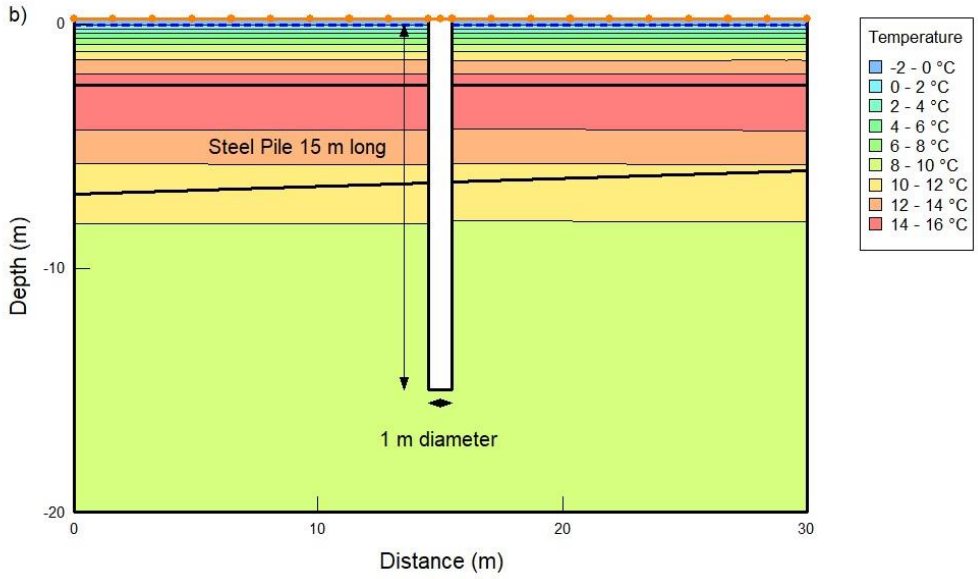
b)
Steel Pile 15 m long
1 m diameter
Depth (m)
Distance (m)
Temperature
-2 - 0 °C
0 - 2 °C
2 - 4 °C
4 - 6 °C
6 - 8 °C
8 - 10 °C
10 - 12 °C
12 - 14 °C
14 - 16 °C

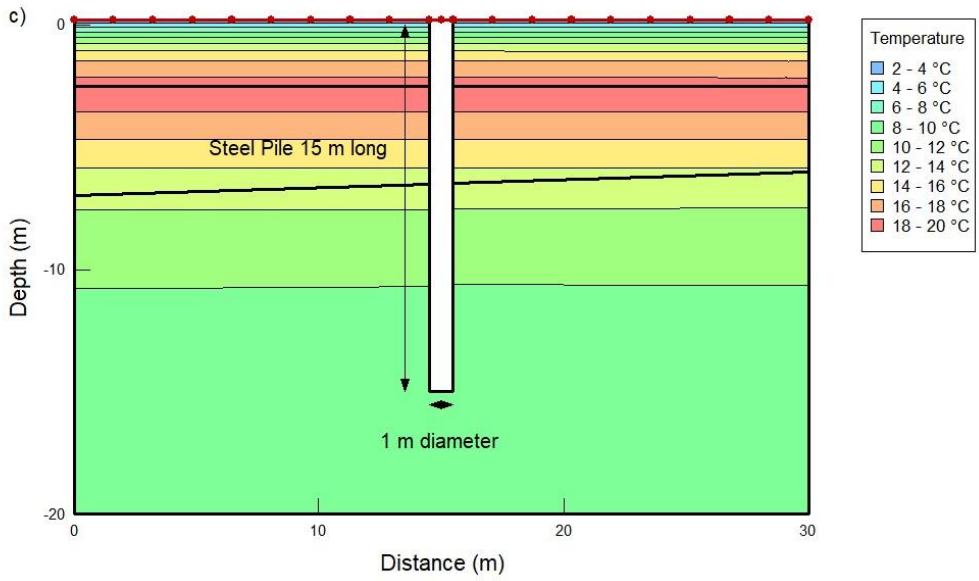

Figure 5.3.3: Ground temperature distribution around the pile structure in December 31st, a) 2020, b) 2060 and c) 2100 for RCP 8.5

Figure 5.3.4 a,b and c represents the porewater pressure distribution along the pile structure. The results were reported in December 31s, 2020, 2060 and 2100 for RCP 8.5.

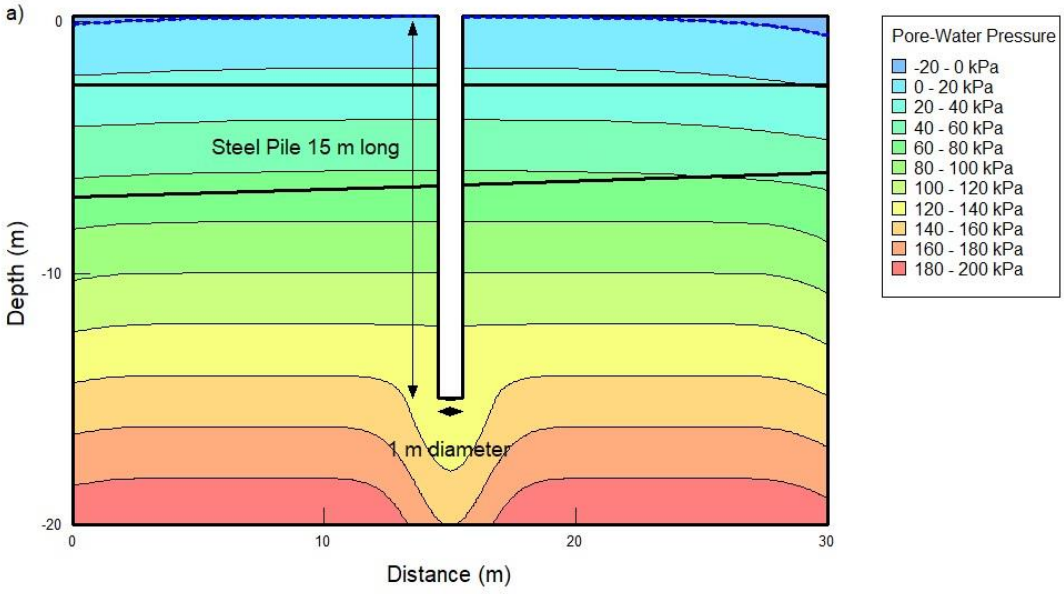

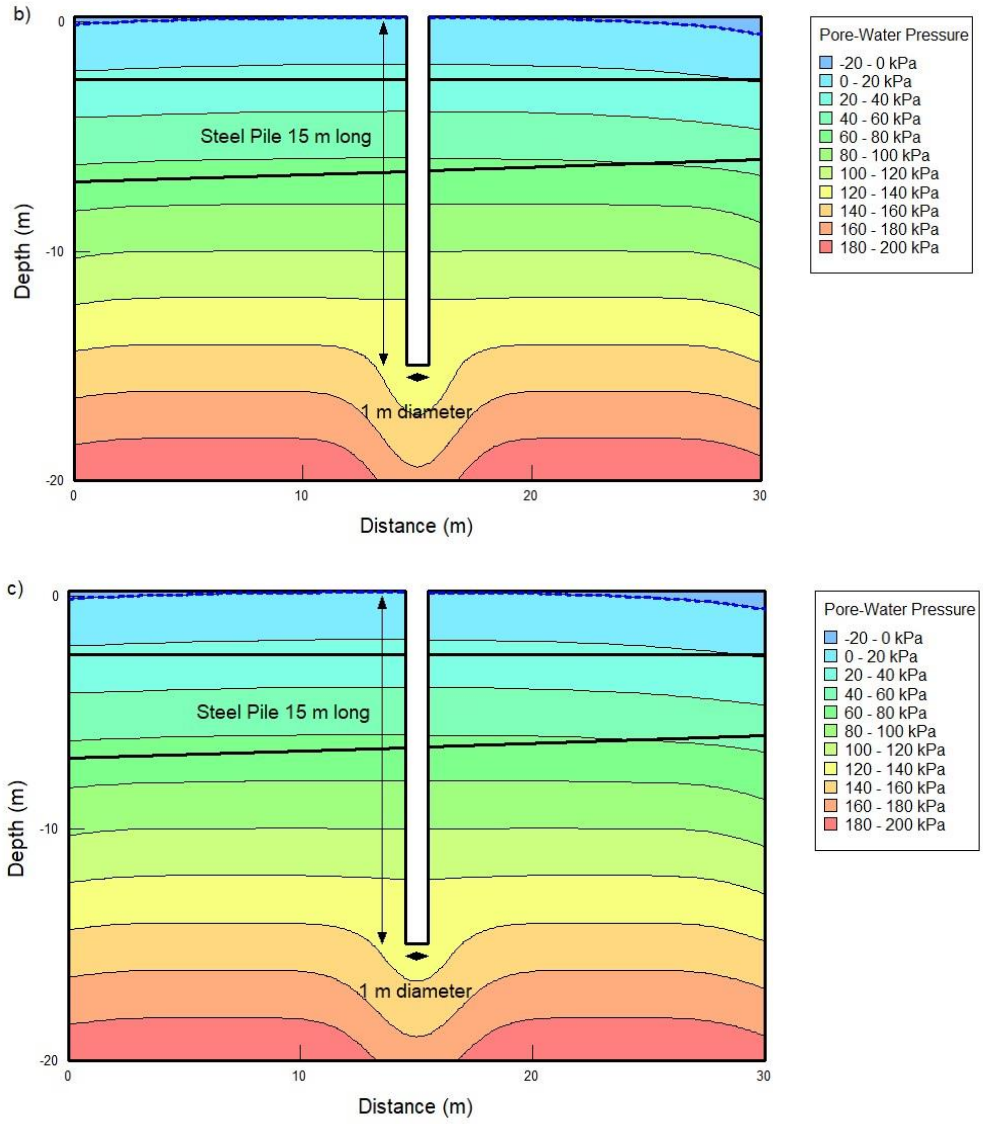

Figure 5.3.4: Porewater pressure distribution along the pile structure. The results were reported in December 31s,a) 2020, b) 2060 and c) 2100 for RCP 8.5.

The vertical settlement is also represented as part of the results of coupled hydro-mechanical simulation. Figure 5.3.5 a,b and c represents the ground deformation structure in December 31s, 2020, 2060 and 2100 for RCP 8.5.

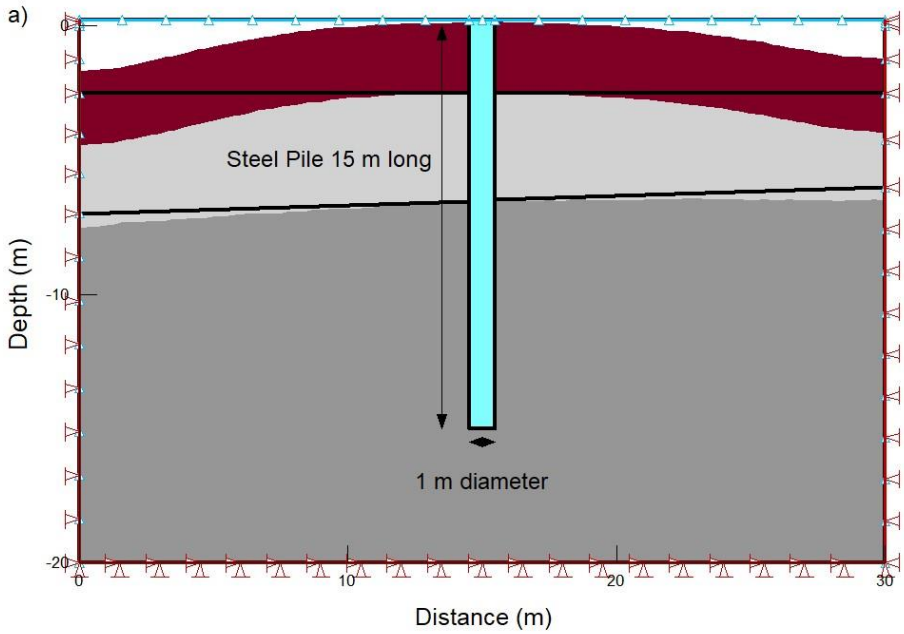
a)
Steel Pile 15 m long
1 m diameter
Depth (m)
0
-10
-20
0
10
20
30
Distance (m)

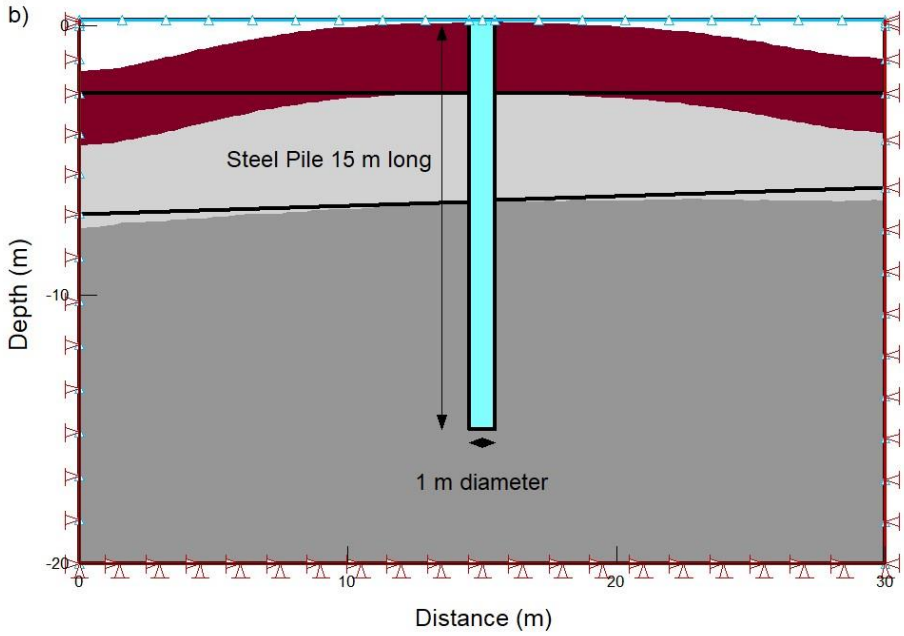
b)
Steel Pile 15 m long
1 m diameter
Depth (m)
0
-10
-20
0
10
20
30
Distance (m)

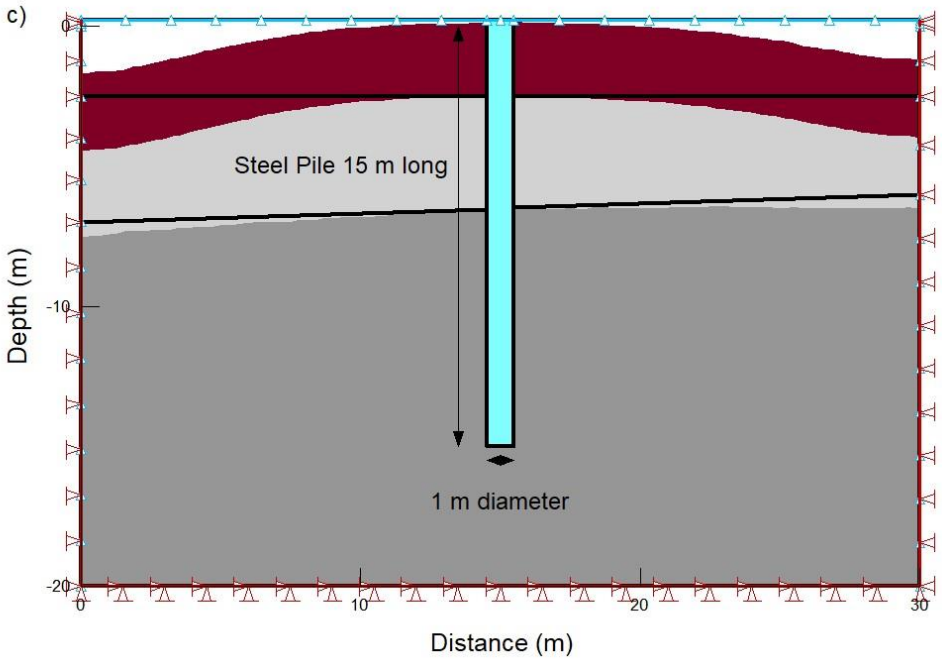

Figure 5.3.5: Ground deformation structure in December 31s, a) 2020, b) 2060 and c) 2100 for RCP 8.5.

The ground temperature profiles in March 1st and December 31st at 2020, 2060 and 2100, along the pile perimeter are presented in figure 5.3.6 a,b,c. Due to the symmetrical geometry of the model, results are reported only for the right side of the pile perimeter. Results are reported for both RCP4.5 and RCP8.5.

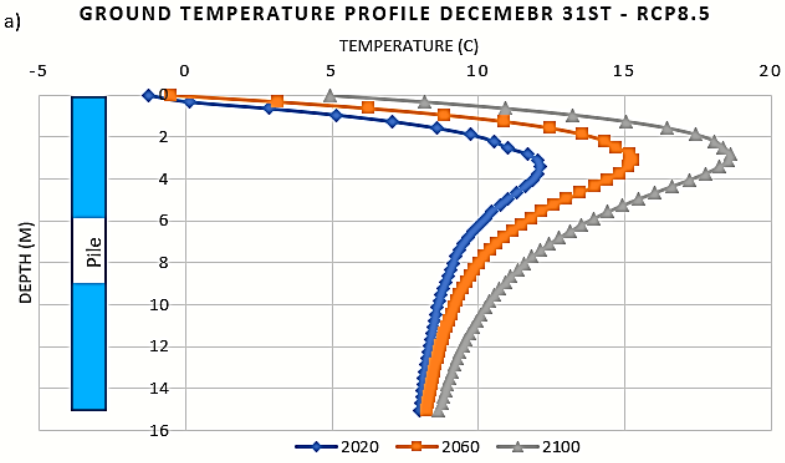

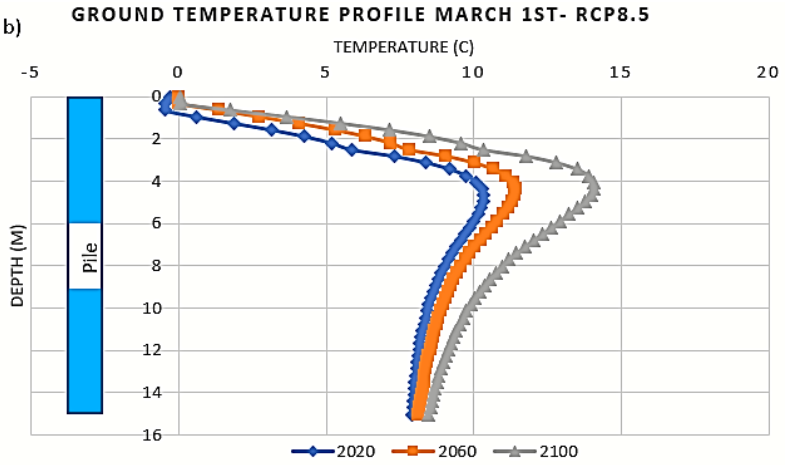

Figure 5.3.6: Ground temperature profiles at a) December 31 st and b) March 1st for 2020– 2060– 2100 – RCP8.5

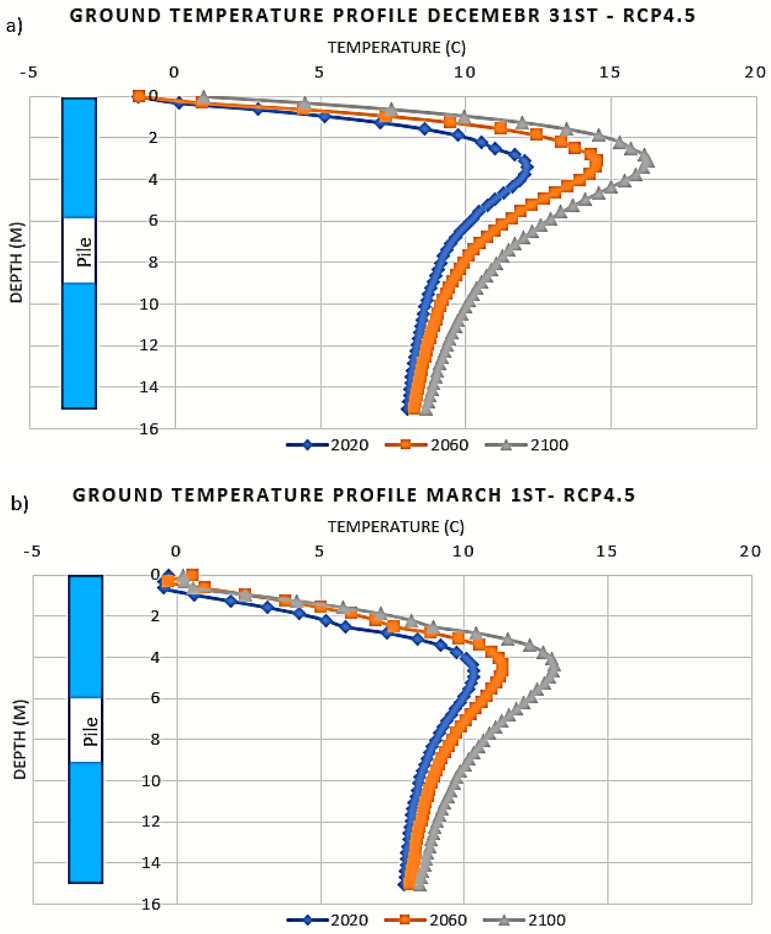

Figure 5.3.7: Ground temperature profiles at a) December 31 st and b) March 1st for 2020– 2060– 2100 – RCP4.5

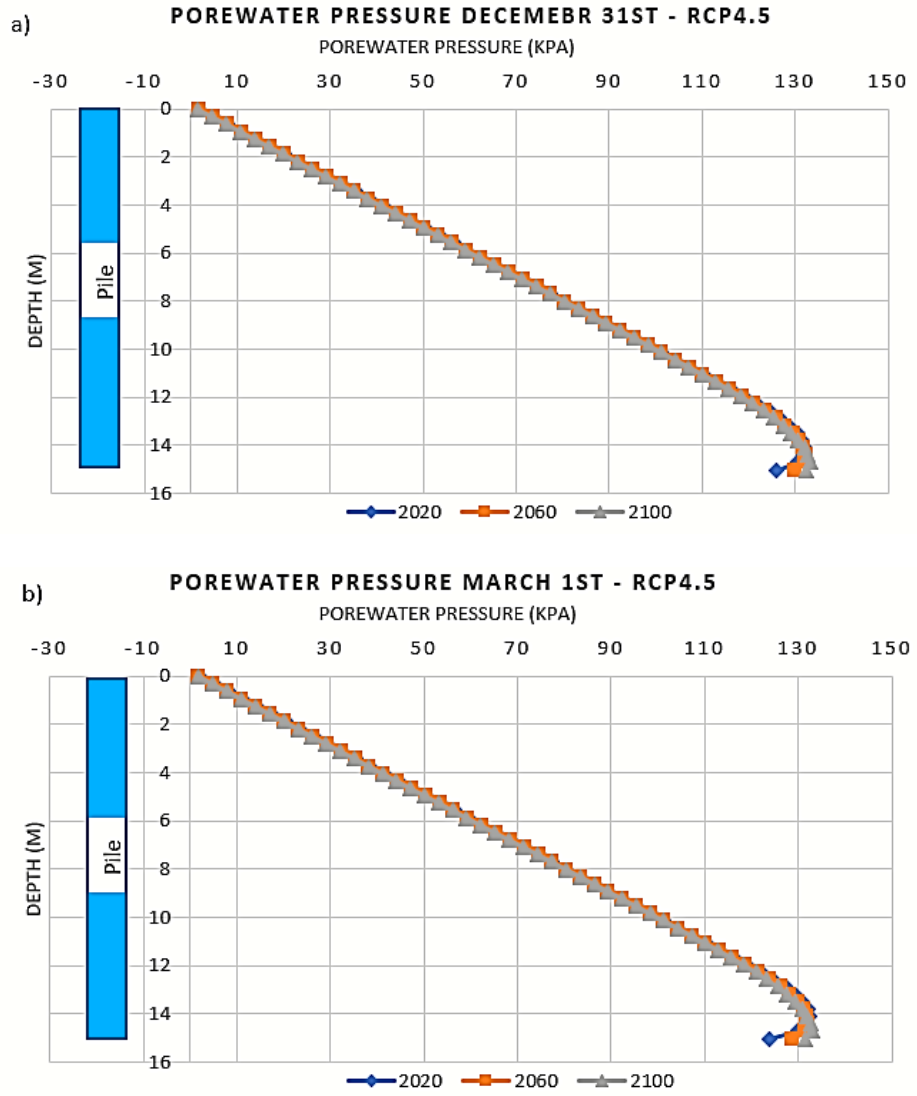

Figure 5.3.8: Porewater pressure distribution at a) December 31st and b) March 1st, 2020, 2040, 2060, 2080 and 2100 – RCP 4.5

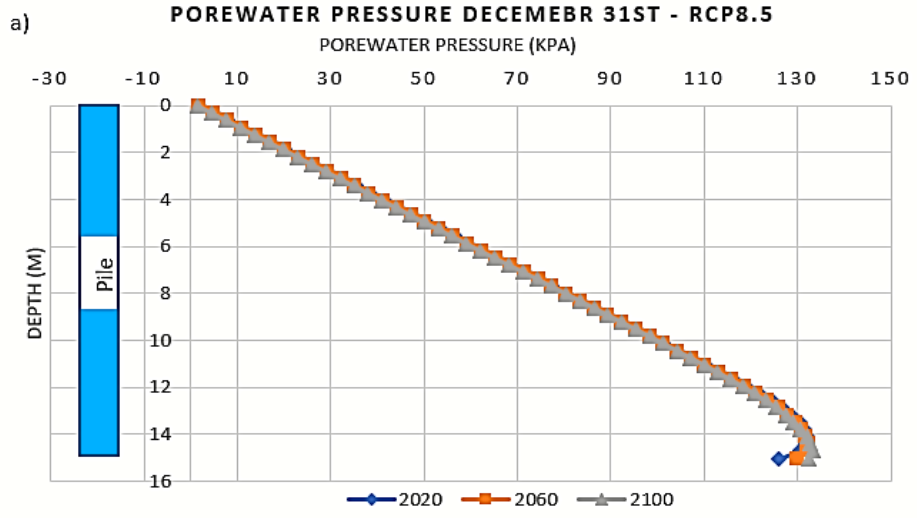

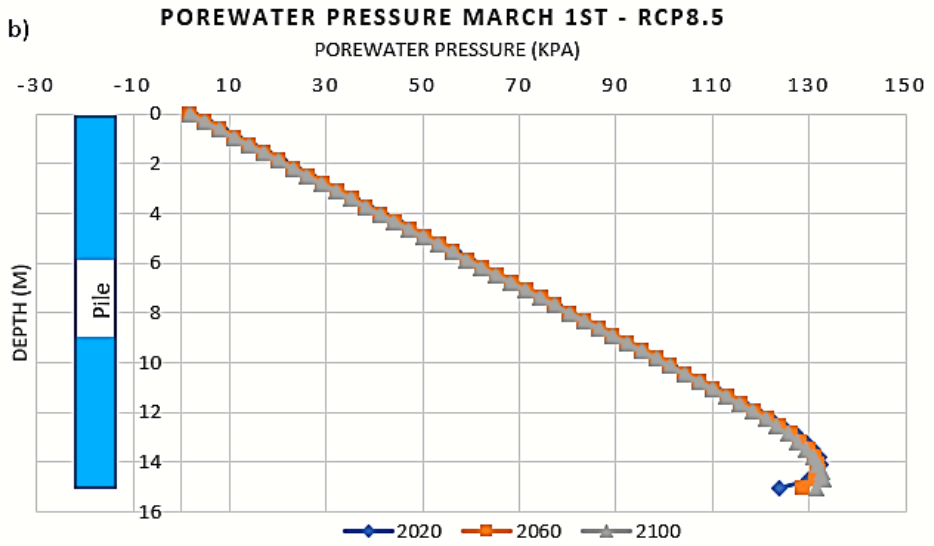

Figure 5.3.9: Porewater pressure distribution at a) December 31st and b) March 1st, 2020, 2040, 2060, 2080 and 2100 – RCP 4.5

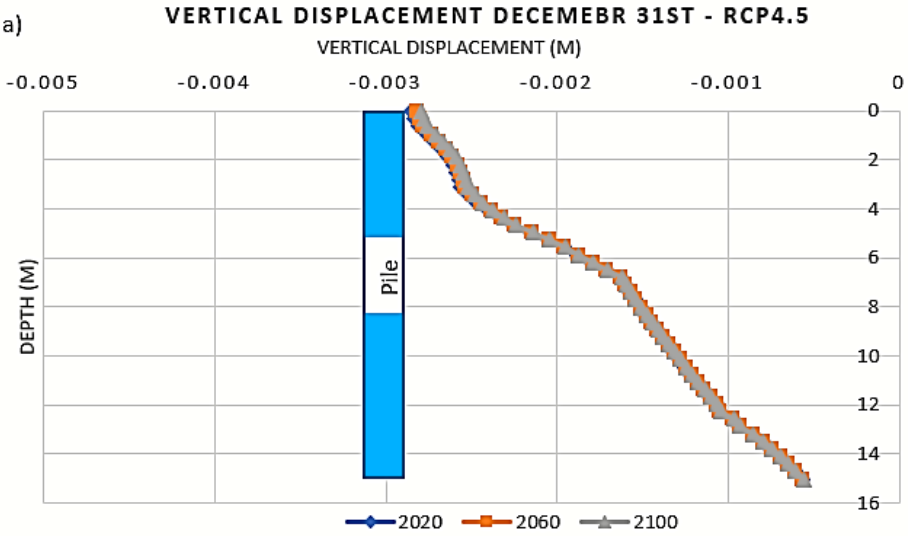

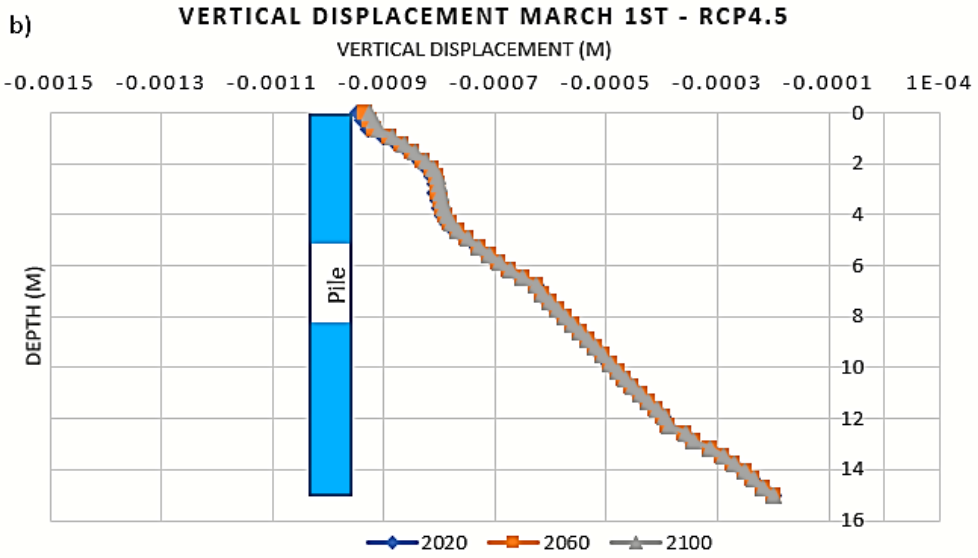

Figure 5.3.10: Vertical Displacement at a) December 31st and b) March 1st, 2020, 2040, 2060, 2080 and 2100 – RCP 4.5

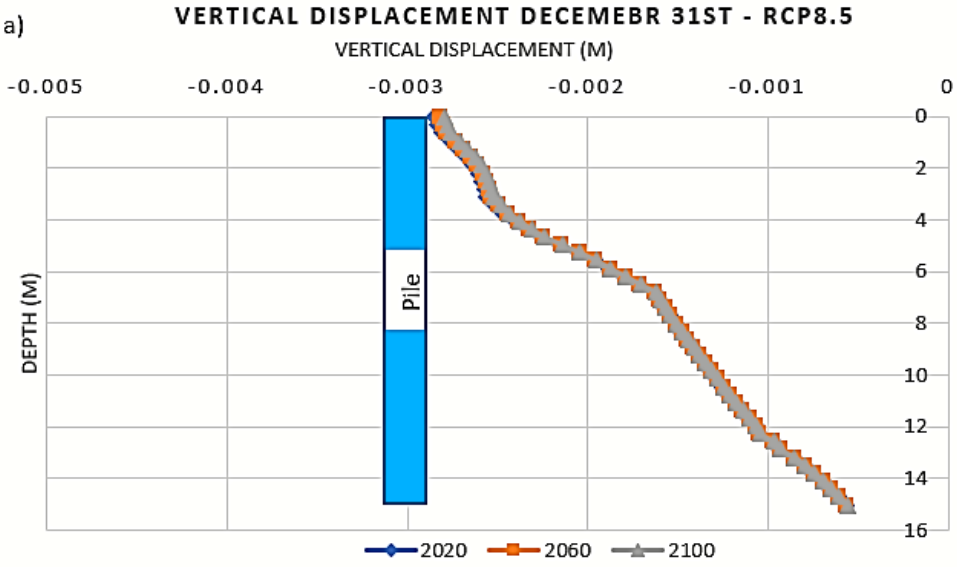

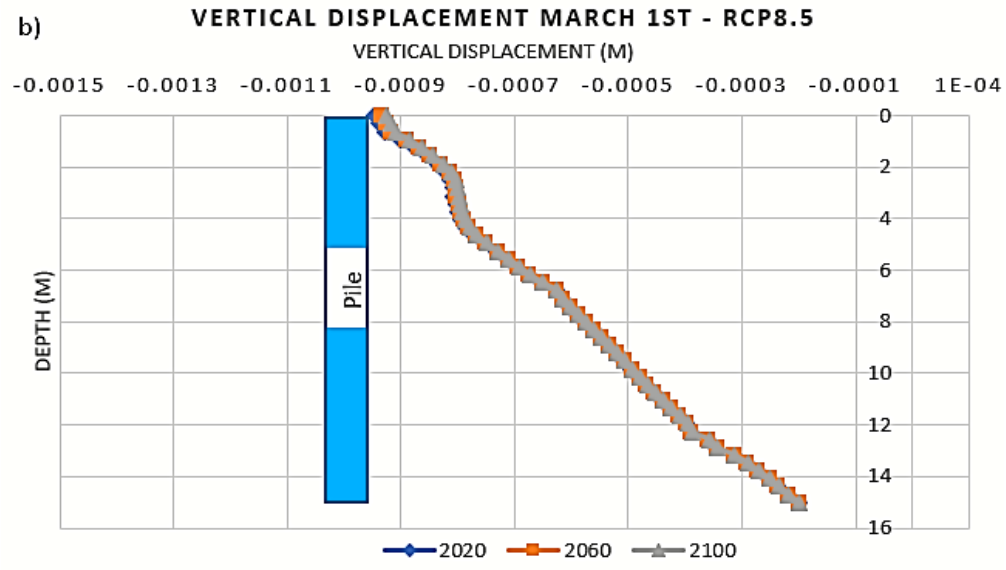

Figure 5.3.11: Vertical Displacement at a) December 31st and b) March 1st, 2020, 2040, 2060, 2080 and 2100 – RCP 8.5

5.4 Discussions of results and conclusions

Figure 5.3.6 through Figure 5.3.7 display the ground temperature profiles along the shaft of the pile on December 31st and March 1st respectively in Ottawa for both climate change scenarios. The results of the coupled thermo-hydraulic simulation of the foundation soil confirmed that ground temperature around the pile structure will experience a continuous rise due to global warming up 2100. Ground temperature will increase by 1 to 5 ° C by 2100 due to future climate changes. The ground thermal regime is not sensitive to climate change scenarios; the ground temperature distribution of both RCPs is approximately similar in shape and magnitude. Furthermore, the depth of the seasonally frozen ground around the pile structure will experience a continuous reduction from 2020 until 2100. In 2100, the seasonally frozen ground layer will not be present around the pile structure by the year 2100. At the toe of the pile the ground temperature tends to be less affected by future climate changes. The ground temperature at the pile toe level is approximately constant with time. The results acquired in the thermal component of this modeling study align with the acquired data obtained in the thermal analysis established in Chapter 3.

The hydraulic component of the bridge pile foundation simulation displayed the changes of the porewater distribution and magnitude induced by global warming around the pile structure. Figure 5.3.8 through Figure 5.3.9 display the porewater pressure profiles along the shaft of the pile on December 31st and March 1st respectively in Ottawa for both climate change scenarios in 2020, 2060 and 2100. The results of the simulation showed a negligible or insignificant effect of future climate changes on the hydraulic regime of

the ground surrounding the pile structure. The distribution of the porewater pressures along the shaft of the pile retained its linear distribution in the years of the analysis. Therefore, the increase of the ground temperature does not seem to significantly influence the in-situ water distribution in the soil matrix. Accordingly, the magnitude of the porewater pressures remains almost constant among the years up to 2100. A reduction of the porewater pressures in the order of 0.5 kPa was noted at the year 2100. Both climate change scenarios RCP4.5 and RCP8.5 provided similar results. Overall, the hydraulic regime or porewater pressure magnitude and distribution around the pile structure will not be significantly affect by future climate changes in the Canadian no-permafrost area. In other words, the effective stress around the pile foundation structure will not be significantly affected by global warming. This means that the impact of global warming on the shear strength of the foundation soils in the study area will be insignificant. These results concords with the obtained results of the thermo-hydraulic simulations established in chapter 4.

The last stage of this study comprises a coupled hydro-mechanical simulation to assess the settlement behavior around the pile structure in response to global warming. At the time of this study, the establishment of a fully coupled THM model is not possible using Gestudio package. Therefore, the resulting porewater pressures from the coupled thermo-hydraulic analysis were used in the mechanical model to include the effect of the escalation of ground temperature in finding the ground settlement around the pile foundation. Figure 5.3.10 through Figure 5.3.11 represent the ground settlement profiles along the shaft of the pile on December 31st and March 1st respectively in Ottawa for both climate change scenarios in 2020, 2060 and 2100. The results of the hydro-mechanical simulation of the foundation soil confirmed that the ground settlement around the pile structure will not experience a significant change with time. The settlement profiles represented the settlement behavior of the ground at different depths along the shaft of the pile. A tiny reduction of the ground settlement was observed at 2100 compared to 2020 around the pile structure. Therefore, the mechanical regime of the foundation ground in the Canadian no-permafrost region is not affected by future climate changes.

The THM simulation of the foundation soil aims to determine if the design of pile foundation in the Canadian no-permafrost region need to be adapted to meet the climate change requirement. In fact, the results of the modeling study confirmed that the ground temperature around the pile structure will increase by an average of 4 ° C in 2100. The ground temperature increase induced by global warming will impact the length of the frost period and the depth of the frost penetration of the foundation soil. The simulation of the foundation soil in Ottawa showed that the seasonally frozen layer will most likely disappear by 2100. Therefore, design matters related to uplift forces and down drag movements due to thawing may not be present by 2100 in Ottawa. Frost heave actions affect the operation of the piles due to the heaving forces in the winter and the down drag forces in the summer. In the winter season, the heaving movements of the frozen ground produce uplift forces which pull out the pile structure out of the soil. Nevertheless, due to

future climate changes, the ground will likely not experience the freezing process in the winter season, Therefore, the uplift forces due to frost heave actions may disappear around the pile foundation. In the summer season, the thawing settlement of the thawed layer, induces negative skin friction (down drag forces) acting on the pile and reducing its bearing capacity. The negative skin friction applies additional loads on the pile and reduces the pile load capacity. Consequently, in the absence of the freeze-thawing cycle, due to global warming, the seasonally frozen layer will likely be completely unfrozen along the year. Therefore, the seasonally thaw settlement and thaw consolidation processes will likely not occur in the foundation soil Ottawa in 2100. Consequently, the negative skin friction action on the pile foundation will likely, similarly, be reduced.

Uplift forces could be caused by several factor including hydrostatic pressures. Hydrostatic uplift is the condition of greater porewater pressure than the overburden pressure of the structure. The hydraulic simulation of the foundation soil showed a minimal effect of future climate changes on the magnitude and the distribution of the porewater pressures around the pile foundation in the Canadian no-permafrost region. Therefore, it is reasonable to conclude that the hydrostatic uplift forces will not likely change due global warming. Consequently, the design of pile foundation against the hydrostatic uplift forces in the no-permafrost region will likely not be affected by future climate changes.

The main serviceability limit state criterion for the design of axially loaded piles is the settlement. The coupled hydro-mechanical simulation of the foundation soil displayed a very small or insignificant change in the settlement behavior of the ground around the pile structure in 2100. The results of the coupled hydro-mechanical simulation provide a conservative engineering evaluation of the settlement behavior of the ground. At the time being, SIGMA/W is not able to simulate the ground settlement induced by thermal processes such as thaw settlement and thaw consolidation. However, the results of the thermal simulation confirmed the absence of these processes by 2100 due to future climate changes. therefore, less settlement is predicted to occur in the ground in 2100.

Chapter 6 – Summary, conclusions and future research recommendations

6.1 Summary

The purpose of the research project was to examine the effect of climate change on the design of pile foundation in the Canadian no-permafrost region through understanding the impact of global warming on the THM behaviour of grounds in this region. Three Canadian no-permafrost cities located in east Ontario, were selected as a study area. Sudbury, Ottawa and Sudbury were selected in this research to represent the north, the center and the south of the Canadian no permafrost region. The new research carried out by the authors established numerical simulations to assess the impact of climate warming on ground temperature in the study area. TEMP/W program from GeoStudio software was used to construct the numerical models. The model geometries were retrieved from the National geological survey of Canada, whereas climate conditions and climate change projections were downloaded from the Environment of Canada website. Three climate change scenarios; RCP8.5, RCP4.5, RCP2.5, were considered in this stage of the analysis. The climate change scenarios provided different projections of air temperature change by 2100. The combined effect of climate change and snow cover variation was also examined in the thermal analysis conducted in the first part of the present research. Four snow cover depths were simulated in each study area. The results of the thermal analysis are reported in Chapter 3 of this report.

To investigate the effect of ground temperature change on the hydraulic and mechanical regime of the ground in the study areas, coupled THM simulations were established using TEMP/W, SEEP/W and SIGMA/W from GeoStudio package. Since a fully THM coupled analysis is still not possible using GeoStudio package, a coupled thermo-hydraulic analysis was first established to examine the effect of climate change on the porewater pressure distribution in the ground in the three selected no-permafrost sites. The resulting porewater pressures were than incorporated in a coupled hydro-mechanical simulation, using SEEP/W and SIGMA/W, to assess the change in the settlement of the ground due to global warming. Two climate change scenarios were considered in this part of the study namely RCP8.5 and RCP4.5. The results of the THM simulations are reported in Chapter 4 of this report.

Finally, a practical application to a foundation soil was established. For this purpose, a pile structure of 1m diameter and 15 m long was incorporated in the numerical model of the city of Ottawa. THM changes around the pile structure were assessed using the same THM methodology conducted in chapter 4.

6.2 Conclusions

The following conclusions were made based on the research conducted:

(1) The thermal regime of the ground can be accurately simulated using the developed methodology and simulation tool. This simulation tool was validated against existing field data and succeeded to model the average monthly ground temperature of an Ottawa clay ground from May 1954 to April 1955.

(2) The results of the future climate change simulations confirmed that global warming will influence the thermal behaviour of the ground in the three study areas. In fact, a clear increase of the ground temperature was observed as a result of increasing air temperature in the simulation models. A ground temperature increases of 2 to 4 ° C was observed in the three studied sites by 2100.

(3) The thermal regime of the ground is not sensitive to climate change scenarios as the three climate change scenarios considered in the present study, led to slightly different effect on the ground temperature in the three study areas.

(4) The depth of the snow cover in the no-permafrost study area did not seem to affect the thermal response of the soil to global warming. The maximum snow cover depth provides a stronger insulation if compared with the minimum snow cover depth. Therefore, the ground tends to be cooler under the maximum snow depth and less impacted by future climate changes. Nevertheless, the difference between the temperature profiles of different snow covers is hardly noticeable.

(5) The frost penetration depth and the frost period duration will experience a gradual loss due to global warming until 2100. In fact, the simulation results confirmed that the frost duration in Ottawa will vanish in 2100 compared to 5 months in 2020. Similarly, the frost period in Toronto will disappear by 2100. In Sudbury, the frost duration will last for 70 days in the winter season, as the weather is cooler in the north of the Canadian no-permafrost region.

(6) The future climate changes will likely impact the thermal regime of the first 5 m of the ground. The results confirmed that starting from a depth of 6m the ground temperature remains constant with time. This behaviour was observed in the three studied sites for the three climate change scenarios.

(7) The results of the TH simulations confirmed that the ground temperature variation, due to global warming, will not significantly impact the magnitude and distribution of the porewater pressures in the soil, in the no-permafrost study areas. A slight or insignificant reduction of porewater pressures was noticed in one of the study areas, however, no general trend could be observed in the three study sites.

(8) The results of the coupled hydro-mechanical simulations affirmed that future climate changes will not significantly affect the settlement behaviour of the soils in the studied Canadian no-permafrost regions. A slight reduction of the average surface settlement was noticed in 2100 in the three study areas for both days of the analysis. Accordingly, the future climate changes do not seem to significantly affect the frost heave movements in the study areas.

(9) The results of the pile foundation soil simulation are analogous to the results acquired in both the thermal and the THM analyzes. The ground temperature increases around the shaft perimeter of the pile foundation ranges between 4 to 6 °C by 2100, at shallow depths, while the ground temperature at the toe of the pile is relatively constant. Similarly, the magnitude and distribution of the porewater pressures around the pile shaft is not disturbed by future climate changes. The settlement of the ground beneath and adjacent to the pile structure was also assessed. The results displayed a minimal variation of the ground settlement along the pile shaft perimeter. Therefore, future climate changes will likely not significantly affect the mechanical regime around pile foundations as well as their geotechnical stability in the studied no-permafrost region.
(10) As the ground THM changes, due to global warming, are not very significant along the study period, it is reasonable to conclude that the actual design procedure of pile foundation in the Canadian no-permafrost region provides a conservative approach to construct pile foundation in 2100.

6.3 Recommendations

The following suggestions are made by the authors:
(1) Field investigations and laboratory testing can be conducted on specific no-permafrost sites to determine the geotechnical composition of the ground, the in-situ hydraulic conditions and the in-situ stress conditions.
(2) Soil samples can be studied in the laboratory to determine their thermal, hydraulic, and mechanical properties. Furthermore, a soil sample can be exposed to changing freeze-thawing cycles and different air temperatures in the laboratory to produce the same climate change projections. The purpose of the laboratory study is to experimentally assess the impact of future climate changes on the thermal, hydraulic, and mechanical regimes of no-permafrost soil sample. The geometry and boundary conditions of the laboratory study can be modeled using a FEM software, and results can be compared.
(3) Different surface cover types during the winter season and the summer season could be modelled in the thermal analysis. Several other variables that are more difficult to incorporate in a model include net solar radiation, continuity of surface cover and plant and root type and depth.
(4) At the time being, a fully coupled THM simulation is not possible using GeoStudio software. Only thermal-hydro and hydro-mechanical models are possible in GeoStudio, but the company is working to develop a fully coupled THM modeling procedure using TEMP/, SEEP/W and SIGMA/W. Future numerical models could couple thermal and mechanical analyses with groundwater conditions using a fully coupled THM simulation. A thermal-hydro-mechanical coupled numerical model could be developed to simulate thermally induced displacements and convective heat flow from seepage.
(5) Other finite element software could provide a better way to estimate the behaviour of thermal properties near freezing temperatures. Future thermal models could enhance the simulation with 3D modelling in

another finite element software such as SVHEAT or Abaqus.

Appendix

Appendix A

a)

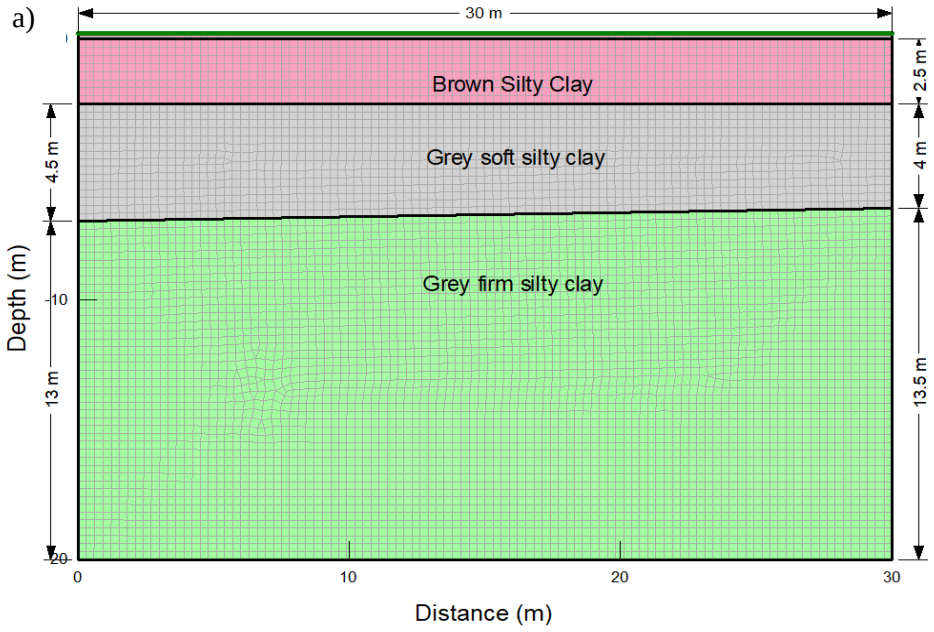
30 m
Brown Silty Clay
Grey soft silty clay
Grey firm silty clay
2.5 m
4 m
13.5 m
4.5 m
13 m
Depth (m)
0
10
20
30
Distance (m)

b)

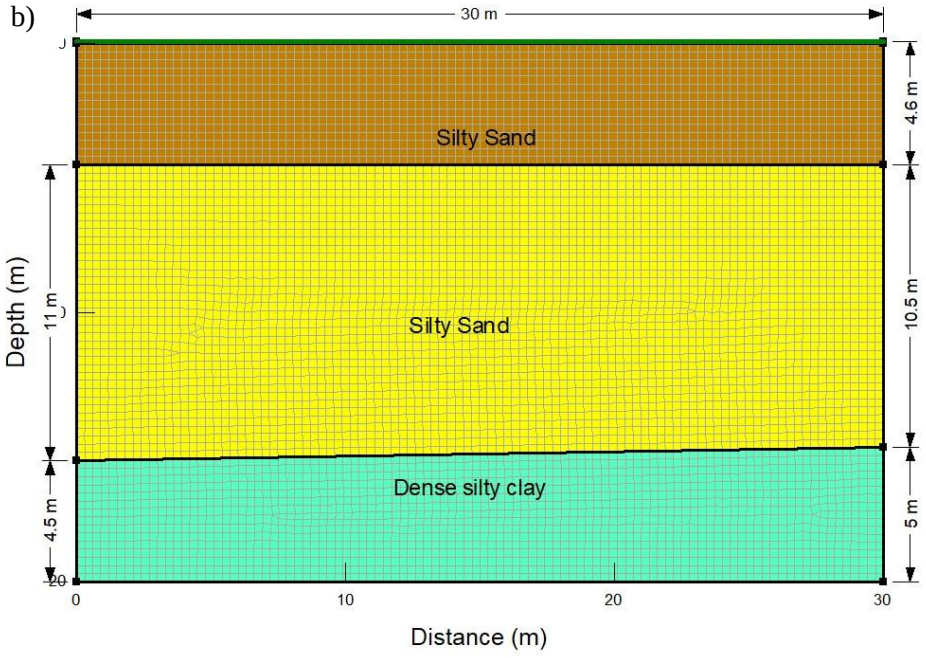
30 m
Silty Sand
Silty Sand
Dense silty clay
4.6 m
10.5 m
5 m
11 m
4.5 m
Depth (m)
0
10
20
30
Distance (m)

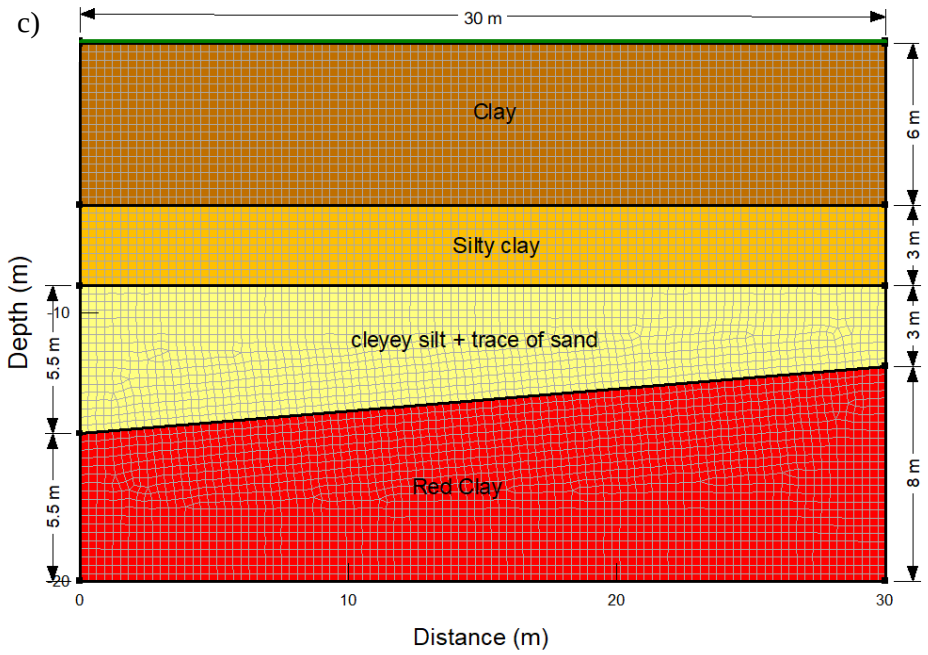

Figure A-1: a) Ottawa simulation model geometry, b) Toronto simulation model geometry, (c) Sudbury simulation model geometry

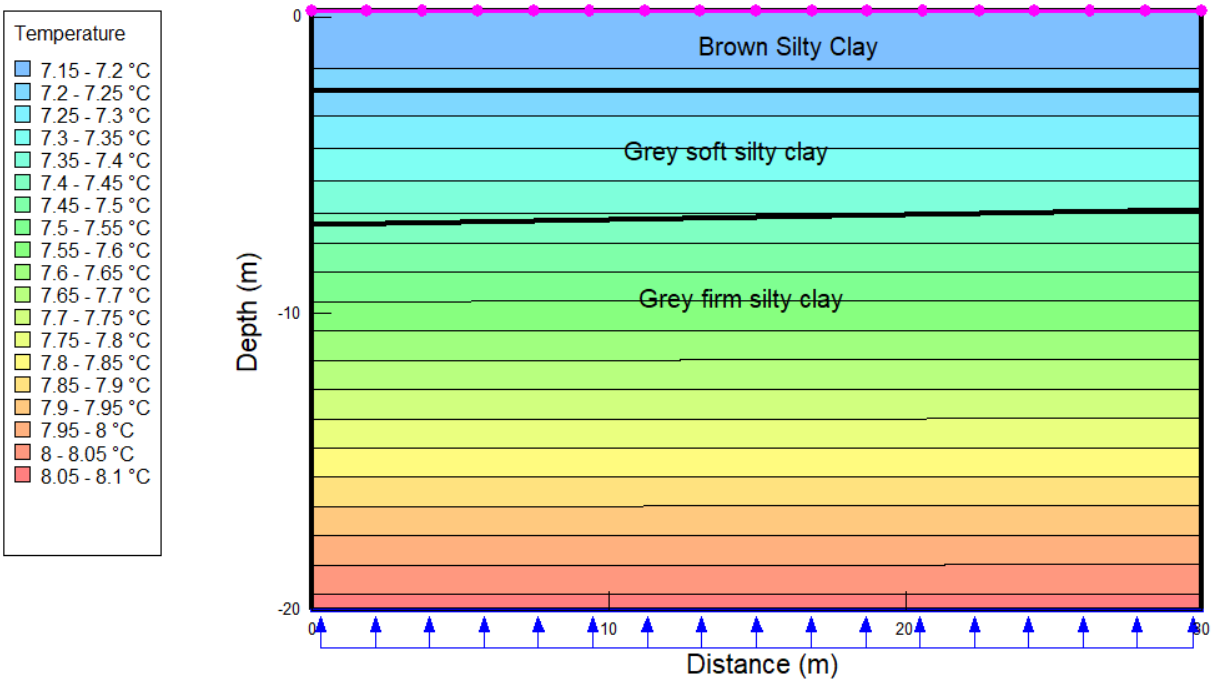
Temperature
7.15 - 7.2 °C
7.2 - 7.25 °C
7.25 - 7.3 °C
7.3 - 7.35 °C
7.35 - 7.4 °C
7.4 - 7.45 °C
7.45 - 7.5 °C
7.5 - 7.55 °C
7.55 - 7.6 °C
7.6 - 7.65 °C
7.65 - 7.7 °C
7.7 - 7.75 °C
7.75 - 7.8 °C
7.8 - 7.85 °C
7.85 - 7.9 °C
7.9 - 7.95 °C
7.95 - 8 °C
8 - 8.05 °C
8.05 - 8.1 °C
Brown Silty Clay
Grey soft silty clay
Grey firm silty clay
Depth (m)
0
-10
-20
0
10
20
30
Distance (m)

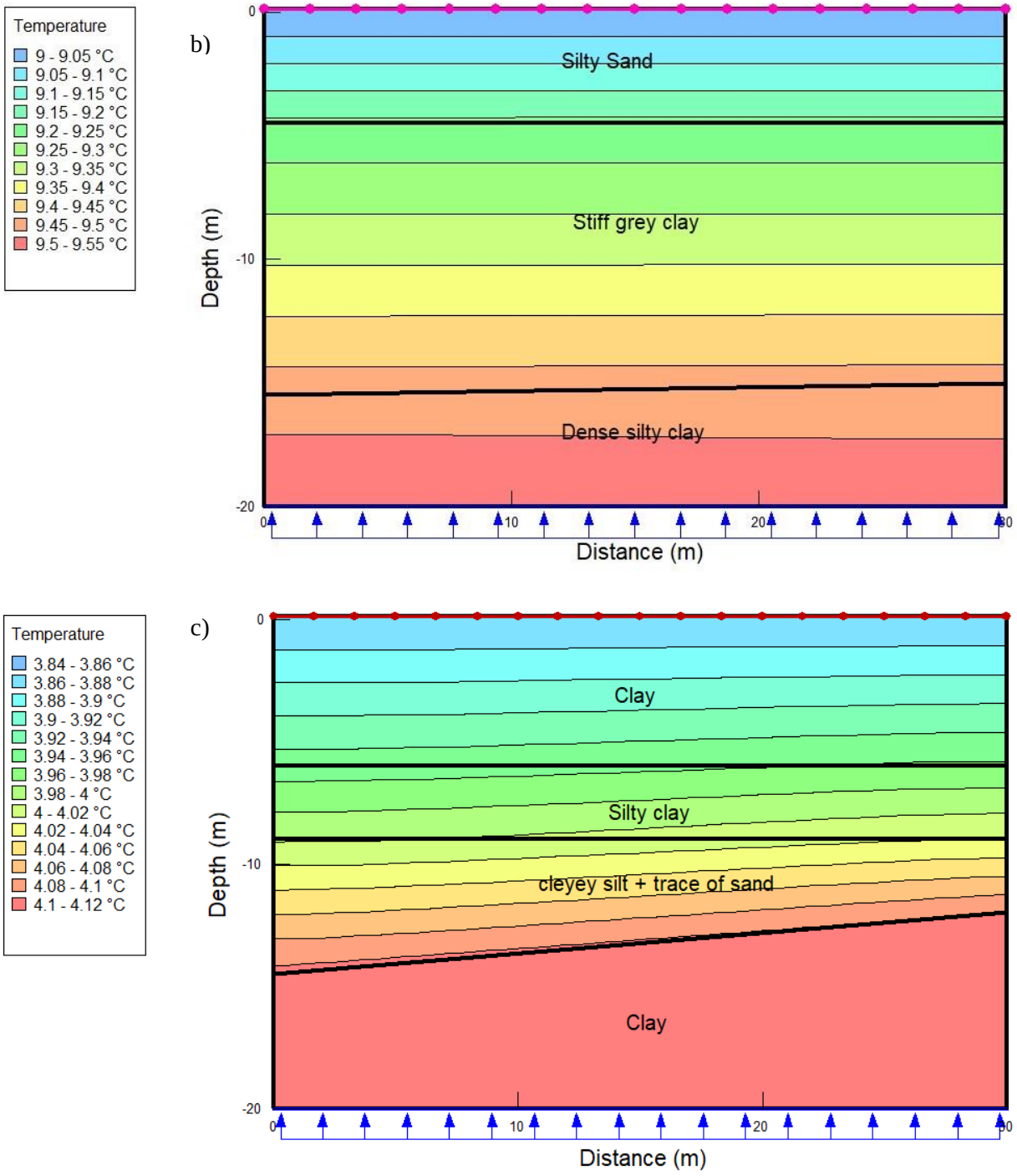

Figure A-2: TEMP/W Model for Initial Conditions for the first day of the analysis – RCP 8.5 - a) Ottawa, b) Toronto c) Sudbury

Appendix B

Ottawa RCP 8.5:

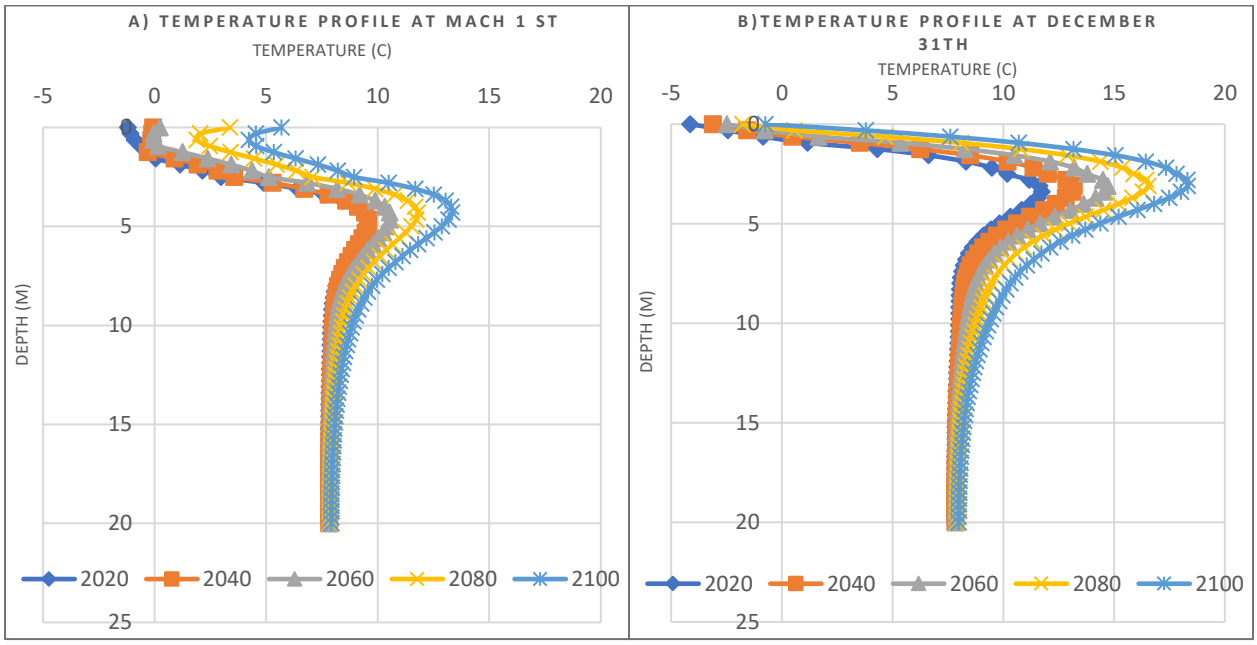

Figure B-1: Ground temperature profiles at a) March 1st and b) December 31 st for 2020 – 2040 – 2060 – 2080 – 2100 – RCP8.5

Ottawa RCP 4.5:

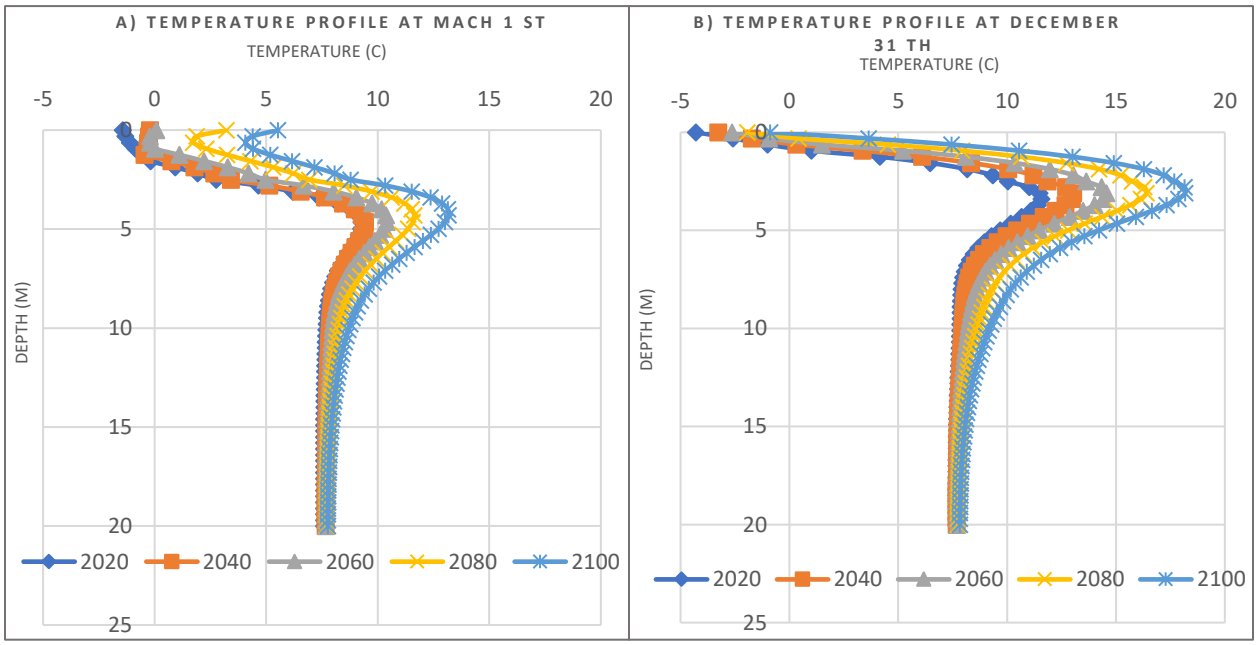

Figure B-2: Ground temperature profiles at a) March 1st and b) December 31 st for 2020 – 2040 – 2060 – 2080 – 2100

Ottawa RCP 2.5:

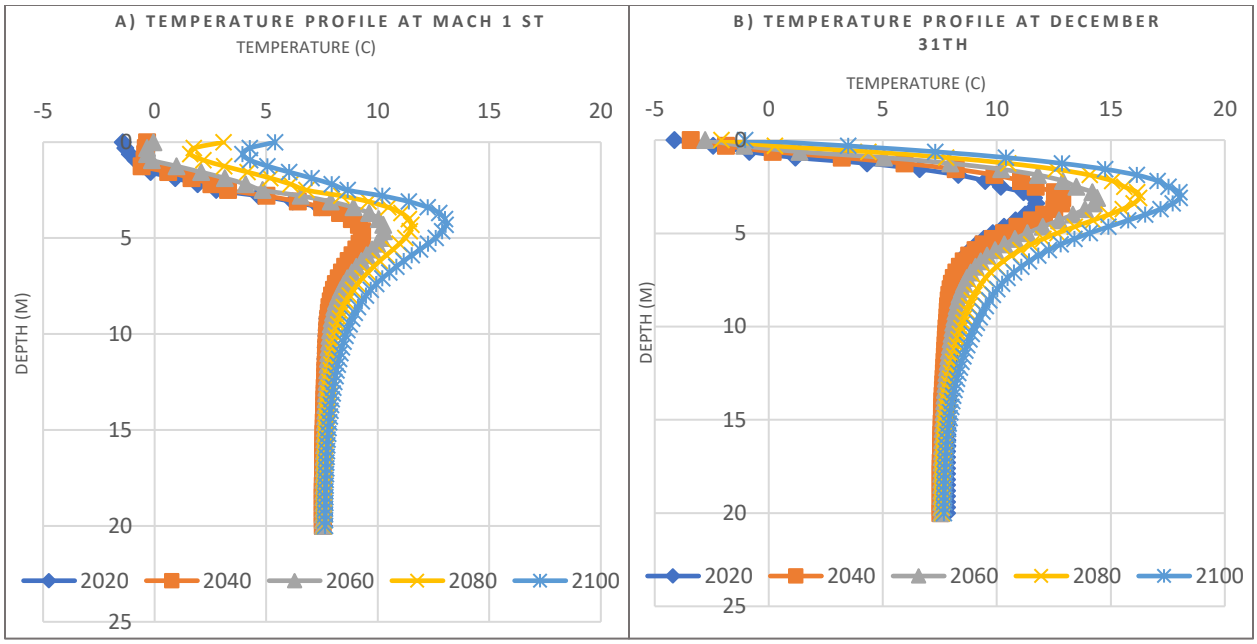

Figure B-3: Ground temperature profiles at a) March 1st and b) December 31 st for 2020 – 2040 – 2060 – 2080 – 2100 – RCP 2.5

Toronto RCP 8.5:

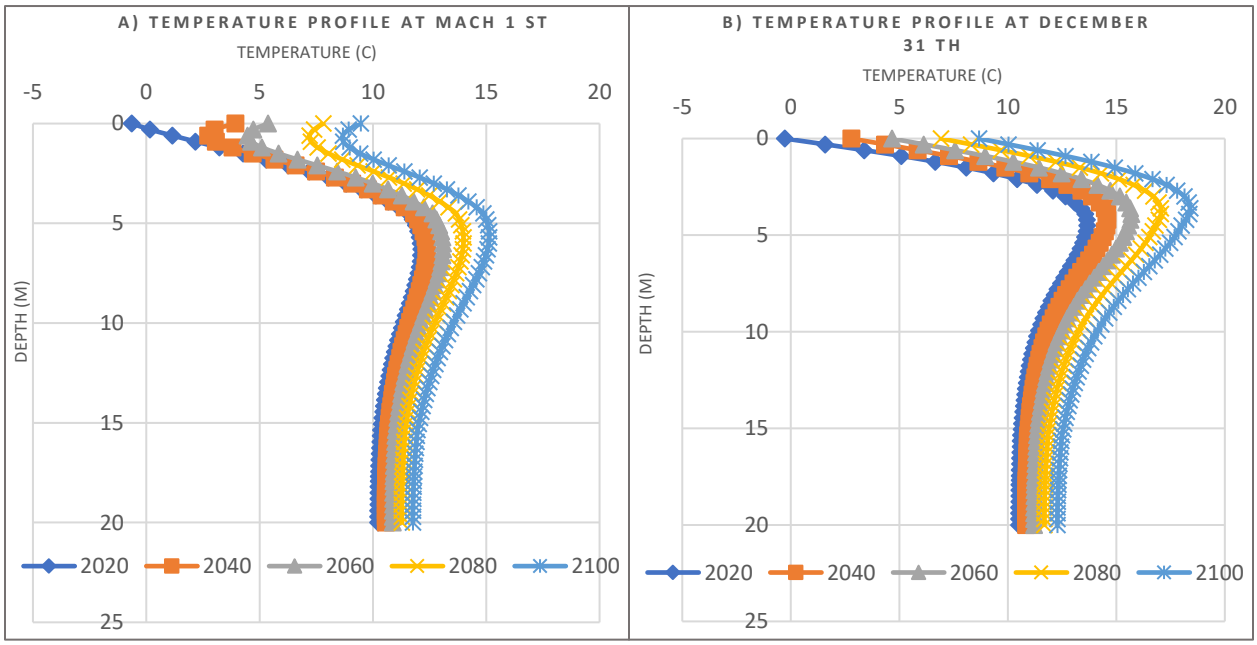

Figure B-4: Ground temperature profiles at a) March 1st and b) December 31 st for 2020 – 2040 – 2060 – 2080 – 2100 – RCP8.5

Toronto RCP 4.5:

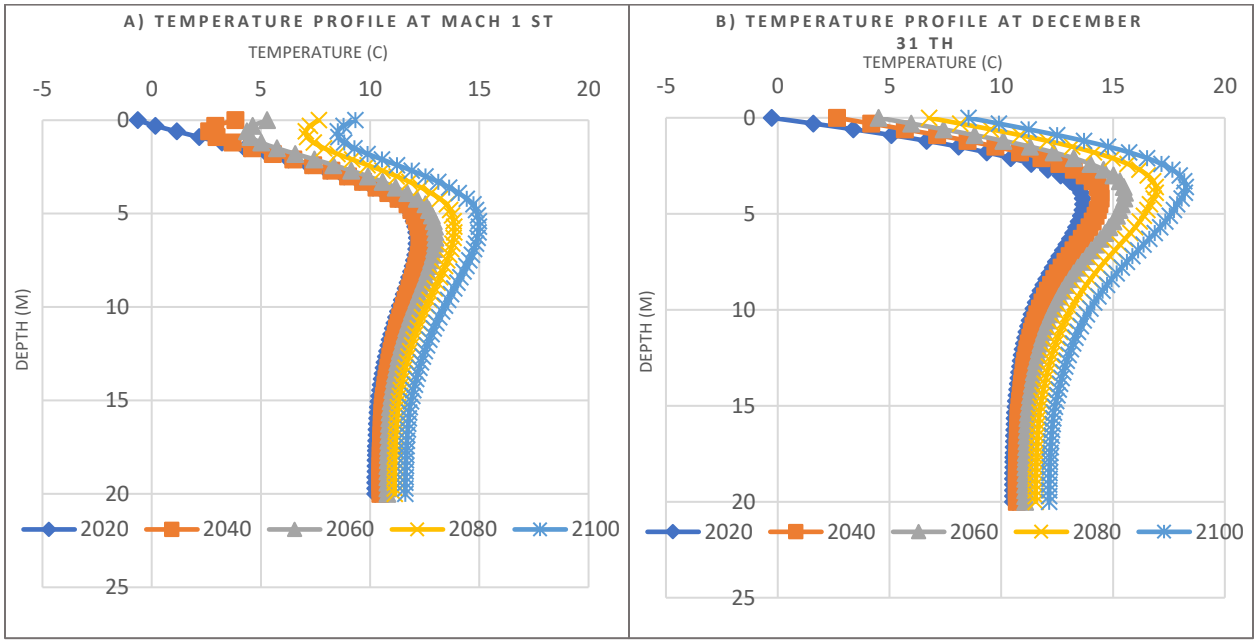

Figure B-5: Ground temperature profiles at a) March 1st and b) December 31 st for 2020 – 2040 – 2060 – 2080 – 2100 – RCP 4.5

Toronto RCP 2.5:

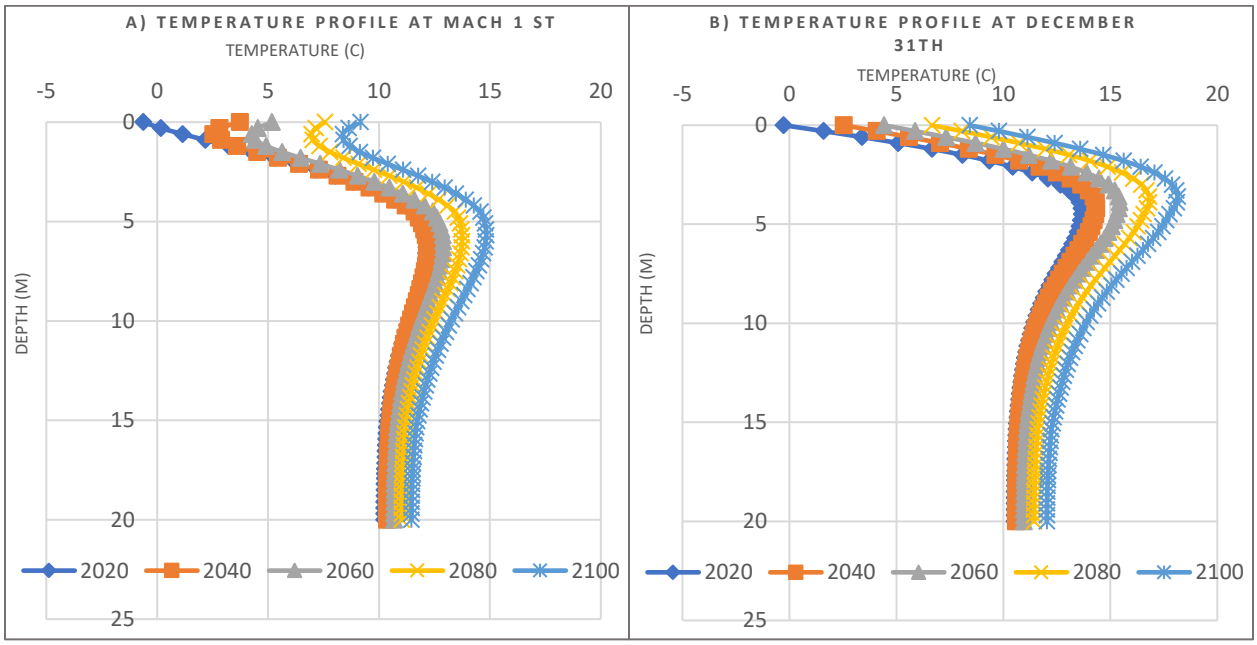

Figure B-6: Ground temperature profiles at a) March 1st and b) December 31 st for 2020 – 2040 – 2060 – 2080 – 2100 – RCP 2.5

Sudbury RCP 8.5:

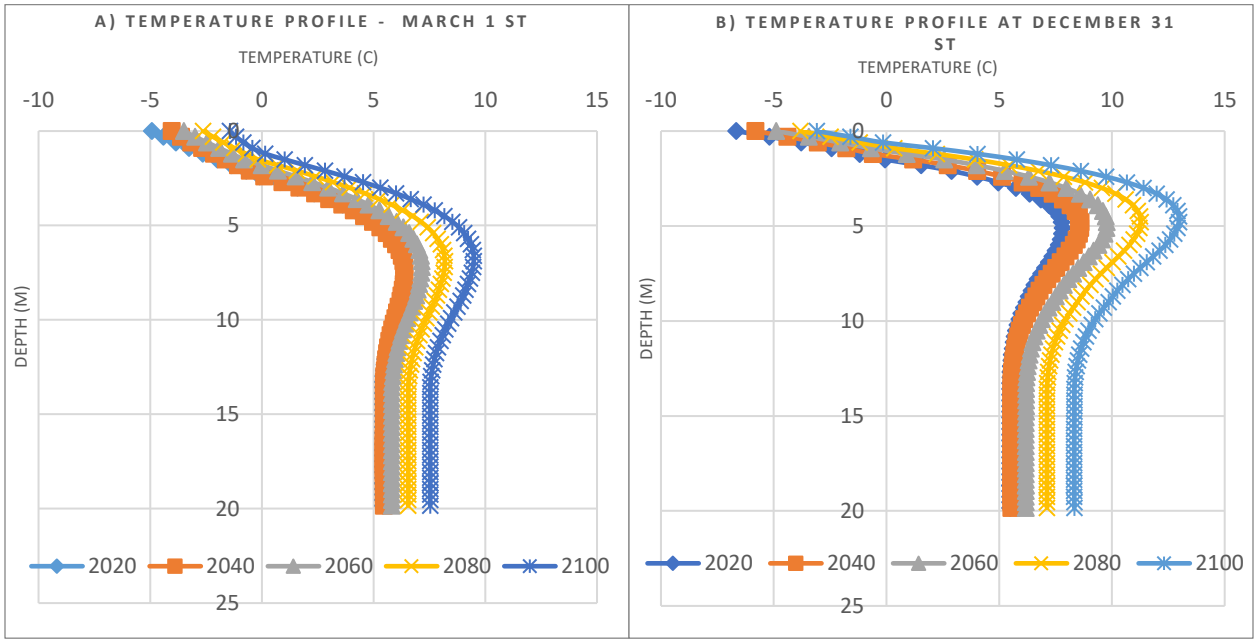

Figure B-7: Ground temperature profiles at a) March 1st and b) December 31 st for 2020 – 2040 – 2060 – 2080 – 2100 – RCP8.5

Sudbury RCP 4.5:

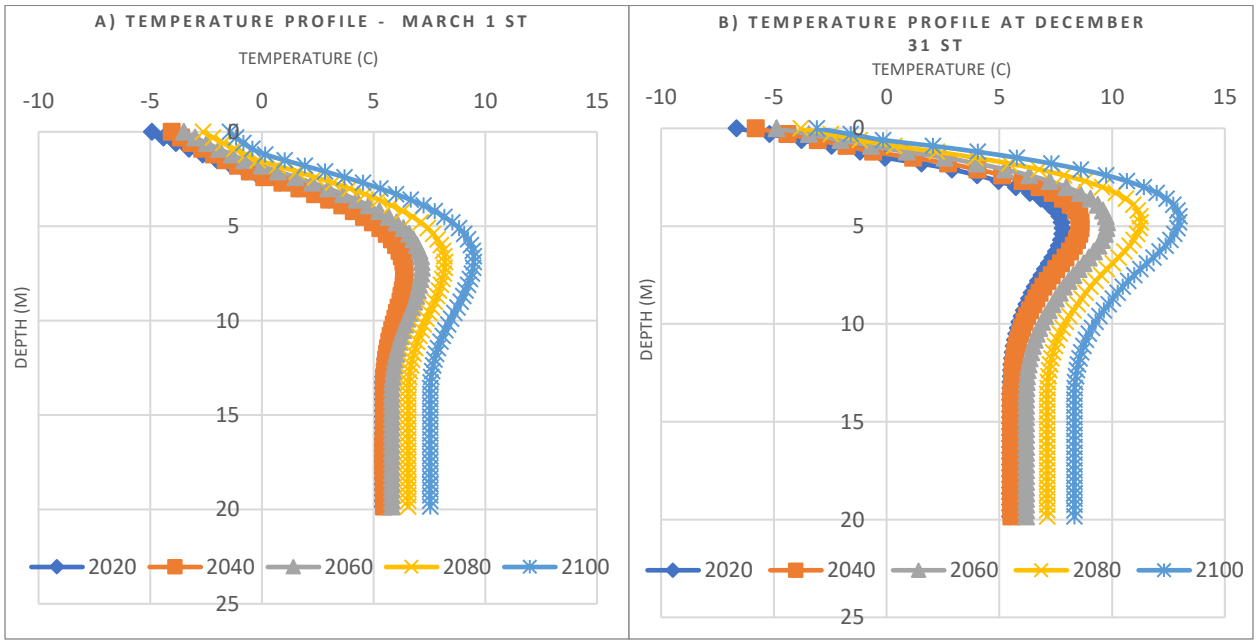

Figure B-8: Ground temperature profiles at a) March 1st and b) December 31 st for 2020 – 2040 – 2060 – 2080 – 2100 – RCP 4.5

Sudbury RCP 2.5:

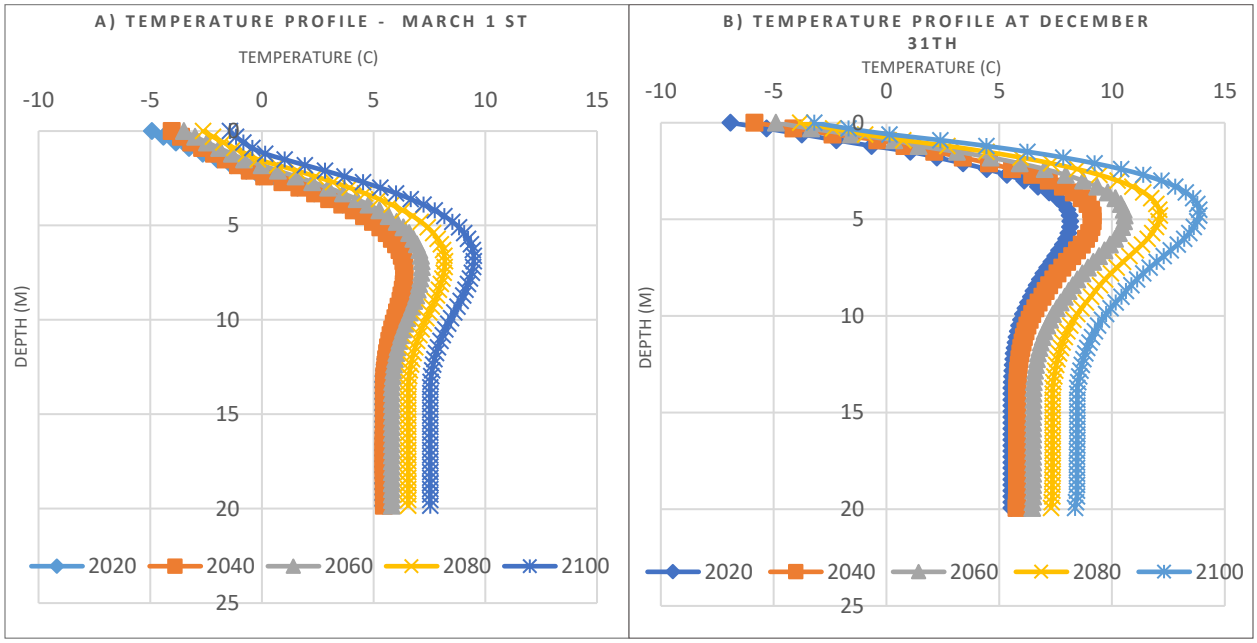

Figure B-9: Ground temperature profiles at a) March 1st and b) December 31 st for 2020 – 2040 – 2060 – 2080 – 2100 – RCP 2.5

Appendix C

Ottawa:

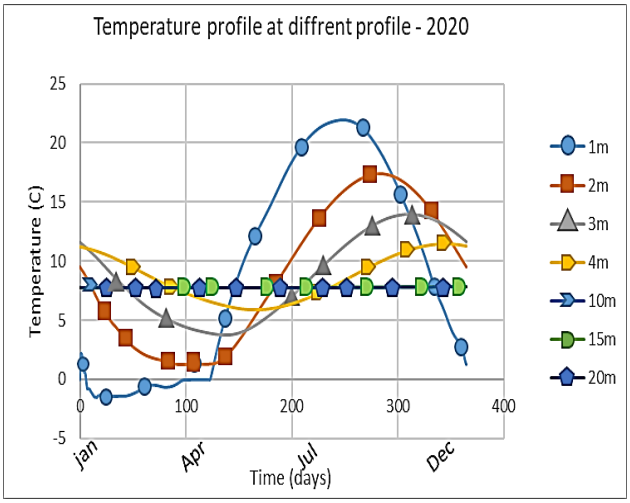

Figure C-1: Temperature profile at different depths -2020 – Ottawa

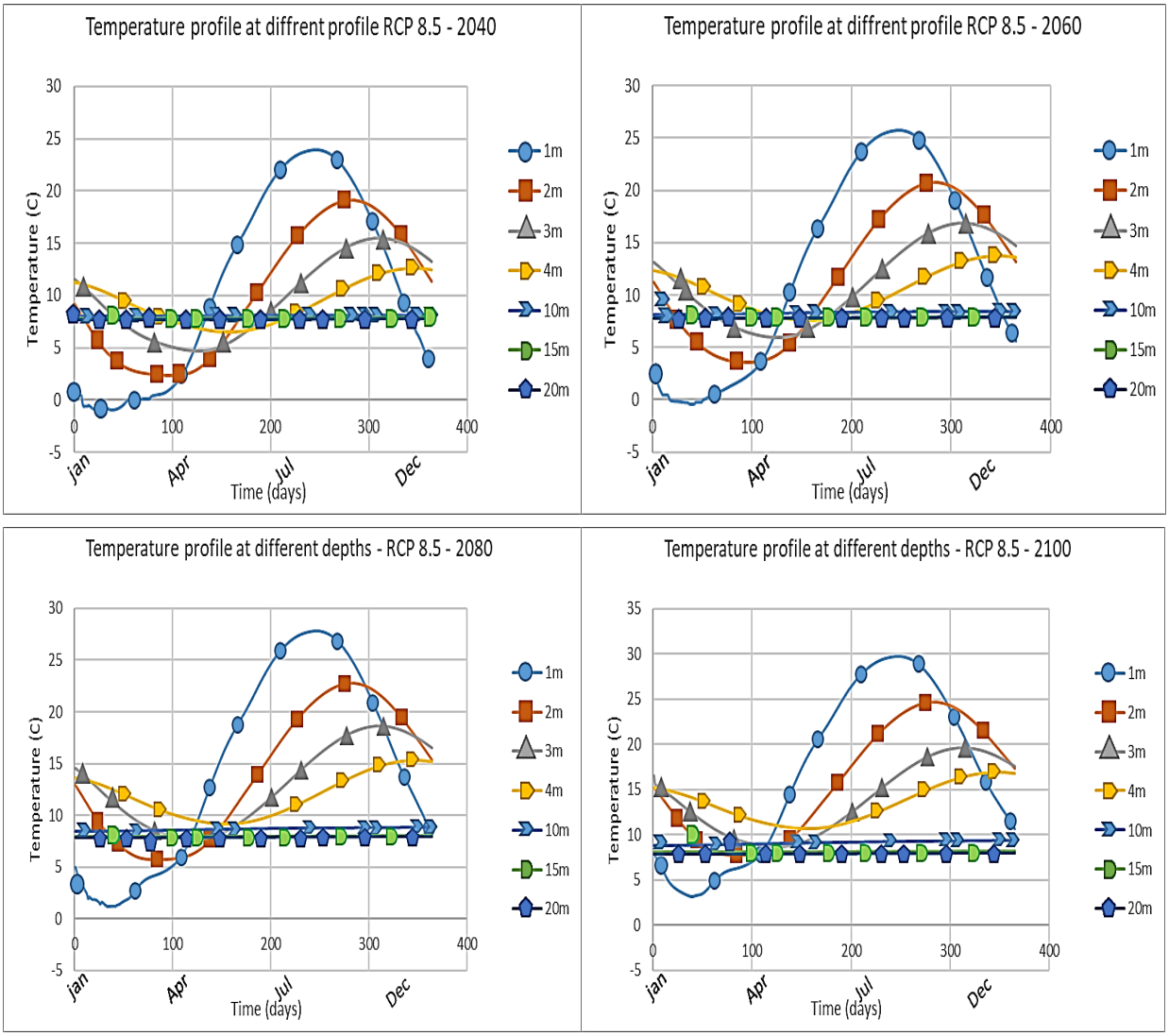

Figure C-2: Temperature profile at different depths - RCP 8.5 - at 2040, 2060, 2080, 2100 - Ottawa

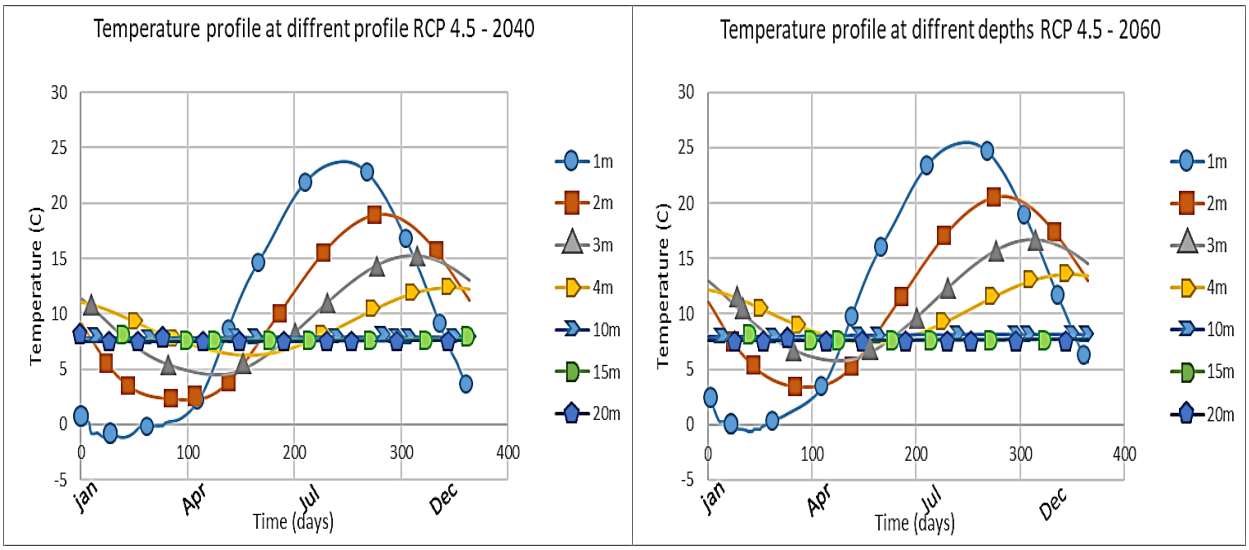

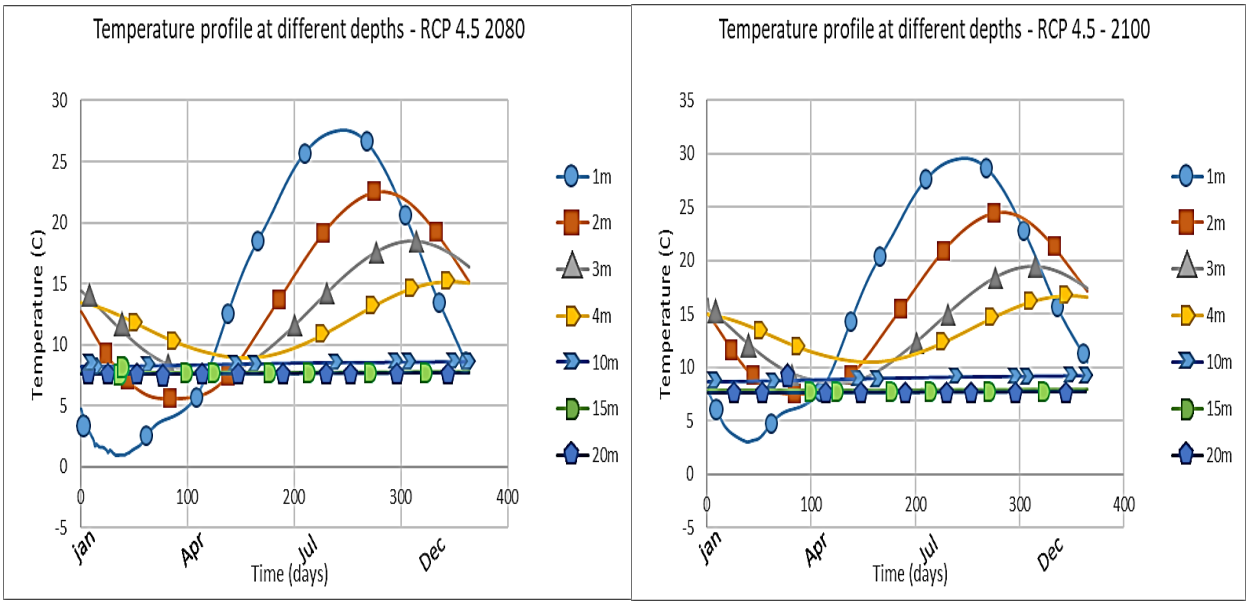

Figure C-3: Temperature profile at different depths - RCP 4.5 - at 2040, 2060, 2080, 2100 - Ottawa

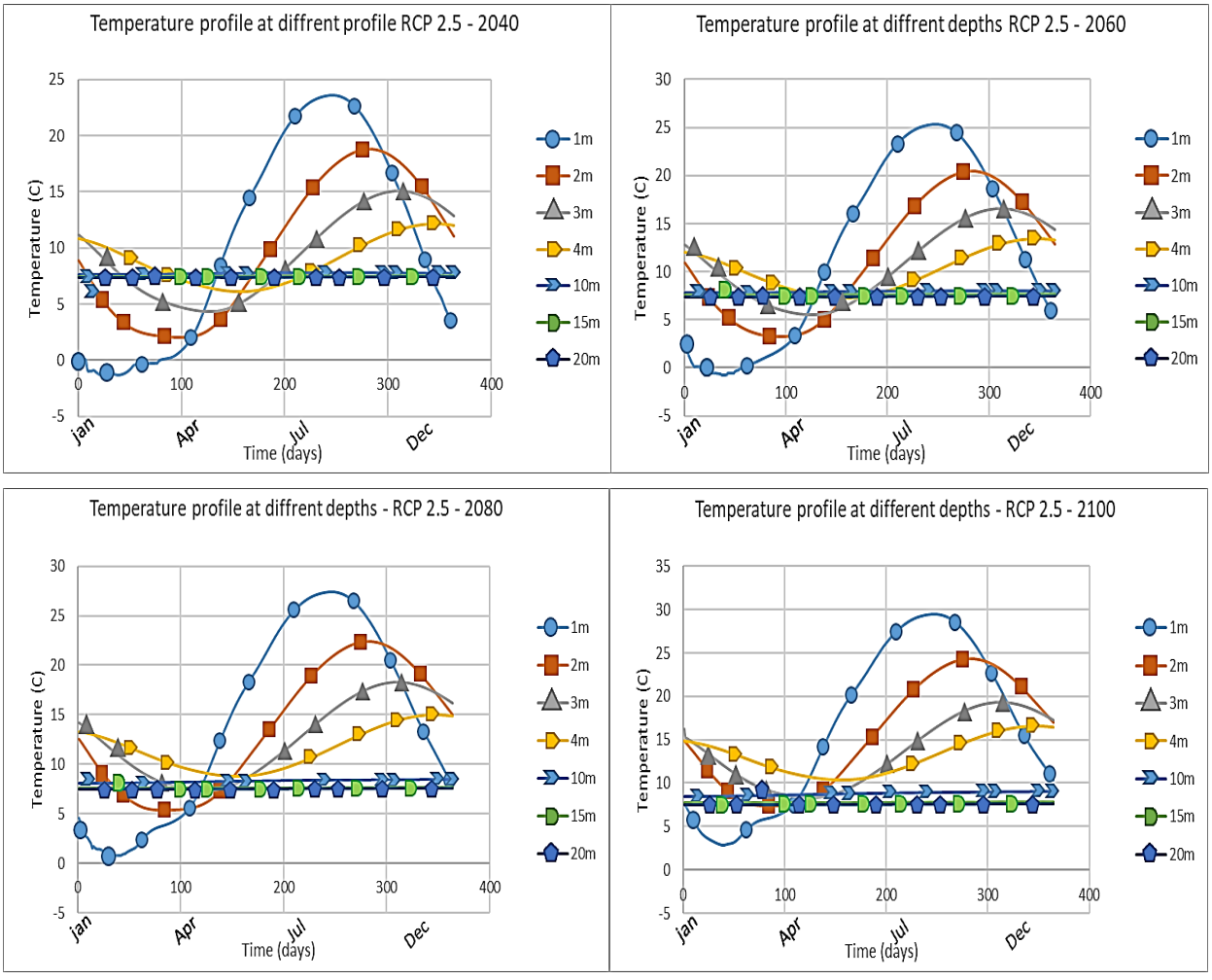

Figure C-4: Temperature profile at different depths - RCP 2.5 - at 2040, 2060, 2080, 2100 – Ottawa

Toronto:

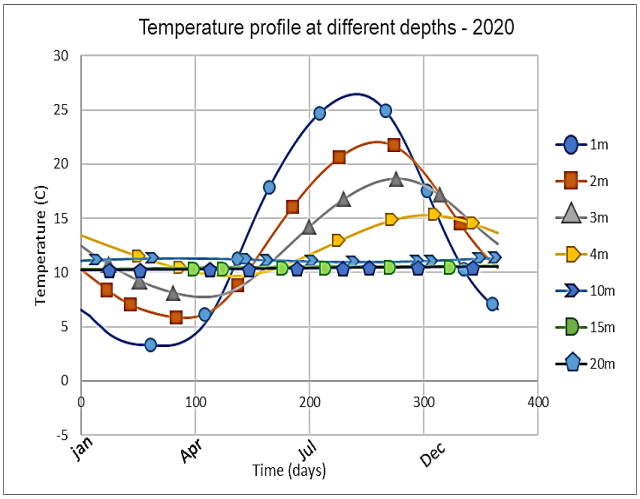

Figure C-5: Temperature profile at different depths - 2020 - Toronto

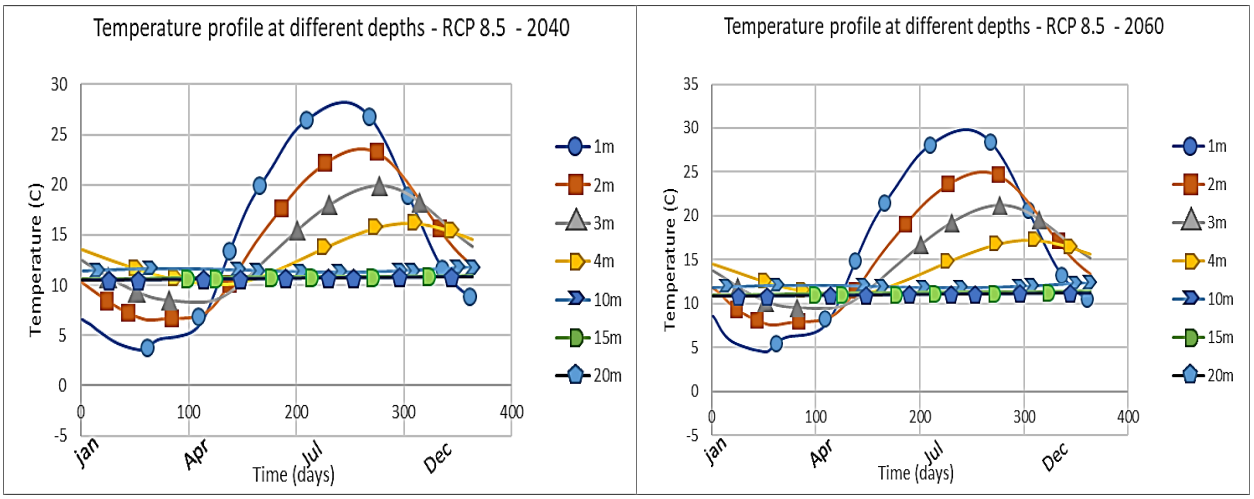

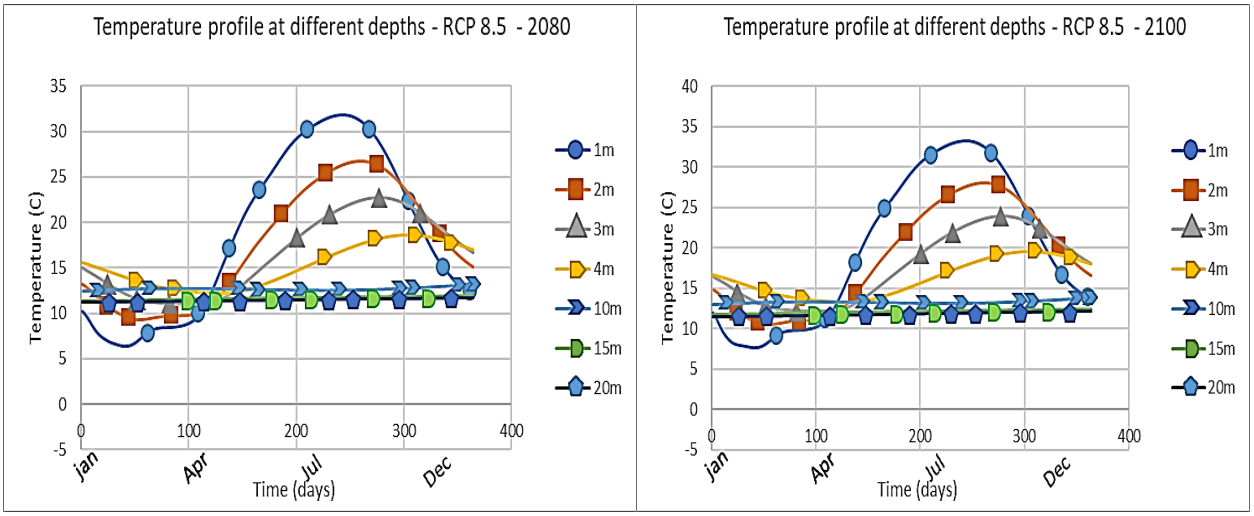

Figure C-6: Temperature profile at different depths - RCP 8.5 at 2040, 2060, 2080, 2100 - Toronto

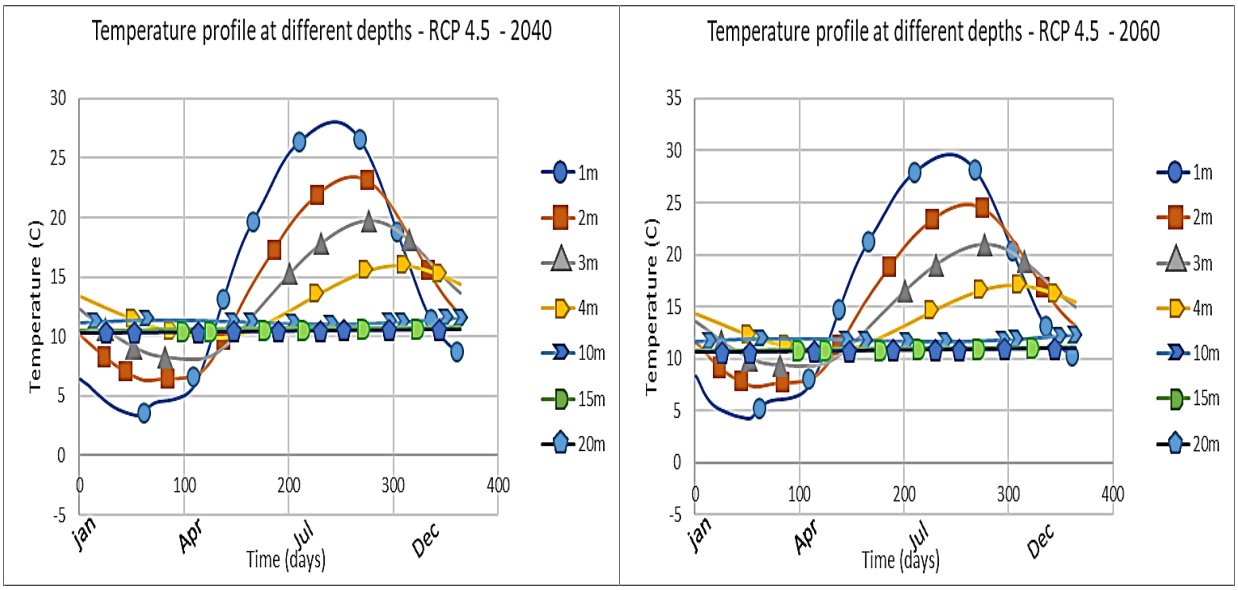

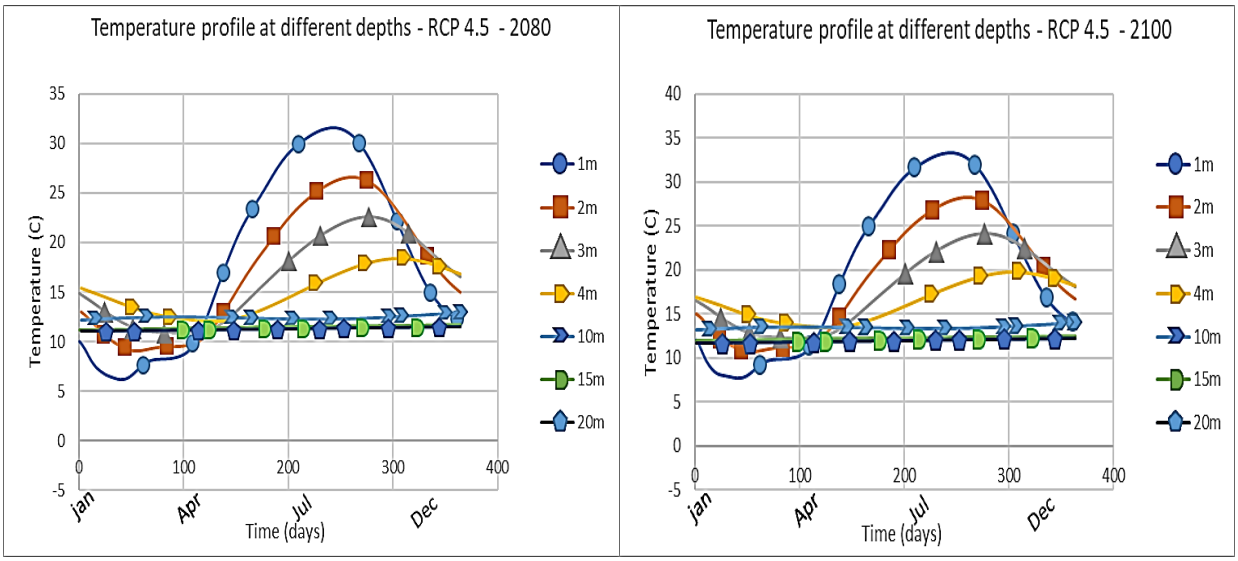

Figure C-7: Temperature profile at different depths - RCP 4.5 at 2040, 2060, 2080, 2100 – Toronto

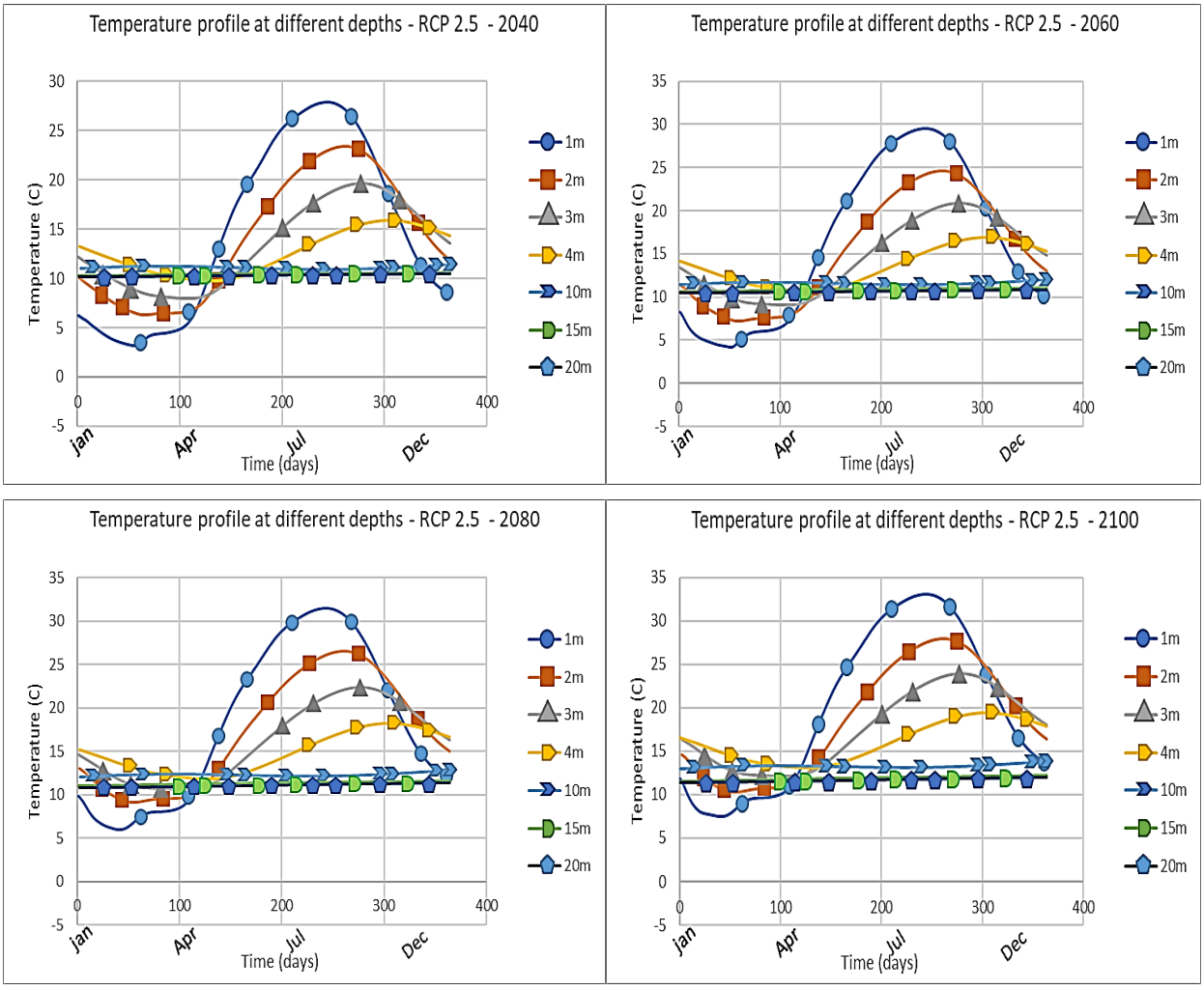

Figure C-8: Temperature profile at different depths - RCP 2.5 at 2040, 2060, 2080, 2100 – Toronto

Sudbury:

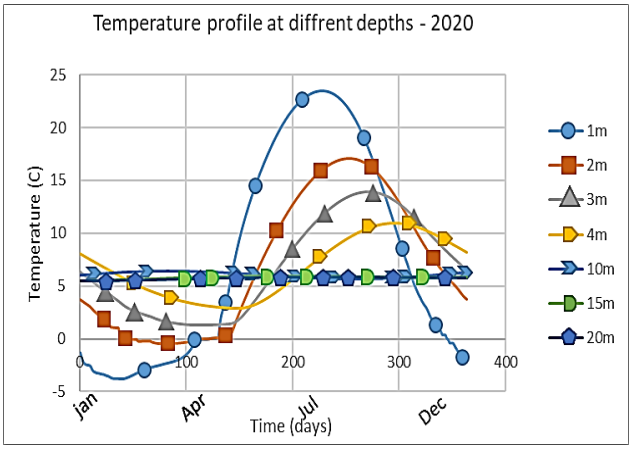

Figure C-9: Temperature profile at different depths - 2020 - Sudbury

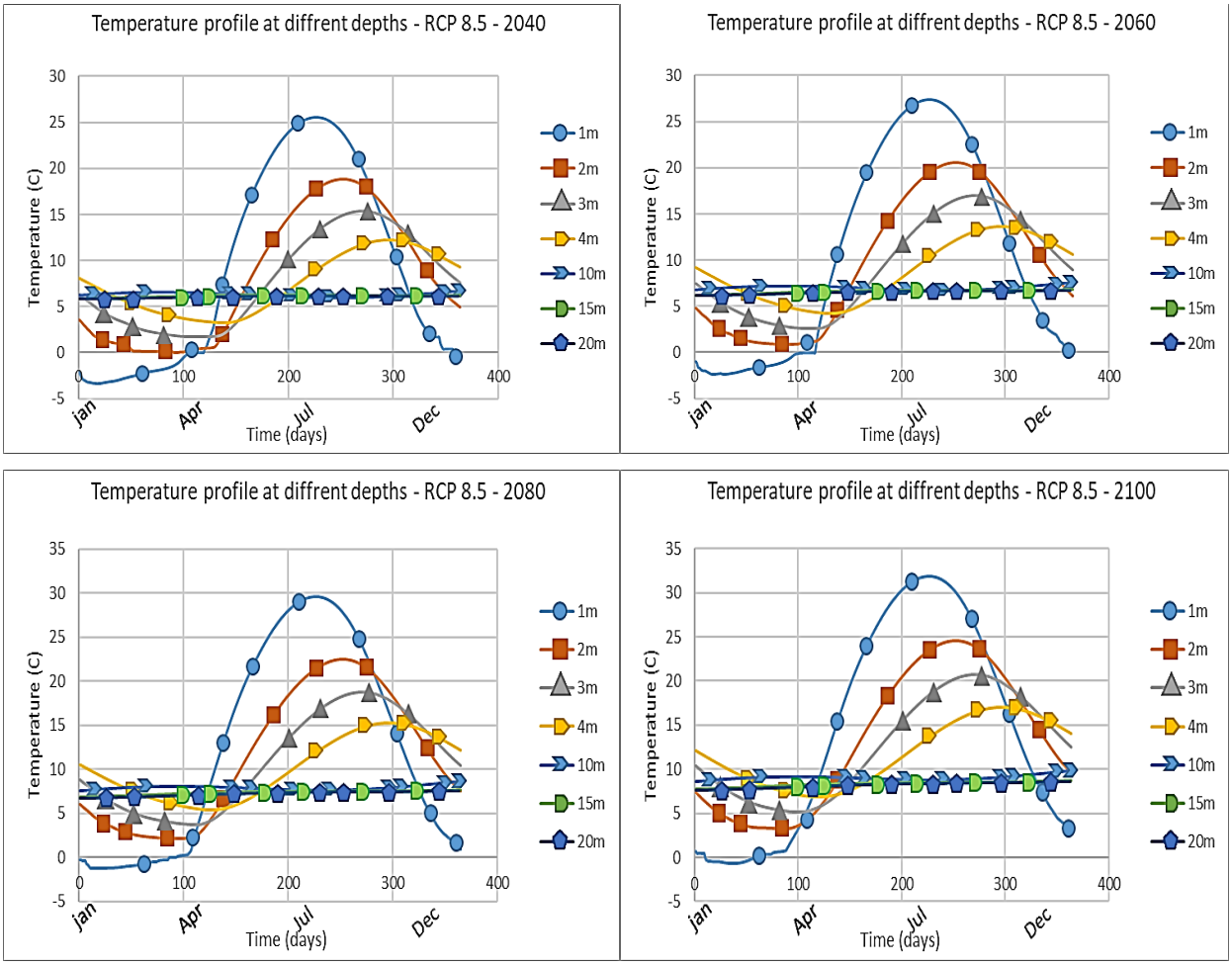

Figure C-10: Temperature profile at different depths - RCP 8.5 at 2040, 2060, 2080, 2100 – Sudbury

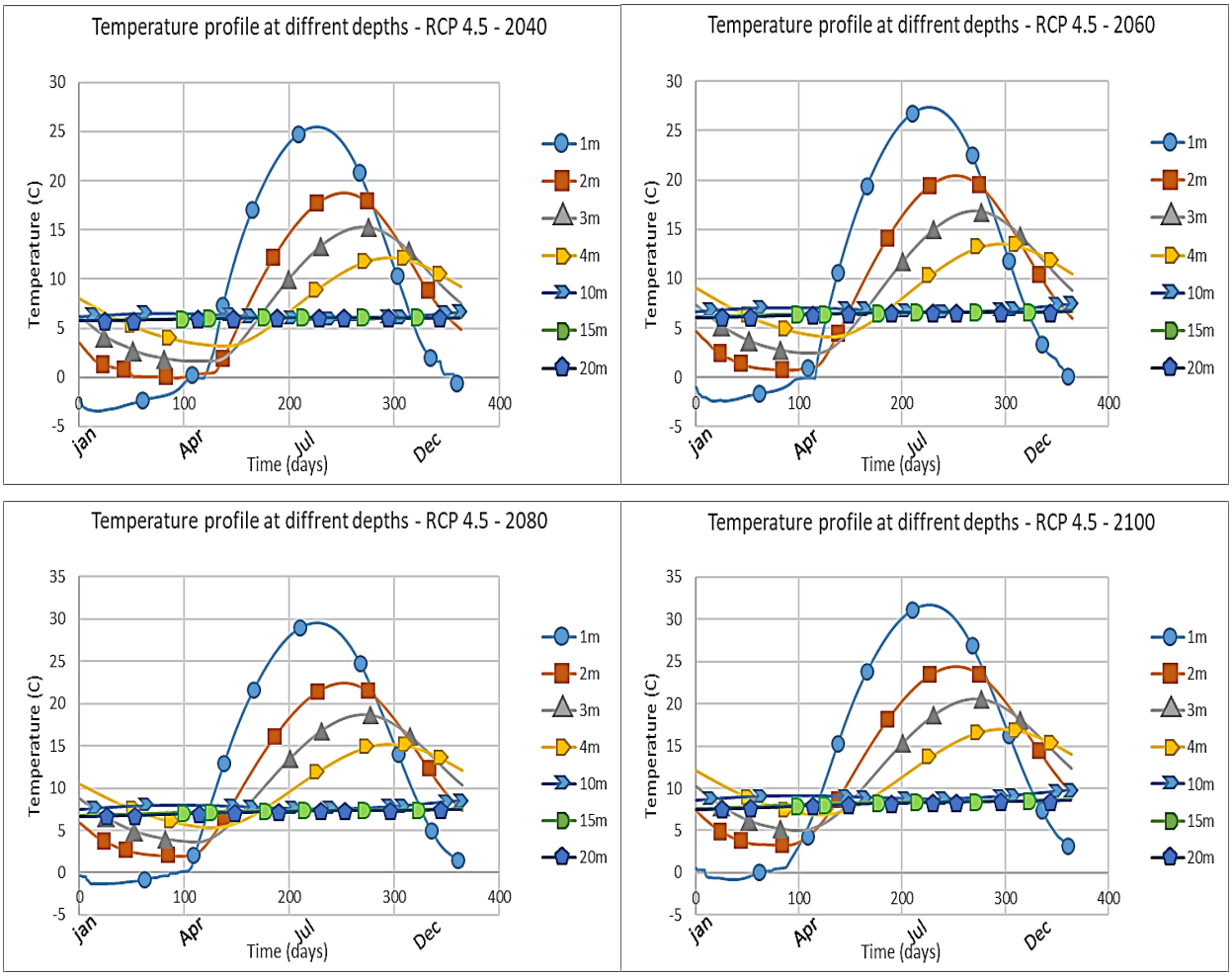

Figure C-11: Temperature profile at different depths - RCP 4.5 at 2040, 2060, 2080, 2100 - Sudbury

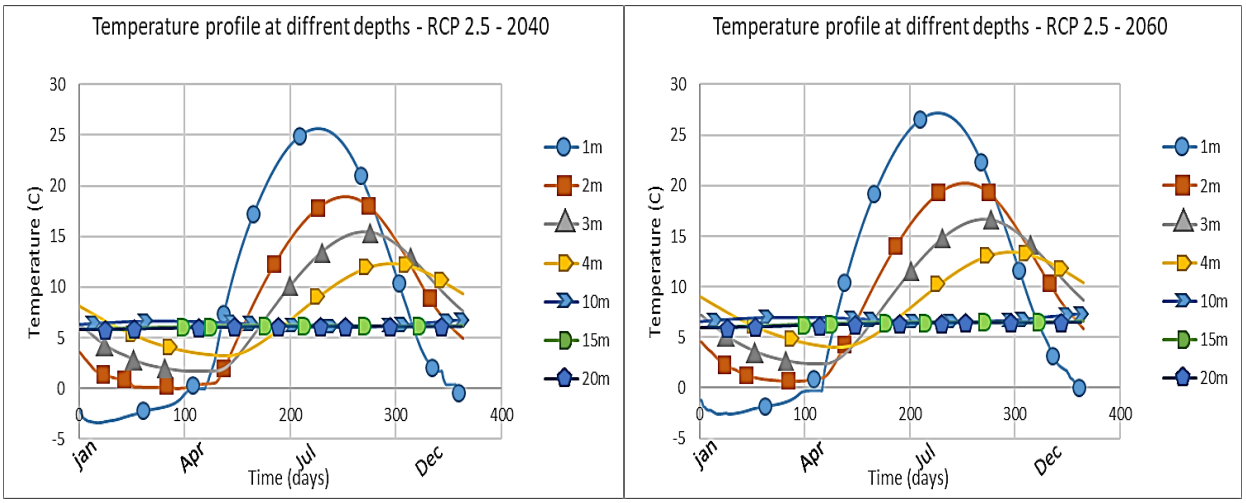

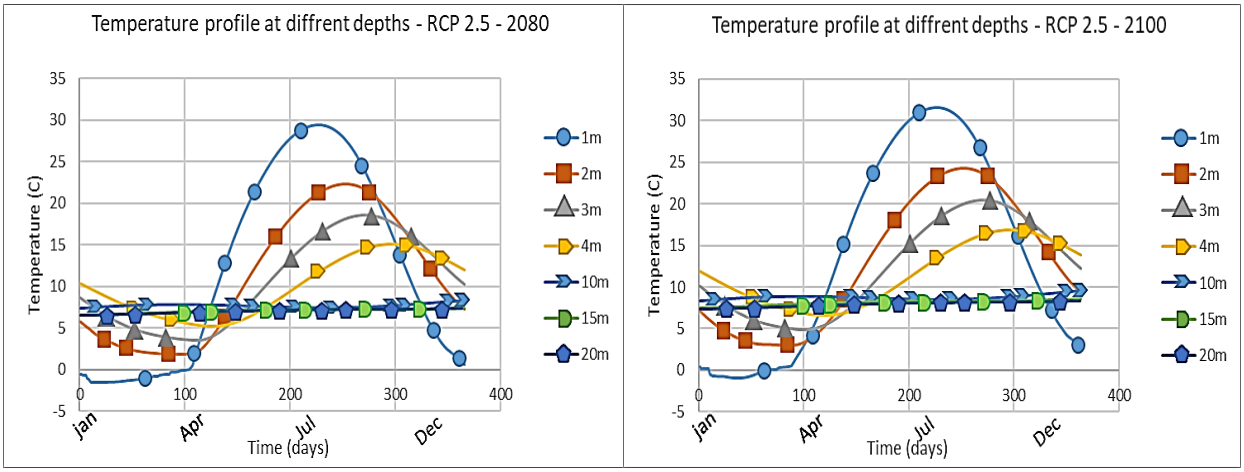

Figure C-12: Temperature profile at different depths - RCP 2.5 at 2040, 2060, 2080, 2100 – Sudbury

Appendix D

a)

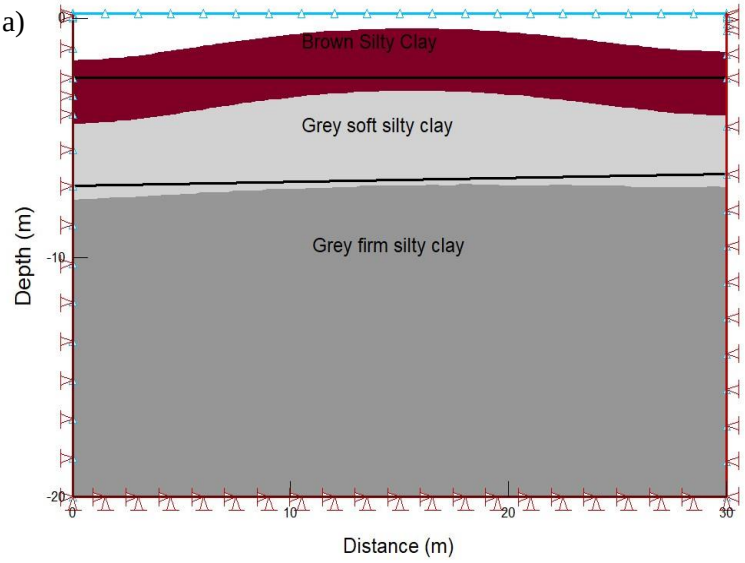
Brown Silty Clay
Grey soft silty clay
Grey firm silty clay
Depth (m)
0
-10
-20
0
10
20
30
Distance (m)

b)

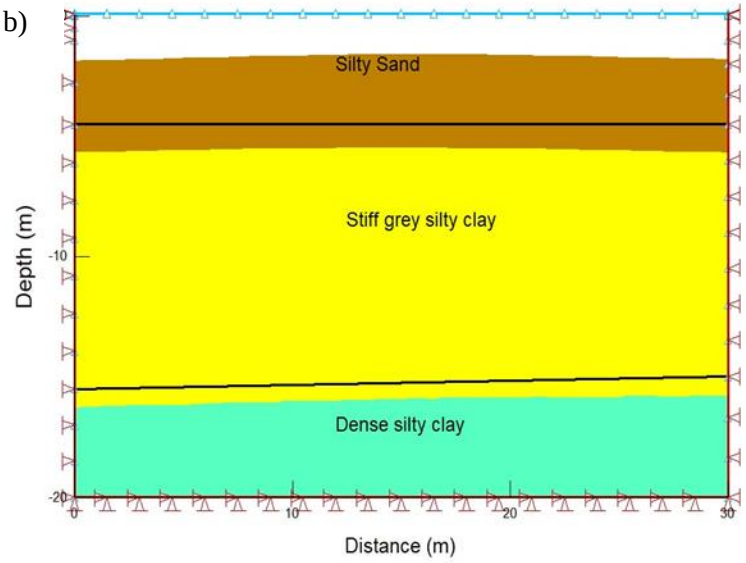
Silty Sand
Stiff grey silty clay
Dense silty clay
Depth (m)
0
-10
-20
0
10
20
30
Distance (m)

c)

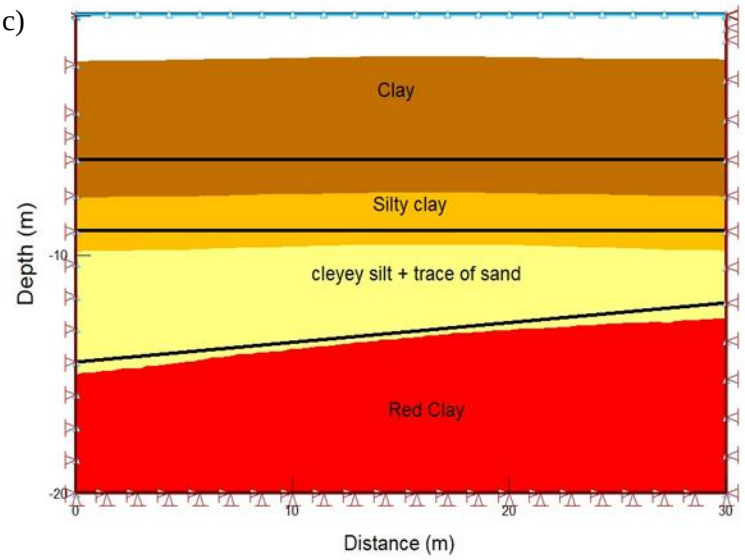

Figure D-1: Deformation model a) Ottawa, b) Toronto and c) Sudbury

Ottawa:

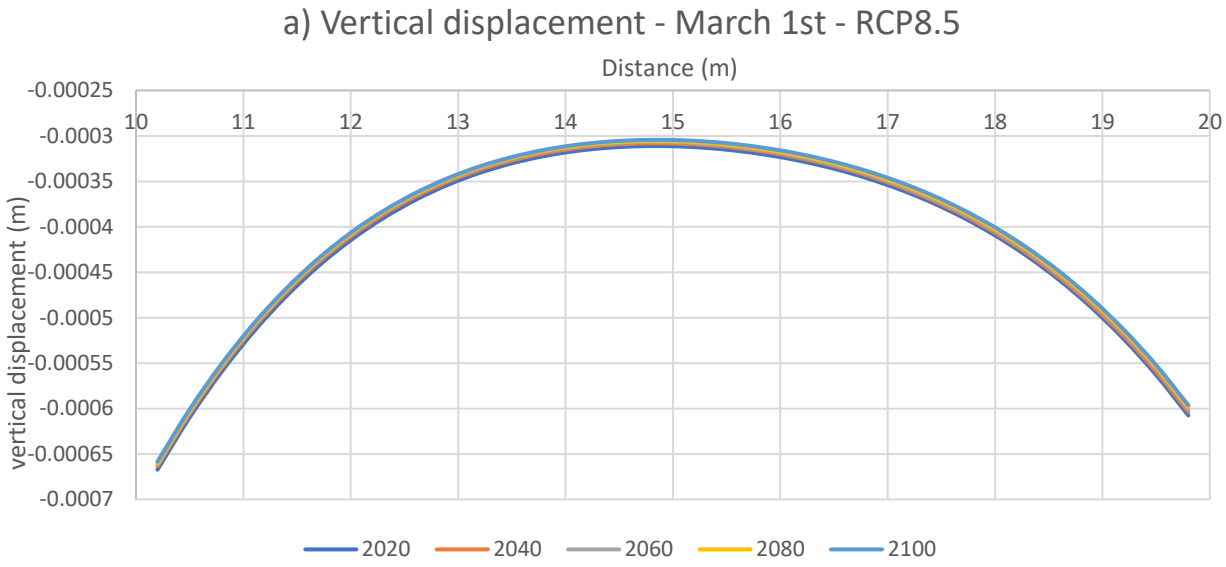

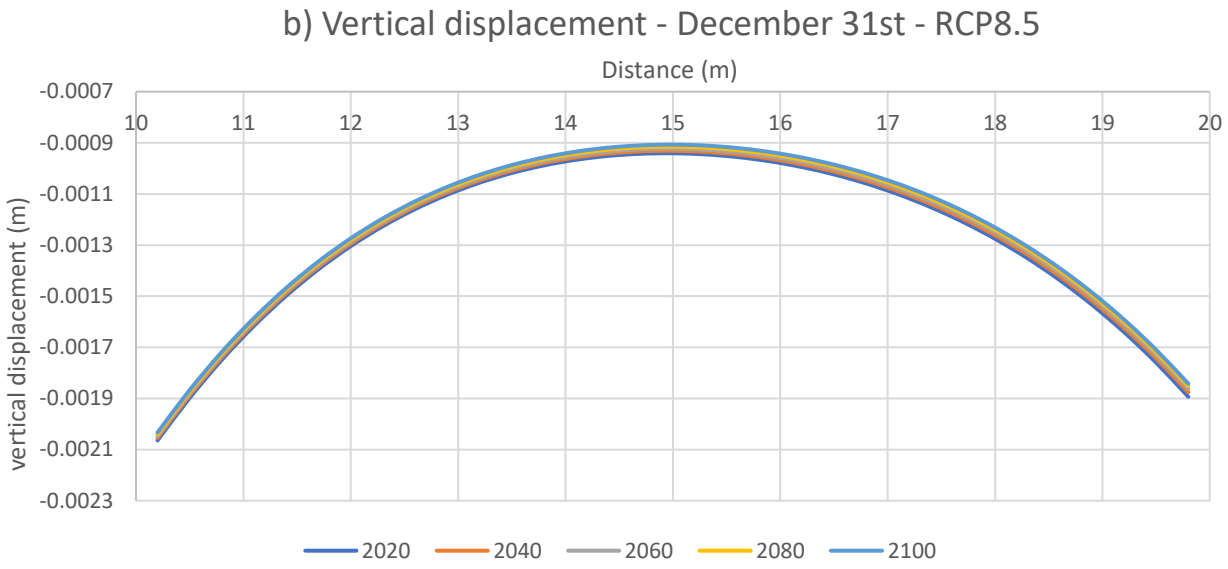

Figure D-2: Ground surface settlement at a) March 1st and b) December 31 st for 2020 – 2040 – 2060 – 2080 – 2100 – RCP8.5

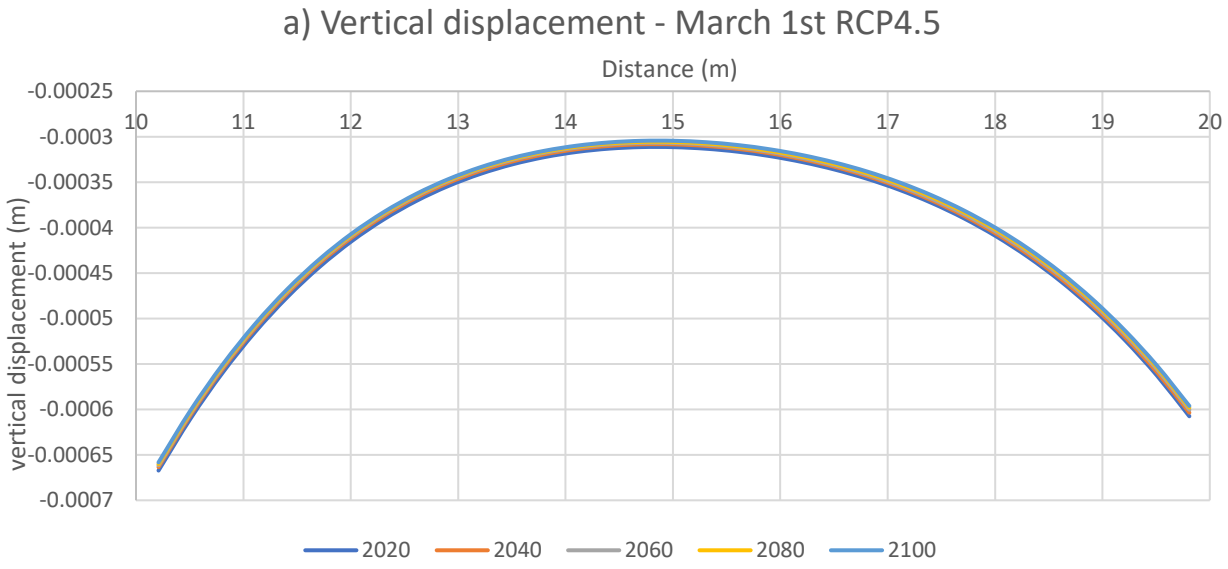

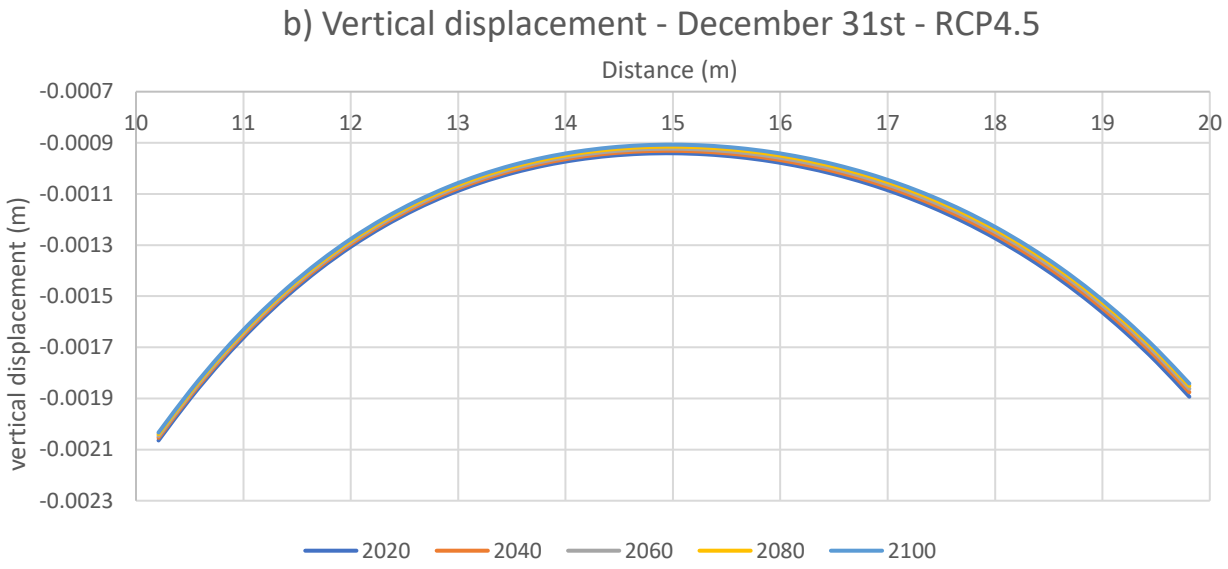

Figure D-3: Ground surface settlement at a) March 1st and b) December 31 st for 2020 – 2040 – 2060 – 2080 – 2100 – RCP4.5

Toronto:

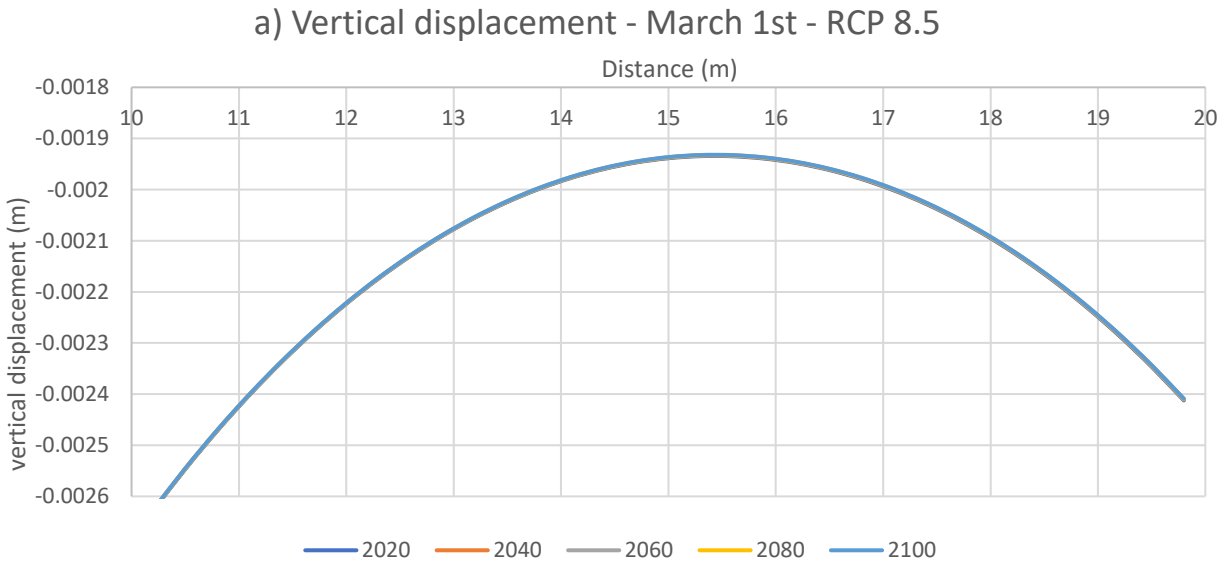

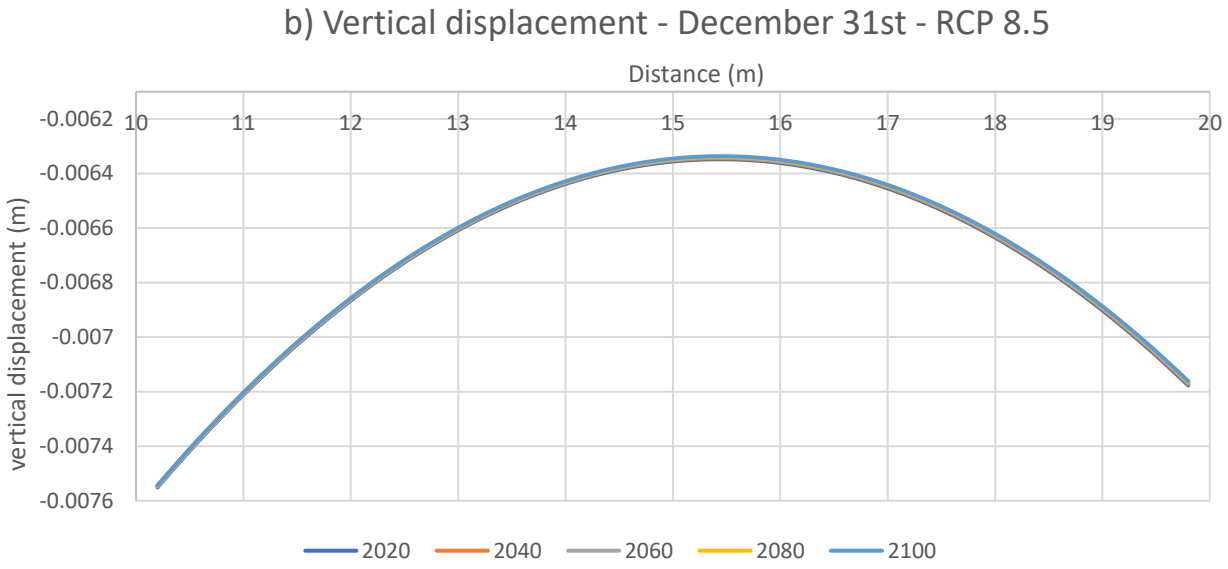

Figure D-4: Ground surface settlement at a) March 1st and b) December 31 st for 2020 – 2040 – 2060 – 2080 – 2100 – RCP4.5

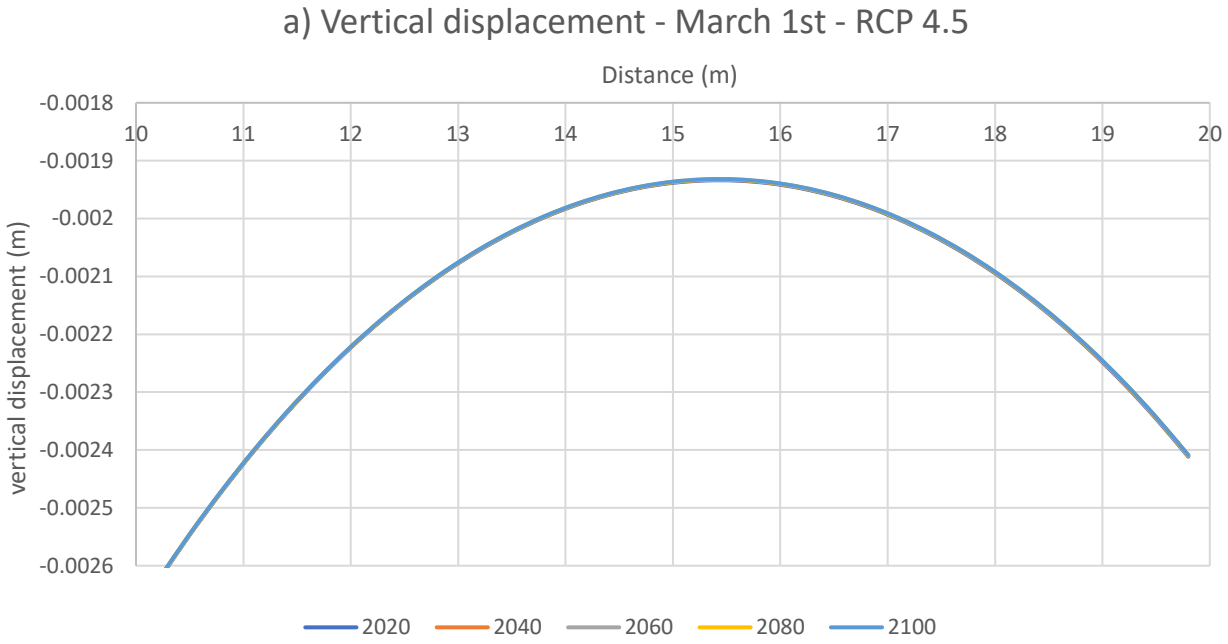

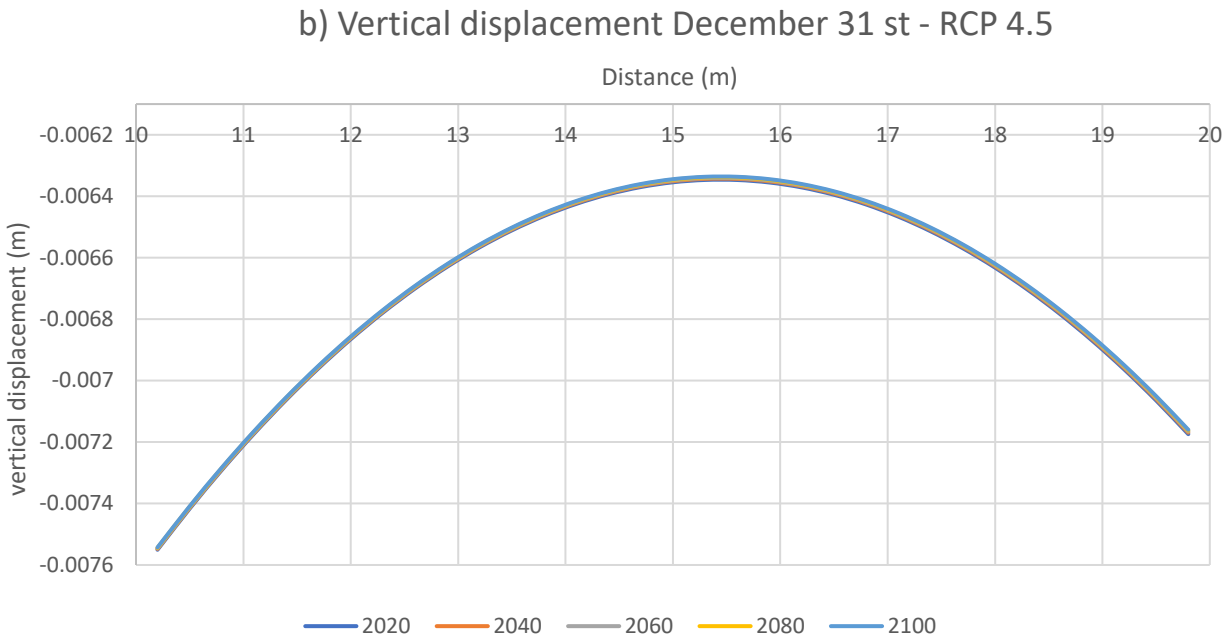

Figure D-5: Ground surface settlement at a) March 1st and b) December 31 st for 2020 – 2040 – 2060 – 2080 – 2100 – RCP4.5

Sudbury:

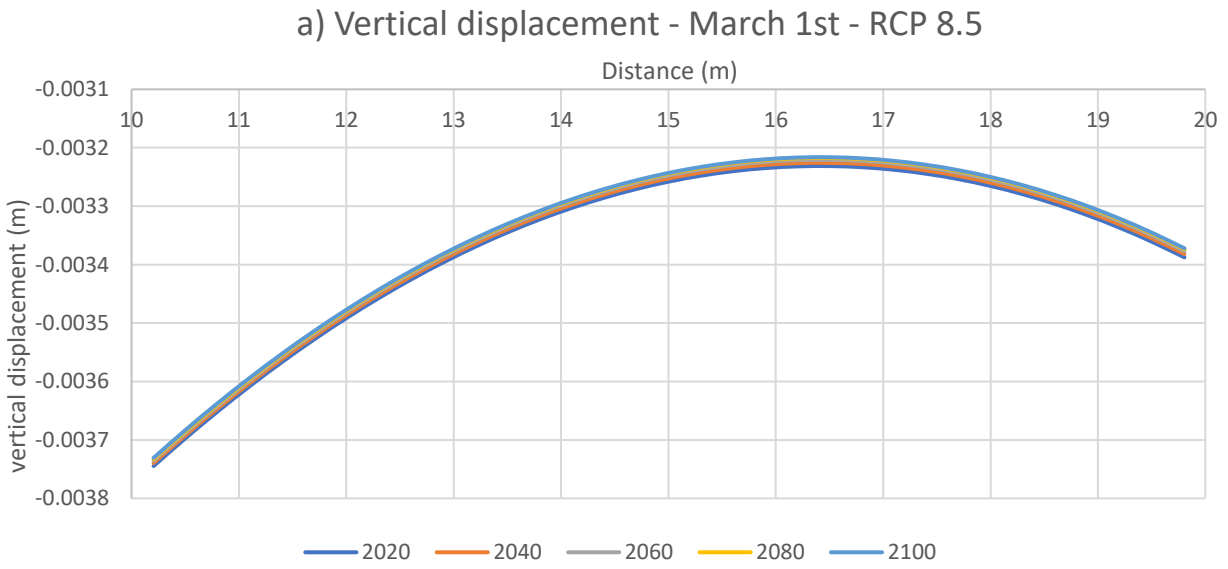

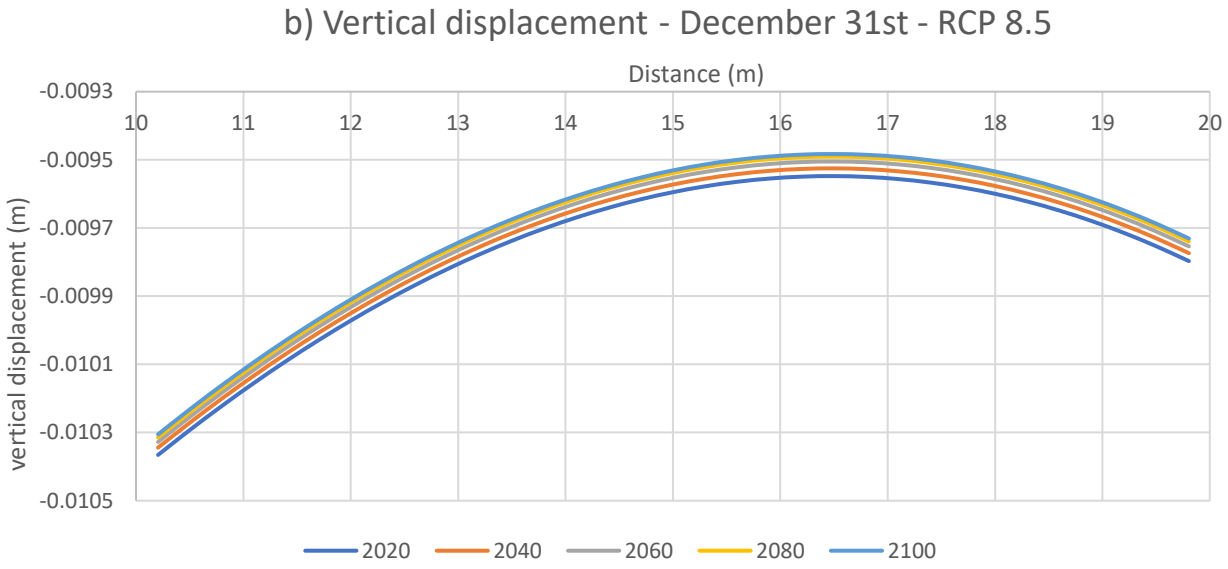

Figure D-6: Ground surface settlement at a) March 1st and b) December 31 st for 2020 – 2040 – 2060 – 2080 – 2100 – RCP8.5

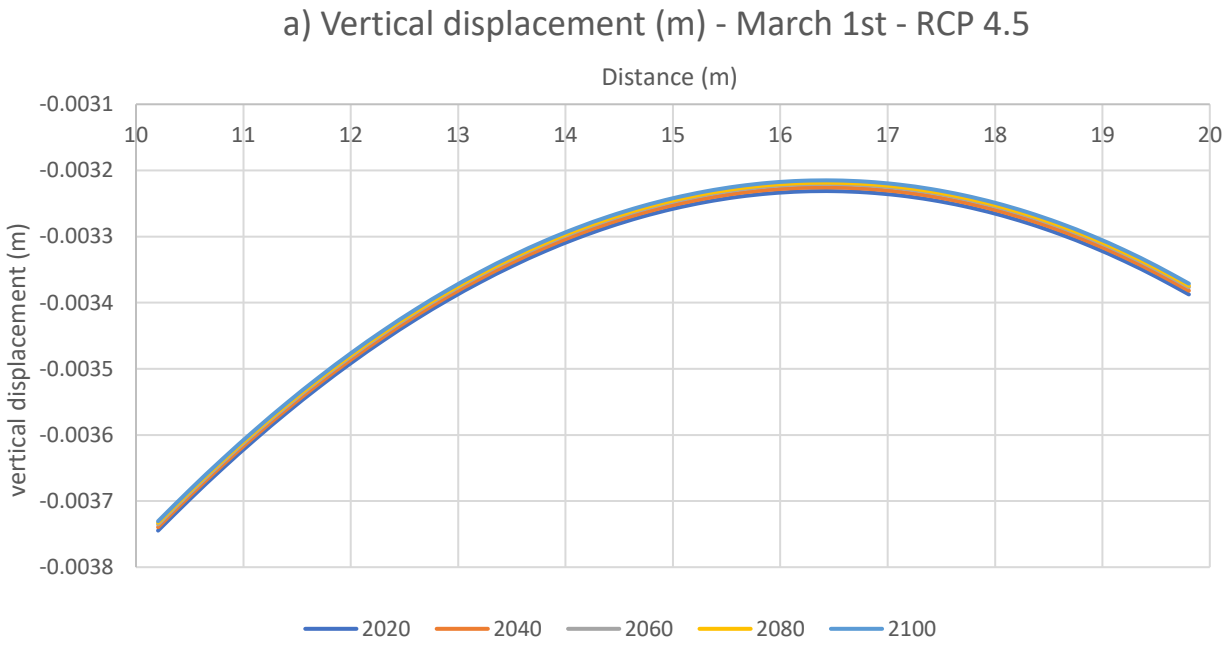

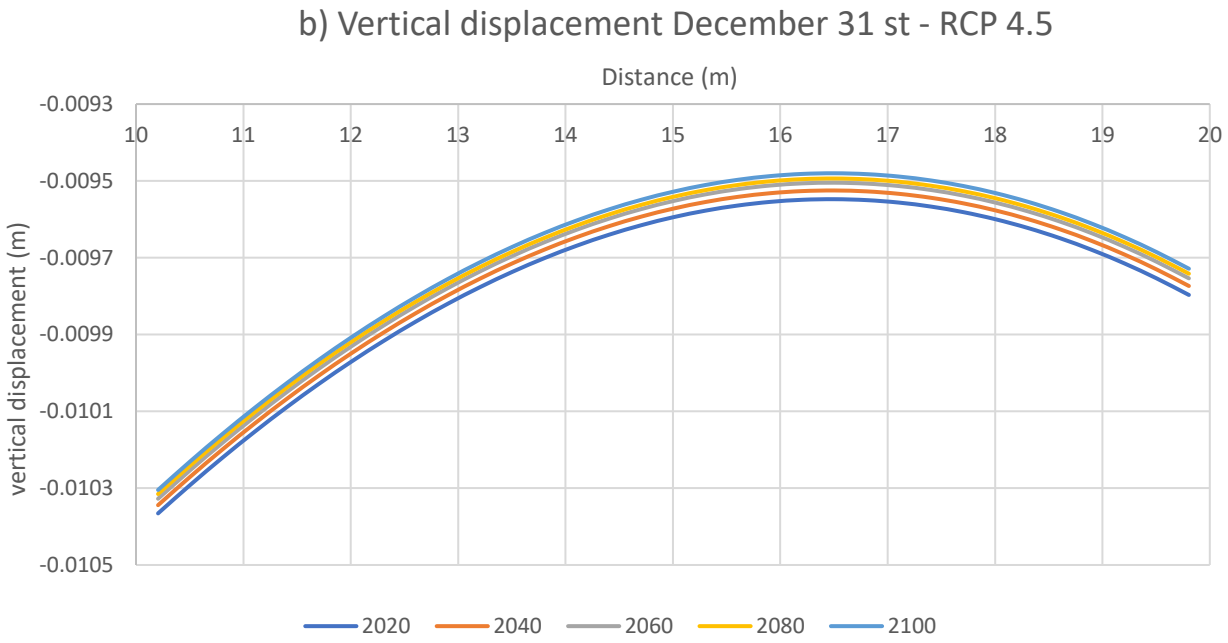

Figure D-7: Ground surface settlement at a) March 1st and b) December 31 st for 2020 – 2040 – 2060 – 2080 – 2100 – RCP4.5

Appendix E

E.1- Finite element formulation for coupled hydro-mechanical analysis

In a coupled consolidation analysis, both equilibrium and flow equations are solved simultaneously. In SIGMA/W, the finite element equilibrium equations are formulated using the principle of virtual work, which states that for a system in equilibrium, the total internal virtual work is equal to the external virtual work (GEO-SLOPE International Ltd, 2013). The finite element equations that SIGMA/W solves are given by:

Equation 6.3.1: SIGMA/W finite element equilibrium equation (GEO-SLOPE International Ltd, 2013):

$$\sum [B]^T[D][B]\{\Delta\delta\} + \sum [B]^T[D]\{m_H\}\langle N\rangle\{\Delta u_w\} = \sum F$$

$$[K] = [B]^T[D][B]$$

$$[L_d] = [B]^T[D]\{m_H\}\langle N\rangle$$

And,

$$\{m_H\}^T = \langle \frac{1}{H}\frac{1}{H}\frac{1}{H}\ 0\rangle$$

Where:

[B] = gradient matrix, (also called the strain matrix),

[D] = drained constitutive matrix,

[K] = stiffness matrix,

[Ld] = coupling matrix,

$\{\Delta\delta\}$ = incremental displacement vector, and

$\{\Delta u_w\}$ = incremental pore-water pressure vector.

For a fully saturated soil, the coupling matrix, [Ld], can be written as:

$$[L_d] = [B]^T\{m\}\langle N\rangle$$

With,

$\{m\}^T$ = unit isotropic tensor, < 1 1 1 0 >.

The flow equation can similarly be formulated for finite element analysis using the principle of virtual work in terms of pore-water pressure and volumetric strains. If virtual pore-water pressures, u_w*, are applied to the flow equation and integrated over the volume, the following virtual work equation can be

obtained.

Equation 6.3.2: Flow equation (GEO-SLOPE International Ltd, 2013):

$$\int u_w^* \left(\frac{k_x}{\gamma_w} \frac{\partial u_w^*}{\partial x^2} + \frac{k_y}{\gamma_w} \frac{\partial^2 u_w}{\partial y^2} + \frac{\partial \theta_w}{\partial t} \right) dV = 0$$

Where:

kx, ky = the hydraulic conductivity in x and y direction, respectively,

uw = pore-water pressure,

γ_w = the unit weight of water,

θ_w = the volumetric water content, and

t = time.

Applying integration by parts to equation E.1.2 gives:

$$-\int \left(\frac{k_x}{\gamma_w} \frac{\partial u_w^*}{\partial x} \frac{\partial u_w}{\partial x} + \frac{k_y}{\gamma_w} \frac{\partial u_w^*}{\partial y} \frac{\partial u_w}{\partial y} \right) dV + \int u_w^* \frac{\partial \theta_w}{\partial t} \, dV = \int u_w^* v_n dA$$

Where:

v_n = boundary flux.

The volumetric water content for an elastic material is given by the following expressions (Dakshanamurthy et al., 1984):

$$\theta_w = \frac{\beta}{3} \varepsilon_v - \omega u_w$$

Where:

$$\beta = \frac{E}{H} \frac{1}{1 - 2v}$$

And,

$$\omega = \frac{1}{R} - \frac{3\beta}{H}$$

Where:

H = unsaturated soil modulus for soil structure with respect to matrix suction (ua - uw),

R = a modulus relating the change in volumetric water content with change in matric suction.

E = elastic modulus for soil structure, and

v = Poisson's ratio.

ε_v= normal strain,

Therefore, substituting in the expression for the volumetric water content, θ_w, gives:

$$-\int\left(\frac{k_x}{\gamma_w}\frac{\partial u_w^*}{\partial x}\frac{\partial u_w}{\partial x}+\frac{k_y}{\gamma_w}\frac{\partial u_w^*}{\partial y}\frac{\partial u_w}{\partial y}\right)dV+\int u_w^*\frac{\partial\theta_w}{\partial t}\,dV=\int u_w^* v_n dA$$

Using finite element approximations, this equation can be written as:

$$-\int\frac{1}{\gamma_w}[B]^T[K_w][B]\{u_w\}dV-\int\langle N\rangle^T\langle N\rangle\left\{\frac{\partial(\omega u_w)}{\partial t}\right\}+\int\langle N\rangle^T\{m\}^T[B]\left\{\frac{\partial(\beta\delta)}{\partial t}\right\}\,dV=\int\langle N\rangle^T v_n dV$$

Where:

$$[K_f]=\int[B]^T[K_w][B]dV$$

$$[M_N]=\langle N\rangle^T\langle N\rangle$$

$$[L_f]=\int\langle N\rangle^T\{m\}^T[B]\;dV$$

With:

[B] = gradient matrix,

[Kw] = hydraulic conductivity matrix,

[Kf] = element stiffness matrix,

$\langle N\rangle$ = row vector of shape functions,

$[M_N]$ = mass matrix,

$[L_f]$ = coupling matrix for flow,

$\{m\}^T$: isotropic unit tensor, < 1 1 1 0 >, and

δ: nodal displacement.

Integrating the equation above from time t to time t +Δt gives:

$$-\int_{t}^{t+\Delta t}\frac{1}{\gamma_w}[K_f]\{u_w\}\,dt-\int_{t}^{t+\Delta t}[M_N]\left\{\frac{\partial(\omega u_w)}{\partial t}\right\}dt+\int_{t}^{t+\Delta t}[L_f]\left\{\frac{\partial(\beta\delta)}{\partial t}\right\}dt=\int_{t}^{t+\Delta t}\langle N\rangle^T v_n\,dA dt$$

Applying the time differencing technique using as the time stepping factor to this equation and when the backward (fully implicit) time-stepping scheme is used (by setting θ = 1) and assuming that ω and β remain constant within a time increment, the equation above becomes:

$$-\frac{\Delta t}{\gamma_w}[K_f]\{u_w\}|_{t+\Delta t}-\omega[M_N]\{u_w\}+\beta[L_f]\{\Delta\delta\}=\Delta t\,\{Q\}|_{t+\Delta t}$$

Where:

{Q} = the flow at boundary nodes.

To obtain an equation involving an incremental pore-water pressure only, the first term, $\frac{\Delta t}{\gamma_w}[K_f]\{u_w\}|_t$, is added to both sides of the equation. The resultant equation describing the flow of pore-water is:

$$\beta[L_f]\{\Delta\delta\}-\left(\frac{\Delta t}{\gamma_w}[K_f]+\omega[M_N]\right)\{\Delta u_w\}=\Delta t\left(\{Q\}|_{t+\Delta t}+\frac{1}{\gamma_w}[K_f]\{\Delta u_w\}|_t\right)$$

Therefore, the coupled consolidation analysis for saturated/unsaturated soils is formulated using incremental displacement and incremental pore-water pressure as field variables.
In summary, the coupled equations for finite element analysis are rewritten in the following form.

$$[K]\{\Delta\delta\}+[L_d]\{\Delta u_w\}=\{\Delta F\}$$

And,

$$\beta[L_f]\{\Delta\delta\}-\left(\frac{\Delta t}{\gamma_w}[K_f]+\omega[M_N]\right)\{\Delta u_w\}=\Delta t\left(\{Q\}|_{t+\Delta t}+[K_f]\{y\}+\frac{1}{\gamma_w}[K_f]\{\Delta u_w\}|_t\right)$$

Where:

$$[K]=\sum[B]^T[D][B]$$

$$[L_d] = \sum [B]^T [D]\{m_H\} < N >$$

$$\{m_H\} = < \frac{1}{H} \frac{1}{H} \frac{1}{H} 0 >$$

$$[K_f] = \sum [B]^T [K_w][B]$$

$$[M_N] = \sum < N >^T < N >$$

$$[L_f] = \sum < N >^T \{m\}[B]$$

And,

[Kf]{y}: Gravitational term

For these equations to model the fully saturated case, the following conditions must be satisfied:

$$\beta = 1,$$

$$\omega = 0, \text{and}$$

$$[L_f] = [L_d]^T$$

E.2- References:

GEO-SLOPE International Ltd. (2013). Stress-Deformation Modeling with SIGMA/W. July, 223. http://downloads.geo-slope.com/geostudioresources/books/8/15/sigma modeling.pdf

Dakshanamurthy, V., Fredlund, D.G, and Rahardjo, H., (1984). Coupled three-dimensional consolidation theory of unsaturated porous media. Proceedings of the Fifth International Conference on Expansive Soils, Adelaide, Australia, pp. 99 -103.

Appendix F

F.1- Engineering properties of Canadian no-permafrost soils

F.1.1- Geotechnical properties of frozen soils:

Since the Canadian no-permafrost region comprises frozen soil in the winter season, it is essential to understand the geotechnical properties of frozen soil in general. In fact, there is more than fifty years of history of studies on the effect of temperature on the geotechnical properties of soils (Flynn, 2015). The following section is an analysis of geotechnical properties of frozen soils.

F.1.1.1- The shear strength of frozen soils:

Shear stress is a function of both normal stress and temperature. The shear strength of frozen sand, silt, clay and polycrystalline ice, was the object of a research project conducted by Knutsson in the University of Luleå in Sweden (1981). In this study, undisturbed samples of sandy, silty and clay soils were prepared in the laboratory and placed in a cold room in which the temperature was kept constant at -15 ° C before shearing. The study concluded that samples of frozen saturated silt behave like ice, with respect to Mohr-Coulomb shear failure, and their shear strength increases significantly after freezing. The investigated clay samples showed a higher shear resistance which can be related to the preserved continuity of the particle connection after freezing (Munro, 2018).

In other studies, conducted by Chen (1988) and Chen et al. (1991), samples of clay soil were tested in the laboratory to determine their strength-deformation behavior. Results showed that, with soils of clay fraction greater than 50%, all the stress-strain curves show a strain-hardening character, resulting from a gradual mobilization of friction, dilatancy, and interference of particles. Regarding the shear strength, the study concluded that frozen clay develops a significant shear strength similar to cemented clay. Chen et al.'s (1991) tests concluded that the friction angle is not much affected by temperature change. Therefore, they concluded that the increase of shear strength is essentially contained almost entirely in the cohesion term. These results concord with those reported by Vyalov et al. (1988) (Czurda & Hohmann, 1997).

Many investigators have studied the shear behavior of frozen sands (e.g., Goughnour and Andersland 1968; Andersland and Al-Nouri 1970; Alkire and Andersland 1973; Chamberlain, Groves and Perham 1972; Sayles 1973). Ting (1981) and Martin and Ladd (1983) concluded that the shear behavior of frozen sands is controlled by four main factors: (1) pore ice strength, (2) soil strength related to interparticle friction, (3) increase in the effective stress due to adhesive ice bonds resisting dilation during shear of a dense soil , and (4) synergistic strengthening effects between the soil and ice matrix preventing shearing the soil skeleton (Orlando & Ladanyi, 2004). These four mechanisms are significantly influenced by temperature and confining pressures. For instance, the effect of ice bounding, and the pore ice strength will disappear when global ice melting occurs at a high confining pressure, which will significantly reduce the shear strength of

the soil (Orlando & Ladanyi, 2004).

F.1.1.2- Uniaxial compressive strength and modulus of elasticity of frozen soils:

A research was conducted by Shelman et al. (2014) to capture the changes in soil behavior and engineering properties at freezing temperatures. Samples of Alluvial deposits (soil Type I, figure F-1.2) were prepared in the laboratory and tested under compressive force at different temperatures ranging from -20 ° C to + 20 ° C. The results show that when decreasing temperature, the soil sample experienced an increase in the elastic modulus, an increase in the ultimate compressive strength, and a decrease in the strain at peak stress. For the alluvial soil samples tested in this study, the elastic modulus increased by a factor of 300, the ultimate compressive strength increased by a factor of 80, and the strain at peak stress decreased by 5% strain. The results are reported in the figures bellow (Shelman et al., 2014):

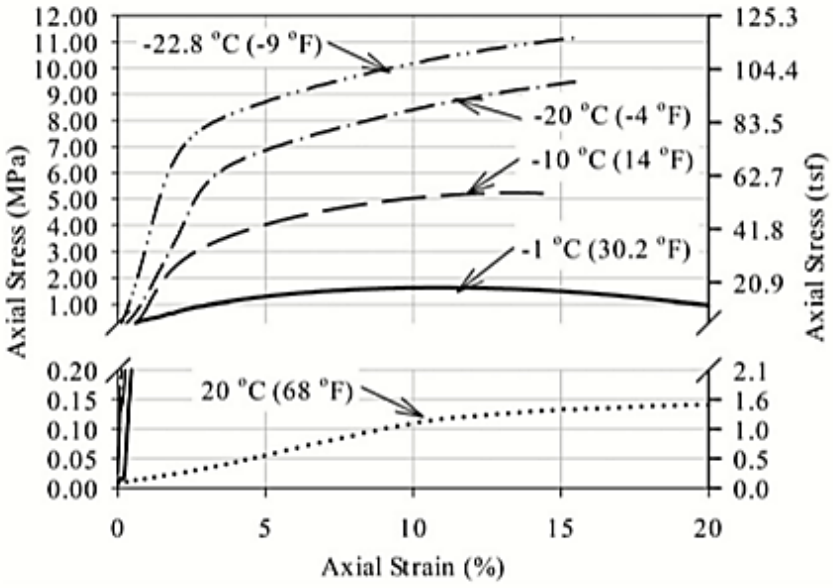

Figure 6.3.1: Stress-strain response of a Type I soil subjected to monotonic loading at various test temperatures (Shelman et al., 2014)

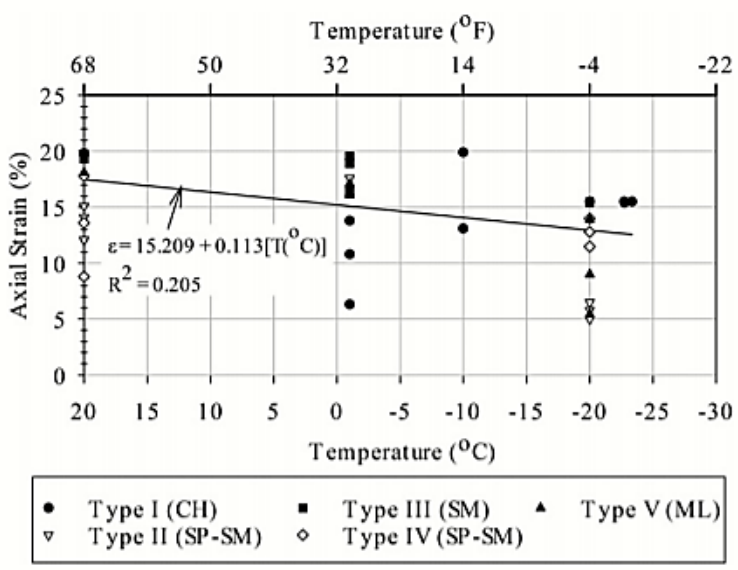

Figure 6.3.2: Variation of ultimate strain with temperature – Soil type I (Shelman et al., 2014)

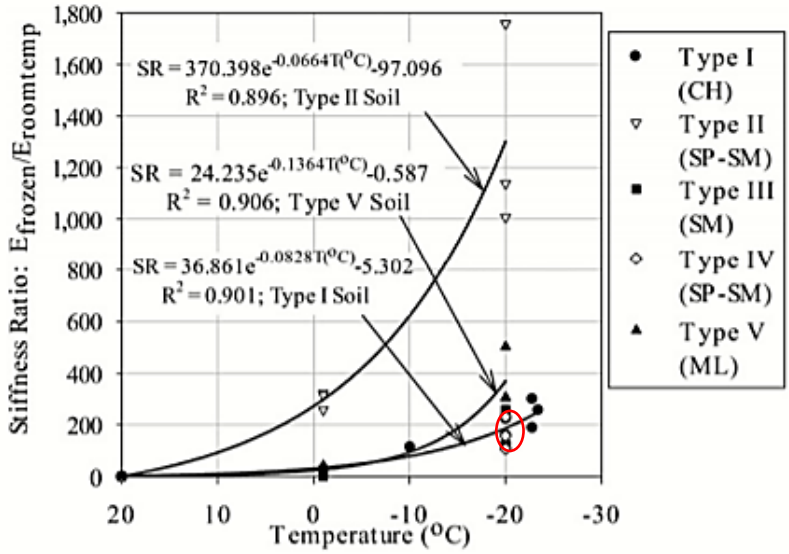

Figure 6.3.3: Effects of temperature on the stiffness ratio under monotonic loading (Shelman et al., 2014)

In general, a decrease in temperature results in an increase in compressive strength of a frozen soil (Jiang and Fall, 2017), but at the same time it increases its brittleness, which is manifested by a larger drop of strength after the peak and an increase in the ratio of compressive to tensile strength (Shelman et al., 2014). The embrittlement effect of temperature is observed more in frozen sand or silt than in a frozen clay, for example, down to about -10 °C, frozen clay still contains enough unfrozen water to maintain its plastic behavior (Orlando & Ladanyi, 2004).

F.1.1.3- Poisson's ratio of frozen soils:

Many studies were carried out to determine the effect of temperature on soil's Poisson ratio. A research by He and Zhu (1999) concluded that the Poisson's ratio of frozen sand is strongly dependent on temperature but is rarely affected for frozen silt and frozen clay (Wang et al., 2015). Furthermore, a study conducted by Wang et al. (2015) showed that the Poisson's ratio for frozen silt and frozen clay is not significantly influenced by frozen temperature and a constant value of Poison ratio can be used in analyzing the dynamic responses for frozen silt and clay soils. Wang's study involved a laboratory examination of three main soil types: frozen sand (water content 17.3%), frozen silt (water content =18.86 %), and frozen clay (water content 31 %). As shown in figure 2.3.4, a relatively small variation of Poisson ratio for silt and clay was recorded in this laboratory test. Unlike for clay and silt, Poisson ration for sand appears to be strongly affected by decreasing temperature (Wang et al., 2015).

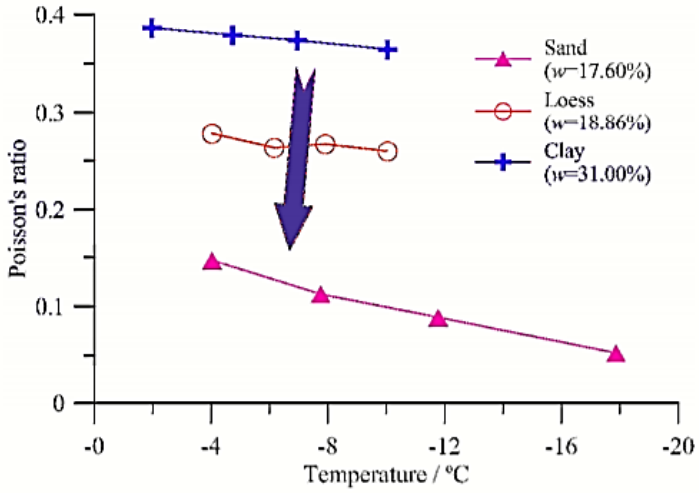

Figure 6.3.4: Relationship of dynamic Poisson's ratio vs. temperature (Wang et al., 2015)

F.1.2- Physical properties of frozen soils

Soil physical properties are related to the elements constituting the soil. They are determined based on laboratory testing of soil samples and involve measurements of soil sample volume V, the total mass, the mass of dry solids M_s, the mass of water in both physical forms; ice M_i and unfrozen water M_{un} and the total mass of water ($M_w = M_i + M_{uw}$) in the soil. Some physical properties are not sensitive to frozen state of the soil, they are calculated using same quantities and equations for both frozen and unfrozen soils. Other physical properties are slightly influenced by the presence of ice, in the composition of soil, and therefore, their equations change slightly to incorporate the existence of ice. Figure F-1.5 represent a schematization of the different soil elements including their volumes and masses.

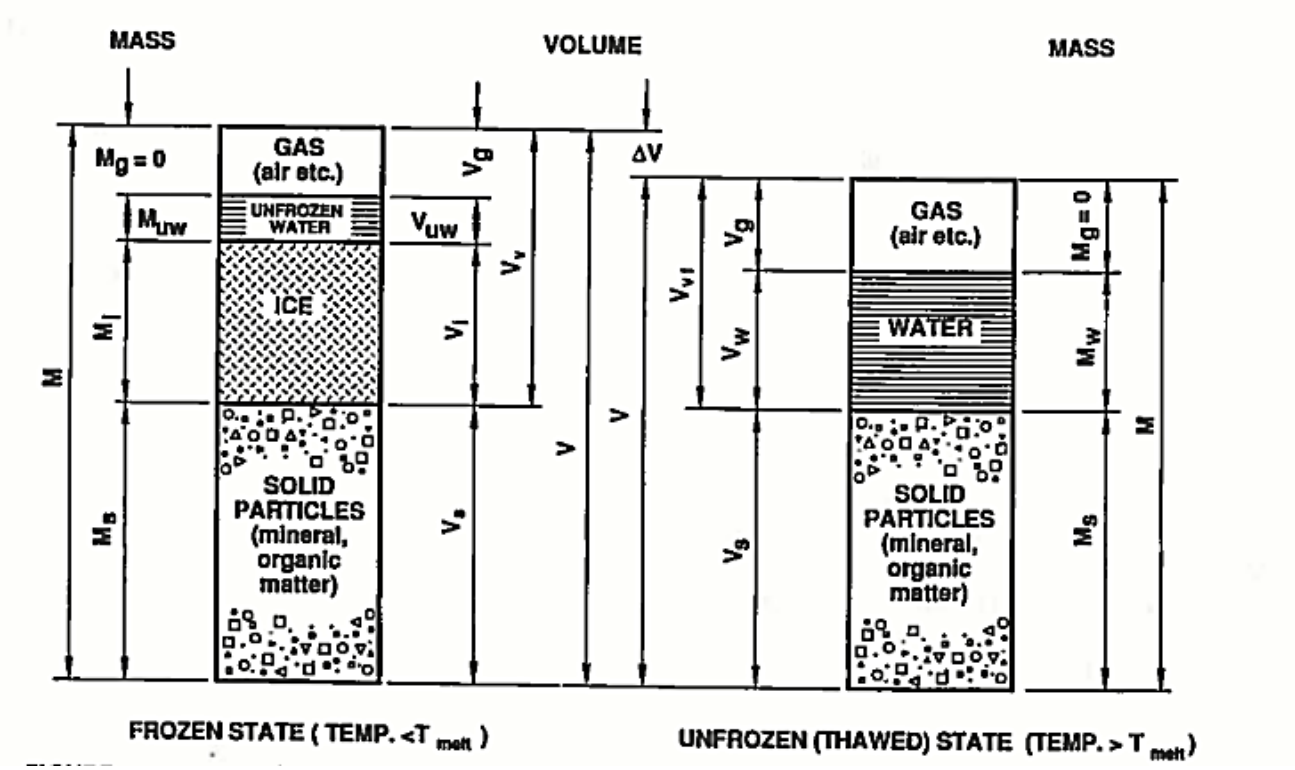

Figure 6.3.5: Mass-Volume relationship for frozen and unfrozen soils (Orlando & Ladanyi, 2004)

F.1.2.1- Gravimetric water content:

The gravimetric water content is defined as the amount of water in the soil. Considering the four elements in the frozen soil composition, the amount of water in the soil includes both unfrozen water and ice; therefore, gravimetric water content for frozen ground is calculated as the ratio of the total mass of water M_w to the mass of solid particles. The water content is usually expressed as percentage (Bilskie, 2001). In the context of frozen soils, the total gravimetric water content w_t is divided to two parts: frozen w_f and unfrozen w_u. An empirical formulation was developed to compute the unfrozen water content w_u using the soil grain surface area $S(m2\ /g)$ and the temperature T(°C) as follows:

Equation 6.3.1: unfrozen water content equation Farouki, (1981):

$$\log_e w_u = 0.2618 + 0.5519 \log_e S - 1.449 S^{-0.264} \log_e T$$

The frozen water content w_f is deducted from the total and unfrozen water contents, as follow:

Equation 6.3.2: frozen water content equation (Orlando & Ladanyi, 2004)

$$w_f = w_t - w_{uf}$$

Where: w_t: total water content and w_{uf}: unfrozen water content.

F.1.2.2- Volumetric water content:

The volumetric water content (Θ) is an essential parameter commonly used to identify the amount of water existing in soils. It represents the percentage of the water volume in the ground to the total volume of the soil. The volumetric water content is calculated as follows:

Equation 6.3.3: Volumetric water content equation (Orlando & Ladanyi, 2004)

$$\Theta = \left(\frac{\mathrm{w_t}}{\mathrm{W_t} + 1}\right) * \left(\frac{\rho_{\mathrm{bulk}}}{\rho_{\mathrm{w}}}\right) = \mathrm{n\ S}$$

Where:

- $\mathrm{W_t}$: Gravimetric water content,
- ρ_{bulk}: Bulk density,
- ρ_{w}: Density of water,
- n: Soil's porosity,
- S: Soil's degree of saturation.

F.1.2.3- Degree of saturation:

The degree of saturation is the parentage of total voids volume filled with water. For unfrozen grounds, the degree of saturation is defined as the volume of water in the pore to the total volume of voids; however, for frozen engineering practice, two degrees of saturation are calculated:

Ice degree of saturation: defined as the ratio of ice volume to pore volume in frozen soil.

Unfrozen water degree of saturation: defined as the ratio of unfrozen water volume to pore volume.

The total degree of saturation (ice and unfrozen water) for frozen soil is calculated as the sum of the ice degree of saturation and the unfrozen water degree of saturation of a soil sample.

Crory (1973) proposed an equation to compute the total degree of saturation for frozen soil as follows (Crory, 1973):

Equation 6.3.4: Degree of saturation for frozen soil (Crory, 1973):

$$S_r = \frac{G_s\left(1.09\ w_f - 0.09\ w_u\right)}{e}$$

Where:

- G_s: the specific gravity of the soil particles,
- w_f: frozen water content,
- w_u: unfrozen water content,
- e : void ratio of the soil at the dry state,

F.1.2.4- Relative ice content:

The relative ice content can be calculated as the ratio of ice mass to total water mass (in both state frozen and unfrozen). The relative ice content is also called iceness ratio (i_r). (Orlando & Ladanyi, 2004).

F.1.2.5-Atterberg limits:

Atterberg limits are basic measures of the water contents of fine-grained soil at a certain limiting or critical stages of soil behavior including its shrinkage limit, plastic limit, and liquid limit. Atterberg limits are represented on a straight line as shown in figure F-1.6. The horizontal line represents qualitatively the water content of the soil from the dry state on the left to wet state on the right.

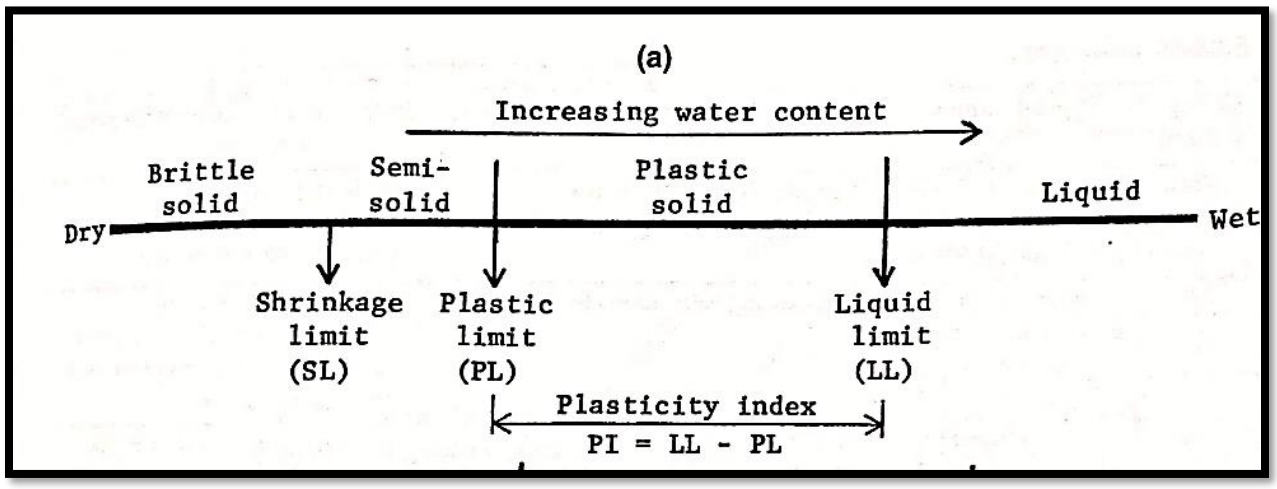

Figure F-1.6: Atterberg limits - (Orlando & Ladanyi, 2004)

The effect of decreasing temperature on the Atterberg limits is first studied by Ctori (1989), who concluded that a decrease in temperature from 35 °C to 6 °C changes the behavior of clay from low to medium plasticity. Atterberg limits will increase with lower temperatures as shown in figure F-1.6 (Ctori, 1989).

Table 6.3.1: Temperature dependence of Atterberg limit - (Orlando & Ladanyi, 2004)

Temperature	liquid limit %	Plastic limit %	Plasticity index (%)
6	41	20	21
20	36.5	18	18.5
35	26	15	11

F.1.3- Thermal properties of frozen soils:

Thermal properties command the heat transfer process in soils and govern the response of ground to thermal variations. They vary with temperature, soil type, soil density, water and ice contents, and the degree of saturation of the soil (Wolfe & Thieme, 1964). The thermal properties include the thermal conductivities, heat capacities, thermal diffusivity, latent heat of fusion, and thermal expansion coefficient.

F.1.3.1-Thermal conductivity:

The thermal conductivity is defined as the quantity of heat transmitted through a unit thickness of a material due to a unit temperature gradient under steady state conditions (Orlando & Ladanyi, 2004). Thermal conductivity varies greatly depending on the soil type and the ground temperature. Several methods were developed to estimate the thermal conductivity of frozen soils. Johnsen's (1975) method gives a good result for thermal conductivity of frozen and unfrozen coarse and fine soils, at a degree of saturation above 0.1 (Orlando & Ladanyi, 2004).

Johnsen's equation is valid for unfrozen and frozen mineral soils, and is presented as follows:

Equation 6.3.5: Thermal conductivity equation (Johnsen, 1975):

$$K\left(\frac{W}{m.K}\right) = \left(K_{sat} - K_{dry}\right)K_e + K_{dry}$$

Where:

- K: thermal conductivity if the soil,
- K_{sat}: Saturated thermal conductivity,
- K_{dry}: Dry thermal conductivity,
- K_e: is defined as follow:

For coarse-grained unfrozen soils with the degree of saturation Sr>0.05:

$$K_e = 0.7\log(S_r) + 1\ ,$$

For fine- grained unfrozen soils with Sr > 0.1:

$$K_e = 0.7 \log(S_r) + 1,$$

For all type of frozen soils: $K_e = S_r$,

Johansen (1975) developed a semi-empirical equation to compute the dry and saturated soil conductivities as follow:

Equation 6.3.6: Dry Thermal conductivity equation (Johnsen, 1975):

$$K_{dry}\left(\frac{W}{m.K}\right) = \frac{0.137\rho_d + 64.7}{2700 - 0.947\rho_d} \pm 20\%$$

Where:

ρ_d: soil dry density

For saturated unfrozen soils, Johansen proposed the following equation to compute the saturated thermal conductivity:

Equation 6.3.7: Saturated unfrozen thermal conductivity equation (Johnsen, 1975):

$$K_{sat}\left(\frac{W}{m.K}\right) = K_s^{1-n}.K_w^n$$

For saturated frozen soils, Johansen proposed the following equation to compute the saturated thermal conductivity:

Equation 6.3.8: Saturated frozen thermal conductivity equation (Johnsen, 1975):

$$K_{sat}\left(\frac{W}{m.K}\right) = K_s^{1-n}.K_i^{n-w_u}.K_w^{w_u}$$

Where:

- n: porosity,
- w_u: unfrozen water content,
- K_i: ice thermal conductivity = $2.2\frac{W}{m.K}$,
- K_w: water thermal conductivity = $0.57\frac{W}{m.K}$,

Ks is defined by Johansen (1975) as follow:

Equation 6.3.9: Ks equation (Johnsen, 1975):

$$K_s\left(\frac{W}{m.K}\right) = K_q^q . K_0^{1-q}$$

Where:

- K_q : thermal conductivity of quartz; $K_q = 7.7 \frac{W}{m.K}$,
- K_0 : Thermal conductivity of other minerals; $K_o = 2.0 \frac{W}{m.K}$. For coarse grained soils with quartz content less than 20% è $K_o = 3.0 \frac{W}{m.K}$,

Kersten (1949) has conducted experiments on natural soils samples and crushed rocks and developed empirical equation to compute their thermal conductivity. These equations were revised and converted to the SI units with k (w/m.K) is expressed in terms of water content w(%) and dry density ρ_{dry} (g/cm^3) .
For unfrozen coarse-grained soils (silt-clay content<20%) with a great quartz content, Farouki (1981) estimated the thermal conductivity as follows:
Equation 6.3.10: Unfrozen thermal conductivity equation for coarse-grained soils (Farouki, 1981):

$$k = 0.1442\ (0.7\log(w) + 0.4) * (10)^{0.6243\rho_{dry}}$$

For frozen coarse-grained soils (-4 C) :
Equation 6.3.11: Frozen thermal conductivity equation for coarse-grained soils ((Farouki, 1981):

$$k = 0.01096\ (10)^{0.8116*\rho_{dry}} + 0.00461 * (10)^{0.9115\rho_{dry}}\ w$$

For unfrozen fine-grained soils (silt-clay content>50%), the thermal conductivity is calculated as follows (Farouki, 1981):
Equation 6.3.12: Unfrozen thermal conductivity equation for fine-grained soils (Farouki, 1981):

$$k = 0.1442\ (0.9\log(w) - 0.2) * (10)^{0.6243\rho_{dry}}$$

For frozen fine-grained soils:
Equation 6.3.13: Frozen thermal conductivity equation for fine-grained soils (Farouki, 1981):

$$k = 0.001442\ (10)^{1.373*\rho_{dry}} + 0.01226 * (10)^{0.4994\rho_{dry}}\ w$$

Where:

- W: water content of the soil,
- ρ_{dry}: dry density.

Harlan and Nixon (1978) summarized much of Kersten's (1949) work. They developed representative graphs to find the frozen and unfrozen thermal conductivities based on the soil type, dry density, water content and degree of saturation (Harlan & Nixon, 1978). These graphs are shown in figure F-1.7.

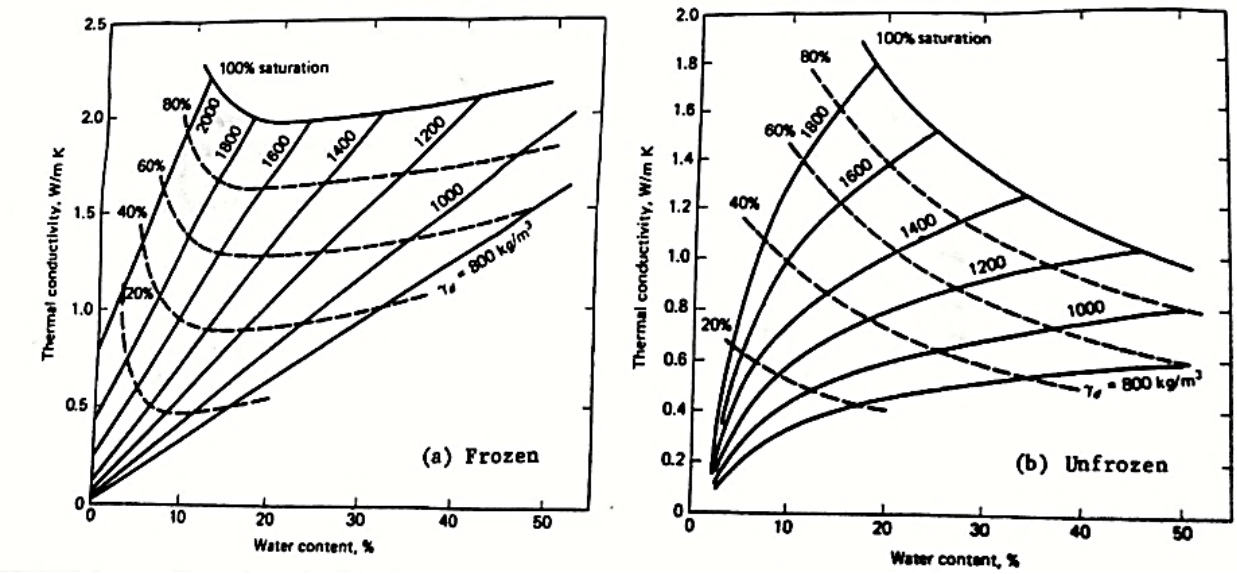

Figure F-1.7: Average thermal conductivity for silt and clay: (a) frozen, (b) unfrozen - (Harlan & Nixon, 1978)

F.1.3.2- Heat capacity and volumetric heat capacity:

The amount of heat required to increase the temperature of a soil by 1-degree Celsius is noted the heat capacity (Williams, 1962).

The volumetric heat capacity is the heat capacity per unit volume of soil. Orlando and Ladanyi (2004) established simplified empirical equation to compute the volumetric heat capacity for both unfrozen and frozen soils.

For unfrozen soil, the volumetric heat capacity is calculated as follows (Orlando & Ladanyi, 2004) :

Equation 6.3.14: Unfrozen volumetric heat capacity equation (Orlando & Ladanyi, 2004)

$$c_{vu}\left(\frac{MJ}{m^3.C}\right) = \left(\frac{\rho_{dry}}{\rho_w}\right) * \left(0.17 + \frac{w}{100}\right) c_{vw}$$

For frozen soil, the volumetric heat capacity can be calculated as follows (Orlando & Ladanyi, 2004):

Equation 6.3.15: Frozen volumetric heat capacity equation (Orlando & Ladanyi, 2004)

$$c_{vf}(\frac{MJ}{m^3.C}) = \left(\frac{\rho_{dry}}{\rho_w}\right) * [\left(0.17 + \frac{w}{100}\right) + 0.5 * \left(\left(w - \frac{w_u}{100}\right)\right)] * c_{vw}$$

Where:

- c_{vu} ($\frac{MJ}{m^3.C}$): unfrozen volumetric het capacity,
- c_{vf}: frozen heat capacity,
- ρ_{dry}: soil dry density,
- ρ_{water}: water density,
- w: soil water content,
- c_{vw}: water volumetric heat capacity = $c_{vw} = 4.187 \frac{Mj}{m^3.C}$,

The mass heat capacity can be deducted from the volumetric heat capacity as follows:
Equation 6.3.16: The mass heat capacity (Orlando & Ladanyi, 2004)

$$c_m(\frac{Mj}{Kg.C}) = \frac{c_v}{\rho_{dry}(1+w)}$$

Where:

- c_v ($\frac{Mj}{m^3.C}$): Soil volumetric heat capacity,
- w: soil water content,
- ρ_{dry} ($\frac{Kg}{m^3}$): Soil dry density.

F.1.3.3- Thermal diffusivity:

Thermal diffusivity is defined as the rate at which the heat is transferred in the soil mass. It depends on the thermal conductivity, the bulk density and the heat capacity of the soil (Haynes et al., 1980). Thermal diffusivity is computed using the following equation:

Equation 6.3.17: Thermal diffusivity (Haynes et al., 1980):

$$\alpha\left(\frac{m^2}{s}\right) = \frac{k}{C * \rho}$$

Where:

- K ($\frac{w}{m.C}$) : Soil thermal conductivity,
- C ($\frac{kj}{kg.C}$) : Soil heat capacity,
- ρ $\left(\frac{kg}{m^3}\right)$: Soil bulk density.

Thermal diffusivity of ice is much higher than that of water, therefore, the diffusivity of frozen soil is much higher than that of the same soil in the unfrozen condition. This means that the average temperature of a mass of saturated frozen soil will increase quicker than of a mass of unfrozen soil with equal dimensions and in the same in-situ conditions (Orlando & Ladanyi, 2004).

F.1.3.4- Latent heat of fusion:

The latent heat of fusion also called the enthalpy of fusion of a substance is defined as the amount of heat energy required for a unit mass of this substance to change its state from the solid to a liquid, at constant pressure (Emerson, 1994). In the context of frozen soil, the main component responsible for the phase change is water in the soil's pore. At the freezing point where temperature is at 0 °C, the total energy involved in the phase change process will depend on the total water contained in the soil volume and the fraction of this water that changes the phase (Orlando & Ladanyi, 2004) .

The latent heat of fusion for a given soil is calculated as follows:

Equation 6.3.18: Latent heat of fusion equation (Orlando & Ladanyi, 2004)

$$L\left(\frac{KJ}{m^3}\right) = \rho_{dry} * L' * \frac{w - w_u}{100}$$

Where:

- ρ_{dry} $\left(\frac{kg}{m^3}\right)$: Soil dry density,
- $L'\left(\frac{KJ}{kg}\right)$: The mass latent heat for water, $L'\left(\frac{KJ}{kg}\right) = 333.7\frac{KJ}{Kg}$,
- w (%) : Total soil water content,
- w_u(%): Soil unfrozen water content.

Sand and gravel quickly dissipate the water in the unfrozen state, therefore, the w_u term will be negligible. The assumption that w_u= 0 gives acceptable latent heat of fusion values (Emerson, 1994).

F.1.3.5- Thermal expansion coefficient:

The thermal expansion coefficient (α) describes the extent to which a material expands or contract

upon heating or freezing. It is related to the micro-composition of the material and the magnitude of temperature change (Song, 2007). The cyclic phenomenon of expansion-contraction induces significant serviceability and ultimate issues in civil engineering structures in the cold regions. For example, the fracturing of topsoil layers by thermal contraction induces major maintenance problems for highways and roads. It may also, weaken apart landfill covers by creating major cracks and joints in the fill soil (Orlando & Ladanyi, 2004).

The coefficient of thermal expansion is defined as the rate of change of length relatively to temperature per unit length. It can be expressed as follows:

Equation 6.3.19: The coefficient of thermal expansion equation (Orlando & Ladanyi, 2004)

$$\alpha\ (°C)^{-1} = \frac{1}{L_0} * \frac{dL}{dT} = \frac{d\varepsilon}{dT}$$

Where:

- L_0 : reference length at a reference temperature,
- $d\varepsilon = \frac{dL}{L_0}$: strain in a given direction,
- dT : temperature variation,

For isotropic material, with homogenous micro composition, the thermal expansion is assumed to be equal in all directions. Therefore, the thermal expansion coefficient is identical in all directions.

The impact of decreasing temperature on the thermal expansion coefficient of sand was studied by Al-Moussawi (1988) where saturated sand samples with a bulk density of $2.27\frac{mg}{m^3}$ were tested in temperatures up to -60 $°C$. It was concluded that the thermal expansion coefficient for frozen sand experiences a small reduction before reaching a temperature of -60 $°C$. For temperature < -60 $°C$, Bourbonnais (1984), concluded that the thermal expansion coefficient undergoes a significant and continuous drop to minimal values at -170 $°C$ (Orlando & Ladanyi, 2004).

The figure below represents the temperature dependency of the thermal expansion coefficient of frozen sand, ice, and quartz in freezing temperatures up to -170 $°C$.

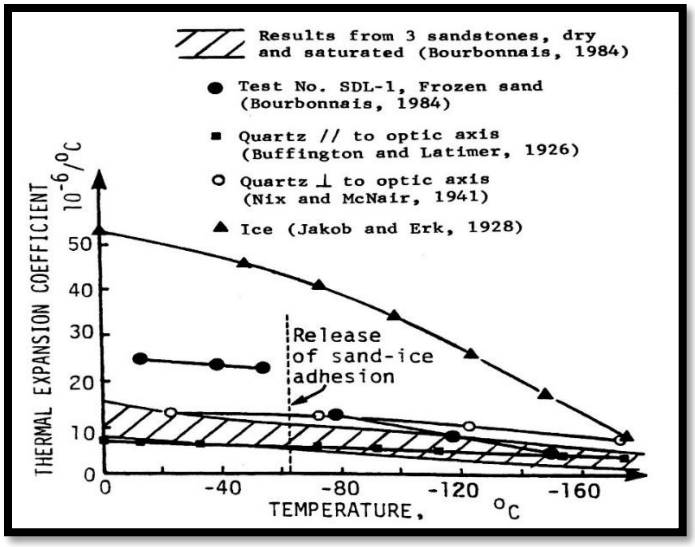

Figure F-1.8: Temperature dependency of the thermal expansion coefficient of frozen sand, ice and quartz (Orlando & Ladanyi, 2004).

F.2- References:

Bilskie, J. (2001). Soil Water Status: Content and potential: Campbell Scientific. Campbell Scientific, 1784(435), 84321. https://s.campbellsci.com/documents/us/technical-papers/soilh20c.pdf

Crory, F., Settlement associated with the thawing of permafrost, in Proc. 2nd Int. Permafrost Conf., Yakutsk, 1973, pp. 599–607

Ctori, P. (1989). The effects of temperature on the physical properties of cohesive soil. NBER Working Paper Series, 58(58), 99–104. https://www.unhcr.org/publications/manuals/4d9352319/unhcr protection-training-manual-european-border-entry-officials-2-legal.html?query=excom 1989

Czurda, K. A., & Hohmann, M. (1997). Freezing effect on shear strength of clayey soils. Applied Clay Science, 12(1–2), 165–187. https://doi.org/10.1016/S0169-1317(97)00005-7

Emerson, D. G. (1994). A heat and water transfer model for seasonally frozen soils with application to a precipitation-runoff model. US Geological Survey Water-Supply Paper, 2389. https://doi.org/10.3133/wsp2389

Farouki, O.T. (1981). Thermal Properties of Soils. CRREL Monograph 81-1. U.S. Army Corps of Engineers, Cold Regions Research and Engineering Laboratory, Hanover, New Hampshire.

Flynn, D. J. (2015). Field and Numerical Studies of an Instrumented Highway Embankment in Degrading Permafrost By.

Harlan, R.L., and Nixon, J.F. (1978). Ground thermal regime. Chapter 3 in Geotechnical Engineering for Cold Regions, ed. O.B. Andersland and D.M. Anderson. New York: McGraw-Hill, pp. 103-163

Haynes, F. D., Carbee, D. L., & Van Pelt, D. J. (1980). Thermal Diffusivity of Frozen Soil. CRREL Special Report (US Army Cold Regions Research and Engineering Laboratory), 80–38.

Jiang, H. & Fall, M. (2017). Yield stress and strength of saline cemented tailings materials in sub-zero environments: slag-paste backfill. Journal of Sustainable Cement-Based Materials 6 (5), 314-331.

Johansen, O., (1975). Thermal Conductivity of Soils. Ph.D. thesis. Trondheim, Norway. (CRREL Draft Translation 637, 1977), ADA044002.

Moghbel, F. & Fall, M. (2018). Thermal properties of compost biocover subjected to freeze-thaw cycles Journal of Cold Regions Engineering 32 (3), 04018008.

Munro, R. (2018). The Shear Strength of Frozen Soils. INTERNATIONAL SOCIETY FOR SOIL Mechanics and geotechnical engineering, 536–537. https://doi.org/10.1007/978-3-319-73568-9_174

Orlando, B. A., & Ladanyi, B. (2004). Frozen Ground Engineering (4th ed.). John Wiley & sons.

Shelman, A., Tantalla, J., Sritharan, S., Nikolaou, S., & Lacy, H. (2014). Characterization of Seasonally Frozen Soils for Seismic Design of Foundations. Journal of Geotechnical and Geoenvironmental Engineering, 140(7), 04014031. https://doi.org/10.1061/(asce)gt.1943-5606.0001065

Song, W. K. (2007). Effective thermal expansion coefficient of frozen granite soil. Canadian Geotechnical Journal, 44(10), 1137–1147. https://doi.org/10.1139/T07-047

Wang, S., Qi, J., & Yin, Z. Y. (2015). A review of the dynamic behaviour of frozen soils. Geotechnical Engineering, 46(3), 37–45.

Williams, P. J. (1962). Specific Heats and Unfrozen Water Content of Frozen Soils. Proceedings of the First Canadain Conference on Permafrost, 109–126.

Wolfe, L. H., & Thieme, J. O. (1964). Physical and Thermal Properties of Frozen Soil and Ice. Society of Petroleum Engineers Journal, 4(01), 67–72. https://doi.org/10.2118/675-pa

Appendix G

G.1- Thaw behavior of soils

G.1.1- Thaw depth:

In the thawing season, the soil surface experiences an increase in temperature (>0 °C). The thawing process is then defined as the movement of the surface thermal boundary condition (T_s> 0 °C) through the frozen soil to a depth X(t). Nixon and McRoberts (1973) estimate the movement of the thawing depth into the soil with time as follows (Nixon & McRoberts 1973):

Equation 6.3.1: Thawed depth equation (Nixon & McRoberts 1973):

$$X\,(m) = \alpha\sqrt{t}$$

Where:

- X (m): the thawed depth,
- t (s) : time,
- $\alpha(\frac{m}{\sqrt{s}})$: constant,

Nixon and McRoberts (1973) proposed an empirical equation to compute the constant $\alpha(\frac{m}{\sqrt{s}})$ as follows:

Equation 6.3.2: α constant equation (Nixon & McRoberts 1973):

$$\alpha\left(\frac{m}{\sqrt{s}}\right) = 2\sqrt{\alpha_u}\left(\frac{Ste}{2}\right)^{\frac{1}{2}}\left(1-\frac{Ste}{8}\right)$$

Where:

- α_u: the unfrozen soil thermal diffusivity,
- $Ste = c_{vu}T_s(L)^{-1}$: Stefan number,
- c_{vu}: the unfrozen volumetric heat capacity,
- T_s : the constant surface temperature,
- L : the volumetric latent heat,

For partially frozen soils containing certain amount of water, Nixon and McRoberts (1973) proposed a modified equation to estimate the thaw depth:

Equation 6.3.3: Thaw depth equation (Nixon & McRoberts 1973):

$$X\,(m) = \left(\frac{2k_u T_s}{L}\right)^{\frac{1}{2}} \sqrt{t}$$

Where k_u the soil unfrozen thermal conductivity and all other parameters are as defined in the equation above.

For soil strata incorporating two different soil layers with different thermal and geotechnical properties, the thaw depth can be calculated as follows:

Equation 6.3.4: Thaw depth in two different soil layers equation (Nixon & McRoberts 1973):

$$X = \left(\left(\frac{k_2}{k_1}H\right)^2 + \left(2\frac{k_2 T_s (t - t_o)}{L_2}\right)\right)^{\frac{1}{2}} - \left(\frac{k_2}{k_1} - 1\right) H$$

Where:

- k_1, k_2: thermal conductivity of layer 1 and 2 respectively,
- L_1, L_2 : volumetric latent heat of layer 1 and 2 respectively,
- H: height of the first layer (at the surface),
- t: time at the end of the thawing process,
- to: the time to thaw the first layer,
- T_S: surface temperature,

G.1.2- Thaw settlement:

Two factors are responsible for soil thawing settlement: Ice phase change (ice to water) and the dissipation of excess water out of the soil. In the case of a saturated soil, frozen under closed drainage condition, the soil will expand in volume due to the change of pore water to ice (Sinnathamby et al., 2015). The volumetric expansion (strain) is estimated as:

Equation 6.3.5: The volumetric expansion equation (Sinnathamby et al., 2015)

$$\frac{\Delta V}{V_o} \approx 0.09\ n$$

Where “n" is the soil porosity.

Similarly, for undrained conditions, in thawing, the soil will return to its initial volume V_o.

Nevertheless, in open fields, the ground experiences significant drainage forces inducing a flow of excess water out the soil. Drainage of thawed ground leads to additional volume change depending on soil composition, and previous consolidation changes that occurred during the previous freezing-thawing cycles (Orlando & Ladanyi, 2004).

Several factors influence the amount and distribution of ice in frozen ground. This includes the geotechnical composition and thermal properties of the soil and moisture and structural changes histories. The amount of thaw settlement can be roughly estimated through visual inspections for ice rich grounds; nevertheless, the exact amount of thaw settlement should be determined through experiment and laboratory observation on representative samples (Orlando & Ladanyi, 2004).

Thaw settlement can be measured in a triaxial cell or in a one-dimensional consolidation device. In the thawing season, the frozen soil void ratio "e_f" drops to e_{th} the thawed void ration (b to c), figure G.1.1. At a constant pressure σ_o, large change in void ratio occurs due to water phase change and the primary drainage of excess water (Orlando & Ladanyi, 2004).

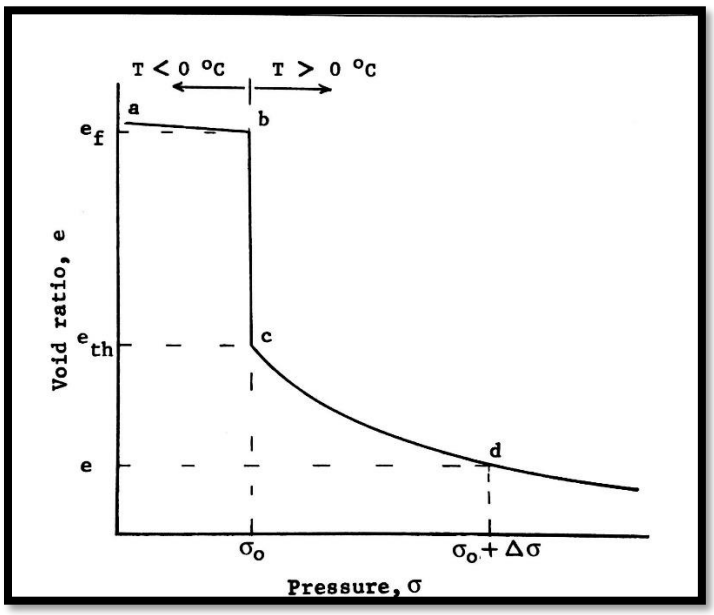

Figure 6.3.1: Typical void ratio vs pressure curve for frozen soils subjected to thawing (Orlando & Ladanyi, 2004)

Consolidation settlement occurs under soil self-weight and increasing external applied loads"$\Delta\sigma$" (c to d figure G.1.1). Consolidation settlement continues until a new equilibrium void “e” is attained.

The vertical strain of a soil sample thawed under a stress σ_o and exposed to a stress increase of "$\Delta\sigma$" can be found as follows:

Equation 6.3.6: Vertical strain of thawed soil (Orlando & Ladanyi, 2004)

$$\varepsilon_{vertical} = \frac{\Delta H}{H} = A_o + m_v \, \Delta\sigma$$

Where:

- m_v : the coefficient of volume compressibility as defined in section 1-2-2,
- A_o : Thaw-strain parameter calculated as follow: $A_o = \frac{e_f - e_{th}}{1+e_f}$,

The thaw settlement of the soil sample is than calculated as follow:

Equation 6.3.7: The thaw settlement equation (Orlando & Ladanyi, 2004)

$$\Delta H = A_o H_f + m_v \, \Delta\sigma \, H_{th}$$

Where:

- H_f : The height of the frozen sample,
- H_{th} : The height of the soil sample after phase change and dissipation of excess water before consolidation occurs.

Crory (1973) gives an alternative relationship to calculate thaw settlement (no consolidation yet) as follows:

Equation 6.3.8: Thaw settlement (no consolidation) equation (Orlando & Ladanyi, 2004)

$$\Delta H = H_f \left(1 - \frac{\rho_{df}}{\rho_{th}}\right)$$

where ρ_{df} and ρ_{th} are the frozen and thawed dry densities of the soil respectively.

(Crory 1973) provides equation to calculate the thaw strain parameter A_o using the basic physical properties of frozen soil. The equation is as follow (Crory, 1973):

Equation 6.3.9: Thaw strain parameter Ao equation (Orlando & Ladanyi, 2004

$$A_o = \frac{\Delta H}{H_f} = \frac{w_f + 0.09 \, i_r w_f - w}{\left(\frac{S_r}{G_s}\right) + w_f + 0.09 i_r w_f}$$

Where:

- w_f and w: the total frozen and thawed soil water content respectively,
- S_r: the total degree of saturation as defined in section 1.3.5,

- G_s: the specific gravity of the soil as defined in section 1.3.6,
- i_r: the iciness ratio as defined in section 1.3.7,

Seep, Watson and Rowley (1973) and Johnson (1981) conducted field investigations and oedometer tests at a constant pressure (σ_o = 100 kpa) to estimate the thaw settlement of silty and sandy soils from several sites along the Makenzie king valley. The results showed a correlation between the unit thaw settlement and the density of the frozen soil samples. Ladanyi (1978) proposed an empirical equation to estimate the thaw strain (%) using the bulk density of the frozen soil ρ_f and the density of water ρ_w as follow:

Equation 6.3.10: Thaw strain equation (1978) (Orlando & Ladanyi, 2004)

$$\varepsilon(\%) = 100\frac{\Delta H}{H_f} = 85 * \left(1 - \left(\frac{\rho_f}{\rho_w} - 1.1\right)^{\frac{1}{2}}\right) \pm 8$$

The equation above also gives a good approximation of the thaw strain for low plasticity clays. Nixon and Ladanyi (1994) modified the equation above and estimate the thaw strain as follows (Orlando & Ladanyi, 2004):

Equation 6.3.11: Thaw strain equation (1994) (Orlando & Ladanyi, 2004)

$$\varepsilon = \frac{\Delta H}{H_f} = 0.9 - 0.868\left(\frac{\rho_f}{\rho_w} - 1.15\right)^{\frac{1}{2}} \pm 0.05$$

Similarly, results of the same study showed a correlation between the thaw strain (%) and total frozen water content. Ladanyi (1994) proposed an empirical equation to estimate the thaw strain (%) using the total frozen water content "w":

Equation 6.3.12: Thaw strain equation (1994) (Orlando & Ladanyi, 2004)

$$\varepsilon(\%) = 102.75 - (5480.75(w + 27.43)) \pm 8$$

For silts and clayey silts within the interval $1.2 < \frac{\rho_f}{\rho_w} < 2.0$ Nixon and Ladanyi (1978) proposed and empirical equation to estimate the thaw strain as follow (Orlando & Ladanyi, 2004):

Equation 6.3.13: Thaw strain equation (1978) (Orlando & Ladanyi, 2004)

$$\varepsilon = \frac{\Delta H}{H_f} = 0.8 - 0.86\left(\frac{\rho_f}{\rho_w} - 1.1\right)^{\frac{1}{2}} \pm 0.05$$

G.1.3- Thaw consolidation:

Thaw consolidation theory was first established by Morgenstern and Nixon to describe the consolidation process that occurs in fine grained soils in the thawing season. Consolidation in the thawed soil is induced by the soil self-weight and external applied load at the surface (Morgenstern & Nixon, 1971). The first thaw-consolidation tests were performed by Tsytovich approximately 70 years ago. Tsytovich conducted thaw consolidations tests using a simple oedometer and measured settlement in rapid thawing soils under different loading conditions. Tsytovich experiments concluded that the compressible behavior of the soil skeleton could be modeled using the Terzaghi consolidation theory (Tsytovich, 1941). Morgenstern and Nixon (1971) used Tsytovich results and relayed on the theories of heat conduction and soil consolidation to build the thaw consolidation theory (Lesage, 2008). They considered one dimensional configuration as shown in figure G.1.2:

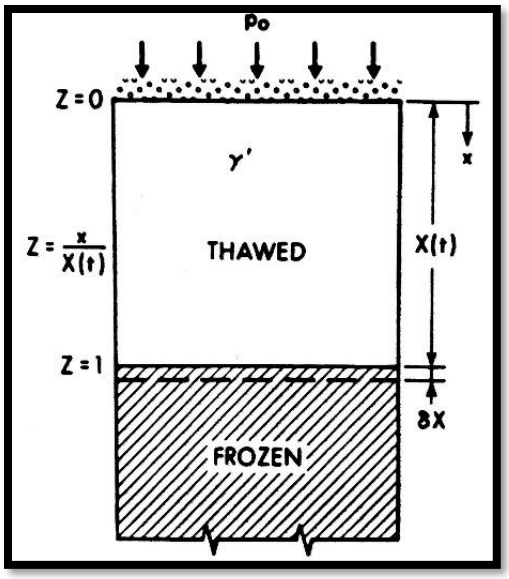

Figure 6.3.2: one-dimensional thaw consolidation (Orlando & Ladanyi, 2004)

Morgenstern and Nixon (1971) described the movement of the thaw plane X(t) in soil with no unfrozen water and assumes compressible ground. The boundary conditions for the one-dimensional configuration were defined as follows (Morgenstern & Nixon, 1971):

1- Initially, the time is zero and the distance to the thaw plane from the soil surface is zero

2- Free draining at the upper surface of the soil mass,
3- Porewater pressures are zero during thawing at the soil surface.

Considering the boundary conditions above, the classical Terzaghi consolidation equation for a saturated compressible soil under constant applied stress could be expressed as follows:

Equation 6.3.14: Terzaghi consolidation equation (Orlando & Ladanyi, 2004):

$$c_v\left(\frac{\partial^2 u}{\partial x^2}\right) = \left(\frac{\partial u}{\partial t}\right)$$

where:

- c_v: Coefficient of consolidation; varies from $10\frac{mm^2}{s}$ for sandy silt to $0.01\frac{mm^2}{s}$ for clays (Orlando & Ladanyi, 2004),
- u : Excess pore pressure,
- x : Depth measured from the ground surface,

Using Darcy's law, boundary conditions as above, and theories of heat conduction and of consolidation, Morgenstern and Nixon (1971) described the stress condition at the thaw line as follows:

Equation 6.3.15: Stress condition at the thaw line (Morgenstern & Nixon, 1971):

$$P_o + \gamma' X - u(X,t) = \frac{1}{\frac{dx}{dt}}\left[c_v \frac{\partial u}{\partial t}\,(X,t)\right]$$

Where:

- P_0: Load applied to the surface
- γ': submerged unit weight of the soil,
- X: Thaw depth,

Morgenstern and Nixon (1971) proposed an empirical solution to estimate the excess pore pressures caused by thaw consolidation as follows:

Equation 6.3.16: Excess pore pressures equation caused by thaw consolidation (Morgenstern & Nixon, 1971):

$$u(x,t) = \frac{P_0}{\mathrm{erf}(R) + \frac{e^{-R^2}}{\sqrt{\pi}}}\,\mathrm{erf}\left(\frac{x}{2\sqrt{c_v t}}\right) + \left(\frac{\gamma' x}{1 + \frac{1}{2R^2}}\right)$$

Where:

- $R = \left(\frac{\alpha}{2\sqrt{c_v}}\right)$: Thaw consolidation ratio and α as defined in section 2.5.1,
- erf() : error function,
- Other parameter as defined above,

Morgenstern and Nixon (1971) introduce two directionless parameters as follows:

$$B = \frac{1}{1 + \frac{1}{2R^2}}$$

And,

$$Z = \left(\frac{x}{X(t)}\right)$$

The equation to calculate the excess pore pressures caused by thaw consolidation could be modified and written as follows:

Equation 6.3.17: Modified excess pore pressures equation caused by thaw consolidation (Orlando & Ladanyi, 2004):

$$u(x,t) = \left(\frac{1}{1 + W_r}\right)\frac{erf(RZ)}{erf(R) + \frac{e^{-R^2}}{\sqrt{\pi R}}} + \left(\frac{Z}{\left(1 + \frac{1}{2R^2}\right)\left(1 + \frac{1}{W_r}\right)}\right)$$

Where:

- $W_r = \left(\frac{\gamma' X(t)}{P_o}\right)$, and all parameters as defined above,

For a weightless material consolidated under external applied load P_o, the excess pore pressures caused by thawing could be modified and written as follows (Lesage, 2008):

Equation 6.3.18: Weightless material excess pore pressures equation caused by thaw consolidation (Orlando & Ladanyi, 2004):

$$u(x,t) = \frac{u(Z,t)}{P_o} = \frac{erf(RZ)}{erf(R) + \frac{e^{-R^2}}{\sqrt{\pi R}}}$$

Similarly, Morgenstern and Nixon (1971) proposed the following equation to calculate the excess pore pressures caused by thawing for soil consolidating under its own weight:

Equation 6.3.19: Self consolidating material excess pore pressures equation caused by thaw consolidation (Morgenstern & Nixon, 1971):

$$u(x,t) = \frac{u(Z,t)}{\gamma' X} = \frac{Z}{\left(1 + \frac{1}{2R^2}\right)}$$

Figure G.1.3 represents a graphical correlation for weightless material consolidation based on the equation developed by Morgenstern and Nixon (1971), it includes the normalized values of excess pore pressures that have been computed for different thaw consolidation ratios as a function of the normalized depth Z (Morgenstern & Nixon, 1971):

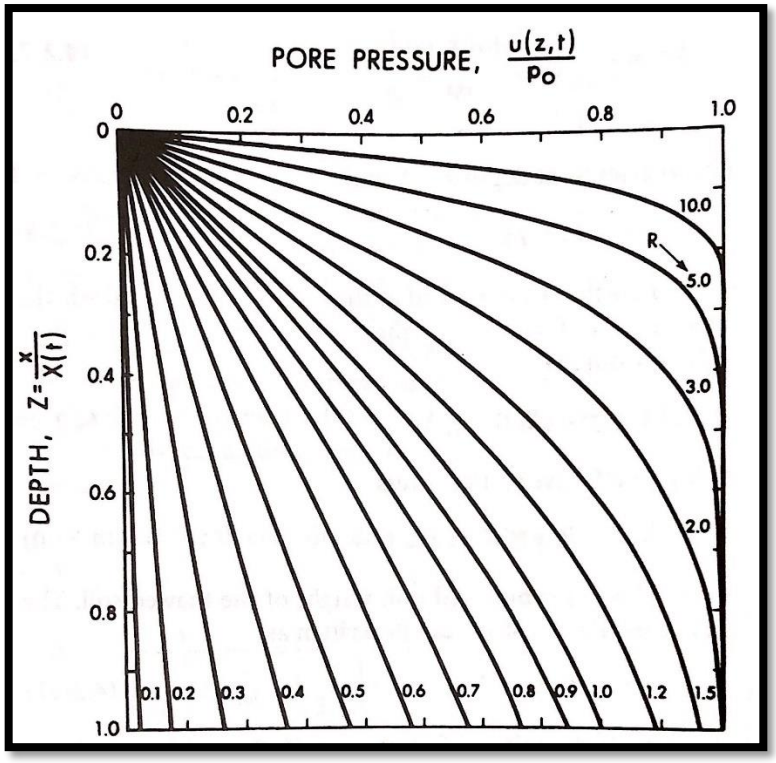

Figure 6.3.3: Excess pore pressure correlation for weightless materials (Orlando & Ladanyi, 2004)

Similarly, figure G.1.4 represents a graphical correlation for weightless soil consolidated under its unit weight with no external load applied based on the equation developed by Morgenstern and Nixon (1971), it includes the normalized values of excess pore pressures that have been computed for different thaw

consolidation ratios as a function of the normalized depth Z:

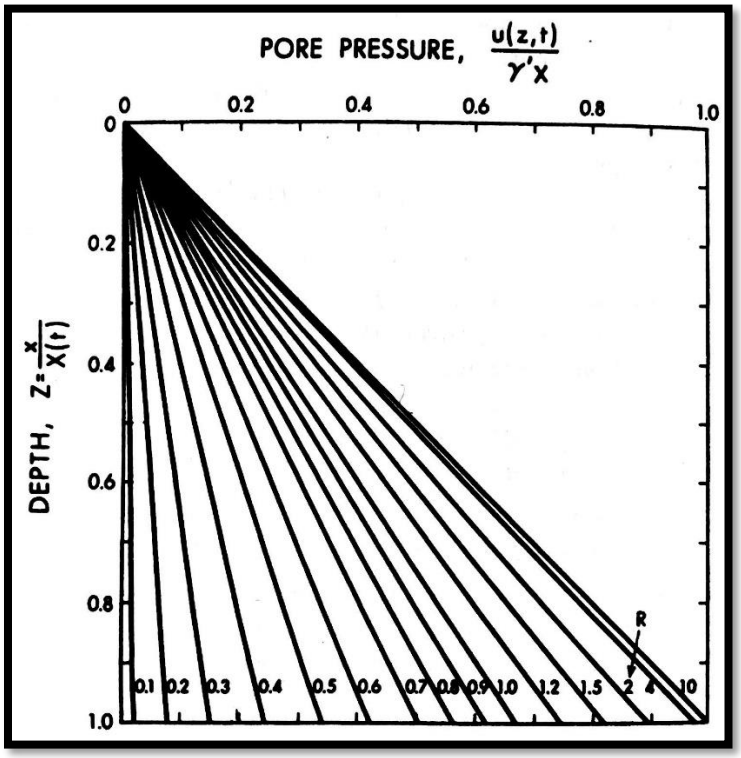

Figure 6.3.4: Excess pore pressure correlation for weightless materials (Orlando & Ladanyi, 2004)

Morgenstern and Nixon (1975) calculated the thaw consolidation settlement at time "t" as follows (Morgenstern & Nixon, 1975):

Equation 6.3.20: Thaw consolidation settlement equation (Morgenstern & Nixon, 1975):

$$S_t = \int_0^X P_o + \gamma' x - \sigma_o' - u(x,t)\, dx$$

The general formulation to calculate the total settlement S_{max} is given as follows:

Equation 6.3.21: Total settlement equation (Orlando & Ladanyi, 2004)

$$S_{max} = m_v \left((P_0 - \sigma_o')X + \frac{\gamma' X^2}{2} \right)$$

Where σ_o' is the effective stress in the soil at the thaw depth (residual stress in the soil if not neglected) and all variables are as defined above.

The average degree of consolidation of the thawed soil is defined as the ratio of the consolidation settlement that has occurred at time t; "S_t", to the total consolidation that would occur if thawing were stopped at time t; S_{max} (Orlando & Ladanyi, 2004). Morgenstern and Nixon (1971) proposed two equations to calculate the degree of consolidation as follows:

- For weightless materials ($\gamma' = 0$):

Equation 6.3.22: Degree of thaw consolidation for weightless material equation (Morgenstern & Nixon, 1971):

$$\frac{S_t}{S_{max}} = 1 - \frac{\text{erf}(R) + \frac{e^{-R^2} - 1}{\sqrt{\pi}R}}{\text{erf}(R) + \left(\frac{e^{-R}}{\sqrt{\pi}R}\right)}$$

- For self-weight consolidation ($P_o = 0$):

Equation 6.3.23: Degree of thaw consolidation for self-weight consolidation material equation (Morgenstern & Nixon, 1971):

$$\frac{S_t}{S_{max}} = \frac{1}{1 + 2R^2}$$

Where all parameters are defined as above,

The average degree of consolidation has been plotted as a function of the thaw consolidation ratio for both consolidation scenarios (self-weight consolidation and weightless materials) as presented in figure G.1.5:

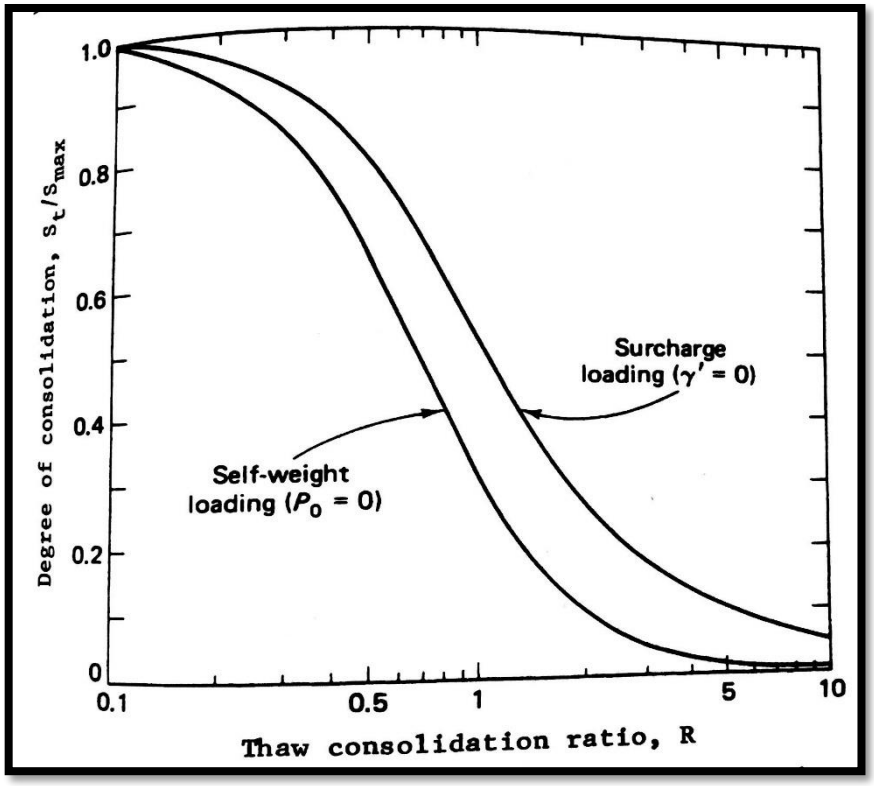

Figure 6.3.5: Variation of degree of consolidation with thaw consolidation ratio (Orlando & Ladanyi, 2004)

G.1.1- Thaw consolidation in layered strata

Thaw consolidation in layered soil strata should be assessed to establish adequate geotechnical design of foundation systems and embedded structures. The difference of the thermal and geotechnical properties between two subsequent soil layers can influence the thaw consolidation behavior of the ground (Orlando & Ladanyi, 2004).

Assuming a configuration as in figure G.1.6:

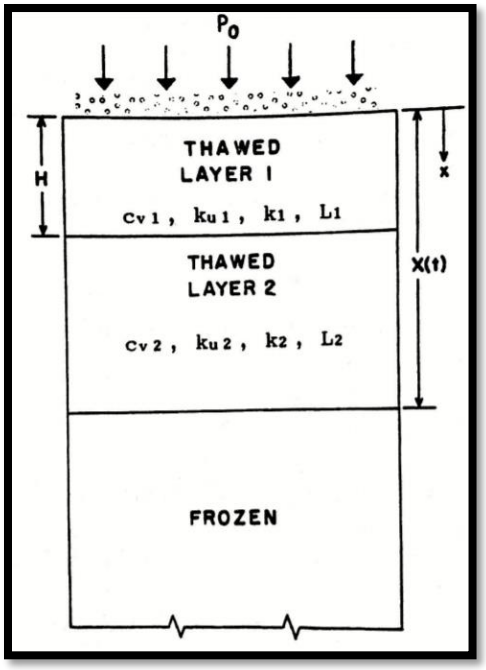

Figure 6.3.6: Thaw configuration in layered soil - (Orlando & Ladanyi, 2004)

The Terzaghi consolidation settlement could be used to describe the consolidation process in both layers, therefore:

For layer 1:

Equation 6.3.24 : Terzaghi consolidation equation (Orlando & Ladanyi, 2004)

$$c_{v_1}\left(\frac{\partial^2 u_1}{\partial x^2}\right) = \left(\frac{\partial u_1}{\partial t}\right)$$

For layer 2:

Equation 6.3.25: Terzaghi consolidation equation (Orlando & Ladanyi, 2004)

$$c_v\left(\frac{\partial^2 u_2}{\partial x^2}\right) = \left(\frac{\partial u_2}{\partial t}\right)$$

Morgenstern and Nixon (1971) proposed a solution for Terzaghi thaw consolidation equation using the continuity of pore fluids at the thaw line. This theory assumes that the porewater pressures $u_1 = u_2$ when the thaw plane reaches the interface between the two layers (Orlando & Ladanyi, 2004).

Therefore, when the thaw plane reaches the interface between the two layers the consolidation problem can be expressed as follows:

Equation 6.3.26 : Terzaghi consolidation equation at the interface between the two layers (Orlando & Ladanyi, 2004)

$$k_1 \frac{\partial u_1}{\partial x} = k_2 \frac{\partial u_2}{\partial x}$$

And the stress condition at the thaw line:

Equation 6.3.27: Stress condition at the thaw line equation (Orlando & Ladanyi, 2004)

$$P_o + \gamma' X - \sigma_o - u_2(x,t) = \frac{1}{\frac{dx}{dt}}\left[c_{v_2} \frac{\partial u}{\partial t}\right]$$

Where σ_o' is the effective stress in the soil at the thaw depth (residual stress in the soil if not neglected) and all variables are as defined above.

Morgenstern and Nixon (1971) solution can be used to describe the stress condition at the thaw line of multilayered soil using the same rational and assuming the continuity of the pore fluids at the thaw line (Morgenstern & Nixon, 1971).

G.2- References:

Crory, F., Settlement associated with the thawing of permafrost, in Proc. 2nd Int. Permafrost Conf., Yakutsk, 1973, pp. 599–607

Lesage, K. (2008). Experimental studies of thaw consolidation of fine grained frozen soils from the Mackenzie Valley.

Morgenstern, N.R., and Nixon, J.F. 1971. One-dimensional consolidation of thawing soils. Canadian Geotechnical Journal, 8(4): 558–565.

Nixon, J.F., and McRoberts, E.C., 1973. A Study of Some Factors Affecting the Thawing of Frozen Soils. Canadian Geotechnical Journal, Vol. 10.

Orlando, B. A., & Ladanyi, B. (2004). Frozen Ground Engineering (4th ed.). John Wiley & sons.

Sinnathamby, G., Gustavsson, H., & Korkiala-tanttu, L. (2015). Frost Heave and Thaw Settlement Estimation of a Frozen Ground Frost Heave and Thaw Settlement Estimation of a Frozen Ground. November. https://doi.org/10.3233/978-1-61499-603-3-891

Tsytovich, N.A., An analysis of foundation settlement on melting grounds, in Tr. LISI (Bull. Leningrad. Civil Eng. Inst), 1941, vol. 3, pp. 15–21